INTEGRATION OF SCHEDULING AND CONTROL WITH CLOSED-LOOP PREDICTION

Integration of Scheduling and Control with Closed-loop Prediction

by

Daniela Dering, M.Sc.

A Thesis
Submitted to the School of Graduate Studies
in Partial Fulfillment of the Requirements
for the Degree of
Doctor of Philosophy

McMaster University

DOCTOR OF PHILOSOPHY (2023) McMaster University

(Chemical Engineering) Hamilton, Ontario, Canada

TITLE:	Integration of Scheduling and Control with Closed-loop Prediction
AUTHOR:	Daniela Dering
	M.Sc. (Chemical Engineering),
	McMaster University, Hamilton, Canada
SUPERVISOR:	Dr. Christopher L.E. Swartz
NUMBER OF PAGES:	xvii, 178

Abstract

Deregulation of electricity markets, increased usage of intermittent energy sources, and growing environmental concerns have created a volatile process manufacturing environment. Survival under this new paradigm requires chemical manufactures to shift from the traditional steady-state operation to a more dynamic and flexible operation mode. Under more frequent operating changes, the transition dynamics become increasingly relevant, rendering the traditional steady-state based scheduling decision-making suboptimal. This has motivated calls for the integration of scheduling and control.

In an integrated scheduling and control framework, the scheduling decisions are based on a dynamic representation of the process. While various integration paradigms are proposed in the literature, our study concentrates on the *closed-loop* integration of scheduling and control. There are two main advantages to this approach: (i) seamless integration with the existing control system (i.e. it does not require a new control system infrastructure), (ii) the framework is aware of the control system dynamics, and hence has knowledge of the *closed-loop* process dynamics. The later aspect is particularly important as the control system plays a key role in determining the transition dynamics.

The first part of our work is dedicated to developing an integrated scheduling and control framework that computes set-point trajectories, to be tracked by the lower-level linear model predictive control system, that are robust to demand uncertainty. We employ a piecewise linear representation of the nonlinear process model to obtain a mixed-integer linear programming (MILP) problem, thus alleviating the computational complexity compared to a mixed-integer nonlinear programming formulation. The value of the stochastic solution is used to confirm the superiority of the robust formulation against a nominal one that disregards uncertainty. In the second part of this study, we expand the framework to accommodate additional uncertainty types, including model and cost uncertainty.

In the third part of this thesis, a *deterministic* integrated scheduling and control framework for processes controlled by distributed linear model predictive control is developed. The integrated problem is formulated as a MILP. To reduce the solution time, we introduce strategies to approximate the feedback control action. Through case studies, we demonstrate

that knowledge of the control system enables the framework to effectively coordinate the MPC subsystems. The framework performs well even under conditions of plant-model mismatch conditions.

In the final part of this study, we introduce an integrated scheduling and control formulation for processes controlled by nonlinear model predictive control (NMPC). Here, discrete scheduling decisions are represented using complementarity conditions. Additionally, we use the first-order Karush-Kuhn-Tucker conditions of the NMPC controller to compute the input values in the integrated problem. The resulting problem is a mathematical program with complementarity constraints that we solve using a regularization approach. For all case studies, the complementarity formulation effectively capture discrete scheduling decisions, and the KKT conditions always provides a local optimum of the associated NMPC problem.

In summary, this study of the integration of scheduling and control addresses various control systems, uncertainty, and strategies for enhancing the solution time. Furthermore, we assess the performance of the proposed frameworks under conditions of plant-model mismatch, a common scenario in real-life applications.

Acknowledgments

I extend my deepest gratitude to Dr. Christopher Swartz for his unwavering guidance and support. His mentorship, availability, and positive attitude, combined with several insightful discussions is what made this thesis possible. I am also grateful to him for allowing me to follow my curiosity, and explore various topics and ideas outside the main scope of this thesis. This greatly helped me improve my technical skills and achieve a more profound understanding of important concepts.

I am grateful to Dr. Kamil Khan for being always available to answer my questions regarding optimization theory, providing invaluable input and untangling my thoughts. My gratitude to Dr. Tim Davidson for his insightful suggestions and feedback during my committee meetings, including the box plots in chapter three, which greatly improved the quality of the manuscript.

Throughout my almost six years at McMaster, I had the privilege of getting to know wonderful people, and food, from all over the world. I am extremely grateful to all my MACC and CHEMENG friends, who not only shared their diverse cuisines but also provided valuable collaborative criticism and emotional support. A special thanks goes to Praveen, Mina, Nina, Carlos and Anthony.

Moreover, I would like to acknowledge the unwavering support of my family.

I dedicate this thesis to a handful of strong women that tailored my personality and life choices. My grandma Teresinha, by far the most kind person I know. My mom Regina for being unfailingly caring and protective. My aunties Lilia and Alice who always radiate positivity and warmth despite the hardship of life. My cousin Helena Maria for being such a good-hearted person and hosting me for about three years. My cousin Juliana for being so loving, caring, and tolerating me as a roommate for three years. My Canadian hosts Alicia, Lily and Deborah for welcoming me in their house, and giving me a place to call home. J.K. Rowling for Hermione Granger, who, in my teenage years, served as an inspiring role model and motivated me to excel academically.

Last, I am grateful to God.

Table of Contents

List of Figures

List of Tables

Chapter 1

Introduction

In this chapter we present an overview and literature review on the integration of scheduling and control, followed by the main contributions of this work and the thesis outline.

1.1 Integration of scheduling and control

In the chemical process industry, scheduling is historically carried out using a steady-state process model where process transition times are either ignored, or an estimate thereof is used. Scheduling involves defining the production sequencing, production amounts, equipment usage, among others, for a period of hours to days. The relevant scheduling information is provided as targets to an underlying decision-making layer, or applied directly

to the plant.

Fig. 1.1, adapted from Darby et al. [10], illustrates the process automation hierarchy commonly implemented in refineries and large chemical plants. Also indicated are the time scales typically associated with the decision-making layers. Model predictive control (MPC) is the advanced control method of choice in the chemical process industry, and is typically configured to provide set-points to local plant PID-type controllers [23]. Fig. 1.1 includes real-time optimization (RTO), an economic optimization layer that traditionally utilizes a steady-state plant model, and provides set-points to the underlying MPC system. Production scheduling is the next level up. We remark that there are several variations of this process automation architecture. For example, the RTO layer may be replaced by a dynamic RTO (DRTO) system that utilizes a dynamic plant model [17, 29, 16], or the RTO layer could be entirely absent, with the scheduling decisions passed directly to the MPC system [4].

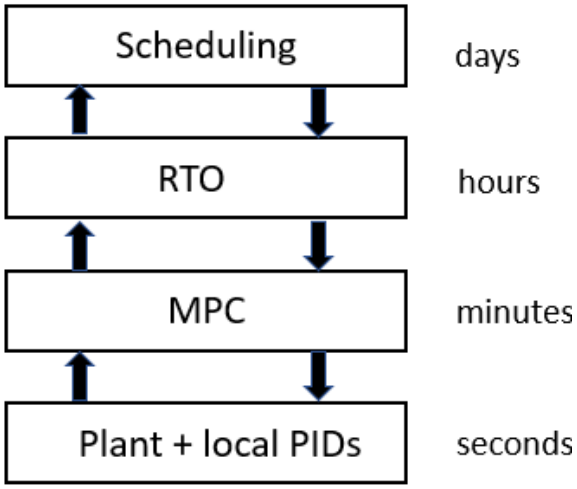

Figure 1.1. Process automation hierarchy.

Current trends toward increased globalization and deregulation of energy markets have resulted in significant variation in demand, supply, raw material costs, and energy prices, that together have created a highly dynamic environment in which plants are required to operate. Associated with the more dynamic plant operating environment is an increased frequency of scheduling decisions. Neglecting plant and control system dynamics under these conditions would generally lead to suboptimal decisions - a notion that underpins recent research activity in the integration of scheduling and control. Key conceptual paradigms

toward achieving this integration are identified in Baldea and Harjunkoski [4] and Caspari et al. [7] as "bottom-up" and "top-down" approaches.

In the "bottom-up" approach, the scheduling task is incorporated by the control layer, allowing for direct computation of the control input values and scheduling decisions applied to the process. An example is the integration of scheduling and economic model predictive control [20]. While this approach eliminates the need for the traditional set-point tracking MPC controller, it entails significant changes to the process control architecture currently in place in industry. Conversely, the "top-down" approach consists of augmenting the optimization problem solved at the scheduling layer with information regarding the process dynamics and control. The integrated problem is solved to compute set-point targets for the process control layer that is, then, kept intact.

The "bottom-up" and "top-down" paradigms find parallel in a more recent categorization scheme due to Flores-Cerrilo et al. [14] and illustrated in Fig. 1.2. They classify integrated scheduling and control (ISC) formulations as plant-dynamics aware or control-dynamics aware. In the first, the scheduler is unaware of the existence of the control system (if any) and its closed-loop interaction with the plant. The computed input trajectories are either applied directly to the plant, following the paradigm of economic model predictive control (EMPC), or tracked by a suitable controller. Note that in the EMPC paradigm, the plant dynamics-aware scheduler also takes on the function of the control system layer, dispensing the use of a set-point tracking controller. In control-dynamics aware scheduling formulations, a closed-loop dynamic representation of the plant is utilized at the scheduler level, thus making it aware of the feedback control action. Various strategies to obtain a closed-loop dynamics representation can be found in the literature. They include utilizing closed-loop data to develop data-driven models [28], and incorporating a suitable model of the control system to compute the input action [24, 27, 13, 9, 11]. Note that control-dynamics aware scheduling formulations are often referred to as "closed-loop" formulations. Conversely, plant-dynamics aware scheduling formulations are said to be "open-loop" formulations.

For the purposes of this study, we also make a distinction between implementation strategies for the ISC formulation. We use the term *closed-loop implementation* to mean that the ISC

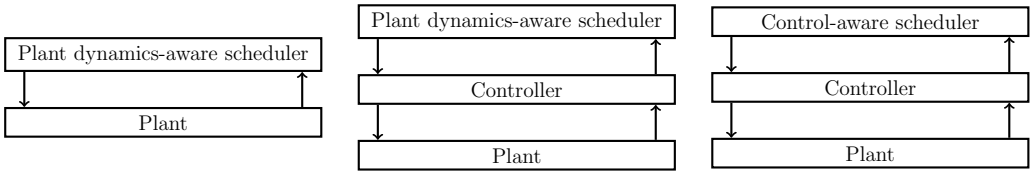

Figure 1.2. Schematic representation of paradigms for the integration of scheduling and control.

problem is solved online and receives feedback information from the actual process. On another hand, in open-loop implementations, the ISC problem is solved offline, providing optimal targets that are tracked online by an appropriate controller, or optimal inputs that are applied directly to the plant. Several studies focus on the formulation and solution of the ISC problem, and hence do not provide results regarding its implementation [15, 22, 31]. For these cases, we assume that the optimal inputs are directly applied to the plant, and the ISC implementation is said be open-loop. A categorization of several studies is presented in Table 1.1.

Table 1.1. Categorization of ISC formulations and implementations as open-loop (OL) or closed-loop (CL).

Study	ISC Formulation	Implementation
Flores-Tlacuahuac and Grossmann [15]	OL	OL
Zhuge and Ierapetritou [32]	OL	CL
Zhuge and Ierapetritou [31]	CL	OL
Zhuge and Ierapetritou [30]	OL	CL
Du et al. [13]	CL	OL
Pattison et al. [22]	CL	OL
Pattison et al. [21]	CL	CL
Dias et al. [12]	CL	OL
Burnak et al. [6]	CL	CL
Simkoff and Baldea [27]	CL	OL
Remigio and Swartz [24]	CL	CL
Simkoff and Baldea [28]	OL	OL

In the next paragraphs we present a literature review of plant-dynamics and control-dynamics aware scheduling formulations. We focus mostly on continuous processes.

1.1.1 Plant-dynamics aware scheduling formulations

One of the first ISC formulations is due to Flores-Tlacuahuac and Grossmann [15]. They compute the optimal cyclic production sequencing and control input values for multiproduct CSTRs. Process transitions times are calculated interactively as part of the proposed solution algorithm that involves the solution of mixed-integer nonlinear programming (MINLP) problems for fixed transition times. Zhuge and Ierapetritou [32] present an ISC formulation for online closed-loop operation of a nonlinear process. The closed-loop implementation consists of solving the ISC problem and applying the optimal input values to the process. The ISC problem is re-solved and new input values computed when the difference between the process states and the ISC prediction exceeds a given threshold. Mathur et al. [19] developed an ISC formulation for hydropower systems that accounts for on/off switching of the generators. The ISC computed input trajectories are implemented in a receding horizon manner. However, differing from typical EMPC implementations, a subset of the inputs rather than only the first input value is implemented on the process. Plant-dynamics aware scheduling formulationn for HVAC systems have also been developed [25, 26].

Due to the elevated solution times, a number of strategies have been proposed to reduce the computational burden of plant-dynamics aware scheduling formulations. In Zhuge and Ierapetritou [30], the nonlinear process model is approximated via piecewise affine (PWA) segments, allowing formulation of the ISC problem as a mixed-integer linear programming (MILP) problem as opposed to an MINLP. The optimal state profiles are tracked by a model predictive controller. Large deviations between predicted and measured state values trigger execution of the ISC calculation. Andres-Martinez and Ricardez-Sandoval [1] propose reformulating mixed-integer ISC formulations as a switched system, which leads to a nonlinear programming (NLP) problem. The computational benefits of their approach are demonstrated through case studies. In a later work, Andrés-Martínez and Ricardez-Sandoval [2] report results for the case where the optimal state trajectories are tracked by a nonlinear model predictive controller, and there are disturbances affecting the process. Simkoff and Baldea [28] propose the use of piecewise linear Hammerstein-Wiener models to capture scheduling relevant dynamics, reducing the computational burden associated with a rigorous

first-principles model. Some studies also proposed methods based on Benders and Lagrangian decomposition to reduce the solution time of integrated scheduling and control formulations [8, 26].

1.1.2 Control-dynamics aware scheduling formulations

As previously mentioned, process and control dynamics are accounted for in control-dynamics aware scheduling formulations.

Simkoff and Baldea [27] and Remigio and Swartz [24] propose an ISC formulation that accounts for the action of the lower-level linear model predictive control (LMPC). The embedded MPC subproblems, used to generate the closed-loop plant response along the prediction horizon, are replaced by their equivalent first-order Karush-Kuhn-Tucker (KKT) conditions. This draws on the closed-loop DRTO (CL-DRTO) formulation proposed in Jamaludin and Swartz [16], where the performance benefit of a closed-loop over an open-loop predicted response is demonstrated. Replacing the MPC subproblems by their KKT conditions yields a single-level mathematical program with complementarity constraints (MPCC), for which efficient solution techniques exist. In Simkoff and Baldea [27], the binary decisions introduced with the scheduling constraints are also reformulated using complementary constraints, maintaining an overall MPCC structure. Remigio and Swartz [24], on the other hand, reformulate the complementarity constraints introduced via the MPC-KKT conditions using binary variables. Since a linear dynamic process model and linear objective function are used, the resulting problem is a MILP. Dias et al. [12] propose an ISC formulation for a MPC controlled air separation unit. The resulting problem is solved using simulation-based optimization, an iterative procedure where an optimization problem is solved to compute the set-points provided to the closed-loop process simulation from which relevant data is extracted for the next optimization iteration.

At it would be expected, considering the control dynamics worsens the computational burden compared to an open-loop formulation. To deal with this issue, a number of studies replace the complex high fidelity process model with a reduced-order model. A control-aware

scheduling formulation for processes controlled by input-output linearizing controllers is developed in Du et al. [13]. This type of controller leads to linear closed-loop dynamics between the process inputs and outputs, even if the open-loop process dynamics are nonlinear. By employing this low-order linear model in place of the original nonlinear process model, the computational complexity and solution time of the integrated scheduling and control formulation is significantly reduced, with minimal impact in the economic performance. This idea is further extended in Baldea et al. [3]. Particularly, they develop a scheduling-oriented MPC formulation that leads to a linear closed-loop dynamics. The MPC is tasked with tracking the optimal trajectories computed by the integrated framework with the low-order linear model. In a separate study, Pattison et al. [22] develop a low-order nonlinear Hammerstein-Wiener model representation of the closed-loop dynamics of an air separation unit. Taking a different approach, Kelley et al. [18] utilizes piecewise linear Hammerstein-Wiener models to capture the closed-loop process dynamics. This leads to a mixed-integer linear (MILP) formulation for the integrated scheduling and control problem, for which a special solution strategy is proposed. A polymerization reactor case study is used to demonstrate the performance of their framework. Chu and You [9] propose strategies for efficient online solution of an integrated scheduling and controller selection problem.

The capabilities of multiparametric programming have also been extensively used to reduce the online solution time of control-aware scheduling formulations. Zhuge and Ierapetritou [31] make use of multi-parametric MPC (mp-MPC) [5], and obtain a solution map of the MPC problem. This solution map is embedded in the ISC formulation as piecewise affine functions. They also suggest utilizing a piecewise affine approximation of the nonlinear plant model and objective function to yield a MILP formulation. Burnak et al. [6] go a step further and use multiparametric programming to obtain offline solution maps of the ISC problem itself, thus, reducing the online solution of the control-aware scheduler to a lookup table and a function evaluation.

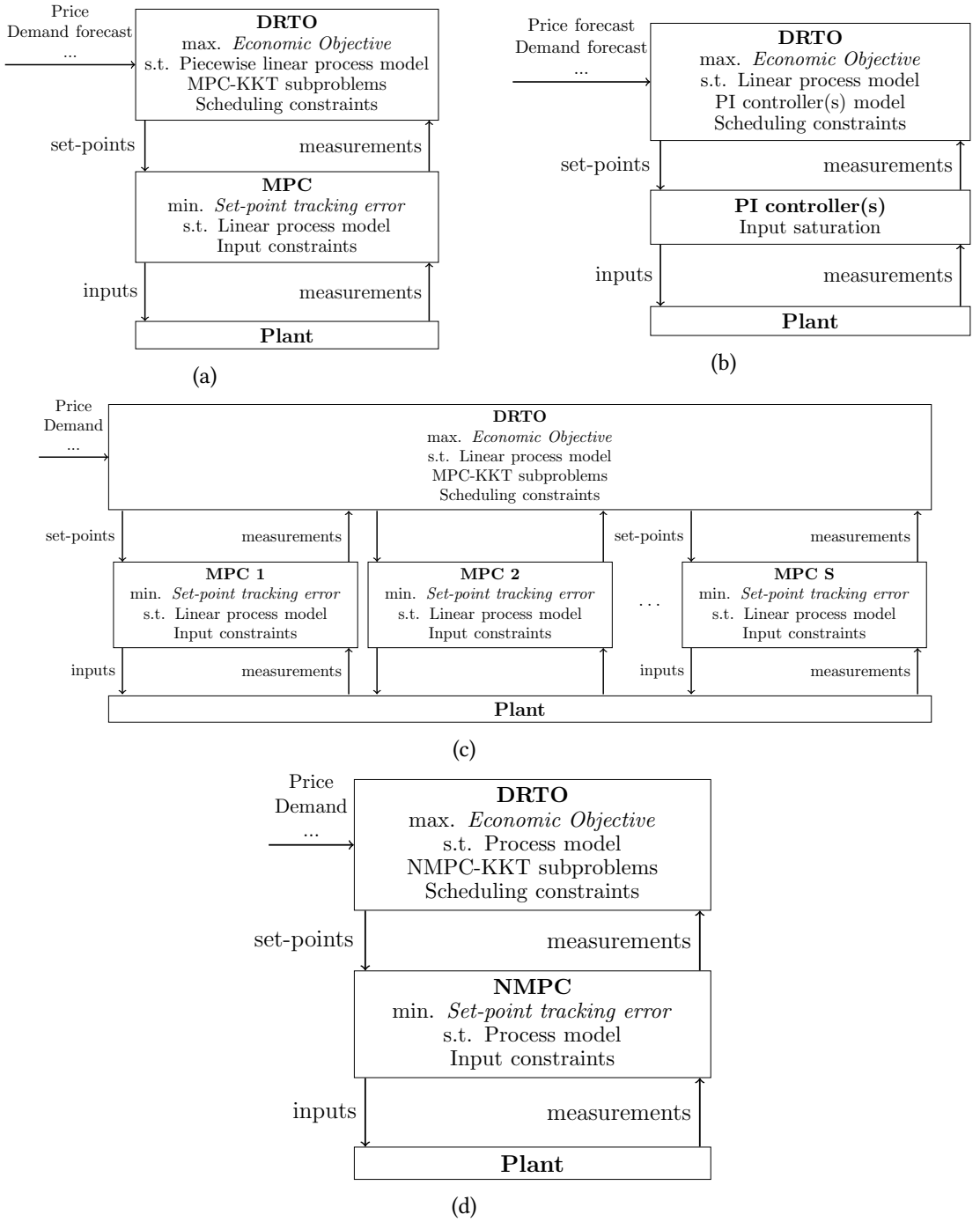

Figure 1.3. Schematic representation of the control-aware scheduling formulations developed in this study. The integrated scheduling and control problem is solved at the DRTO level to compute set-point trajectories to the lower-level control system. The DRTO and control layers receive feedback information from the plant in the form of measurements. In (a) and (b) we have a stochastic ISC formulation. In (c) and (d) a nominal ISC formulation is used.

1.2 Main contributions

This thesis addresses a number of research gaps in the field of the integration of scheduling and control. In particular, we propose robust control-aware formulations for multi-product processes controlled by linear MPC and PI controller, and develop nominal closed-loop formulations for multi-product processes controlled by distributed linear MPC and centralized nonlinear MPC. An schematic representation is presented in Fig. 1.3. In contrast to some earlier studies [15], the transition times are directly computed as part of the solution of the ISC problem, and an iterative solution approach is not required. The ISC problem is solved at the DRTO level and computes optimal set-point trajectories tracked by the lower-level control system. Production sequencing is communicated to the plant exclusively through the set-points trajectories.

The main contributions of this work are outlined bellow:

1. An integrated scheduling and control framework for processes operated under demand uncertainty. The framework accounts for an underlying linear model predictive control system and predicts the closed-loop process response. We use simulation studies to assess the benefits of the proposed robust ISC formulation compared to a nominal formulation where uncertainty is neglected.

2. A robust integrated scheduling and control framework for processes operated under multiple uncertainties including demand, cost, and model uncertainty. In particular, we consider the case where the underlying control system is formed by one or more PI controllers. Input saturation is rigorously handled in the ISC formulation. The efficacy of the framework in handling multiple uncertainties under conditions of plant-model mismatch is demonstrated. We also evaluate the benefits of the proposed robust ISC formulations compared to a nominal formulation where uncertainty is neglected.

3. An integrated scheduling and control formulation for processes controlled by distributed linear model predictive control systems. Knowledge of the control subsystems enables the ISC layer to coordinate the control subsystems exclusively through the

set-point trajectories. A number of strategies are proposed to reduce the computational burden and their efficacy demonstrated.

4. An integrated scheduling and control formulation for processes controlled by nonlinear model predictive control. Discrete scheduling decisions, including production sequencing, are formulated using complementarity conditions. The resulting problem is a mathematical program with complementarity constraints (MPCC) that is solved using an suitable approach. We use the first-order Karush-Kuhn-Tucker conditions of the NMPC problem to compute the input action in the integrated scheduling and control formulation. In all our cases studies, the KKT conditions provided a local optimum of the associated NMPC problem and the complementarity formulation effectively captured the discrete scheduling decisions.

1.3 Thesis outline

Each chapter of this thesis is dedicated to the development of one of the frameworks in Fig. 1.3.

In Chapter 2, we develop a closed-loop stochastic formulation for the integrated scheduling and control problem that accounts for demand uncertainty. Our formulation accounts for the feedback action of the underlying linear model predictive control system enabling prediction of the closed-loop process response. Discrete scheduling decisions, such as production sequencing, are captured using binaries. To obtain a mixed-integer linear programming problem, nonlinear process models are approximated using piecewise linear segments. Additionally, we explore the use of closed-loop approximations to reduce the computational burden. The performance of the framework is shown through cases studies, where the value of the stochastic solution is used to compare the efficacy of the robust formulation against a nominal formulation where uncertainty is neglected.

The formulation in Chapter 2 is extended in Chapter 3 to account for multiple uncertainty types, and instead of linear model predictive control, we consider processes controlled by

one or more PI controllers. PI input saturation is rigorously handled by the framework. We use the value of the stochastic solution to compare the performance of the stochastic formation against that of a nominal formulation where uncertainty is neglected under conditions of perfect model knowledge and plant-model mismatch. Additionally, we explore the performance impact of the solution frequency of the integrated scheduling and control problem.

In Chapter 4, we develop a *deterministic* integrated scheduling and control formulation for processes controlled by distributed linear model predictive control. Knowledge of the underlying control system enables the framework to coordinate the MPC subsystems. Such coordination is achieved purely through set-point trajectories assigned to each MPC subsystem. Through case studies, we explore the computational and economic performance of different closed-loop approximation strategies to reduce the solution time. We also consider implementation of the proposed framework under conditions of plant-model mismatch.

While in Chapters 2-4 we utilize a linear process model (approximation) within the integrated scheduling and control formulation, in Chapter 5 we consider a nonlinear process representation. Moreover, we focus on processes controlled by nonlinear model predictive control (NMPC). To avoid a mixed-integer nonlinear programming (MINLP) problem formulation, we use complementarity conditions to model discrete decisions yielding a mathematical program with complementarity constraints (MPCC). This MPCC problem is solved using a regularization method. In all our case studies, the Karush-Kuhn-Tucker conditions led to a local optimum of the associate NMPC problem, and the complementarity formulation effectively captured discrete scheduling decisions.

Finally, in Chapter 6 we present the conclusion of this thesis and future work directions.

References

[1] O. Andres-Martinez and L. A. Ricardez-Sandoval. “A switched system formulation for optimal integration of scheduling and control in multi-product continuous processes”. In: *Journal of Process Control* 106 (2021), pp. 94–109 (cit. on p. 5).

[2] O. Andrés-Martínez and L. A. Ricardez-Sandoval. “A nested online scheduling and nonlinear model predictive control framework for multi-product continuous systems”. In: *AIChE Journal* 68.5 (2022), e17665 (cit. on p. 5).

[3] M. Baldea, J. Du, J. Park, and I. Harjunkoski. “Integrated production scheduling and model predictive control of continuous processes”. In: *AIChE Journal* 61.12 (2015), pp. 4179–4190 (cit. on p. 7).

[4] M. Baldea and I. Harjunkoski. “Integrated production scheduling and process control: A systematic review”. In: *Computers & Chemical Engineering* 71 (2014), pp. 377–390 (cit. on pp. 2, 3).

[5] A. Bemporad, M. Morari, V. Dua, and E. N. Pistikopoulos. “The explicit linear quadratic regulator for constrained systems”. In: *Automatica* 38.1 (2002), pp. 3–20 (cit. on p. 7).

[6] B. Burnak, J. Katz, N. A. Diangelakis, and E. N. Pistikopoulos. “Simultaneous process scheduling and control: a multiparametric programming-based approach”. In: *Industrial & Engineering Chemistry Research* 57.11 (2018), pp. 3963–3976 (cit. on pp. 4, 7).

[7] A. Caspari, C. Tsay, A. Mhamdi, M. Baldea, and A. Mitsos. “The integration of scheduling and control: Top-down vs. bottom-up”. In: *Journal of Process Control* 91 (2020), pp. 50–62 (cit. on p. 3).

[8] Y. Chu and F. You. “Integration of production scheduling and dynamic optimization for multi-product CSTRs: Generalized Benders decomposition coupled with global mixed-integer fractional programming”. In: *Computers & Chemical Engineering* 58 (2013), pp. 315–333 (cit. on p. 6).

[9] Y. Chu and F. You. "Integration of scheduling and control with online closed-loop implementation: Fast computational strategy and large-scale global optimization algorithm". In: *Computers & Chemical Engineering* 47 (2012), pp. 248–268 (cit. on pp. 3, 7).

[10] M. L. Darby, M. Nikolaou, J. Jones, and D. Nicholson. "RTO: An overview and assessment of current practice". In: *Journal of Process Control* 21.6 (2011), pp. 874–884 (cit. on p. 2).

[11] D. Dering and C. L. E. Swartz. "A scenario-based framework for the integration of scheduling and control under multiple uncertainties". In: *Journal of Process Control* 129 (2023), p. 103055 (cit. on p. 3).

[12] L. S. Dias, R. C. Pattison, C. Tsay, M. Baldea, and M. G. Ierapetritou. "A simulation-based optimization framework for integrating scheduling and model predictive control, and its application to air separation units". In: *Computers & Chemical Engineering* 113 (2018), pp. 139–151 (cit. on pp. 4, 6).

[13] J. Du, J. Park, I. Harjunkoski, and M. Baldea. "A time scale-bridging approach for integrating production scheduling and process control". In: *Computers & Chemical Engineering* 79 (2015), pp. 59–69 (cit. on pp. 3, 4, 7).

[14] J. Flores-Cerrilo, C. L. E. Swartz, K. Ankur, and D. Dering. "Integration of Chemical Process Operation with Energy, Global Market, and Plant Systems Infrastructure". In: *Computers and Chemical Engineering* (2023). Under review (cit. on p. 3).

[15] A. Flores-Tlacuahuac and I. E. Grossmann. "Simultaneous cyclic scheduling and control of a multiproduct CSTR". In: *Industrial & Engineering Chemistry Research* 45.20 (2006), pp. 6698–6712 (cit. on pp. 4, 5, 9).

[16] M. Z. Jamaludin and C. L. E. Swartz. "Dynamic real-time optimization with closed-loop prediction". In: *AIChE Journal* 63.9 (2017), pp. 3896–3911 (cit. on pp. 2, 6).

[17] J. V. Kadam, M. Schlegel, W. Marquardt, R. L. Tousain, D. H. van Hessem, J. van den Berg, and O. H. Bosgra. "A Two-Level Strategy of Integrated Dynamic Optimization and Control of Industrial Processes - A Case Study". In: *European Symposium on*

Computer Aided Process Engineering-12. Ed. by J. Grievink and J. van Schijndel. Vol. 10. Computer Aided Chemical Engineering. Elsevier, 2002, pp. 511–516 (cit. on p. 2).

[18] M. T. Kelley, R. C. Pattison, R. Baldick, and M. Baldea. "An efficient MILP framework for integrating nonlinear process dynamics and control in optimal production scheduling calculations". In: *Computers & Chemical Engineering* 110 (2018), pp. 35–52 (cit. on p. 7).

[19] P. Mathur, C. L. E. Swartz, D. Zyngier, and F. Welt. "Uncertainty management via online scheduling for optimal short-term operation of cascaded hydropower systems". In: *Computers & Chemical Engineering* 134 (2020), p. 106677 (cit. on p. 5).

[20] R. D. McAllister, J. B. Rawlings, and C. T. Maravelias. "Rescheduling Penalties for Economic Model Predictive Control and Closed-Loop Scheduling". In: *Industrial & Engineering Chemistry Research* 59.6 (2019), pp. 2214–2228 (cit. on p. 3).

[21] R. C. Pattison, C. R. Touretzky, I. Harjunkoski, and M. Baldea. "Moving horizon closed-loop production scheduling using dynamic process models". In: *AIChE Journal* 63.2 (2017), pp. 639–651 (cit. on p. 4).

[22] R. C. Pattison, C. R. Touretzky, T. Johansson, I. Harjunkoski, and M. Baldea. "Optimal process operations in fast-changing electricity markets: framework for scheduling with low-order dynamic models and an air separation application". In: *Industrial & Engineering Chemistry Research* 55.16 (2016), pp. 4562–4584 (cit. on pp. 4, 7).

[23] S. J. Qin and T. A. Badgwell. "A survey of industrial model predictive control technology". In: *Control Engineering Practice* 11.7 (2003), pp. 733–764 (cit. on p. 2).

[24] J. E. Remigio and C. L. E. Swartz. "Production scheduling in dynamic real-time optimization with closed-loop prediction". In: *Journal of Process Control* 89 (2020), pp. 95–107 (cit. on pp. 3, 4, 6).

[25] M. J. Risbeck, C. T. Maravelias, J. B. Rawlings, and R. D. Turney. "A mixed-integer linear programming model for real-time cost optimization of building heating, ventilation, and air conditioning equipment". In: *Energy and Buildings* 142 (2017), pp. 220–235 (cit. on p. 5).

[26] M. J. Risbeck, C. T. Maravelias, J. B. Rawlings, and R. D. Turney. "Mixed-integer optimization methods for online scheduling in large-scale HVAC systems". In: *Optimization Letters* 14 (2020), pp. 889–924 (cit. on pp. 5, 6).

[27] J. M. Simkoff and M. Baldea. "Production scheduling and linear MPC: Complete integration via complementarity conditions". In: *Computers & Chemical Engineering* 125 (2019), pp. 287–305 (cit. on pp. 3, 4, 6).

[28] J. M. Simkoff and M. Baldea. "Stochastic scheduling and control using data-driven nonlinear dynamic models: application to demand response operation of a chlor-alkali plant". In: *Industrial & Engineering Chemistry Research* 59.21 (2020), pp. 10031–10042 (cit. on pp. 3–5).

[29] T. Tosukhowong, J. M. Lee, J. H. Lee, and J. Lu. "An introduction to a dynamic plant-wide optimization strategy for an integrated plant". In: *Comput. Chem. Eng.* 29.1 (2004), pp. 199–208 (cit. on p. 2).

[30] J. Zhuge and M. G. Ierapetritou. "An integrated framework for scheduling and control using fast model predictive control". In: *AIChE Journal* 61.10 (2015), pp. 3304–3319 (cit. on pp. 4, 5).

[31] J. Zhuge and M. G. Ierapetritou. "Integration of scheduling and control for batch processes using multi-parametric model predictive control". In: *AIChE Journal* 60.9 (2014), pp. 3169–3183 (cit. on pp. 4, 7).

[32] J. Zhuge and M. G. Ierapetritou. "Integration of scheduling and control with closed loop implementation". In: *Industrial & Engineering Chemistry Research* 51.25 (2012), pp. 8550–8565 (cit. on pp. 4, 5).

Chapter 2

A stochastic optimization framework for integrated scheduling and control under demand uncertainty

The study in this chapter has been published and presented in:

[1] D. Dering and C. L. Swartz. "A stochastic optimization framework for integrated scheduling and control under demand uncertainty". In: *Computers & Chemical Engineering* 165 (2022), p. 107931

[3] D. Dering and C. L. Swartz. "Integrated Scheduling and Control under Uncertain

Demand with Closed-Loop Dynamic Prediction". In: *2021 Virtual Canadian Chemical Engineering Conference (CCEC)*. Chemical Institute of Canada (CIC). 2021

2.1 Introduction

In this chapter, we present an integrated scheduling and control (ISC) formulation for explicit handling of demand uncertainty. We build on the work of Remigio and Swartz [17], but introduce a number of significant extensions, including the use of a piecewise affine formulation [12] for approximating a nonlinear dynamic process model to maintain the ISC problem an MILP. The ISC problem is formulated as a two-stage stochastic programming problem, whose solution (including the production sequence) is communicated to the plant via set-point trajectories provided to the plant MPC. The ISC scheme is applied in a moving horizon manner, incorporating feedback from the plant and storage units. To the authors' knowledge, there is only one recent study that tackles uncertainty in the ISC formulation. Simkoff and Baldea [19] propose an open-loop two-stage stochastic formulation for scheduling and control of a chlor-alkali plant where the random variables are the electricity cost and demand. Different from Simkoff and Baldea [19], the formulation presented in this study accounts for the closed-loop process response, and the ISC problem is solved online. We compare the performance of the deterministic and stochastic formulation for closed-loop operation of a linear and nonlinear process.

2.2 Formulation

This study considers processes where real-time optimization of the plant performance is achieved using a two–layer control architecture shown in Fig. 2.1.

In the upper layer, the closed-loop dynamic real–time optimization (CL–DRTO) problem is solved at an execution interval of Δt^{DRTO} to compute the set-point trajectories y_j^{SP} and u_j^{SP} ascribed to the lower–level model predictive control (MPC). The MPC computes the input values $u_j^{\mathrm{MPC}} \in \mathcal{R}^{n_u}$ applied directly to the plant or assigned as set-points to local PID controllers. Plant measurements $y_j^m \in \mathcal{R}^{n_y}$ and inventory values $I_j \in \mathcal{R}^{n_g}$ are provided as feedback to the CL-DRTO, and are taken into account when computing the optimal amount to be produced of each product, and the new set-point trajectories. If the current inventory

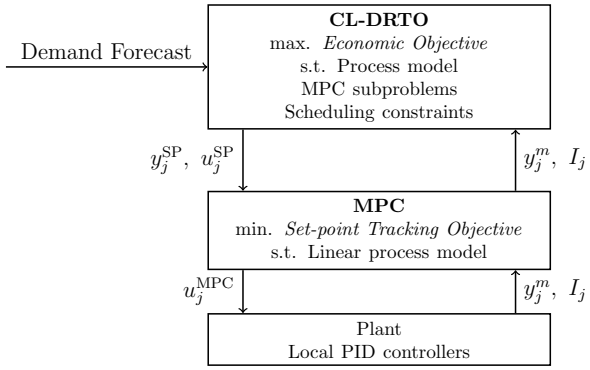

Figure 2.1. Two–layer control architecture.

level (or an estimation thereof) is not provided, the CL–DRTO will not be aware of the quantities of each product in stock, and is likely to give a suboptimal solution regarding the amount to be produced of each grade. The lower-level MPC is executed more frequently than the CL-DRTO, such that $\Delta t^{\text{DRTO}}/\Delta t^{\text{MPC}} \in \mathcal{Z}^+$.

The CL-DRTO formulation used in this study builds on that first proposed by Jamaludin and Swartz [11] for online economic optimization of plants with centralized model predictive control, and later extended to processes with distributed MPCs [13]. More recently, Remigio and Swartz [17] integrated scheduling within the CL-DRTO formulation, leading to an integrated scheduling and control problem. The DRTO is deemed closed-loop because it models the plant response under the action of the model predictive control (MPC). At every prediction time-step, an MPC subproblem is formulated to provide the control input value. The MPC subproblems have a similar formulation to the lower–level MPC controlling the plant. In this study, we extend the work of Remigio and Swartz [17] by proposing a CL-DRTO formulation that accounts for demand uncertainty directly within the DRTO optimization formulation through use of a two-stage stochastic programming approach. While the feedback inherent in the closed-loop DRTO implementation, shown in Fig. 2.1, provides a level of uncertainty mitigation, enhanced performance may be achieved by the proposed approach as demonstrated in the case studies. Similar improvement is shown in the robust real-time scheduling formulation of Mathur et al. [15] that utilizes both feedback and two-stage stochastic optimization, applied to a cascaded hydropower generation system.

The integrated scheduling and control problem solved at the CL-DRTO level computes

the optimal production sequence and production amounts, while taking into account the dynamics of the transitions between products, as well as the various constraints in effect. The optimal solution is communicated to the plant through set-point trajectories for the plant MPC to track. Thus, the plant MPC system remains intact, requiring no modification to accommodate either the production scheduling or the uncertainly handling capability of the overall decison-making scheme.

The CL-DRTO optimization problem may be conceptually partitioned into the following key components: (a) a process model that captures the dynamic behavior of the plant, (b) MPC subproblems, one correponding to each control interval along the DRTO prediction horizon, to determine inputs that are applied to the process model to generate the predicted closed-loop response of the plant under the action of constrained MPC, (c) scheduling constraints required for determination of the production sequence, production amounts, and inventory levels, and (d) operating and auxiliary constraints that include the mapping between set-point targets and the production sequence. The MPC subproblems are replaced by their equivalent first-order KKT conditions in which the complemetarity constraints are handled through a mixed-integer formulation. The nonlinear dynamic process model is approximated through a piecewise affine formulation. Two-stage stochastic optimization involves first-stage decisions that are made prior to the uncertainty realization, and second-stage or recourse decisions that are made in response to the uncertainty realization [2]. In the present study, the first-stage decisions comprise the amounts to be produced of each grade, while the second-stage variables correspond to the unmet demand, the demand met, and the inventory level upon realization of the demand. Furthermore, we assume that the demand is the main source of uncertainty, and consider orders not met at the designated nominal due time as lost sales. The integrated CL-DRTO problem ultimately takes the form of a MILP in which the expected profit over the DRTO prediction horizon is maximized. The detailed formulation is described in the following subsections.

2.2.1 CL-DRTO plant model and associated constraints

A discretized dynamic model is used to represent the plant in the CL-DRTO formulation,

$$x_{j+1}^{\mathrm{DRTO}} = f^{\mathrm{DRTO}}(x_j^{\mathrm{DRTO}}, u_j^{\mathrm{DRTO}}) \qquad \forall\, j \in \mathcal{J}_0^{N-1} \tag{2.1a}$$

$$y_j^{\mathrm{DRTO}} = h^{\mathrm{DRTO}}(x_j^{\mathrm{DRTO}}, y^{\mathrm{m}}) \qquad \forall\, j \in \mathcal{J}_1^{N} \tag{2.1b}$$

where $x_j^{\mathrm{DRTO}} \in \mathcal{R}^{n_x}$ is a vector of the state values at time-step j, $u_j^{\mathrm{DRTO}} \in \mathcal{R}^{n_u}$ is a vector of inputs, $y_j^{\mathrm{DRTO}} \in \mathcal{R}^{n_y}$ is the output vector, $y_j^{\mathrm{m}} \in \mathcal{R}^{n_y}$ is a vector of the most recent measurement of the outputs, and N is the DRTO or scheduling horizon. The relationship between the discrete time j and continuous time t is given by $t = j\Delta t^{\mathrm{MPC}}$. The functions $f^{\mathrm{DRTO}}(\cdot)$ and $h^{\mathrm{DRTO}}(\cdot)$ denote the discrete-time dynamic model used to compute the state and output values, respectively. To simplify the notation, $\mathcal{J}_a^b = \{j | a \leq j \leq b, j \in \mathcal{Z}_0^+\}$ is used to represent the time-steps between a and b. For instance, $\mathcal{J}_1^N = \{1, 2, \ldots, N\}$. We also define $\mathcal{Y} = \{1, \ldots, n_y\}$ and $\mathcal{U} = \{1, \ldots, n_u\}$, where n_y and n_u are the number of measured outputs and manipulated inputs respectively.

The optimization degrees of freedom are the reference trajectories [11]

$$y^{\mathrm{ref}} = \left[(y_1^{\mathrm{ref}})^T, \ldots, (y_{N+P-1}^{\mathrm{ref}})^T\right]^T,$$

$$u^{\mathrm{ref}} = \left[(u_0^{\mathrm{ref}})^T, \ldots, (u_{N+M-2}^{\mathrm{ref}})^T\right]^T$$

for the output and input variables, where $y_j^{\mathrm{ref}} \in \mathcal{R}^{n_y}$ and $u_j^{\mathrm{ref}} \in \mathcal{R}^{n_u}$ are the vectors of reference values at time-step j. P and M are the MPC output and input horizon, respectively. The reference trajectory is held at a constant value for $j > N$ [11]:

$$y_j^{\mathrm{ref}} = y_N^{\mathrm{ref}} \qquad j \in \mathcal{J}_{N+1}^{N+P-1}$$

$$u_j^{\mathrm{ref}} = u_{N-1}^{\mathrm{ref}} \qquad j \in \mathcal{J}_{N}^{N+M-2}$$

Bounds are imposed on the reference trajectories and outputs,

$$y_{\min}^{\mathrm{DRTO}} \leq y_j^{\mathrm{DRTO}} \leq y_{\max}^{\mathrm{DRTO}} \qquad \forall j \in \mathcal{J}_1^N \tag{2.2a}$$

$$y_{\min}^{\mathrm{ref}} \leq y_j^{\mathrm{ref}} \leq y_{\max}^{\mathrm{ref}} \qquad \forall j \in \mathcal{J}_1^N \tag{2.2b}$$

$$u_{\min}^{\mathrm{ref}} \leq u_j^{\mathrm{ref}} \leq u_{\max}^{\mathrm{ref}} \qquad \forall j \in \mathcal{J}_0^{N-1} \tag{2.2c}$$

while constraints on the input values are enforced in the MPC subproblems. The set-point trajectories

$$y_j^{\mathrm{SP}} = \left[(y_{j,1}^{\mathrm{SP}})^T, \ldots, (y_{j,P}^{\mathrm{SP}})^T\right]^T,$$
$$u_j^{\mathrm{SP}} = \left[(u_{j,0}^{\mathrm{SP}})^T, \ldots, (u_{j,M-1}^{\mathrm{SP}})^T\right]^T$$

can be obtained from the reference trajectory using different approaches, two of which are:

- Moving window [11, 13]:

$$y_{j,k}^{\mathrm{SP}} = y_{j+k}^{\mathrm{ref}} \qquad \forall\, k \in \mathcal{J}_1^P,\ j \in \mathcal{J}_0^{N-1} \tag{2.3a}$$

$$u_{j,k}^{\mathrm{SP}} = u_{j+k}^{\mathrm{ref}} \qquad \forall\, k \in \mathcal{J}_0^{M-1},\ j \in \mathcal{J}_0^{N-1} \tag{2.3b}$$

- Constant set-point [16]:

$$y_{j,k}^{\mathrm{SP}} = y_{j+1}^{\mathrm{ref}} \qquad \forall\, k \in \mathcal{J}_1^P,\ j \in \mathcal{J}_0^{N-1} \tag{2.4a}$$

$$u_{j,k}^{\mathrm{SP}} = u_j^{\mathrm{ref}} \qquad \forall\, k \in \mathcal{J}_0^{M-1},\ j \in \mathcal{J}_0^{N-1} \tag{2.4b}$$

where $y_{j,k}^{\mathrm{SP}} \in \mathcal{R}^{n_y}$ and $u_{j,k}^{\mathrm{SP}} \in \mathcal{R}^{n_u}$. A schematic representation of the first method is given in Fig. 2.2. Consider the MPC subproblem solved at time-step j. In the first method, the set-point trajectory is given by $y_j^{\mathrm{SP}} = \left[(y_{j+1}^{\mathrm{ref}})^T, \ldots, (y_{j+P}^{\mathrm{ref}})^T\right]^T$ and $u_j^{\mathrm{SP}} = \left[(u_j^{\mathrm{ref}})^T, \ldots, (u_{j+M-1}^{\mathrm{ref}})^T\right]^T$, while in the second method the set-point is constant, $y_j^{\mathrm{SP}} = \left[(y_{j+1}^{\mathrm{ref}})^T, \ldots, (y_{j+1}^{\mathrm{ref}})^T\right]^T$ and $u_j^{\mathrm{SP}} = \left[(u_j^{\mathrm{ref}})^T, \ldots, (u_j^{\mathrm{ref}})^T\right]^T$.

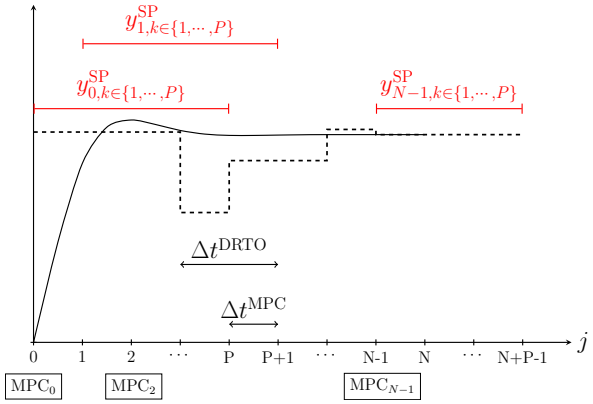

Figure 2.2. Schematic representation of the moving window set-point selection method. The solid black line is the output trajectory y^{DRTO}, and the dashed black line is the reference trajectory y^{ref}.

As in previous studies [9, 11, 17], we impose a set-point hold (SPH) constraint of the form:

$$\sum_{j=1}^{N} b^{\text{ref}}_{i,j} \leq N^{\text{ref}}_{i} \qquad \forall\, i \in \mathcal{Y} \tag{2.5a}$$

$$\sum_{h=0}^{H-1} b^{\text{ref}}_{i,j+h} \leq 1 \qquad \forall\, i \in \mathcal{Y},\ j \in \mathcal{J}_1^{N-H+1} \tag{2.5b}$$

$$b^{\text{ref}}_{i,1} = 1, \qquad \forall\, i \in \mathcal{Y} \tag{2.5c}$$

$$y^{\text{ref}}_{i,j+1} - y^{\text{ref}}_{i,j} \geq \left(y^{\text{ref}}_{\text{min},i} - y^{\text{ref}}_{\text{max},i}\right) b^{\text{ref}}_{i,j+1} \qquad \forall\, i \in \mathcal{Y},\ j \in \mathcal{J}_1^{N-1} \tag{2.5d}$$

$$y^{\text{ref}}_{i,j+1} - y^{\text{ref}}_{i,j} \leq \left(y^{\text{ref}}_{\text{max},i} - y^{\text{ref}}_{\text{min},i}\right) b^{\text{ref}}_{i,j+1} \qquad \forall\, i \in \mathcal{Y},\ j \in \mathcal{J}_1^{N-1} \tag{2.5e}$$

where $b^{\text{ref}}_{i,j}$ is a binary variable and N^{ref}_{i} is the maximum allowable number of changes in the reference trajectory for output i. From Eq. (2.5b) we have that $b^{\text{ref}}_{i,j}$ can equal one only once in every H time-steps, while the last two constraints prevent the reference trajectory from changing when $b^{\text{ref}}_{i,j}$ equals zero. For example, consider $H = 2$. If a reference trajectory change occurs at $j = 5$, then according to Eqs. (2.5d) and (2.5e), $b_{i,5} = 1$. Eq. (2.5b) ensures that the trajectory can only change again for $j \geq 7$. A similar set of constraints can be introduced for u^{ref}. Set-point hold constraints serve the purpose of regularizing the objective function when the optimal trajectory is not unique, or when the objective function surface at the optimum is quite flat - situations that are not uncommon in real-time economic optimization. Jamaludin et al. [9] showed that a set-point hold constraint on the reference trajectory considerably reduces the solution time and leads to less aggressive changes in

set-point, without significantly impacting the optimal objective value. The SPH formulation given in this study differs from previous works in the sense that it specifies the frequency rather than the exact time-steps where the reference trajectory can change.

If $f^{\mathrm{DRTO}}(\cdot)$ and $h^{\mathrm{DRTO}}(\cdot)$ are linear, it enables the final problem to be cast as a MILP and a global optimum to be found using state of the art MILP solvers (e.g. Gurobi, CPLEX). Otherwise, the final problem is a MINLP, a class of problems notoriously difficult and time-consuming to solve. A nonlinear model may be linearized to yield an approximate discrete-time linear model of the form,

$$x_{j+1}^{\mathrm{DRTO}} = Ax_j^{\mathrm{DRTO}} + Bu_j^{\mathrm{DRTO}} \qquad \forall\, j \in \mathcal{J}_0^{N-1} \tag{2.6a}$$

$$y_j^{\mathrm{DRTO}} = Cx_j^{\mathrm{DRTO}} + d_j^{\mathrm{DRTO}} \qquad \forall\, j \in \mathcal{J}_1^{N} \tag{2.6b}$$

where $A \in \mathcal{R}^{n_x \times n_x}$ and $B \in \mathcal{R}^{n_x \times n_u}$ are matrices obtained from the linearization of the nonlinear model, and $d_j^{\mathrm{DRTO}} \in \mathcal{R}^{n_y}$ is a disturbance estimate, determined here as

$$d_j^{\mathrm{DRTO}} = y^{\mathrm{m}} - Cx_0^{\mathrm{DRTO}}, \qquad \forall\, j \in \mathcal{J}_1^{N} \tag{2.7}$$

Because the linearized model may provide a poor representation of the plant, the profit may be significantly lower than if a more accurate model were used. Another challenge is choosing the point of linearization in multiproduct plants. Linearizing the model at the set-points for producing grade A, for example, may lead to good prediction capabilities concerning the production targets for grade A, but poor prediction for the other grades. An alternative strategy to have a more accurate model while keeping the problem a MILP is to approximate the nonlinear model using piecewise linear segments.

Piecewise affine approximation of a nonlinear model

A strategy to obtain a piecewise affine (PWA) approximation of nonlinear separable functions, proposed by Kvasnica et al. [12], is presented in this section. A function $f(v) : \mathcal{R}^{n_v} \to \mathcal{R}$ is deemed separable if it can be expressed as a linear combination of nonlinear univariate

terms, that is $f(v) = \sum_{j=1}^{n} b_j f_j(v_j)$ [12], where $f_j(v_j) : \mathcal{R} \rightarrow \mathcal{R}$. Obtaining a piecewise linear approximation for $f(v)$ consists of deriving a piecewise linear approximation for each univariate nonlinear function $f_j(v_j)$.

Consider the nonlinear function $f(v) : \mathcal{R} \rightarrow \mathcal{R}$ for $v \in [v_{\min}, v_{\max}]$. The domain can be partitioned to yield a set of grid points $v_0 < v_1 < \ldots < v_K$ where $v_0 = v_{\min}$ and $v_K = v_{\max}$. A linear approximation $\widetilde{f}(v) = a_i v + c_i$ of the nonlinear function $f(v)$ in the interval $[v_{i-1}, v_i]$ can then be developed, such that:

$$f(v) \approx \widetilde{f}(v) = \begin{cases} a_1 v + c_1, & \text{if} \quad v \in [v_0, v_1] \\ a_2 v + c_2, & \text{if} \quad v \in [v_1, v_2] \\ \quad \vdots & \\ a_K v + c_K, & \text{if} \quad v \in [v_{K-1}, v_K] \end{cases} \tag{2.8}$$

The optimal $a_i,\ c_i$ and and v_i values are obtained via minimization of the squared error between the true function and the piecewise linear approximation

$$\min_{a', c', v'} \quad \sum_{i=1}^{K} \int_{v_{i-1}}^{v_i} \left(f(v) - (a_i v + c_i)\right)^2 dv \tag{2.9a}$$

$$\text{subject to} \quad v_i \leq v_{i+1} \quad i \in \{1, \ldots, K-1\} \tag{2.9b}$$

$$v_0 = v_{\min},\ v_K = v_{\max} \tag{2.9c}$$

$$a_i v_i + c_i = a_{i+1} v_i + c_{i+1} \quad i \in \{1, \ldots, K-1\} \tag{2.9d}$$

where continuity at the breakpoints v_i is imposed by Eq. (2.9d), K is a parameter defining the number of piecewise segments, or regions, and a', c' and v' are vectors of the a_i, c_i and v_i, respectively. A schematic representation, and the approximation of the cubic function $f(v) = v^3$, $v \in [-3, 3]$ for $K = 5$ is shown in Fig. 2.3.

Once the coefficients and breakpoints values have been computed, the piecewise expression in Eq. (2.8) can be put into a form suitable for optimization by introducing a binary variable

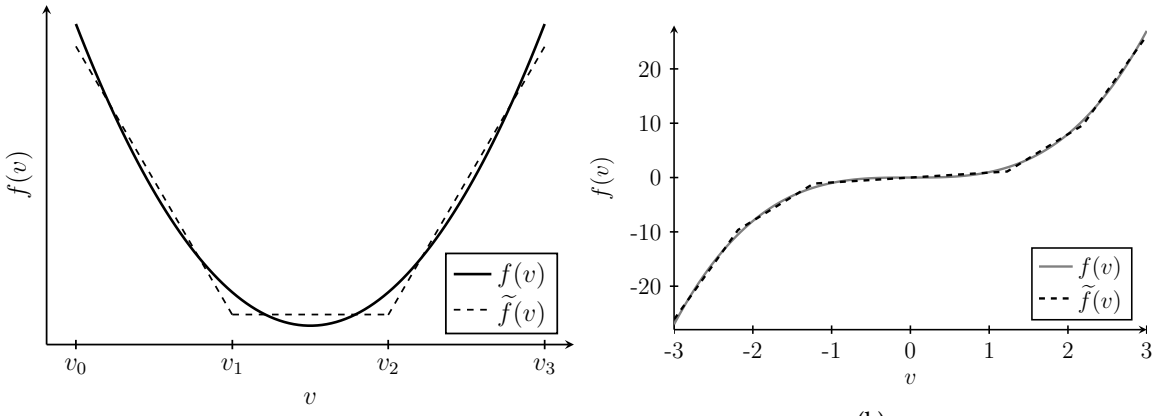

Figure 2.3. (a) Schematic representation of the approximation of a nonlinear function for $K = 3$, and (b) piecewise affine approximation of $f(v) = v^3$ for $K = 5$.

β_l for each interval $[v_l, v_{l+1}]$ and using Eqs. (2.10a)-(2.10c) to select the active region.

$$\sum_{l=1}^{K} \beta_l = 1 \tag{2.10a}$$

$$v \leq \sum_{l=1}^{K} \beta_l v_l - 2\theta \tag{2.10b}$$

$$v \geq \sum_{l=1}^{K} \beta_l v_{l-1} \tag{2.10c}$$

θ is a small number chosen to equal the solver tolerance. Eq. (2.10a) guarantees that one and only one β_l is different from zero, while Eqs. (2.10b) and (2.10c) impose that β_l can only be one if $v \in [v_{l-1}, v_l)$. An approximate value $\widetilde{f}(v) = \widetilde{y}$ for the nonlinear function $f(v)$ is then given by

$$f(v) \approx \widetilde{y} = \sum_{l=1}^{K} \widetilde{y}_l, \tag{2.11}$$

where $\widetilde{y}_l$ is computed via Eqs. (2.12a) to (2.12d):

$$\widetilde{y}_l - (a_l v + c_l) \leq -(1 - \beta_l) m_l, \qquad \forall\, l \in \{1, \ldots, K\} \tag{2.12a}$$

$$\widetilde{y}_l - (a_l v + c_l) \geq -(1 - \beta_l) M_l, \qquad \forall\, l \in \{1, \ldots, K\} \tag{2.12b}$$

$$\widetilde{y}_l \leq \beta_l M_l, \qquad \forall\, l \in \{1, \ldots, K\} \tag{2.12c}$$

$$\widetilde{y}_l \geq \beta_l m_l, \qquad \forall\, l \in \{1,\ldots,K\} \tag{2.12d}$$

m_l and M_l are appropriately chosen bounds. $\widetilde{y}_l$ equals $a_l v + c_l$ if the corresponding binary β_l is one (Eqs. (2.12a) and (2.12b)), and it is zero otherwise (Eqs. 2.12c and 2.12d).

While we do not quantify the loss in performance due to the use of the piecewise approximation *in lieu* of the original nonlinear model in the DRTO optimization problem, it is reasonable to assume that the more accurate the PWA approximation, the more closely we approximate the optimal solution of the DRTO problem with the original nonlinear model. The accuracy of the approximation can be improved by increasing the number of discrete segments K.

Extension to dynamic systems

Application of the above-described PWA method to obtain an approximate solution for the separable nonlinear ODE,

$$\frac{dx}{dt} = f(x,u) \tag{2.13}$$

where $f : \mathcal{R}^{n_x+n_u} \rightarrow \mathcal{R}$, in the time interval $[0, t_f]$ is straightforward. Because $f(x,u)$ is separable, we can define new variables $w_i \in \mathcal{R}$ such that $f(x,u) = \sum_{i=1}^{n} f_i(w_i)$ where $f_i(w_i) : \mathcal{R} \rightarrow \mathcal{R}$, and w_i is a function of x and u. For example, consider $f(x,u) = xu$, $x,u \in \mathcal{R}$. Defining $w_1 = x + u$ and $w_2 = x - u$ we can write $xu = 0.25(w_1^2 - w_2^2)$. A PWA approximation $\widetilde{y}_i = \sum_{l=1}^{K_i} \widetilde{y}_{i,l}$ (see Eq. (2.11)) for each $f_i(w_i)$ can then be obtained using the method presented in the previous section, such that:

$$\frac{dx}{dt} = \sum_{i=1}^{n} f_i(w_i) \approx \sum_{i=1}^{n} \widetilde{y}_i \tag{2.14}$$

Integration of the expression above can be carried out using an appropriate numerical method. For example, for $N = t_f / \Delta t$ where Δt is the integration time-step, the forward-Euler method

gives

$$x_{j+1} = x_j + \Delta t \sum_{i=1}^{n} \widetilde{y}_{j,i} \quad \forall\, j \in \mathcal{J}_0^{N-1} \tag{2.15}$$

where $\sum_{i=1}^{n} \widetilde{y}_{j,i}$ is the approximate value of the nonlinear function $f(x,u)$ at the point (x_j, u_j). For example:

$$f(x_j, u_j) \approx \sum_{i=1}^{n} \widetilde{y}_{j,i} = \sum_{i=1}^{n} \sum_{l=1}^{K_i} \widetilde{y}_{j,i,l}. \tag{2.16}$$

The time discretization increases the complexity of the PWA models by a factor of N. The reason is that a new set of binary variables (e.g. β_l) and equations needs to be introduced for each time-step j. Therefore, in a CL–DRTO application where N is considerably large, it may be convenient to use the more accurate PWA model for only part of the horizon and a linearized model for the remainder, that is

$$x_{j+1}^{\mathrm{DRTO}} = x_j^{\mathrm{DRTO}} + \Delta t \sum_{i=1}^{n} \widetilde{y}_{j,i}, \qquad \forall\, j \in \mathcal{J}_0^{N^{PWA}-1} \tag{2.17a}$$

$$x_{j+1}^{\mathrm{DRTO}} = A x_j^{\mathrm{DRTO}} + B u_j^{\mathrm{DRTO}}, \qquad \forall\, j \in \mathcal{J}_{N^{PWA}}^{N-1} \tag{2.17b}$$

where $N^{\mathrm{PWA}} < N$.

2.2.2 MPC subproblems

The MPC formulation used in this work corresponds to the quadratic dynamic matrix control (QDMC) formulation proposed in Garcia and Morshedi [6], but utilizes a state-space model formulation instead of a finite step response model, and takes the form

$$\min_{u_j^{\mathrm{MPC}}, x_j^{\mathrm{MPC}}, y_j^{\mathrm{MPC}}} \quad \Phi_j^{MPC} = \sum_{k=1}^{P} (y_{j,k}^{\mathrm{MPC}} - y_{j,k}^{\mathrm{SP}})^{\mathrm{T}} Q (y_{j,k}^{\mathrm{MPC}} - y_{j,k}^{\mathrm{SP}}) + \sum_{k=0}^{M-1} \Delta u_{j,k}^{\mathrm{T}} R \Delta u_{j,k} + (u_{j,k}^{\mathrm{MPC}} - u_{j,k}^{\mathrm{SP}})^{\mathrm{T}} S (u_{j,k}^{\mathrm{MPC}} - u_{j,k}^{\mathrm{SP}}) \tag{2.18a}$$

$$\text{subject to} \qquad x_{j,k+1}^{\mathrm{MPC}} = A x_{j,k}^{\mathrm{MPC}} + B u_{j,k}^{\mathrm{MPC}}, \qquad \forall\, k \in \mathcal{J}_0^{M-1} \tag{2.18b}$$

$$x^{\text{MPC}}_{j,k+1} = Ax^{\text{MPC}}_{j,k} + Bu^{\text{MPC}}_{j,M-1}, \qquad \forall\, k \in \mathcal{J}^{P-1}_{M} \tag{2.18c}$$

$$y^{\text{MPC}}_{j,k} = Cx^{\text{MPC}}_{j,k} + d^{\text{MPC}}_{j,k}, \qquad \forall\, k \in \mathcal{J}^{P}_{1} \tag{2.18d}$$

$$\Delta u_{j,k} = u^{\text{MPC}}_{j,k} - u^{\text{MPC}}_{j,k-1}, \qquad \forall\, k \in \mathcal{J}^{M-1}_{0} \tag{2.18e}$$

$$u^{\text{MPC}}_{\min} \leq u^{\text{MPC}}_{j,k} \leq u^{\text{MPC}}_{\max}, \qquad \forall\, k \in \mathcal{J}^{M-1}_{0} \tag{2.18f}$$

where

$$u^{\text{MPC}}_{j} = [(u^{\text{MPC}}_{j,0})^T, \ldots, (u^{\text{MPC}}_{j,M-1})^T]^{\text{T}},$$

$$x^{\text{MPC}}_{j} = [(x^{\text{MPC}}_{j,1})^T, \ldots, (u^{\text{MPC}}_{j,P})^T]^{\text{T}},$$

$$y^{\text{MPC}}_{j} = [(y^{\text{MPC}}_{j,1})^T, \ldots, (y^{\text{MPC}}_{j,P})^T]^{\text{T}}.$$

$Q \in \mathcal{R}^{n_y \times n_y}$, $R \in \mathcal{R}^{n_u \times n_u}$, $S \in \mathcal{R}^{n_u \times n_u}$ are diagonal weighting matrices, $u^{\text{MPC}}_{j,k} \in \mathcal{R}^{n_u}$, $x^{\text{MPC}}_{j,k} \in \mathcal{R}^{n_x}$, $y^{\text{MPC}}_{j,k} \in \mathcal{R}^{n_y}$ are, respectively, vectors of the input, state and output values for the j^{th} MPC subproblem at time-step k. The disturbance estimates $d^{\text{MPC}}_{j,k} \in \mathcal{R}^{n_y}$ are given by

$$d^{\text{MPC}}_{0,k} = y^m - Cx^{\text{MPC}}_{0,0}, \qquad k \in \mathcal{J}^{P}_{1} \tag{2.19a}$$

$$d^{\text{MPC}}_{j,k} = y^{\text{DRTO}}_{j} - Cx^{\text{MPC}}_{j-1,1}, \qquad k \in \mathcal{J}^{P}_{1},\ j \in \mathcal{J}^{N-1}_{1} \tag{2.19b}$$

The first embedded MPC subproblem uses the plant measurement in the disturbance estimate (Eq. (2.19a)), and subsequent MPC subproblems along the DRTO prediction horizon use the DRTO model output as a surrogate measurement (Eq. (2.19b)). The input value applied to the DRTO process model, u^{DRTO}_{j}, is extracted from u^{MPC}_{j} as

$$u^{\text{DRTO}}_{j} = u^{\text{MPC}}_{j,0} \quad j \in \mathcal{J}^{N-1}_{0} \tag{2.20}$$

Because problem (2.18) is convex, the first-order KKT conditions are necessary and sufficient for global optimality and are used in place of Eq. (2.18) in the DRTO formulation. More details can be found in Jamaludin and Swartz [11].

We consider in this work also an approximation strategy utilized in Jamaludin and Swartz [10], in which the input bound constraints, Eq. (2.18f), are removed, resulting on an unconstrained

QP which can be solved analytically, drastically reducing the solution of the DRTO problem with embedded MPC subproblems. A clipping mechanism is applied to ensure that the DRTO process model receives inputs that are within the original constraint bounds. In this case, u_j^{DRTO} is given by Eq. (2.21) rather than Eq. (2.20):

$$u_j^{\text{DRTO}} = \begin{cases} u_{\max}^{\text{MPC}}, & u_{j,0}^{\text{MPC}} \geq u_{\max}^{\text{MPC}} \\ u_{j,0}^{\text{MPC}}, & u_{\min}^{\text{MPC}} \leq u_{j,0}^{\text{MPC}} \leq u_{\max}^{\text{MPC}} \\ u_{\min}^{\text{MPC}}, & u_{j,0}^{\text{MPC}} \leq u_{\min}^{\text{MPC}} \end{cases} \tag{2.21}$$

The above construct can be captured using slack and binary variables as

$$u_j^{\text{DRTO}} = u_{j,0}^{\text{MPC}} - \mu_j^1 + \mu_j^2 \tag{2.22a}$$
$$u_j^{\text{DRTO}} = u_{\max}^{\text{MPC}} - s_j^1 \tag{2.22b}$$
$$u_j^{\text{DRTO}} = u_{\min}^{\text{MPC}} + s_j^2 \tag{2.22c}$$
$$0 \leq \mu_j^1 \leq (1 - \nu_j^1)M \tag{2.22d}$$
$$0 \leq \mu_j^2 \leq (1 - \nu_j^2)M \tag{2.22e}$$
$$0 \leq s_j^1 \leq \nu_j^1 M \tag{2.22f}$$
$$0 \leq s_j^2 \leq \nu_j^2 M \tag{2.22g}$$

where ν_j^i is a binary variable, M is a sufficiently large positive constant and $s_j^i \in \mathcal{R}^{n_u}$ and $\mu_j^i \in \mathcal{R}^{n_u}$ are slack variables. Note that s_j^1 and s_j^2 can not be simultaneously zero. If $\mu_j^1 > 0$, follows from Eq. (2.22d) that $\nu_j^1 = 0$ and from Eq. (2.22f) that $s_j^1 = 0$. Thus, by Eq. (2.22b) we have that $u_j^{\text{DRTO}} = u_{\max}^{\text{MPC}}$. This corresponds to the first case in Eq. (2.21) and the other ones can be obtained via similar analysis. A similar construct using complementarity conditions instead of binaries can be found in Li and Swartz [13].

A comparison of CL–DRTO implementations using the rigorous constrained MPC formulation (Eq. (2.18)) against the input-clipping formulation (unconstrained MPC subproblems and Eq. (2.22)) can be found in Jamaludin and Swartz [10] and Li and Swartz [13]. The solution given by both formulations match exactly when the optimal solution u_j^{MPC} of problem (2.18)

is strictly within the lower and upper bounds defined in Eq. (2.18f).

2.2.3 Scheduling constraints

The scheduling formulation presented in this section is used to compute the inventory levels of each grade, the optimal production sequencing, to identify whether or not the output is within the desired quality specifications, and to constrain the values taken by the optimization decision variables when some criteria, defined *a priori*, are met. Not only the process dynamics but also the control dynamics are accounted for in the solution of the scheduling problem since the CL–DRTO process model reflects the plant response under the MPC control action. This construct leads to a more accurate representation of the process transitions. The optimal production sequence is communicated to the plant via set-point trajectories given to the lower MPC, which retains the standard MPC formulation.

The second–stage decision variables and non-anticipativity constraints are directly linked to the scheduling constraints. Consider the inventory level I_g of grade g, and that there is a probability ρ_s that the demand of grade g at time-step t_g^D in scenario s is ξ_{s,g,t_g^D}. The amount to be produced of grade g has to be decided before the demand realization at time-step t_g^D. That is, before the demand realization, the inventory level of grade g is the same across all scenarios. After time t_g^D, the inventory level is dependent on the demand realization. Moreover, the inventory amount may or may not be enough to satisfy the demand in a given scenario. To account for this, two additional variables $D_{s,g,j}$ and $B_{s,g,j}$ for the met and unmet demand amount of grade g at time-step j, respectively, are introduced for each scenario s. $B_{s,g,j}$ is zero if the inventory at time-step j is sufficient to completely meet the demand $\xi_{s,g,j}$ in scenario s, which means that $D_{s,g,j} = \xi_{s,g,j}$. Therefore, $D_{s,g,j}$ and $B_{s,g,j}$ are second-stage decisions and $\xi_{g,j} = \{\xi_{s,g,j} | s \in \mathcal{S}\}$ is the random variable for the demand of grade g at time-step j. We use $\mathcal{G}$ and $\mathcal{S}$, respectively, to represent the discrete set of grades and scenarios, respectively.

Discrete scheduling decisions, such as choosing which grade to produce and determining whether or not the output meets the quality specifications, are formulated using binary

variables [17]. Alternatively, these discrete decisions could also be formulated using complementarity conditions [18].

The inventory model is given by

$$I_{s,g,j} = I_{s,g,j-1} + m_{g,j} - D_{s,g,j}, \qquad \forall\, s \in \mathcal{S},\ g \in \mathcal{G},\ j \in \mathcal{J}_1^N \tag{2.23a}$$

$$D_{s,g,j} + B_{s,g,j} = \xi_{s,g,j}, \qquad \forall\, s \in \mathcal{S},\ g \in \mathcal{G},\ j \in \mathcal{J}_1^N \tag{2.23b}$$

$$I_{s,g,j},\ D_{s,g,j},\ B_{s,g,j} \geq 0, \qquad \forall\, s \in \mathcal{S},\ g \in \mathcal{G},\ j \in \mathcal{J}_1^N \tag{2.23c}$$

where $I_{s,g,j}$ represents the amount of grade g in inventory at time step j in scenario s, $D_{s,g,j}$ is the demand met, $B_{s,g,j}$ is the unmet demand amount, and $\xi_{s,g,j}$ is the discrete random variable for the demand level. $m_{g,j}$ is the amount of grade g produced at time–step j. We have that $I_{s,g,0} = I_{g,0}$ for all $s \in \mathcal{S}$, where $I_{g,0}$ is the current or estimated inventory of grade g provided as feedback information to the DRTO. Note that $m_{g,j}$ is a first-stage decision variable since the amount to be produced has to be decided before realization of the demand uncertainty. Since there is no upper bound on the value of $B_{s,g,j}$, and $\xi_{s,g,j}$ is always positive, the constraints above are always satisfied. Nevertheless, we note that having an end-point constraint $I_{s,g,N} > 0$ can potentially lead to higher profit over multiple scheduling executions by indirectly accounting for future information that is not within the DRTO horizon N [7].

The binary variable $\gamma_{g,j}$ and Eq. (2.24a) are used to select the output target, where $y_{g,i}^{targs}$ is the desired value of quality i in grade g. Eq. (2.24b) ensures that only one grade can be targeted for production at any time-step j.

$$y_{i,j}^{target} = \sum_{g \in \mathcal{G}} y_{g,i}^{targs} \gamma_{g,j}, \qquad \forall\, i \in \mathcal{Y},\ \mathcal{J}_1^N \tag{2.24a}$$

$$\sum_{g \in \mathcal{G}} \gamma_{g,j} = 1, \qquad \forall\, j \in \mathcal{J}_1^N \tag{2.24b}$$

The product is deemed acceptable if all the outputs are within $\pm\epsilon_{g,i}$ of the target value $y_{g,i}^{targs}$, with the quality target band accordingly given by $y_{g,i}^{targs} \pm \epsilon_{g,i}$. We introduce an auxiliary binary variable $b_{l,g,i,j}$ to track if the ith component of the output vector y_j^{DRTO} is below ($l = 1$), within ($l = 2$) or above ($l = 3$) the respective quality target band. This is achieved

through two sets of equations, the first of which is

$$y_{i,j}^{\text{DRTO}} \leq \sum_{g\in\mathcal{G}} b_{1,g,i,j}\left(y_{g,i}^{targs} - \delta_{g,i}\epsilon_{g,i}\right) + \sum_{g\in\mathcal{G}} b_{2,g,i,j}\left(y_{g,i}^{targs} + \delta_{g,i}\epsilon_{g,i}\right) + \sum_{g\in\mathcal{G}} b_{3,g,i,j} y_{i,\max}^{\text{DRTO}}, \quad \forall\, i \in \mathcal{Y},\ j \in \mathcal{J}_1^N \tag{2.25a}$$

$$y_{i,j}^{\text{DRTO}} \geq \sum_{g\in\mathcal{G}} b_{1,g,i,j} y_{i,\min}^{\text{DRTO}} + \sum_{g\in\mathcal{G}} b_{2,g,i,j}\left(y_{g,i}^{targs} - \delta_{g,i}\epsilon_{g,i}\right) + \sum_{g\in\mathcal{G}} b_{3,g,i,j}\left(y_{g,i}^{targs} + \delta_{g,i}\epsilon_{g,i}\right), \quad \forall\, i \in \mathcal{Y},\ j \in \mathcal{J}_1^N \tag{2.25b}$$

where $y_{i,\min}^{\text{DRTO}}$ and $y_{i,\max}^{\text{DRTO}}$ are, respectively, the lower and upper bounds on the output variable $y_{i,j}^{\text{DRTO}}$ (Eq. (2.2)), and $\delta_{g,i} \in [0,1]$ is a parameter used to define a backoff amount from the boundaries of the quality target band. The idea of the backoff is to drive the predicted output value to the interior of the quality target band. That way, even in the presence of plant-model mismatch, the output at the plant level may still meet the actual quality specifications. A schematic representation of the target quality band, and backoff implementation, is given in Fig. 2.4a, while Fig. 2.4b indicates the value assumed by the binary variable $b_{l,g,i,j}$, depending on whether the output is within, below and above the target quality band for a given grade.

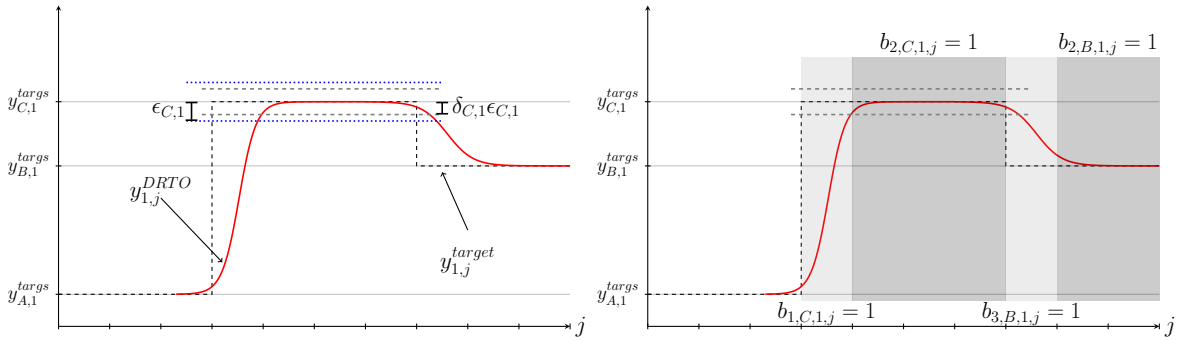

(a) (b)

Figure 2.4. Schematic representation of scheduling constraints in Eqs. (2.24)– (2.26): (a) quality target band and backoff, (b) tracking whether or not the output is within, below or above the quality target band.

Additional constraints are required to make sure that only the binaries $b_{l,g,i,j}$ associated with the grade g targeted for production can assume a nonzero value (Eq. (2.26a)), and that only

one binary $b_{l,g,i,j}$ can equal one for each output i and time-step j (Eq. (2.26b)).

$$\sum_{l=1}^{3} b_{l,g,i,j} \leq \gamma_{g,j} \qquad \forall\, g \in \mathcal{G},\ i \in \mathcal{Y},\ j \in \mathcal{J}_1^N \tag{2.26a}$$

$$\sum_{l=1}^{3} \sum_{g \in \mathcal{G}} b_{l,g,i,j} = 1 \qquad \forall\, i \in \mathcal{Y},\ j \in \mathcal{J}_1^N \tag{2.26b}$$

From Eqs. (2.25) and (2.26), we have that if grade g has been targeted ($\gamma_{g,j} = 1$) and $y_{i,j}^{\text{DRTO}}$ is within the respective quality target band, then and only then $b_{2,g,i,j} = 1$; otherwise, if grade g has been targeted but $b_{1,g,i,j} = 1$, then $y_{i,j}^{\text{DRTO}}$ is below the quality target band, and if $b_{3,g,i,j} = 1$, the output is above the quality target band. If grade g has not been targeted, the corresponding $b_{l,g,i,j}$ terms are zero via Eq. (2.26a).

The product can be sent to inventory only if all outputs simultaneously meet the quality specifications of the targeted grade. This is captured using a binary variable $z_{g,j}$.

$$z_{g,j} \leq \gamma_{g,j}, \qquad \forall\, g \in \mathcal{G},\ j \in \mathcal{J}_1^N \tag{2.27a}$$

$$\sum_{i \in \mathcal{Y}} b_{2,g,i,j} \geq z_{g,j} n_y, \qquad \forall\, g \in \mathcal{G},\ j \in \mathcal{J}_1^N \tag{2.27b}$$

Eq. (2.27a) ensures $z_{g,j}$ equals zero if grade g has not been targeted for production at time-step j ($\gamma_{g,j} = 0$), while Eq. (2.27b) allows $z_{g,j}$ to equal one only if all outputs are within the quality target band for grade g at step j. Note that $z_{g,j}$ can also equal zero when all the outputs are within the targeted specifications since this does not violate the constraints in Eq. (2.27). Therefore, three potential situations arise:

1. $z_{g,j} = 1$. The product is within the quality specifications and being stored;
2. $z_{g,j} = 0$. The product is within the quality specifications but not being stored;
3. $z_{g,j} = 0$. The product is not within the quality specifications and not being stored;

Item number 2 corresponds to a situation where the DRTO deems storing viable product as suboptimal. From a mathematical standpoint this could happen, for example, to reduce

inventory cost. Therefore, it is possible to avoid the situation in item 2 via appropriate formulation of the objective function. Accounting for the raw material cost, for instance, will prevent the DRTO from wasting resources producing something that will not be stored. Another option is to impose an additional constraint to force $z_{g,j}$ to equal one any time all outputs are within the quality target band:

$$\sum_{i \in \mathcal{Y}} b_{2,g,i,j} \leq n_y - (1 - z_{g,j}) \quad \forall\, g \in \mathcal{G},\ j \in \mathcal{J}_1^N \tag{2.28}$$

For this study, we choose the first avenue since imposing Eq. (2.28) has its own drawbacks. In oscillatory systems, for instance, one may wish to only start storing the product once the oscillation is reduced to an acceptable level. In this situation, Eq. (2.28), as it stands, is inadequate and additional constraints and variables may be required to achieve the desired behavior.

A parameter N_g^{target} is introduced to define the maximum number of times a given grade can be produced and simultaneously sent to storage. An auxiliary binary variable $\tilde{\gamma}_{g,j}$ is used to track when the binary variables for target selection $\gamma_{g,j}$ and for storing the output $z_{g,j}$ change from 1 to 0 in the DRTO scheduling horizon. The objective is to prevent excessive target changes.

$$\sum_{j \in \mathcal{J}_1^N} \tilde{\gamma}_{g,j} \leq N_g^{target} - z_{g,N}, \qquad \forall\, g \in \mathcal{G} \tag{2.29a}$$

$$z_{g,j} - z_{g,j-1} \geq -\tilde{\gamma}_{g,j}, \qquad \forall\, g \in \mathcal{G},\ j \in \mathcal{J}_2^N \tag{2.29b}$$

$$\gamma_{g,j} - \gamma_{g,j-1} \geq -\tilde{\gamma}_{g,j}, \qquad \forall\, g \in \mathcal{G},\ j \in \mathcal{J}_2^N \tag{2.29c}$$

$$\gamma_{g,j} \leq 1 - \tilde{\gamma}_{g,j}, \qquad \forall\, g \in \mathcal{G},\ j \in \mathcal{J}_1^N \tag{2.29d}$$

From Eqs. (2.29b) and (2.29c), storage and target selection can change status from active to inactive at step j for product g only if $\tilde{\gamma}_{g,j} = 1$. Eq. (2.29d) links the auxiliary binary variable to the target selection status, and Eq. (2.29a) limits the number of times the active to inactive status change can occur. In order to prevent the DRTO from starting storage of grade g after it has stopped for the N_g^{target}th time, and remaining in the active storage state until the end

of the horizon, we subtract $z_{g,N}$ from the right hand side of Eq. (2.29a).

Another construct that may be useful is to ensure that once storage commences, it has to continue for at least a specified minimum number of consecutive time periods. For $N_g^{target} = 1$, Eq. (2.30) can be used to ensure that once $z_{g,j}$ equals one, meaning the product is being stored, it is one for at least L consecutive time-steps.

$$\sum_{n \in \mathcal{J}_1^N} z_{g,n} \geq L z_{g,j} \quad \forall\, g \in \mathcal{G},\ j \in \mathcal{J}_1^N \tag{2.30}$$

An alternative formulation, valid for any N_g^{target} is:

$$\sum_{i=1}^{L} z_{g,j-i} \geq L \widetilde{\gamma}_{g,j} \quad \forall\, g \in \mathcal{G},\ j \in \mathcal{J}_{L+1}^N \tag{2.31}$$

Consider $L = 2$; if $\widetilde{\gamma}_{g,3} = 1$ then the constraint above is only satisfied if $z_{g,2} + z_{g,1} = 2$.

The amount $m_{g,j}$ produced and stored of each grade at every time-step is given by

$$m_{g,j} \geq z_{g,j} M_{\min}, \qquad \forall\, g \in \mathcal{G},\ j \in \mathcal{J}_1^N \tag{2.32a}$$

$$m_{g,j} \leq z_{g,j} M_{\max}, \qquad \forall\, g \in \mathcal{G},\ j \in \mathcal{J}_1^N \tag{2.32b}$$

$$m_{g,j} - f^m\left(x_j, u_{j-1}\right) \leq -(1 - z_{g,j}) M_{\min}, \qquad \forall\, g \in \mathcal{G},\ j \in \mathcal{J}_1^N \tag{2.32c}$$

$$m_{g,j} - f^m\left(x_j, u_{j-1}\right) \geq -(1 - z_{g,j}) M_{\max}, \qquad \forall\, g \in \mathcal{G},\ j \in \mathcal{J}_1^N \tag{2.32d}$$

where $M_{\min}$ and $M_{\max}$ are sufficiently large constants, that could be taken as the minimum and maximum value, respectively, of the function $f^m(\cdot)$ in the domain of x_j and u_j. $m_{g,j}$ is zero if $z_{g,j} = 0$, otherwise the two first inequalities are inactive, and $m_{g,j}$ equals the amount being produced of grade g. In order for the overall problem to take the form of a MILP rather than MINLP, we consider the amount produced to be a linear function $f^m(\cdot)$ of the state and input values.

The reference trajectory is constrained to be within the quality target band if $z_{g,j} = 1$

$$y_{i,j}^{\text{ref}} \geq \sum_{g \in G} z_{g,j} \left(y_{g,i}^{targs} - \delta_{g,i}^{\text{ref}} \epsilon_{g,i} \right) + \left(1 - \sum_{g \in \mathcal{G}} z_{g,j} \right) y_{i,\min}^{\text{ref}} \qquad \forall\, i \in \mathcal{Y},\ j \in \mathcal{J}_1^N \tag{2.33a}$$

$$y_{i,j}^{\text{ref}} \leq \sum_{g \in G} z_{g,j} \left(y_{g,i}^{targs} + \delta_{g,i}^{\text{ref}} \epsilon_{g,i} \right) + \left(1 - \sum_{g \in \mathcal{G}} z_{g,j} \right) y_{i,\max}^{\text{ref}} \qquad \forall\, i \in \mathcal{Y},\ j \in \mathcal{J}_1^N \tag{2.33b}$$

where $y_{i,\min}^{\text{ref}}$ and $y_{i,\max}^{\text{ref}}$ are the lower and upper bounds on $y_{i,j}^{\text{ref}}$, and $\delta^{\text{ref}} \in [0,1]$ defines a backoff amount.

While the lower-level MPC tracks the optimal set-point trajectory, additional decisions such as when to start and stop storing a product, or how much to store, are more intrinsically related to the scheduling part of the CL-DRTO. Deciding how the scheduling decisions of the CL-DRTO are going to be implemented at the plant level is not trivial, and should particularly take into account the level of plant-model mismatch and the frequency of execution of the CL-DRTO. For this study, a product is only sent to inventory at the plant level if it is within the quality specifications and the variable $z_{g,j}$ at the corresponding time-step at the DRTO level is one.

2.2.4 Objective function

In scheduling problems, the objective function formulation is determined by the production goal at a given moment, and need not to be static [8]. For this study, the chosen objective function is to maximize the profit computed as:

$$\Phi = -\sum_{i \in \mathcal{U}} \sum_{j \in \mathcal{J}_0^{N-1}} C_i^U u_{i,j} + \sum_{s \in \mathcal{S}} \sum_{g \in \mathcal{G}} \sum_{j \in \mathcal{J}_1^N} \rho_s \left(C_g^G D_{s,g,j} - C_g^I I_{s,g,j-1} \Delta t^{MPC} - C_g^B B_{s,g,j} \right) \tag{2.34}$$

where C_g^G is the value of grade g, C_g^I is the inventory cost, C_g^B is the cost incurred for not meeting the demand, C_i^U is the cost of input i, $u_{i,j}$ is the value of input i at time-step j. In this formulation, revenue comes from satisfying the demand. If not enough is produced to

satisfy the demand in a given scenario, there is a penalty cost $C_g^B B_{s,g,j}$. There is no incentive to accumulate inventory, and unless lower bounds are imposed, complete depletion of the inventory is possible. On the other hand, the stochastic nature of the problem may prevent complete inventory depletion to some extent. Since the inventory level is determined through maximization of the expected profit over a number of scenarios, it is likely that there will be some inventory remaining.

2.2.5 Scenario generation

The demand for each product grade is assumed to follow a continuous probability distribution that is approximated via discrete scenarios. Fig. 2.5 shows how a normal distribution could be discretized yielding low (L), medium (M) and high (H) demand scenarios. The shaded area under the curve gives the probabilities a, b, and c of each demand level [20].

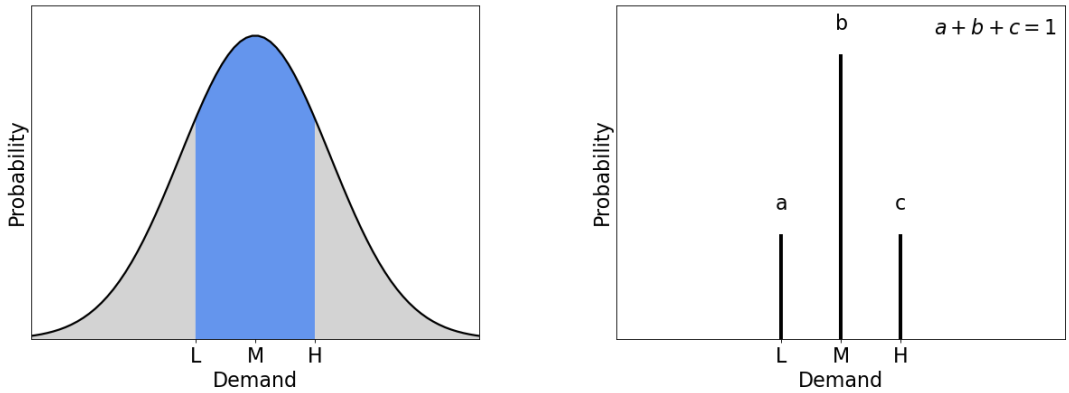

Figure 2.5. (a) Normal distribution and (b) discrete approximation.

Since the demand of each grade is assumed to be independent, we consider the different combinations of the demand levels for each grade to generate scenarios. An example is given in Table 2.1 for when there is one order of A and B each in the scheduling horizon. The expected value of the demand of grade g is computed as $a_g L + b_g M + c_g H$.

Table 2.1. Scenario generation.

Scenario	Demand A	Demand B	Probability
1	L	L	$a_A \times a_B$
2	L	M	$a_A \times b_B$
3	L	H	$a_A \times c_B$
4	M	L	$b_A \times a_B$
5	M	M	$b_A \times b_B$
6	M	H	$b_A \times c_B$
7	H	L	$c_A \times a_B$
8	H	M	$c_A \times b_B$
9	H	H	$c_A \times c_B$
		Sum	1.0

2.2.6 Value of stochastic solution

The value of the stochastic solution (VSS) is evaluated in terms of the profit of the plant at the end of the simulation horizon t_f:

$$VSS = P^{SP} - P^{EVP} \tag{2.35a}$$

$$P^{EVP} = \sum_{s \in \mathcal{S}^r} \rho_s \Phi^{plant} \left(x_{t0}, y^{\text{ref}}(\bar{\xi}), u^{\text{ref}}(\bar{\xi}), \xi_s, t_f \right) \tag{2.35b}$$

$$P^{SP} = \sum_{s \in \mathcal{S}^r} \rho_s \Phi^{plant}(x_{t0}, y^{\text{ref}}(\xi), u^{\text{ref}}(\xi), \xi_s, t_f) \tag{2.35c}$$

The profit of the plant is a function of the state of the system x_{t0} at time t_0 (e.g. inventory level, plant state, previous control action), the reference trajectories computed by the CL–DRTO, the simulation horizon and the actual demand realization ξ_s. $\bar{\xi}$ is the expected value of the demand, and P^{SP} and P^{EVP} denote the profit expectation of the plant when using the reference trajectories computed by solving the stochastic problem (SP) and expected value problem (EVP), respectively, in the CL–DRTO. We write $y^{\text{ref}}(\xi)$ and $u^{\text{ref}}(\xi)$ to emphasize the dependence of the reference trajectory on the random variable rather than meaning that the reference trajectory is only a function of the demand level. The expected value and stochastic problems differ in the CL–DRTO formulation in the number of scenarios. Because the demand in the EVP is assumed to equal its expected value, the expected value problem is deterministic and contains only one scenario. We compute the profit of the plant Φ^{plant} for

the realization of the scenarios in the set $\mathcal{S}^r$ when the EVP and SP problem is solved in the CL-DRTO.

Since the DRTO horizon does not in general coincide with the simulation horizon due to possibly different horizon lengths, coupled with the fact that the DRTO horizon shifts with time, the set of demand scenarios encountered by the DRTO typically differs from that at the plant level over the simulation horizon. The latter set can become quite large as the simulation horizon grows, prohibiting the entire set of scenarios from being included in the VSS calculation. Denoting $\mathcal{S}^p$ as all potential scenarios for the demand realization at the plant level for the entire simulation horizon, for this study we only compute the plant profit for a subset $\mathcal{S}^r \subset \mathcal{S}^p$. The scenarios in $\mathcal{S}^r$ are constructed by randomly sampling from the set of discrete demand levels. Since the probability of realization of a given demand level is accounted for during sampling, all scenarios are equally weighted in Eq. (2.35). While this approach is not entirely rigorous, it provides a tractable way of computing the VSS as defined in Eq. (2.35).

2.3 Case studies

In this section, we compare the performance of the two–stage stochastic and deterministic CL–DRTO formulations for closed-loop scheduling and control of both a linear and a nonlinear dynamic process. In the first case study, we consider both a perfect model and the effect of plant-model mismatch. Results regarding the operation of a nonlinear process when a PWA and a linear model are used to approximate the nonlinear model in the CL–DRTO are presented in the second case study.

Each case study involves the production of a number of product grades. The demand amounts and times at which they are required are given; however, the demand levels are uncertain and assumed here to follow a normal distribution. The production sequence and target amounts of each product grade are determined through periodic solution of the proposed DRTO scheme, which takes into account the demand, the demand uncertainty, and the dynamics of the plant under the action of its associated MPC system. The optimal DRTO decisions are

communicated to the plant MPC through computed set-point trajectories.

For all case studies: (i) the number of consecutive steps L in Eq. (2.30) is set to two, (ii) the objective function is given by Eq. (2.34), (iii) Eq. (2.4) is used for set-point selection. Remaining parameter values such as the values used for the cost coefficients for the objective function (Eq. (2.34)), and the scheduling (N), control (M) and output (P) horizons, are provided in the subsection dedicated to the corresponding case study.

2.3.1 Linear case study

Consider the three-CSTR dynamic process [14] shown in Fig. 2.6. x_A denotes the mass fraction of reactant A, $u = x_{A0}$ and $y = x_{A3}$ are the manipulated and controlled variables, respectively, and F is the volumetric flow rate. The transfer function model is given in Eq. (2.36), where K is the process gain. This process produces three different product grades – A, B and C.

$$y(s) = \frac{K}{(5s+1)^3} u(s) \tag{2.36}$$

The bounds on the control input, DRTO model outputs, and reference trajectory are:

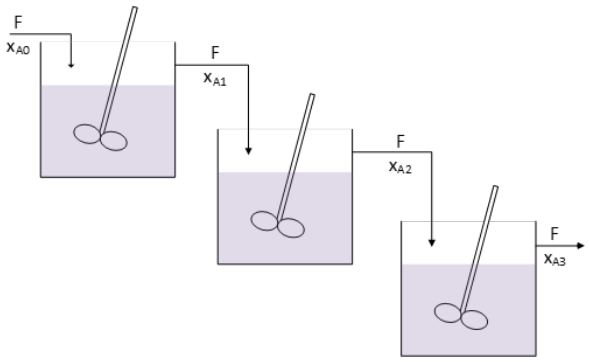

Figure 2.6. SISO CSTR system used in case 1a.

$$0 \leq u_{j,k}^{\text{MPC}} \leq 1, \qquad \forall\, k \in \mathcal{J}_0^{M-1},\ j \in \mathcal{J}_0^{N-1}$$
$$0 \leq y_j^{\text{DRTO}} \leq 1, \qquad \forall\, j \in \mathcal{J}_1^{N}$$
$$0 \leq y_j^{\text{ref}} \leq 1, \qquad \forall\, j \in \mathcal{J}_1^{N}$$

The volume of material produced at every time-step j is given by

$$f^m(x_j, u_{j-1}) = F\Delta t^{\text{MPC}}$$

where $F = 7.04$ m^3/min, and $f^m(\cdot)$ is used in Eq. (2.32). The MPC and CL–DRTO parameter values are given in Table 2.2.

Table 2.2. MPC and CL–DRTO parameter values for Cases 1a and 1b

Parameter	Description	Value
t^{sim}	Simulation horizon	180 min
Δt^{MPC}	MPC sample time	5.0 min
Δt^{DRTO}	DRTO sample time	10 min
P	MPC prediction horizon	20
M	MPC control horizon	3
Q	MPC output weight	1
R	MPC move supression weight	5
δ	Backoff parameter	1
δ^{ref}	Reference trajectory parameter	0
H	Set-point hold	1
N^{target}	Max. number of target changes	1
N^{ref}	Max. number of reference trajectory changes	36
N	DRTO/Scheduling horizon	36

The target specification and cost coefficient values are presented in Table 2.3. The times at which the demand orders are due are also shown. Note that demand times beyond the simulation horizon are included. The reason is that at simulation time 100 min, for example, the DRTO sees all the demand orders until time 280 min (current time plus DRTO horizon of 180 min), which is likely to have an effect on the optimal solution at the current time step. We also remark that the scenario set $\mathcal{S}$ may change between two consecutive DRTO executions as new information becomes available.

The demand for grades A, B and C are assumed to follow a normal probability distribution $N(\mu, \sigma)$ given by $N_A(175, 35)$, $N_B(210, 70)$ and $N_C(280, 105)$, respectively, where μ and σ are in m^3. Following the procedure illustrated in Section 2.2.5, the discretized demand levels for each grade are chosen as $L = \mu - \sigma$, $M = \mu$ and $H = \mu + \sigma$ with consecutive probabilities given by $a = 16$, $b = 68$ and $c = 16\%$ yielding in total 27 scenarios. The

CL–DRTO problem is solved in a rolling horizon fashion, using Gurobi, to an optimality gap of 0.1% on a 2.60 GHz, AMD EPYC 7H12 64-Core processor with 512 GB RAM running Windows Server 2019.

Table 2.3. Product targets (y^{targs}), inventory costs (C^I), unmet demand cost (C^B), input cost (C^U) , product value (C^G), and demand order time t^D for Cases 1a and 1b.

Grade	y^{targs}	C^G (\$/m^3)	C^I (\$/m^3/min)	C^B (\$/m^3)	C^U (\$/frac. of A)	t^D (min)
A	0.3	14	0.01	15	7.04	70, 250
B	0.6	11	0.03	14	7.04	140, 320
C	0.8	15	0.01	16	7.04	180, 360

Case 1a: Perfect model

In this sub-case, it is assumed that there is no plant-model mismatch. The nominal process gain K is set to one. Figures 2.7 and 2.8 show the closed-loop response for the expected value problem (EVP) and stochatic problem (SP), respectively, when the expected value of the demand is realized. We see that the set-point trajectories computed by the CL-DRTO and provided to the lower-level MPC results in a control action that drives the plant to produce grades due earlier first. When the EVP is solved in the CL–DRTO, the amounts produced are enough to satisfy the expected demand of grade A and C, and 84% of the expected demand of grade B. For the stochastic case, enough is produced to also meet the expected demand of grade B.

Due to the objective function formulation, if the inventory cost is higher than the cost incurred for not meeting the demand, the optimal solution will favor lower inventory levels. On the other hand, if the cost of the unmet demand is significantly higher, the optimal solution will lean towards meeting the scenario with the highest demand. For example, in the case study presented in this section, the inventory levels for the stochastic problem are sufficient to meet at least 82% of the demand of grades A and C in all scenarios, while only 75% of the demand of grade B is satisfied in some scenarios. For comparison, the optimal inventory level when the inventory cost of product B is three times lower is given in Fig. 2.9. The lower inventory cost leads to an early start in the production of grades B and C, and as

a result at least 88% of the demand of grade B and 100% of grade C are met in all scenarios.

We carried out 27 closed-loop simulations in order to compute the expected profit of the plant for the stochastic and deterministic problem. The values are given in Table 2.4, together with the VSS. The expected profit is 10% higher when the stochastic problem is solved at the DRTO level, showing that there are economic benefits in accounting for demand uncertainty. The average solution time of the CL-DRTO problem was 20 seconds for the EVP and 33 seconds for the SP.

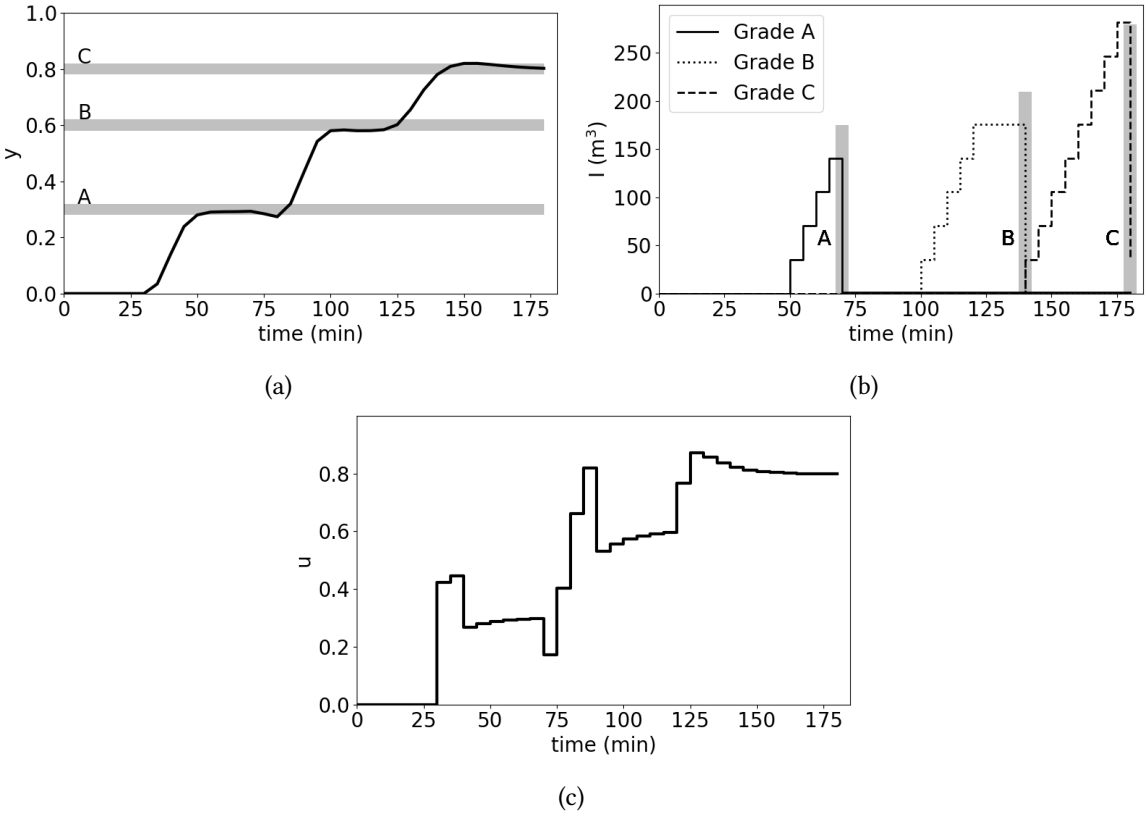

Figure 2.7. (a) Output response, (b) inventory levels, and (c) input values for the expected value problem in case 1a when the expected value of the demand is realized. Horizontal bars indicate the quality target band while vertical bars give the expected value of the demand.

Table 2.4. Expected profit and VSS for cases 1a and 1b (for CL-DRTO implementation)

	P^{EVP} (\$)	P^{SP} (\$)	VSS (\$)
Case 1a	6,593	7,258	665
Case 1b	-1,881	1,477	3,358

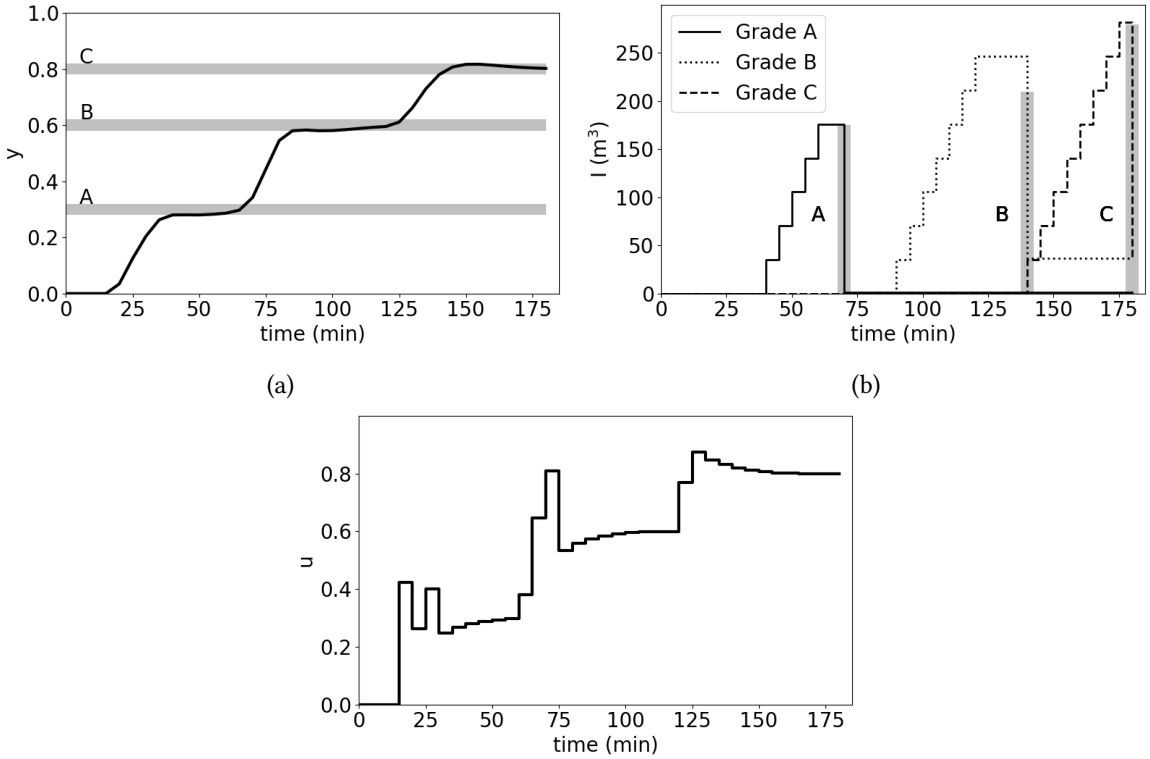

Figure 2.8. (a) Output response, (b) inventory levels, and (c) input values for the stochastic problem in case 1a when the expected value of the demand is realized. Horizontal bars indicate the quality target band while vertical bars give the expected value of the demand.

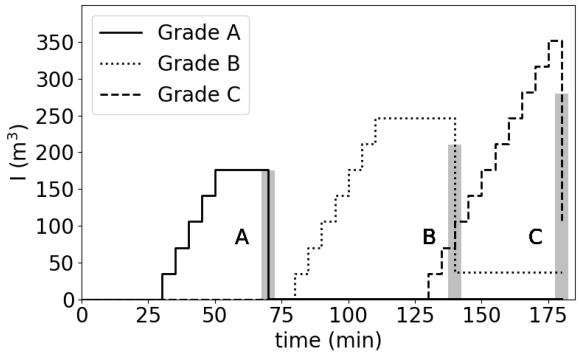

Figure 2.9. Inventory levels for the stochastic problem when the inventory cost of grade B is three times lower in Case 1a. Vertical bars indicate the expected value of the demand.

Case 1b: Introducing plant-model mismatch

For this case, plant-model mismatch is introduced by altering the gain of the linear model in the CL–DRTO and MPC to $K = 1.3$. The gain of the plant is kept at $K = 1$, and the backoff

parameter δ is set to 0.9. All other parameters are kept at the values given in Table 2.2.

We consider three different configurations of the MPC subproblems in the DRTO while the lower-level MPC formulation is kept intact. In the first configuration, denoted CLR–DRTO, we solve the rigorous constrained MPC problem given in Eq. (2.18) at every prediction time-step. In the second, named CLA–DRTO, we use the input–clipping formulation [10] to approximate the control action (see Section 2.2.2). The constraints on the decision variables (Eq. (2.18f)) are dropped from problem (2.18) and an analytical solution obtained [13], thus reducing the computation of the control action to a single function evaluation. The implemented input value at the DRTO level is obtained using Eq. (2.22). Last, the MPC subproblems are completely dropped from the DRTO problem. As a result, the control action is not accounted for and the open-loop problem is solved instead. Under this scenario, the optimization decision variables are u_j^{DRTO} for all $j \in \mathcal{J}_0^{N-1}$, rather than y^{ref} and u^{ref}. This implementation is named OL–DRTO and the reference trajectory is chosen to equal the targeted quality $y_{i,j}^{target}$ at every time-step j: $y_{i,j}^{\text{ref}} = y_{i,j}^{target}\ \forall i \in \mathcal{Y},\ j \in \mathcal{J}_1^N$.

Some deterioration in the economics is expected from the CLR–DRTO to the CLA–DRTO implementation. However, the latter is still expected to significantly outperform OL–DRTO [10]. Fig. 2.10 shows the plant output response and input values for the three configurations for the SP. The inventory is shown in Fig. 2.11.

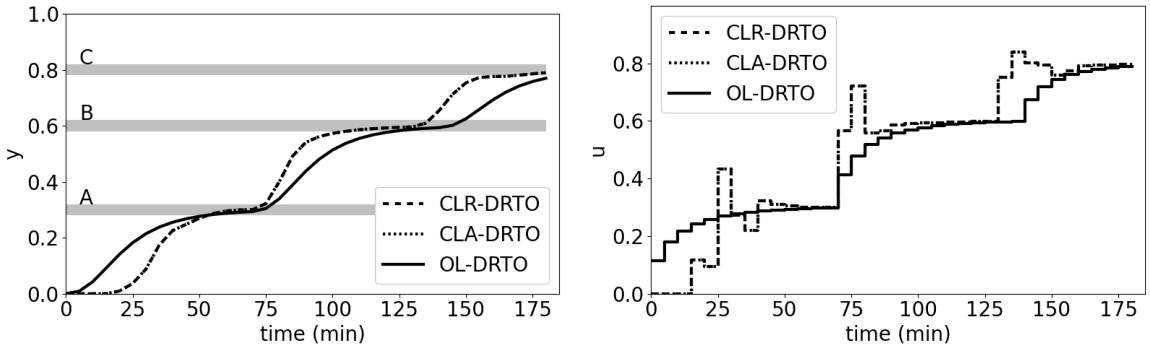

(a) (b)

Figure 2.10. (a) Plant output response and (b) input values for the SP in case 1b for various implementations of the MPC subproblems in the DRTO.

The input and output response values for the CLR–DRTO implementation coincide with those

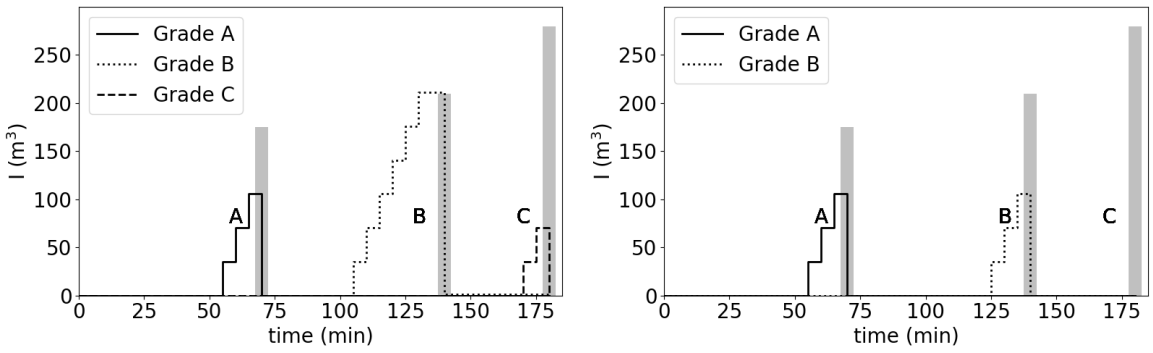

Figure 2.11. Inventory level for (a) CLR–DRTO and CLA–DRTO and (b) OL–DRTO implementations for the stochastic problem when the expected value of the demand is realized in Case 1b. Vertical bars indicate the expected value of the demand.

of the CLA–DRTO. This happens when the optimal input values for the constrained MPC problem do not saturate. For problems where the input saturates, these two configurations provide different results [10]. For the majority of the simulation time, the plant response for the OL–DRTO lags behind that of the CL–DRTO. The expected profit P^{SP} is $ 1,477 for the CL–DRTO and $-3,104 for the OL–DRTO implementations. The average solution time of the CLR-DRTO problem is 30 s, significantly higher than the 3.5 s for the CLA-DRTO and 1.3 s for the OL-DRTO. These results demonstrate the importance of accounting for the control action, but also how it increases the computational burden. The input-clipping formulation provides an exact approximation in operating regions away from the input bounds at a significantly lower computational cost, making it an attractive option in real-time applications.

The expected profit P^{EVP} is $-1,881.36 for the CL–DRTO implementations (Table 2.4), and $-3,104 for the OL–DRTO. Therefore, we have $VSS = \$3,358$ for the CL-DRTO implementation, which is even higher than in the previous case study, showing that accounting for demand uncertainty can also lead to higher profit expectations in the presence of plant-model mismatch. The results also confirm the significant superiority of the CL-DRTO over the OL-DRTO approach. Fig. 2.12 shows the output response and inventory for the expected value problem when the expected value of the demand is realized for the CL-DRTO implementations. Production of grade A starts later in the EVP compared to the SP problem to reduce inventory cost; however, due to plant-model mismatch, the desired quality target

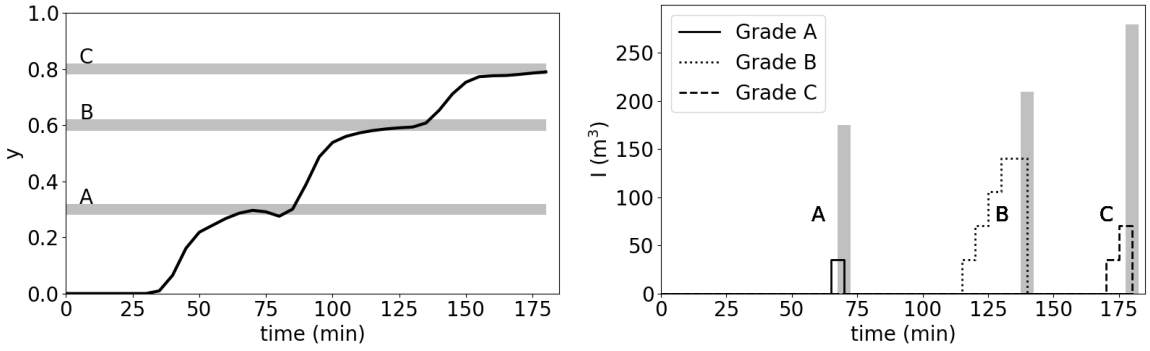

(a) (b)

Figure 2.12. (a) Output response and (b) inventory levels for the expected value problem in case 1b for the CL-DRTO implementations when the expected value of the demand is realized. Horizontal bars indicate the quality target band while vertical bars give the expected value of the demand.

band is reached later than predicted by the CL–DRTO model. In the stochastic problem, the CL–DRTO aims to meet the higher demand level of some of the scenarios, which leads to an earlier production start; thus, despite plant-model mismatch it is able to better satisfy the demand in all the scenarios compared to the expected value problem.

2.3.2 Nonlinear case study

This case study considers the nonlinear model for a CSTR adapted from Flores-Tlacuahuac and Grossmann [5],

$$\frac{dy}{dt} = \frac{u}{V}(C_0 - y) - ky^3 \tag{2.37}$$

where y is the output molar concentration, u is the inlet and output flow rate, V is the reactor volume, C_0 is the molar concentration of reactant in the inlet flow, and k is the reaction rate constant. The parameter values used in this study are shown in Table 2.5.

Table 2.5. Parameter values for nonlinear case study model.

Parameter	Value
C_0	1 mol/L
k	2 $L^2/mol^2/h$
V	5 m^3

By changing the flow rate u, it is possible to alter the output concentration y. Four distinct grades are produced at this plant. The quality targets, cost coefficients and time to meet the demand are given in Table 2.6. The demand for grades B, C, D and E are assumed to follow a normal probability distribution $N(\mu, \sigma)$ given by $N_B(400, 160)$, $N_C(1400, 840)$, $N_D(3000, 1800)$ and $N_E(6250, 3750)$, respectively, where μ and σ are in kg. The discretized demand levels for each grade are chosen as $L = \mu - 0.5\sigma,\ M = \mu$ and $H = \mu + 0.5\sigma$, with consecutive probabilities given by $a = 31,\ b = 38$ and $c = 31\%$. The number of scenarios in each CL–DRTO execution is 3^n, where n is the number of grades for which there is a demand order in the horizon N. For the present case study, there is always one order of two distinct grades within the DRTO horizon, yielding nine scenarios. To compute the expected profit of the plant we perform 30 closed-loop simulations where the realized demand is randomly sampled from the discrete demand set (see Section 2.2.6).

Table 2.6. Quality targets (y^{targs}), molar masses (MM_g), inventory cost (C^I), unmet demand cost (C^B), input costs(C^U), product value (C^G) and demand time (t^D) for the nonlinear case study.

Grade	y^{targs} (mol/L)	MM_g (kg/mol)	C^G ($/kg)	C^I ($/kg/h)	C^B ($/kg)	C^U ($/L)	t^D (h)
B	0.2	4	150	3	225	10	40, 60, 100
C	0.3032	2.298	130	3.6	170	10	10, 50, 110
D	0.393	1.545	125	4	190	10	30, 70, 90
E	0.5	1	120	3.4	140	10	20, 80, 120

The MPC and CL–DRTO parameters are given in Table 2.7. Analyzing the objective function, we see that there is no incentive to produce a grade for which there is no demand in the scheduling horizon. Therefore, to reduce the computational time, the binary variable $\gamma_{g,j}$ associated with the grades for which there is no demand within the horizon N are fixed at zero. We also use the previously discussed input-clipping formulation to approximate the MPC control action in the CL-DRTO in order to reduce the computational effort.

Upper and lower bounds are imposed on the DRTO model outputs, inputs, and on the reference trajectory:

$$0 \leq y_j^{\text{DRTO}} \leq 0.6 \qquad \forall\, j \in \mathcal{J}_1^N \tag{2.38a}$$

$$0.005 \leq u_{j,k}^{\text{MPC}} \leq 3 \qquad \forall\, k \in \mathcal{J}_0^{M-1},\ j \in \mathcal{J}_0^{N-1} \tag{2.38b}$$

Table 2.7. MPC and CL–DRTO parameters for nonlinear case study.

Parameter	Description	Value
t^{sim}	Simulation horizon	80 h
Δt^{MPC}	MPC sample time	0.5 h
Δt^{DRTO}	DRTO sample time	2 h
P	MPC prediction horizon	10
M	MPC control horizon	3
Q	MPC output weight	1
R	MPC move supression weight	1
δ	Backoff parameter	0.9
δ^{ref}	Reference trajectory parameter	0.9
H	Set-point hold	2
N^{target}	Max. number of target changes	1
N^{ref}	Max. number of reference trajectory changes	10
N^{PWA}	PWA horizon	20
N	DRTO/Scheduling horizon	40

$$0 \leq y_j^{\text{ref}} \leq 0.7 \qquad \forall\, j \in \mathcal{J}_1^N \tag{2.38c}$$

The model in Eq. (2.37) is linearized at the point $(y, u) = (0.393, 1)$, and further discretized yielding the matrices A and B used in the MPC subproblems and lower-level MPC. The PWA formulation presented in Section 2.2.1 is used to obtain a piecewise affine approximation of the dynamic process model. Thus, we have two different approximations of the nonlinear model, one linear and one piecewise affine.

The PWA formulation in Section 2.2.1 is ultimately only applicable to univariate functions. Therefore, we introduce two new variables w_1 and w_2 to exactly reformulate the nonlinear term uy in Eq. (2.37) as [12]:

$$\begin{aligned} uy &= 0.25(w_1^2 - w_2^2) \\ w_1 &= u + y \\ w_2 &= u - y \\ 0 &\leq w_1 \leq 3.81 \\ -0.71 &\leq w_2 \leq 3.1 \end{aligned}$$

The bounds on w_1 and w_2 can be obtained from the bounds on u and y (Eq. (2.38)), which are slightly relaxed here to ensure that the PWA approximation does not fail in case there is a small violation of the constraints during the course of the optimization. For instance, using the values on Eq. (2.38), the lower and upper bounds on w_1 would be 0.005 and and 3.6, respectively, which were relaxed to 0 and 3.81. A piecewise linear approximation is derived for each univariate nonlinear term, that is w_1^2, w_2^2 and y^3. The bounds imposed on w_1, w_2 are for the PWA derivation only, and do not affect the input and output bounds in the DRTO optimization problem.

The optimization problem in Eq. (2.9), to determine the PWA model coefficients, was formulated in CasADi [1] and solved using IPOPT [21]. The linear and piecewise linear approximations of the nonlinear model in Eq. (2.37) are shown in Fig. 2.13, where we see that the PWA approximation provides a significantly more accurate representation of the nonlinear model compared to the linear approximation.

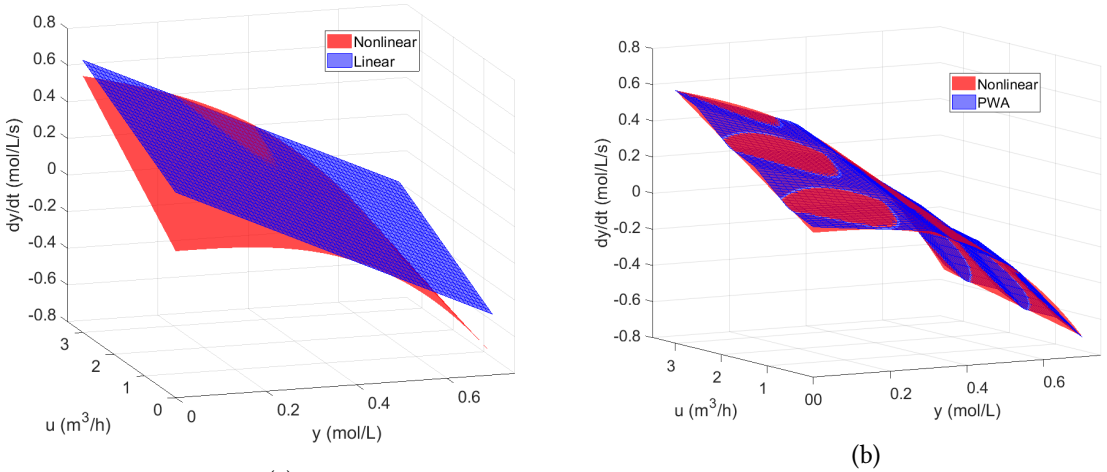

(a) (b)

Figure 2.13. (a) Linear, and (b) PWA approximation of the nonlinear model.

The amount produced at every time-step is given by

$$f^m(x_j, u_{j-1}) = u_{j-1} y_{g,1}^{targs} MM_g \Delta t^{\text{MPC}} \tag{2.40}$$

where MM_g is the molar mass (Table 2.6) and $y_{g,1}^{targs}$ is the desired molar concentration of

the grade g targeted for production at time step j.

In Figs. 2.14 and 2.15, the plant output and inventory levels for realization of the expected value of the demand when using the PWA and linear process models in the DRTO are presented. From the inventory level in Figs. 2.14c and 2.14d, we see that more is produced of each grade when the SP problem is solved at the DRTO level. The reason is that the DRTO is aware of scenarios where the demand is higher. Moreover, to decrease inventory costs, the DRTO tends to push production to start as close as possible to the time an order has to be met. This is especially true for grade D, which has the highest storage cost (Table 2.6). Between 20-25h in Fig. 2.14a, and 60-65h in Figs. 2.14a and 2.14b, the inlet flow rate u is reduced to decrease costs until the DRTO decides it is time to produce grade D. If it started producing grade D earlier, the inventory cost would increase. The exception here is grade B, for which the DRTO at time 40h sees the demand of grade B at 60h, and decides to keep producing B as opposed to producing C and then going back to grade B. We see this in the top two graphs of Figs. 2.14c and 2.14d, where the production of grade B is interrupted by the production of C, with the produced B stored in inventory until the later demand due time for B. Note that the storage cost of grade B is lower and it is also more valuable than grade C. Therefore, the DRTO delays producing grade C to decrease the associated inventory cost, but it also recognizes that it will not be able to produce enough of grade B if it only produces it between 50 and 60 hours, which explains why it decides to keep producing it between 40 and 45 h. Note that a different decision is taken when the process model is linear (Fig. 2.15), which shows how the model prediction into the future, and hence the model accuracy, can influence the scheduling decisions. The DRTO with the linear model fails to drive the plant to produce enough of the grade C to meet even the scenario with the lowest demand.

Table 2.8. Expected profit and VSS for case 2.

Model	P^{EVP} (\$)	P^{SP} (\$)	VSS (\$)
Linear	-387,859	101,483	489,342
PWA	466,568	812,534	345,966

The expected profit and VSS are shown in Table 2.8. The more accurate PWA model leads to a significantly higher plant profit compared to the linear model. We also see significant improvements in the profit expectation by accounting for demand uncertainty. The value

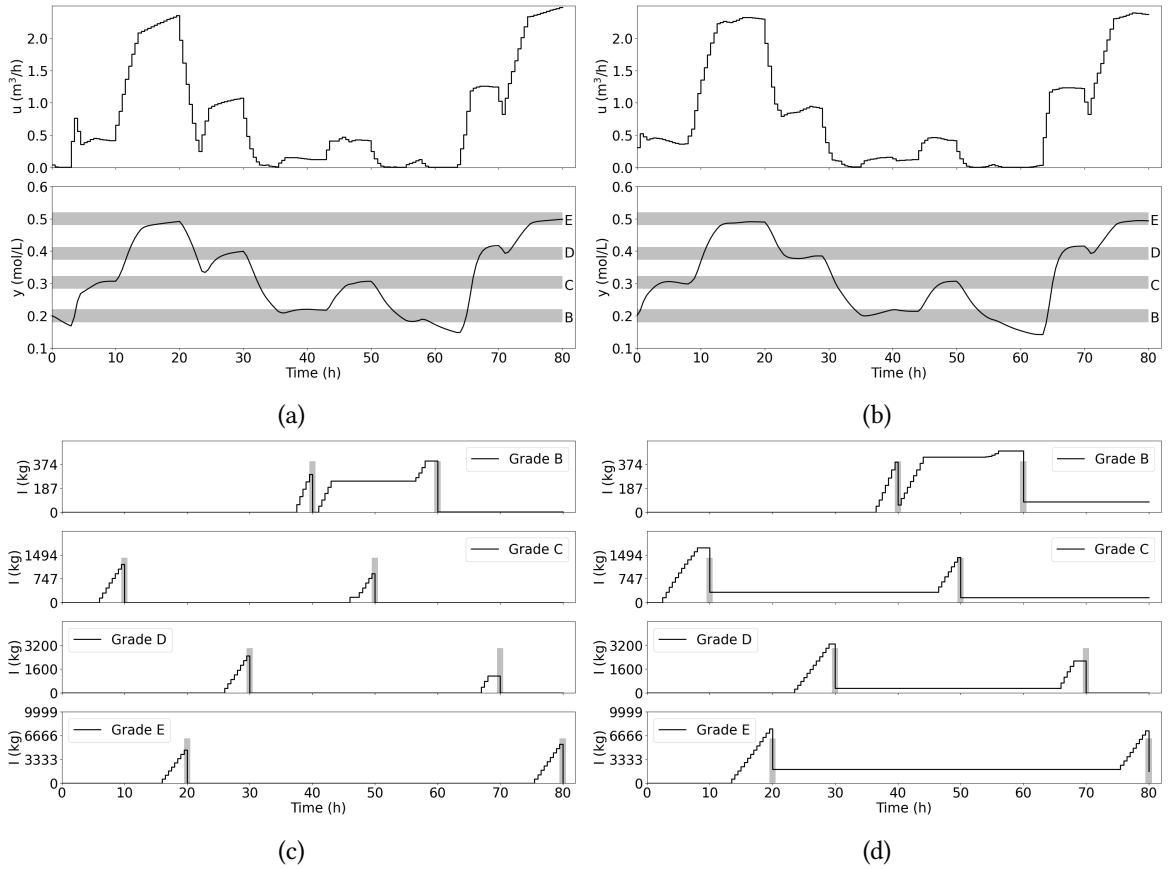

Figure 2.14. Input, output and inventory levels for the EVP ((a) and (c)) and SP ((b) and (d)) implementations when using PWA in the CL–DRTO for case 2. Horizontal bars indicate the quality target band while vertical bars give the expected value of the demand.

of the stochastic solution is $489,342 for the linear implementation, and $345,966 for the PWA. Consistent with the results in the previous case study, we also see that accounting for demand uncertainty seems to help to hedge against model uncertainty providing further motivation to solve the stochastic problem at the DRTO level.

The DRTO problem is solved 40 times in a simulation horizon of 80 hours. Because the demand profile changes, and new information becomes available, a slightly different problem is solved at every execution. In wall clock time, the average solution time for the stochastic DRTO problem is 2s for the linear model and 35s for the PWA. The CL–DRTO problem is always solved in less time than the 30 min sampling time for this case study. Even if the problem could not be solved to the desired optimality gap in less than 30 min, any incumbent solution would be feasible and could be passed to the lower level MPC. This,

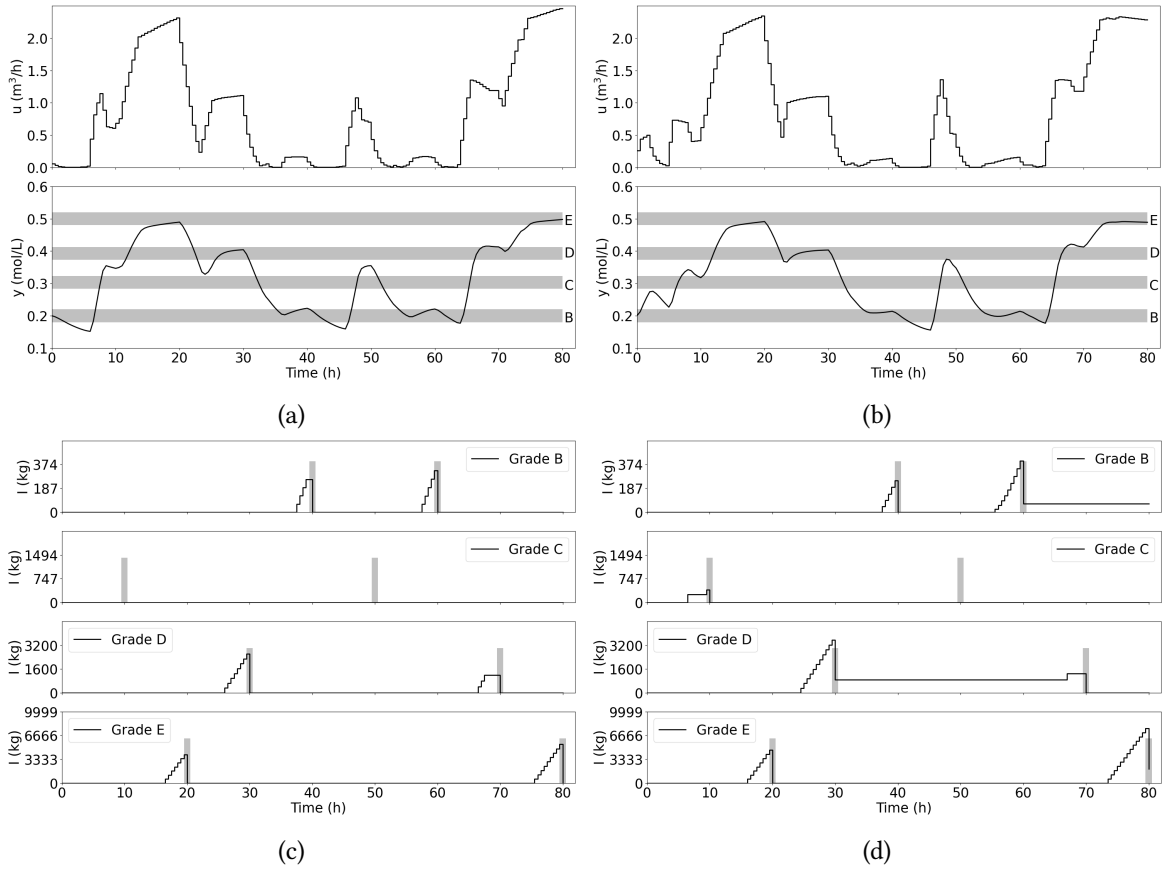

Figure 2.15. Input, output and inventory levels for the EVP ((a) and (c)) and SP ((b) and (d)) implementations when using a linear model approximation in the CL–DRTO for case 2. Horizontal bars indicate the quality target band while vertical bars gives the expected value of the demand.

and the guarantee of global optimality, are the main advantages of formulating the DRTO problem as an MILP as opposed to an MINLP.

2.4 Conclusion

In this work, we proposed a two–stage stochastic formulation for the integrated scheduling and control problem in order to account for demand uncertainty. The integrated problem is solved at the DRTO level in a rolling horizon manner to provide optimal set-point trajectories to the lower-level MPC. The DRTO process model predicts the plant response under the action of the MPC. This is accomplished by formulating an MPC problem at every prediction

time step to determine the control action. Through cases studies, we show that while computationally expensive, accounting for the closed-loop behavior of the plant leads to faster transitions and higher profit – a result that is consistent with previous publications [11]. Moreover, it is possible to significantly decrease the computational burden associated with the modeling of the MPC control action in the DRTO formulation by solving an unconstrained MPC problem followed by input-clipping to provide feasible inputs [10, 13]. The proposed approximation is exact in situations where the optimal solution of the constrained problem is itself unconstrained.

Furthermore, we demonstrate the performance of the proposed DRTO formulation under perfect plant knowledge, and plant-model mismatch. We apply a piecewise affine (PWA) approximation of a nonlinear process model that is implemented via linear mixed-integer constraints in the DRTO formulation, and compare its performance to that achieved when using a linear model. A significantly higher profit was achieved with the PWA approximation. However, the computational cost of solving the DRTO problem with a PWA process model is also higher, which may render applications to large problems intractable. Despite this drawback, PWA formulations are an alternative to avoid MINLP formulations, which are notoriously more difficult to solve. We also implement tighter quality target bands at the DRTO level compared to what is required at the plant level in an attempt to ensure that quality specifications are met even under plant-model mismatch. These tighter constraints implementations constitute contraint back-off – a generally known strategy in optimizing control.

To evaluate whether or not there are real economic gains in accounting for demand uncertainty in the DRTO formulation, the value of the stochastic solution (VSS) was computed using the actual plant profit under different realizations of the demand. A significant large positive VSS was obtained for all case studies, indicating that higher profit expectations can be achieved when demand uncertainty is accounted for in the scheduling and control problem. The VSS was even higher in the presence of plant-model mismatch, which suggests that accounting for demand uncertainty can help to hedge against model uncertainty. A useful avenue for future work is investigation into strategies for decreasing the solution time for accurate approximations of the nonlinear dynamic plant.

References

[1] J. A. E. Andersson, J. Gillis, G. Horn, J. B. Rawlings, and M. Diehl. "CasADi – A software framework for nonlinear optimization and optimal control". In: *Mathematical Programming Computation* 11.1 (2019), pp. 1–36 (cit. on p. 51).

[2] J. R. Birge and F. Louveaux. *Introduction to stochastic programming*. Springer Science & Business Media, 2011 (cit. on p. 20).

[3] D. Dering and C. L. Swartz. "A stochastic optimization framework for integrated scheduling and control under demand uncertainty". In: *Computers & Chemical Engineering* 165 (2022), p. 107931 (cit. on p. 16).

[4] D. Dering and C. L. Swartz. "Integrated Scheduling and Control under Uncertain Demand with Closed-Loop Dynamic Prediction". In: *2021 Virtual Canadian Chemical Engineering Conference (CCEC)*. Chemical Institute of Canada (CIC). 2021 (cit. on p. 16).

[5] A. Flores-Tlacuahuac and I. E. Grossmann. "Simultaneous cyclic scheduling and control of a multiproduct CSTR". In: *Industrial & Engineering Chemistry Research* 45.20 (2006), pp. 6698–6712 (cit. on p. 48).

[6] C. E. Garcia and A. Morshedi. "Quadratic programming solution of dynamic matrix control (QDMC)". In: *Chemical Engineering Communications* 46.1-3 (1986), pp. 73–87 (cit. on p. 28).

[7] D. Gupta, C. T. Maravelias, and J. M. Wassick. "From rescheduling to online scheduling". In: *Chemical Engineering Research and Design* 116 (2016), pp. 83–97 (cit. on p. 32).

[8] I. Harjunkoski, C. T. Maravelias, P. Bongers, P. M. Castro, S. Engell, I. E. Grossmann, J. Hooker, C. Méndez, G. Sand, and J. Wassick. "Scope for industrial applications of production scheduling models and solution methods". In: *Computers & Chemical Engineering* 62 (2014), pp. 161–193 (cit. on p. 37).

[9] M. Z. Jamaludin, H. Li, and C. L. E. Swartz. "The utilization of closed-loop prediction for dynamic real-time optimization". In: *The Canadian Journal of Chemical Engineering* 95.10 (2017), pp. 1968–1978 (cit. on p. 23).

[10] M. Z. Jamaludin and C. L. E. Swartz. “Approximation of closed-loop prediction for dynamic real-time optimization calculations”. In: *Computers & Chemical Engineering* 103 (2017), pp. 23–38 (cit. on pp. 29, 30, 46, 47, 55).

[11] M. Z. Jamaludin and C. L. E. Swartz. “Dynamic real-time optimization with closed-loop prediction”. In: *AIChE Journal* 63.9 (2017), pp. 3896–3911 (cit. on pp. 19, 21–23, 29, 55).

[12] M. Kvasnica, A. Szücs, and M. Fikar. “Automatic derivation of optimal piecewise affine approximations of nonlinear systems”. In: *IFAC Proceedings Volumes* 44.1 (2011), pp. 8675–8680 (cit. on pp. 18, 24, 25, 50).

[13] H. Li and C. L. E. Swartz. “Approximation techniques for dynamic real-time optimization (DRTO) of distributed MPC systems”. In: *Computers & Chemical Engineering* 118 (2018), pp. 195–209 (cit. on pp. 19, 22, 30, 46, 55).

[14] T. E. Marlin. “Process Control, 2nd edn.” In: McGraw-Hill, 2015. Chap. 7, pp. 64–65, 223–224, 366–367 (cit. on p. 41).

[15] P. Mathur, C. L. E. Swartz, D. Zyngier, and F. Welt. “Robust online scheduling for optimal short-term operation of cascaded hydropower systems under uncertainty”. In: *Journal of Process Control* 98 (2021), pp. 52–65 (cit. on p. 19).

[16] P. S. Ramesh, C. L. E. Swartz, and P. Mhaskar. “Closed-loop Dynamic Real-Time Optimization with Stabilizing Model Predictive Control”. In: *AIChE Journal* (2021), e17308 (cit. on p. 22).

[17] J. E. Remigio and C. L. E. Swartz. “Production scheduling in dynamic real-time optimization with closed-loop prediction”. In: *Journal of Process Control* 89 (2020), pp. 95–107 (cit. on pp. 18, 19, 23, 32).

[18] J. M. Simkoff and M. Baldea. “Production scheduling and linear MPC: Complete integration via complementarity conditions”. In: *Computers & Chemical Engineering* 125 (2019), pp. 287–305 (cit. on p. 32).

[19] J. M. Simkoff and M. Baldea. “Stochastic scheduling and control using data-driven nonlinear dynamic models: application to demand response operation of a chlor-alkali

plant". In: *Industrial & Engineering Chemistry Research* 59.21 (2020), pp. 10031–10042 (cit. on p. 18).

[20] S. Subrahmanyam, J. F. Pekny, and G. V. Reklaitis. "Design of batch chemical plants under market uncertainty". In: *Industrial & Engineering Chemistry Research* 33.11 (1994), pp. 2688–2701 (cit. on p. 38).

[21] A. Wächter and L. T. Biegler. "On the implementation of an interior-point filter line-search algorithm for large-scale nonlinear programming". In: *Mathematical Programming* 106.1 (2006), pp. 25–57 (cit. on p. 51).

Chapter 3

A scenario-based framework for the integration of scheduling and control under multiple uncertainties

The study in this chapter has been published and presented in:

[1] D. Dering and C. L. E. Swartz. "A scenario-based framework for the integration of scheduling and control under multiple uncertainties". In: *Journal of Process Control* 129 (2023), p. 103055

[2] D. Dering and C. L. Swartz. "Dynamic Real-Time Scheduling and Control Under

Uncertainty". In: *2022 AIChE Annual Meeting*. AIChE. 2022

3.1 Introduction

In this chapter, we address the integration of scheduling and control under multiple uncertainties. A literature review on this topic is given in [8], which cites several studies that have dealt with uncertainty either within the control or scheduling layer, but reveals only a scant number of studies that have explicitly accounted for uncertainty within an integrated scheduling and control framework by directly taking uncertainty into account in the problem formulation. This is in contrast to approaches that mitigate uncertainty solely via feedback through periodic solution of a deterministic optimization problem [12, 11, 15], or backoff constraints [16, 9].

Simkoff and Baldea [17] account for uncertainty in demand and electricity price in an open-loop integrated scheduling and control formulation for a chlor-alkali plant. They use a scenario-based stochastic formulation to account for the uncertainty. Gupta et al. [12] discuss the relative importance of accounting for uncertainty *a priori* compared to periodic and event triggered scheduling for state task network systems. Insights and guidelines for choosing the scheduling horizon and re-scheduling frequency are provided in [11]. Mathur et al. [14] propose a stochastic EMPC like formulation for optimal scheduling and control of hydropower systems that accounts for uncertainty in electricity prices. Chu and You [4] propose a formulation for scheduling of batch process that takes into account the process dynamics and accounts for model uncertainty via scenarios. A solution procedure based on Benders decomposition is employed to reduce the solution time. In our earlier work [6], we propose a closed-loop stochastic formulation for the integrated scheduling and control problem that addresses demand uncertainty. The formulation is deemed closed-loop because it takes into account the action of an underlying MPC controller.

We extend the integrated scheduling and control paradigm of Dering and Swartz [6] to account for multiple uncertainties types, including model, demand and cost uncertainty. However, instead of an MPC, we consider the case where the underlying tracking controllers are of the PI type. The underlying control system is accounted for in the integrated scheduling and control formulation, which also accommodates input saturation. The result-

ing closed-loop integrated scheduling and control problem is solved at the DRTO level to compute optimal scheduling decisions and output set-points. The production sequencing is communicated to the plant via the output set-points that are tracked by the PI control system. In case of multiple PI loops, the closed-loop formulation allows for the interaction between the feedback loops to be exploited to improve the economic performance of the process. The DRTO problem is solved online in a moving horizon fashion, and receives appropriate feedback information from the plant. Thus, the optimal solution of the closed-loop integrated scheduling and control problem is implemented in closed-loop and online. Since feedback alone has the potential to mitigate uncertainty to a degree [12], this raises the question as to whether or not there is additional benefit in accounting for uncertainty via a stochastic formulation. In this context, it is also relevant to explore the impact of the feedback frequency.

Through case studies, we evaluate the impact of accounting for uncertainty in the presence of feedback. This evaluation is carried out using the value of the stochastic solution for distinct feedback frequencies (that is, distinct execution frequencies of the DRTO layer). We also explore cases where only some of the uncertainty is taken into account in the stochastic formulation (such as accounting only for model uncertainty even though there is also demand uncertainty). This aims to reflect a situation where it is impractical to model all the uncertainties affecting the system. In addition to cases where the true model structure is known, we also consider a situation of structural plant-model mismatch, where the DRTO process model is linear, but the true process model is nonlinear. In summary, key differences from our previous study [6] are (i) consideration of multiple sources of uncertainty, as opposed to only demand uncertainty in the previous study, (ii) consideration here of PI control, including handling of input saturation, as opposed to MPC in the previous study, and (iii) exploration in the present study of the impact of the DRTO execution frequency relative to that of the regulatory PI controller.

The remainder of this chapter is organized as follows. In Section 3.2, we present the overall framework and formulation of the integrated scheduling and control problem. The case studies are presented in Section 3.3, and we finalize with the conclusion in Section 3.4.

3.2 Formulation

In this section, we present a closed-loop formulation for the integrated scheduling and control problem that can account for multiple uncertainty types, including model, demand and cost uncertainty. We follow the two-layer paradigm, illustrated in Fig. 3.1, due to the industrial prevalence of the hierarchical automation architecture. The integrated problem is solved at the DRTO level, and the action of the underlying PI controllers is accounted for in the formulation, enabling it to predict the closed-loop process response. The DRTO layer receives as inputs, the forecast for the selling prices, demand levels and other relevant parameters, and feedback information from the plant regarding current inventory levels I_{j*}, and measured output values y^m_{j*}. It provides optimal reference trajectories y^{ref}_{j*} to the lower level PI controllers, that compute the input values u_{j*} applied to the plant. The subscript $j*$ indicates the current time instance. The DRTO problem is solved periodically at an interval of Δt^{DRTO}, which is typically a multiple of the sampling time of the PI controller, Δt, i.e., $\Delta t^{DRTO}/\Delta t \in \mathcal{Z}^+$.

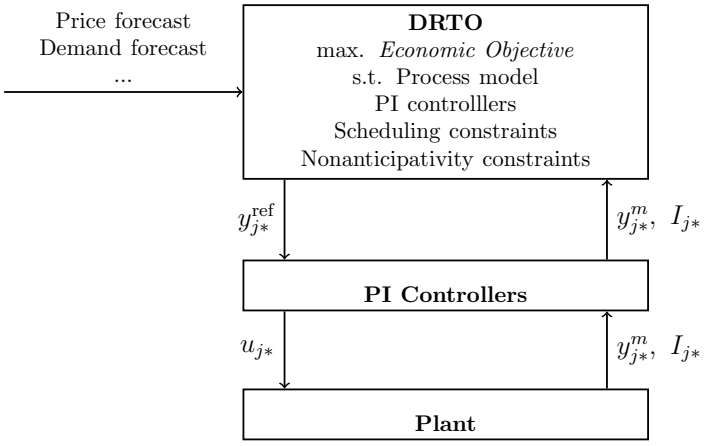

Figure 3.1. Schematic representation of the two-layer control architecture used in the present study. The integrated scheduling and control problem is solved at the DRTO layer. y^{ref}_{j*} denotes the output set-points, u_{j*} denotes the input values applied to the plant, y^m_{j*} stands for the output measurements, and I_{j*} indicates the measured or predicted inventory levels. The subscript $j*$ denotes the current time instance.

3.2.1 The DRTO problem formulation

The formulation of the stochastic integrated scheduling and control problem solved at the DRTO layer is presented in Eq. (3.1),

$$\max_{\eta^{\text{DRTO}}} \quad \Phi = \sum_{s\in\mathcal{S}} \rho_s \phi\left(x_s^{\text{DRTO}}, u_s^{\text{DRTO}}, y_s^{\text{DRTO}}, z_s, \xi_s\right) \tag{3.1a}$$

$$\text{subject to} \quad x_{s,j+1}^{\text{DRTO}} = A_s x_{s,j}^{\text{DRTO}} + B_s u_{s,j}^{\text{DRTO}}, \qquad j \in \mathcal{J}_0^{N-1},\ s \in \mathcal{S} \tag{3.1b}$$

$$y_{s,j}^{\text{DRTO}} = C_s x_{s,j}^{\text{DRTO}} + d_{s,j}, \qquad j \in \mathcal{J}_1^{N},\ s \in \mathcal{S} \tag{3.1c}$$

$$d_{s,j} = y_{j*}^{m} - C_s x_{s,0}^{\text{DRTO}}, \qquad j \in \mathcal{J}_1^{N},\ s \in \mathcal{S} \tag{3.1d}$$

$$\tilde{u}_{s,j}^{\text{PI}} = \tilde{u}_{s,j-1}^{\text{PI}} + K_c \odot \left(\tilde{E}_{s,j} - \tilde{E}_{s,j-1} + \Delta t \tilde{E}_{s,j} \otimes \tau_I\right), j \in \mathcal{J}_0^{N-1},\ s \in \mathcal{S} \tag{3.1e}$$

$$\tilde{E}_{s,j} = y_{s,j+1}^{\text{ref}} - y_{s,j}^{\text{DRTO}}, \qquad j \in \mathcal{J}_0^{N-1},\ s \in \mathcal{S} \tag{3.1f}$$

$$u_{s,j}^{\text{DRTO}} - \tilde{u}_{s,j}^{\text{PI}} + \mu_{s,j}^{1} - \mu_{s,j}^{2} = 0, \qquad j \in \mathcal{J}_0^{N-1},\ s \in \mathcal{S} \tag{3.1g}$$

$$u_{s,j}^{\text{DRTO}} - u_{min} \geq -(1-\beta_{s,j}^{2})M, \qquad j \in \mathcal{J}_0^{N-1},\ s \in \mathcal{S} \tag{3.1h}$$

$$u_{s,j}^{\text{DRTO}} - u_{max} \geq -(1-\beta_{s,j}^{1})M, \qquad j \in \mathcal{J}_0^{N-1},\ s \in \mathcal{S} \tag{3.1i}$$

$$u_{s,j}^{\text{DRTO}} - u_{min} \leq (1-\beta_{s,j}^{2})M, \qquad j \in \mathcal{J}_0^{N-1},\ s \in \mathcal{S} \tag{3.1j}$$

$$u_{s,j}^{\text{DRTO}} - u_{max} \leq (1-\beta_{s,j}^{1})M, \qquad j \in \mathcal{J}_0^{N-1},\ s \in \mathcal{S} \tag{3.1k}$$

$$0 \leq \mu_{s,j}^{1} \leq \beta_{s,j}^{1} M, \qquad j \in \mathcal{J}_0^{N-1},\ s \in \mathcal{S} \tag{3.1l}$$

$$0 \leq \mu_{s,j}^{2} \leq \beta_{s,j}^{2} M, \qquad j \in \mathcal{J}_0^{N-1},\ s \in \mathcal{S} \tag{3.1m}$$

$$u_{min} \leq u_{s,j}^{\text{DRTO}} \leq u_{max} \qquad j \in \mathcal{J}_0^{N-1},\ s \in \mathcal{S} \tag{3.1n}$$

$$y_{min}^{\text{ref}} \leq y_{s,j}^{\text{ref}} \leq y_{max}^{\text{ref}} \qquad j \in \mathcal{J}_1^{N},\ s \in \mathcal{S} \tag{3.1o}$$

$$y_{min} \leq y_{s,j}^{\text{DRTO}} \leq y_{max} \qquad j \in \mathcal{J}_1^{N},\ s \in \mathcal{S} \tag{3.1p}$$

Nonanticipativity constraints (3.1q)

Scheduling constraints: Eqs. (3.3)- (3.10) (3.1r)

We use the index s to denote a scenario in the set of discrete scenarios $\mathcal{S}$, and the index j to indicate the DRTO time step, which differs from the current time instance $j*$. $\mathcal{J}_a^b = \{j | a \leq j \leq b, j \in \mathcal{Z}\}$ is defined as the set of time steps over the range $[a, b]$. We assume a

linear process model in Eqs. (3.1b) and (3.1c) with potential uncertainty in the discrete-time matrices $A_s \in \mathcal{R}^{nx \times nx}$, $B_s \in \mathcal{R}^{nx \times nu}$ and $C_s \in \mathcal{R}^{ny \times nx}$. Nonlinear process models can be linearized or approximated via piecewise linear segments to use the proposed formulation. $d_{s,j}$ is a disturbance estimate computed via Eq. (3.1d), and $y^m_{j*} \in \mathcal{R}^{ny}$ is a vector of the plant output measurements. $x^{\text{DRTO}}_{s,j} \in \mathcal{R}^{nx}$, $u^{\text{DRTO}}_{s,j} \in \mathcal{R}^{nu}$ and $y^{\text{DRTO}}_{s,j} \in \mathcal{R}^{ny}$ are state, input and output vectors, respectively. $y^{\text{ref}}_{s,j} \in \mathcal{R}^{ny}$ is the reference trajectory vector. y^{ref}_s, x^{DRTO}_s, u^{DRTO}_s and y^{DRTO}_s are composite vectors defined as:

$$
\begin{aligned}
y^{\text{ref}}_s &= \left[\left(y^{\text{ref}}_{s,1}\right)^{\text{T}}, \ldots, \left(y^{\text{ref}}_{s,N}\right)^{\text{T}}\right]^{\text{T}}, && s \in \mathcal{S} \\
x^{\text{DRTO}}_s &= \left[\left(x^{\text{DRTO}}_{s,1}\right)^{\text{T}}, \ldots, \left(x^{\text{DRTO}}_{s,N}\right)^{\text{T}}\right]^{\text{T}}, && s \in \mathcal{S} \\
u^{\text{DRTO}}_s &= \left[\left(u^{\text{DRTO}}_{s,0}\right)^{\text{T}}, \ldots, \left(u^{\text{DRTO}}_{s,N-1}\right)^{\text{T}}\right]^{\text{T}}, && s \in \mathcal{S} \\
y^{\text{DRTO}}_s &= \left[\left(y^{\text{DRTO}}_{s,1}\right)^{\text{T}}, \ldots, \left(y^{\text{DRTO}}_{s,N}\right)^{\text{T}}\right]^{\text{T}}, && s \in \mathcal{S}
\end{aligned}
$$

We additionally define $z_s = [(d_s)^T, (v_s)^T]^T$, where $d_s \in \mathcal{Z}^{nd}$ and $v_s \in \mathcal{R}^{nv}$, is a composite vector of the discrete and continuous scheduling decisions. $\xi_s \in \mathcal{R}^{n\xi}$ is the vector of uncertain parameters in scenario s. $\rho_s \in \mathcal{R}$ denotes the probability of realization of a scenario s.

We implement the velocity form of the PI controller in Eqs. (3.1e) and (3.1f) [13], with $K_c \in \mathcal{R}^{nu}$ and $\tau_I \in \mathcal{R}^{nu}$ representing the controller gain and integral time constant. $E_{s,j} \in \mathcal{R}^{nu}$ is the deviation between the predicted output and the reference trajectory $y^{\text{ref}}_{s,j}$. In Eq. (3.1e), $\odot$ and $\otimes$ indicate element-wise multiplication and division, respectively. $\tilde{u}^{PI}_{s,j} \in \mathcal{R}^{nu}$ is the input value computed by the PI controller. Eqs. (3.1g) - (3.1n) account for actuator saturation, and capture the following logic [1]:

$$
u^{\text{DRTO}}_{s,j} = \begin{cases} \tilde{u}^{\text{PI}}_{s,j} & \text{if } u_{min} \leq \tilde{u}^{\text{PI}}_{s,j} \leq u_{max} \\ u^{min} & \text{if } \tilde{u}^{\text{PI}}_{s,j} \leq u_{min} \\ u^{max} & \text{if } \tilde{u}^{\text{PI}}_{s,j} \geq u_{max} \end{cases} \tag{3.2}
$$

where $u_{min} \in \mathcal{R}^{nu}$ and $u_{max} \in \mathcal{R}^{nu}$ are the minimum and maximum input values, respec-

tively. In Eqs. (3.1g)-(3.1m), $\beta^i_{s,j} \in \{0,1\}^{nu}$ are binary variables, while $\mu^i_{s,j} \geq 0$ are slack variables. M is a sufficiently large positive constant. Eqs. (3.1o) and (3.1p) define bounds on the reference trajectory and output values, respectively. Nonanticipativity constraints (NAC) are given in Eq. (3.1q), and are discussed in more detail in Section 3.2.4. The DRTO optimization degrees of freedom are the reference trajectory, and the scheduling decisions. The objective function is an appropriate economic metric Φ.

We define η^{DRTO} as a composite vector of all the optimization variables, it includes y^{ref}_s, x^{DRTO}_s, u^{DRTO}_s, y^{DRTO}_s, z_s, $d_{s,1}, \ldots, d_{s,N}$, $\tilde{u}^{\text{PI}}_{s,0}, \ldots, \tilde{u}^{\text{PI}}_{s,N-1}$, $\tilde{E}_{s,0}, \ldots, \tilde{E}_{s,N-1}$, $\beta^1_{s,0}, \ldots, \beta^1_{s,N-1}$, $\beta^2_{s,0}, \ldots, \beta^2_{s,N-1}$, $\mu^1_{s,0}, \ldots, \mu^1_{s,N-1}$, $\mu^2_{s,0}, \ldots, \mu^2_{s,N-1}$ for all $s \in \mathcal{S}$.

The PI control formulation in the DRTO and that of the PI controllers in the underlying control layer are the same, except that the measured output y^m_{j*} values are used in place of $y^{\text{DRTO}}_{s,j}$ in Eq. (3.1f) in the latter. Therefore, if the predicted and measured output values do not match, the input values u_j computed by the lower level PI controller may also differ from $u^{\text{DRTO}}_{s,j}$ computed by the DRTO. This is especially true in case of plant-model mismatch, or in the presence of unmodeled disturbances affecting the system. At each DRTO execution, $x^{\text{DRTO}}_{s,0}$, $\tilde{E}_{s,-1}$, $\tilde{u}^{\text{PI}}_{s,-1}$ and $y^{\text{DRTO}}_{s,0}$ are respectively set to $x^{\text{DRTO}}_{s,\Delta t^{\text{DRTO}}/\Delta t}$, $E_{s,(\Delta t^{\text{DRTO}}/\Delta t)-1}$, $\tilde{u}^{\text{PI}}_{s,(\Delta t^{\text{DRTO}}/\Delta t)-1}$ and $y^{\text{DRTO}}_{s,\Delta t^{\text{DRTO}}/\Delta t}$ at the previous DRTO execution.

3.2.2 Scheduling constraints

The scheduling formulation presented in this section is largely based on our previous work [6]. However, some differences are introduced via Eqs. (3.5b), (3.6), and (3.10).

The scheduling constraint used are

1. for production sequencing
2. to determine whether or not the output is within the quality target band for a given grade
3. to limit quality target changes

4. to define the minimum number of time steps for which a given grade should be produced

5. to define when to start product storage.

In Eq. (3.3), $\mathcal{Y} = \{1, ..., ny\}$ is the set of measured outputs, and $\mathcal{G}$ is the set of grades. The binary variable $\gamma_{s,g,j}$ is used in Eq. (3.3a) to select the grade g to be produced in scenario s at time step j. $y_{g,i}^{target}$ gives the value of the i^{th} target quality for grade g. Eq. (3.3b) ensures that only one grade can be produced at any time step j.

$$y_{s,i,j}^{targ} = \sum_{g \in \mathcal{G}} \gamma_{s,g,j} y_{g,i}^{target}, \qquad s \in \mathcal{S},\ j \in \mathcal{J}_1^N,\ i \in \mathcal{Y} \tag{3.3a}$$

$$\sum_{g \in \mathcal{G}} \gamma_{s,g,j} = 1, \qquad s \in \mathcal{S},\ j \in \mathcal{J}_1^N \tag{3.3b}$$

To track whether or not the output $y_{s,i,j}^{\text{DRTO}}$ is within the target quality band for any grade g at time step j, we introduce a binary variable $\tilde{b}_{s,k,g,i,j}$. Note that $y_{s,i,j}^{\text{DRTO}}$ denotes the i^{th} element of the vector $y_{s,j}^{\text{DRTO}}$. The target band for quality i of grade g is given by $y_{g,i}^{target} \pm \epsilon_{g,i}$, where $\epsilon_{g,i}$ is the tolerance by which output $y_{s,i,j}^{\text{DRTO}}$ can deviate from $y_{g,i}^{target}$ and still meet the quality specifications for grade g. A schematic representation is provided in Fig 3.2. Eq. (3.4) ensures that $\tilde{b}_{s,2,g,i,j}$ equals one if and only if $y_{s,i,j}^{\text{DRTO}} \in [y_{g,i}^{target} - \epsilon_{g,i},\ y_{g,i}^{target} + \epsilon_{g,i}]$, $\tilde{b}_{s,1,g,i,j}$ equals one if and only if $y_{s,i,j}^{\text{DRTO}} \in [y_{i,\min},\ y_{g,i}^{target} - \epsilon_{g,i}]$, and $\tilde{b}_{s,3,g,i,j}$ equals one if and only if $y_{s,i,j}^{\text{DRTO}} \in [y_{g,i}^{target} + \epsilon_{g,i},\ y_{i,max}]$.

$$\sum_{k=1}^{3} \tilde{b}_{s,k,g,i,j} = 1, \quad s \in \mathcal{S},\ j \in \mathcal{J}_1^N,\ i \in \mathcal{Y},\ g \in \mathcal{G} \tag{3.4a}$$

$$y_{s,i,j}^{\text{DRTO}} \leq \tilde{b}_{s,1,g,i,j} \left(y_{g,i}^{target} - \epsilon_{g,i} \right) + \tilde{b}_{s,2,g,i,j} \left(y_{g,i}^{target} + \epsilon_{g,i} \right) + \tilde{b}_{s,3,g,i,j} y_{i,\max},$$
$$\forall\, g \in \mathcal{G},\ s \in \mathcal{S},\ i \in \mathcal{Y},\ j \in \mathcal{J}_1^N \tag{3.4b}$$

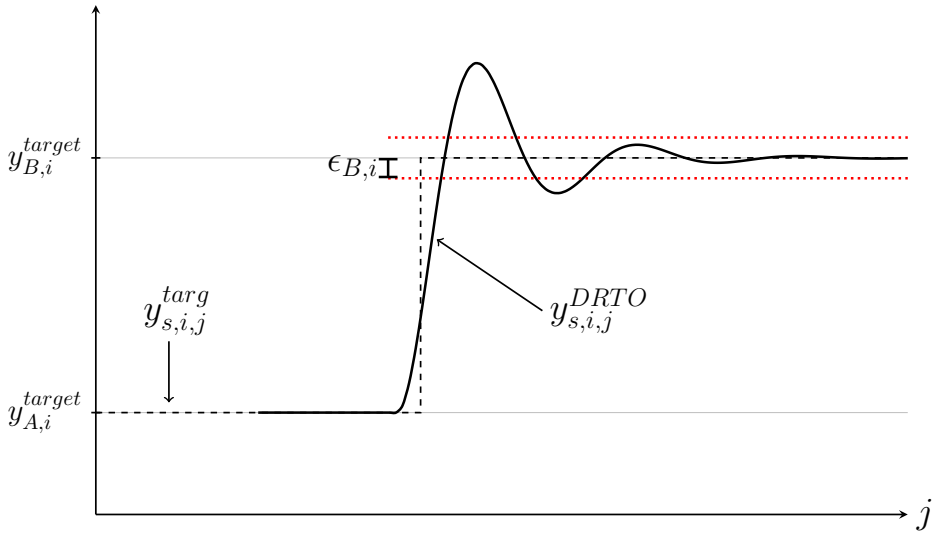

Figure 3.2. Schematic representation of quality target band.

$$y_{s,i,j}^{\text{DRTO}} \geq \tilde{b}_{s,1,g,i,j} y_{i,\min} + \tilde{b}_{s,2,g,i,j} \left(y_{g,i}^{target} - \epsilon_{g,i} \right) + \tilde{b}_{s,3,g,i,j} \left(y_{g,i}^{target} + \epsilon_{g,i} \right), \quad \forall\, g \in \mathcal{G},\ s \in \mathcal{S},\ i \in \mathcal{Y},\ j \in \mathcal{J}_1^N \tag{3.4c}$$

The product is only deemed viable if all outputs are simultaneously within the quality target band, that is $\sum_{i \in \mathcal{Y}} \tilde{b}_{s,2,g,i,j} = ny$ for some grade g at time step j. This can be captured using an auxiliary variable $z_{s,g,j}^{targ} \in [0,1]$ and Eq. (3.5), which guarantees that $z_{s,g,j}$ equal one if and only if all quality target specifications for a given grade are simultaneously met at time step j. Eq. (3.5a) reflects the fact that only one grade can be produced at any time step j.

$$\sum_{g \in \mathcal{G}} z_{s,g,j}^{targ} \leq 1, \qquad s \in \mathcal{S},\ j \in \mathcal{J}_1^N \tag{3.5a}$$

$$\sum_{i \in \mathcal{Y}} \tilde{b}_{s,2,g,i,j} \leq ny - \left(1 - z_{s,g,j}^{targ} \right), \qquad s \in \mathcal{S},\ j \in \mathcal{J}_1^N,\ g \in \mathcal{G} \tag{3.5b}$$

$$\sum_{i \in \mathcal{Y}} \tilde{b}_{s,2,g,i,j} \geq nyz_{s,g,j}^{targ}, \qquad s \in \mathcal{S},\ j \in \mathcal{J}_1^N,\ g \in \mathcal{G} \tag{3.5c}$$

With the constraints introduced until now, we can detect when viable product is being produced, but we may not wish to start storage immediately because the outputs may still be oscillating. To deal with this, we introduce a parameter $H \in \mathcal{Z}^+$, the binary variable

$\tilde{\gamma}_{s,g,j}$ to indicate whether or not grade g is stored at time step j, and the constraint set in Eq. (3.6). In (3.6a) - (3.6b), $\tilde{\gamma}_{s,g,j}$ is one (product is stored) if and only if the quality requirements have been met for H consecutive time steps. Eq. (3.6c) is a tightening constraint, while Eq. (3.6d) ensures that if a product is being stored then it has been targeted for production.

$$\sum_{k \in \mathcal{J}_0^{H-1}} z^{targ}_{s,g,j-k} \leq H - \left(1 - \tilde{\gamma}_{s,g,j}\right), \qquad s \in \mathcal{S},\ j \in \mathcal{J}_0^N,\ g \in \mathcal{G} \tag{3.6a}$$

$$\sum_{k \in \mathcal{J}_0^{H-1}} z^{targ}_{s,g,j-k} \geq H\tilde{\gamma}_{s,g,j}, \qquad s \in \mathcal{S},\ j \in \mathcal{J}_0^N,\ g \in \mathcal{G} \tag{3.6b}$$

$$\tilde{\gamma}_{s,g,j} \leq z^{targ}_{s,g,j}, \qquad s \in \mathcal{S},\ j \in \mathcal{J}_1^N,\ g \in \mathcal{G} \tag{3.6c}$$

$$\gamma_{s,g,j} \geq \tilde{\gamma}_{s,g,j}, \qquad s \in \mathcal{S},\ j \in \mathcal{J}_1^N,\ g \in \mathcal{G} \tag{3.6d}$$

Another parameter $L \in \mathcal{Z}^+$ $(L > H)$ and variable $\tilde{\beta}_{s,g,j} \in [0,1]$ are used to define the minimum number of consecutive time steps for which product should be stored. For that, we use the constraint set in Eq. (3.7) to ensure that once storage starts, it will continue for at least $L - H$ consecutive time steps. Eq. (3.7a) forces $\tilde{\beta}_{s,g,j}$ to equal one when product stops being stored. However, $\tilde{\beta}_{s,g,j}$ can only equal one if the quality requirements for grade g have been met for at least L consecutive time steps, as by Eq. (3.7b). When storage stops, a target change is forced via Eq. (3.7c). Eq. (3.7d) ensures that a target change will only occur if the grade targeted for production at the current time step has been produced, within spec, for at least L time steps. Eq. (3.7e) prevents $\tilde{\beta}_{s,g,j}$ from being one if grade g is not being stored, while Eq. (3.7f) reflects the fact the only one grade can be produced and stored at any given time step j. Finally, Eq. (3.7g) serves to limit the number of target changes via the parameter N^z. For example, if $N^z = 1$ each grade can be produced at most once in the DRTO horizon.

$$\tilde{\gamma}_{s,g,j+1} - \tilde{\gamma}_{s,g,j} \geq -\tilde{\beta}_{s,g,j}, \qquad s \in \mathcal{S},\ j \in \mathcal{J}_0^{N-1},\ g \in \mathcal{G} \tag{3.7a}$$

$$\sum_{k \in \mathcal{J}_0^{L-1}} z^{targ}_{s,g,j-k} \geq L\tilde{\beta}_{s,g,j}, \qquad s \in \mathcal{S},\ j \in \mathcal{J}_0^N,\ g \in \mathcal{G} \tag{3.7b}$$

$$\gamma_{s,g,j+1} \leq 1 - \tilde{\beta}_{s,g,j}, \qquad s \in \mathcal{S},\ j \in \mathcal{J}_0^{N-1},\ g \in \mathcal{G} \tag{3.7c}$$

$$\gamma_{s,g,j+1} - \gamma_{s,g,j} \geq -\tilde{\beta}_{s,g,j}, \qquad s \in \mathcal{S},\ j \in \mathcal{J}_0^{N-1},\ g \in \mathcal{G} \tag{3.7d}$$

$$\tilde{\beta}_{s,g,j} \leq \tilde{\gamma}_{s,g,j}, \qquad s \in \mathcal{S},\ j \in \mathcal{J}_1^N,\ g \in \mathcal{G} \tag{3.7e}$$

$$\sum_{g \in \mathcal{G}} \tilde{\beta}_{s,g,j} \leq 1, \qquad s \in \mathcal{S},\ j \in \mathcal{J}_0^N \tag{3.7f}$$

$$\sum_{j \in \mathcal{J}_0^N} \tilde{\beta}_{s,g,j} \leq N^z - \gamma_{s,g,N}, \qquad s \in \mathcal{S},\ g \in \mathcal{G} \tag{3.7g}$$

The amount of product $m_{s,g,j}$ sent to storage at any time step j is computed via Eq. (3.8) using a big-M formulation, where $f^m(\cdot)$ is a linear function defining the amount produced, and M is a sufficiently large positive constant.

$$m_{s,g,j} \geq -\tilde{\gamma}_{s,g,j} M, \qquad \forall\, s \in \mathcal{S},\ g \in \mathcal{G},\ j \in \mathcal{J}_1^N \tag{3.8a}$$

$$m_{s,g,j} \leq \tilde{\gamma}_{s,g,j} M, \qquad \forall\, s \in \mathcal{S},\ g \in \mathcal{G},\ j \in \mathcal{J}_1^N \tag{3.8b}$$

$$m_{s,g,j} - f^m\left(x_j, u_{j-1}\right) \leq (1 - \tilde{\gamma}_{s,g,j}) M, \qquad \forall\, s \in \mathcal{S},\ g \in \mathcal{G},\ j \in \mathcal{J}_1^N \tag{3.8c}$$

$$m_{s,g,j} - f^m\left(x_j, u_{j-1}\right) \geq -(1 - \tilde{\gamma}_{s,g,j}) M, \qquad \forall\, s \in \mathcal{S},\ g \in \mathcal{G},\ j \in \mathcal{J}_1^N \tag{3.8d}$$

Finally, the inventory model is then given by:

$$I_{s,g,j} = I_{s,g,j-1} + m_{s,g,j} - D_{s,g,j}, \qquad \forall\, s \in \mathcal{S},\ g \in \mathcal{G},\ j \in \mathcal{J}_1^N \tag{3.9a}$$

$$D_{s,g,j} + B_{s,g,j} = D^n_{s,g,j}, \qquad \forall\, s \in \mathcal{S},\ g \in \mathcal{G},\ j \in \mathcal{J}_1^N \tag{3.9b}$$

$$I_{s,g,j},\ D_{s,g,j},\ B_{s,g,j} \geq 0, \qquad \forall\, s \in \mathcal{S},\ g \in \mathcal{G},\ j \in \mathcal{J}_1^N \tag{3.9c}$$

where $I_{s,g,j}$ gives the amount of grade g in inventory in scenario s at time step j, $B_{s,g,j}$ is the amount of the demand $D^n_{s,g,j}$ that could not be met (backorder amount), $D_{s,g,j} \leq D^n_{s,g,j}$ is the demand met.

Remarks

Note that some of the scheduling variables are defined for time steps $j < 1$. That is to allow for some past information to be taken into account when solving the current DRTO problem. If past information is not taken into account, at every DRTO execution, any targeted

grade will have to be produced within spec for at least L consecutive time steps to meet the constraints in Eqs. (3.6) - (3.7), even if storage of the given grade had already started in the immediate previous time steps. To avoid this behavior, we introduce the parameter $z^{plant}_{g,j}$ and Eq. (3.10).

$$z^{targ}_{s,g,j} \leq z^{plant}_{g,j}, \quad s \in \mathcal{S},\ g \in \mathcal{G},\ j \in \mathcal{J}^0_{-L+1} \tag{3.10}$$

$z^{plant}_{g,j}$ is set to one if all the measured plant outputs were within their target quality band for grade g at some previous time step j. The DRTO can then choose whether or not to let $z^{targ}_{s,g,j}$ equal $z^{plant}_{g,j}$ for some $j < 1$ via Eq. (3.10). For appropriate values of $z^{plant}_{g,j}$, this mechanism allows the current DRTO execution to stop storing a given grade at some time step $j < L$, and still meet the constraints in Eqs. (3.6) - (3.7). We also set $\gamma_{s,g,0}$ to one at the current DRTO execution if $\sum_{j \in \mathcal{J}^0_{-H+1}} z^{plant}_{g,j} = H$, since this indicates that at the previous execution, the DRTO was going to start storage of grade g. This forces production of grade g to continue during the current execution.

The parameter values L, H and N^z should be chosen based on process features, and/or via closed-loop simulations. For example, if the process is known to have an oscillatory behavior, H can be set to a higher value to ensure that the outputs are settled within the quality target band before starting storage. L and N^z can be chosen to reflect limitations regarding equipment and personnel when switching production from one grade to another. For instance, if switching production grades is considered complex from an equipment preparation and personnel availability point of view, it may be preferable to have a lower N^z and a higher L.

3.2.3 Objective function

The objective function used in this study aims to achieve good economic and process performance. It is given by:

$$\Phi = c^{ECO}\Phi^{ECO} + c^{P}\Phi^{P} + c^{I}\Phi^{I} \tag{3.11}$$

where $c^i \geq 0$ is a weighting coefficient and Φ^i represents different and potentially competing objective goals. Φ^{ECO} is an economic objective, Φ^P deals with the process and control

performance, and Φ^I imposes soft targets on the inventory levels. Each term is further defined bellow:

- Economic objective Φ^{ECO}

$$\begin{aligned}\Phi^{ECO} = \sum_{s\in\mathcal{S}}\sum_{g\in\mathcal{G}}\sum_{j\in\mathcal{J}_1^N}\rho_s\left(C^G_{s,g,j}D_{s,g,j} - C^I_{s,g,j}I_{s,g,j-1} - C^B_{s,g,j}B_{s,g,j}\right)\\ -\sum_{s\in\mathcal{S}}\sum_{i\in\mathcal{U}}\sum_{j\in\mathcal{J}_0^{N-1}}\rho_s C^U_{s,i,j}u_{s,i,j}\end{aligned} \tag{3.12}$$

$C^k_{s,i,j}$ denotes possibly time-varying cost coefficients that could also be uncertain. The term in parentheses accounts for the revenue from sales, the inventory cost and the cost incurred for not meeting a given demand order. The last term corresponds to the input costs.

- Control and process performance Φ^P

$$\Phi^P = -\sum_{s\in\mathcal{S}}\sum_{j\in\mathcal{J}_1^N}\rho_s\left(\sum_{i\in\mathcal{Y}}c^y_i P^y_{s,i,j} + \sum_{i\in\mathcal{U}}c^u_i P^u_{s,i,j-1}\right) \tag{3.13}$$

The first term between parentheses penalizes deviation of the output from the target value $y^{targ}_{s,i,j}$ during the production period. The deviation is measured by the variable $P^y_{s,i,j}\in\mathcal{R}$ utilizing the construct in Eq. (3.14).

$$y^{\text{DRTO}}_{s,i,j} - y^{targ}_{s,i,j} + p^a_{s,i,j} - p^b_{s,i,j} = 0, \qquad s\in\mathcal{S},\ i\in\mathcal{Y},\ j\in\mathcal{J}_1^N \tag{3.14a}$$

$$P^y_{s,i,j} - p^a_{s,i,j} - p^b_{s,i,j} \geq -\left(1-\sum_{g\in\mathcal{G}}\tilde{\gamma}_{s,g,j}\right)M \qquad s\in\mathcal{S},\ i\in\mathcal{Y},\ j\in\mathcal{J}_1^N \tag{3.14b}$$

$$p^a_{s,i,j}, p^b_{s,i,j}, P^y_{s,i,j} \geq 0, \qquad s\in\mathcal{S},\ i\in\mathcal{Y},\ j\in\mathcal{J}_1^N \tag{3.14c}$$

The second term aims to suppress input moves during the production period. The magnitude of the input move between consecutive time steps is given by $P^u_{s,i,j}\in\mathcal{R}$ computed in Eq. (3.15).

$$u^{\text{DRTO}}_{s,i,j} - u^{\text{DRTO}}_{s,i,j-1} + p^c_{s,j} - p^d_{s,j} = 0, \qquad s\in\mathcal{S},\ i\in\mathcal{U},\ j\in\mathcal{J}_0^{N-1} \tag{3.15a}$$

$$P^u_{s,i,j} - p^c_{s,i,j} - p^d_{s,i,j} \geq -\left(1 - \sum_{g \in \mathcal{G}} \tilde{\gamma}_{s,g,j}\right) M \quad s \in \mathcal{S},\ i \in \mathcal{U},\ j \in \mathcal{J}_0^{N-1} \tag{3.15b}$$

$$p^c_{s,i,j}, p^d_{s,i,j}, P^u_{s,i,j} \geq 0, \quad s \in \mathcal{S},\ i \in \mathcal{U},\ j \in \mathcal{J}_0^{N-1} \tag{3.15c}$$

In Eqs. (3.14) and (3.15), $p^a_{s,i,j}$, $p^b_{s,i,j}$, $p^c_{s,i,j}$ and $p^d_{s,i,j}$ are slack variables. M is a sufficiently large constant that makes the respective constraint inactive outside the production period. $c^y_i \geq 0$ and $c^u_i \geq 0$ in (3.13) are weighting coefficients.

- Inventory level objective Φ^I

$$\Phi^I = \sum_{s \in \mathcal{S}} \sum_{g \in \mathcal{G}} \rho_s V^I_{s,g} \tag{3.16}$$

The term $V^I_{s,g}$ is defined as $C^S_g \min(I_{s,g,N}, I^{max}_g)$, where $C^S_g \geq 0$ is the value of having grade g in inventory. This construct bounds $V^I_{s,g}$ from above by $C^S_g I^{max}_g$. The goal is to prevent complete inventory depletion, and indefinite inventory build-up. To avoid the non-smoothness introduced with a min operator, we can reformulate (3.16) for $c^I > 0$ in Eq. (3.11) as:

$$V^I_{s,g} \leq C^S_g I^{max}_g, \quad s \in \mathcal{S},\ g \in \mathcal{G} \tag{3.17a}$$

$$V^I_{s,g} \leq C^S_g I_{s,g,N}, \quad s \in \mathcal{S},\ g \in \mathcal{G} \tag{3.17b}$$

For $c^I = 0$, Eq. (3.17) does not play any role in the problem solution.

The values of the weighting coefficients c^{ECO}, c^P and c^I can be chosen via trial and error combined with closed-loop process simulations.

3.2.4 Nonanticipativity constraints

Nonanticipativity constraints link some or all of the scenarios, and guarantee that decisions taken before the uncertainty realization and based on the same information are equal [3]. Commonly, nonanticipativity constraints are defined according to the uncertainties modeled,

but they can also be defined in a manner that simplifies the overall problem [2], for example, to reduce a multi-stage to a two-stage stochastic problem. For the DRTO formulation presented in this study, independent of the uncertainties modeled, nonanticipativity constraints are required to ensure that the reference trajectory $y^{\text{ref}}_{s,j}$ and production sequence $\gamma_{s,g,j}$ are equal across all scenarios for at least the first $\Delta t^{\text{DRTO}}/\Delta t$ time steps of each DRTO execution:

$$y^{\text{ref}}_{s',j} = y^{\text{ref}}_{s,j} \qquad s \in \mathcal{S} - \{s'\},\ j \in \mathcal{J}_1^{N_{NAC}}$$
$$\gamma_{s',g,j} = \gamma_{s,g,j} \qquad s \in \mathcal{S} - \{s'\},\ j \in \mathcal{J}_1^{N_{NAC}}$$

where s' is some scenario in $\mathcal{S}$ and $N_{NAC} \geq \Delta t^{\text{DRTO}}/\Delta t$. Additional nonanticipativity constraints may be required depending on the uncertainties considered. For example, in case of demand and model uncertainty, another set of nonanticipativity constraints has to be used to ensure that the reference trajectory and scheduling decisions are the same across scenarios with the same process model for all time steps $j \leq \tau_1^D$, where τ_1^D is the time step that the next immediate uncertain demand order is due. Case specific examples are given in the next section.

3.3 Case studies

In this section, we consider implementation of the proposed integrated scheduling and control formulation, using the two-layer paradigm in Fig. 3.1, to a linear and nonlinear process model.

The integrated scheduling and control problem is solved at the DRTO layer at every time period Δt^{DRTO}. It computes optimal reference trajectories $y^{\text{ref}}_{s,j}$ as set-points to the lower-level PI controllers, which are executed at higher frequency $\Delta t \leq \Delta t^{\text{DRTO}}$. The lower-level PI controllers compute the input values u_j applied to the plant. Mirroring the scheduling constraints implemented at the DRTO layer, if the measured outputs (at the plant level) are within the target quality band for a given grade g and $\gamma_{s,g,j} = 1$ for the corresponding time step j, then $z^{plant}_{g,j}$ is set to one. Note that the nonanticipativity constraints require $\gamma_{s,g,j}$ and

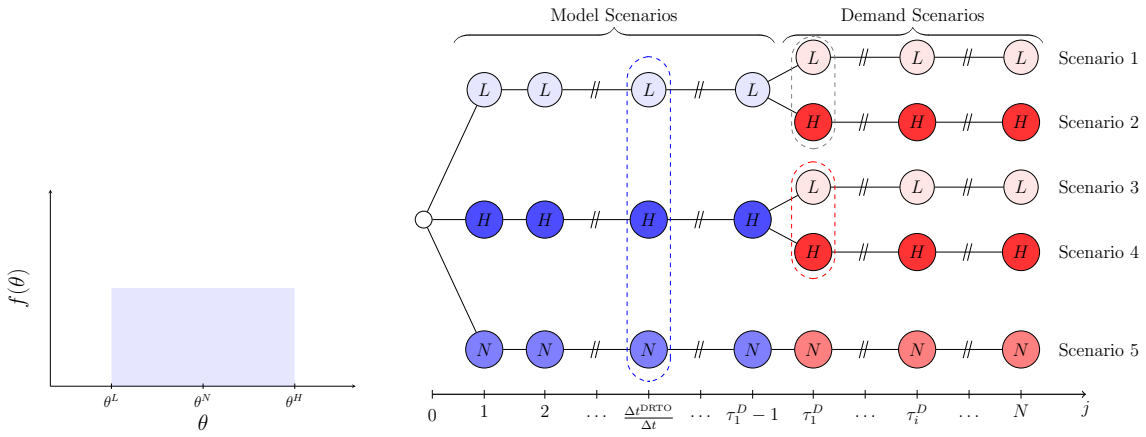

Figure 3.3. Schematic representation of (a) uniform probability distribution and discretization points, and (b) scenario-tree used in the DRTO formulation for Case 1.

$y^{\text{ref}}_{s,j}$ to have the same value across all scenarios for $j \leq \Delta t^{\text{DRTO}}/\Delta t$. Storage at the plant level starts once the quality target requirements for grade g are met for H consecutive steps, that is $\sum_{k\in\mathcal{J}^0_{-H+1}} z^{plant}_{g,k} = H$ at the current time step.

At every DRTO execution, the inventory level $I_{s,g,0}$, measurements y^m_{j*}, $\gamma_{s,g,0}$, and $z^{plant}_{s,k} \forall\, s \in \mathcal{S},\ k \in \mathcal{J}^0_{-L+1}$ are updated using feedback information from the plant. $\gamma_{s,g,0}\ \forall s \in \mathcal{S}$ is set to one if $\sum_{k\in\mathcal{J}^0_{-H+1}} z^{plant}_{g,k} = H$, that is, the output has been meeting the target quality requirements for grade g for the past H time steps. On the other hand, $x^{\text{DRTO}}_{s,0}$, $\tilde{E}_{s,-1}$, $\tilde{u}^{PI}_{s,-1}$, $y^{\text{DRTO}}_{s,0}$ and $u^{\text{DRTO}}_{s,-1}$ are set to their predicted values at the previous DRTO execution.

We assume that all uncertain parameters follow a uniform distribution. Each distribution is discretized yielding three scenarios: nominal (N), high (H) and low (L). The nominal scenario corresponds to the mean of the distribution, while the high and low scenario correspond to its extremities, as indicated in Fig. 3.3a for an uncertain parameter $\theta \in \mathcal{R}$. The discrete scenarios for each uncertain parameter are combined to form the set $\mathcal{S}$ used in the DRTO formulation. This set may be updated at every DRTO execution to take into account new information.

We compare two DRTO formulations. The first one, referred to here as robust DRTO, corresponds to the DRTO formulation presented in the previous sections. It accounts for uncertainty via scenarios. The second one is a nominal DRTO formulation, where uncertainty

is neglected and the uncertain parameters are assumed to equal their expected values, which corresponds to θ^N in Fig. 3.3a. The nominal DRTO constitutes a special case of the robust DRTO with a single scenario, and no nonanticipativity constraints.

To carry out the comparison, we perform 45 simulations for each DRTO implementation, where for each simulation, a scenario $s \in \mathcal{S}^{plant}$ is realized at the plant level. The set $\mathcal{S}^{plant}$ is formed via random sampling of the probability distribution of the uncertain parameters. We define an economic performance metric (EPM) derived from the DRTO objective function, Eq. (3.11), whose value is calculated as follows. Utilizing the simulation data, we compute the expected objective at the plant level using Eqs. (3.11)-(3.17) but with c^P set to zero, the DRTO horizon N replaced by the simulation horizon, $\mathcal{S}$ taken as the set of randomly sampled scenarios $\mathcal{S}^{plant}$, and $\rho_s = 1/45$. The value of the stochastic solution (VSS) is the difference between the expected objective value achieved with the robust and nominal DRTO implementations.

For all case studies, the integrated scheduling and control problem is solved using Gurobi, to an optimality gap of 3% on a 2.60 GHz, AMD EPYC 7H12 64-Core processor with 512 GB RAM running Windows Server 2019.

3.3.1 Case 1: Linear Dynamic System

Consider the two-CSTR model adapted from [13], where a first-order reaction takes place (Fig. 3.4):

$$\frac{dC_{A1}}{dt} = \frac{F}{V}(C_{A0} - C_{A1}) - kC_{A1} \tag{3.18}$$

$$\frac{dC_{A2}}{dt} = \frac{F}{V}(C_{A1} - C_{A2}) - kC_{A2} \tag{3.19}$$

F is the flow rate, V is the volume of each reactor, k is the rate constant, C_{Ai} is the concentration of reactant in reactor i for $i = 1, 2$, and C_{A0} is the inlet concentration of reactant to the first reactor. The manipulated variable u is taken to be the inlet concentration C_{A0} while the output variable y is the outlet concentration of the second tank C_{A2}. This single-input

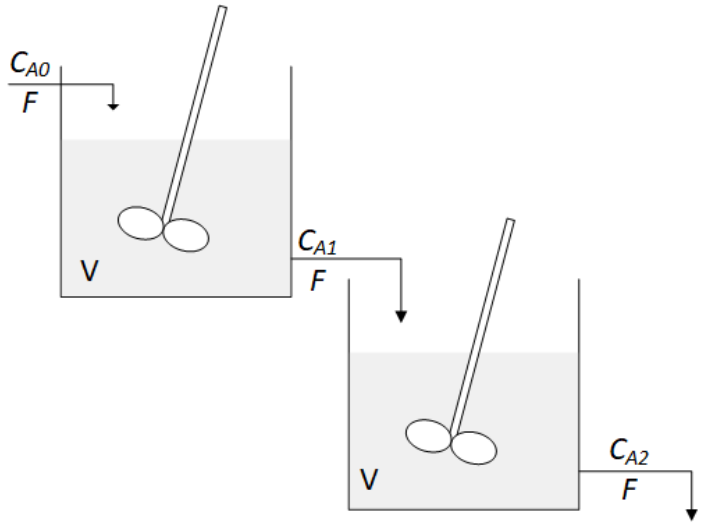

Figure 3.4. Illustration of two-CSTR in series for Case 1.

single-output (SISO) system produces three different product grades. There is uncertainty in the value of the rate constant k and demand levels $D^n_{s,g,j}$. The model uncertainty translates to uncertainty in the gain (K) and time constant (τ) of the process model transfer function $G = K/(\tau s + 1)^2$.

A schematic representation of the scenarios used in the DRTO formulation is given in Fig. 3.3b. The model uncertainty is responsible for the first branching of the tree, while the demand uncertainty leads to the second branching at τ_1^D. The letter within each color coded node indicates the value assume by an uncertain parameter. For example, in Scenario 3 the rate constant k assumes a value corresponding to θ^H (Fig. 3.3a) in its probability distribution, while $D^n_{s,g,j}$ assumes a value corresponding to θ^L for the demand probability distribution at time step j. The nonanticipativity constraints are represented by the dashed enclosures. There is one set of nonanticipativity constraints due to model uncertainty,

$$y^{\text{ref}}_{(L,L)_1,j} = y^{\text{ref}}_{s,j} \qquad \forall\, s \in \mathcal{S} - \{(L,L)_1\},\ j \in \mathcal{J}_1^{N_{NAC}} \tag{3.20a}$$

$$\gamma_{(L,L)_1,g,j} = \gamma_{s,g,j} \qquad \forall\, s \in \mathcal{S} - \{(L,L)_1\},\ j \in \mathcal{J}_1^{N_{NAC}},\ g \in \mathcal{G} \tag{3.20b}$$

and two sets due to demand uncertainty:

$$\text{Set 1}\begin{cases} y^{\text{ref}}_{(L,L)_1,j} = y^{\text{ref}}_{(L,H)_2,j} & j \in \mathcal{J}^{\tau_1^D}_{N_{NAC}+1} \quad (3.21a)\\ \gamma_{(L,L)_1,g,j} = \gamma_{(L,H)_2,g,j} & j \in \mathcal{J}^{\tau_1^D}_{N_{NAC}+1},\ g \in \mathcal{G} \quad (3.21b)\\ m_{(L,L)_1,g,j} = m_{(L,H)_2,g,j} & j \in \mathcal{J}^{\tau_1^D}_{1},\ g \in \mathcal{G} \quad (3.21c)\end{cases}$$

$$\text{Set 2}\begin{cases} y^{\text{ref}}_{(H,L)_3,j} = y^{\text{ref}}_{(H,H)_4,j} & j \in \mathcal{J}^{\tau_1^D}_{N_{NAC}+1} \quad (3.21d)\\ \gamma_{(H,L)_3,g,j} = \gamma_{(H,H)_4,g,j} & j \in \mathcal{J}^{\tau_1^D}_{N_{NAC}+1},\ g \in \mathcal{G} \quad (3.21e)\\ m_{(H,L)_3,g,j} = m_{(H,H)_4,g,j} & j \in \mathcal{J}^{\tau_1^D}_{1},\ g \in \mathcal{G} \quad (3.21f)\end{cases}$$

where $N_{NAC} = \Delta t^{\text{DRTO}}/\Delta t$. We have that $\mathcal{S} = \{(L,L)_1, (L,H)_2, (H,L)_3, (H,H)_4, (N,N)_5\}$, where in the pair $(i,j)_s$, i and j indicate the value assumed by the uncertain parameters k and $D^n_{s,g,j}$, respectively, in scenario s. For any uncertain parameter $\theta \in \mathcal{R}$ in the present case study, we have that $\theta^H = 1.2\theta^N$, and $\theta^L = 0.8\theta^N$ (see Fig. 3.3a). Note that within a given DRTO execution, the demand uncertainty is assumed to be resolved at time τ_1^D. This is to simplify the scenario tree, but in fact the demand levels of future orders, for example at time step τ_i^D, can also be uncertain.

The non-zero nominal demand levels (θ^N) are given in Table 3.1. The nominal value (θ^N) of the rate constant is $k = 0.1$ min^{-1}. We also have that $F = 0.085$m^3/min, and $V = 1.05$ m^3, $0 \le u \le 4$, $0 \le y \le 1$ and $0 \le y^{\text{ref}} \le 1$, and $f^m(\cdot) = F\Delta t$. Additional parameter values are provided in Table 3.1, and Table 3.2.

Table 3.1. Quality targets y^{target} (mol/m^3), quality target tolerance (ϵ), inventory cost C^I (\$/m^3), unmet demand cost C^B (\$/m^3), input costs C^U (\$/mol), product value C^G (\$/m^3), inventory value C^S (\$/m^3), inventory level parameter I^{max} (m^3), mean demand level D^n (m^3) and demand time t^D (min) for Case 1.

Grade	y^{target}	ϵ	C^G	C^S	C^I	C^B	C^U	I^{max}	D^n [t^D]
A	0.25	0.01	200	60	2	205	15	4.5	3.5[60], 2.0[195]
B	0.4	0.015	150	75	1	170	15	4.5	3.0[108], 2.5[270]
C	0.6	0.02	130	110	5	230	15	4.5	2.5[180], 2.5[285]

Table 3.2. DRTO parameters for Case 1.

Parameter	Value
t^{sim}	195 min
Δt	3 min
Δt^{DRTO}	9
N_{NAC}	3
N^z	2
N	30
H	3
L	8
c^{ECO}	0.01
c^P	1
c^I	0.01
c^y	0.5
c^u	0.03

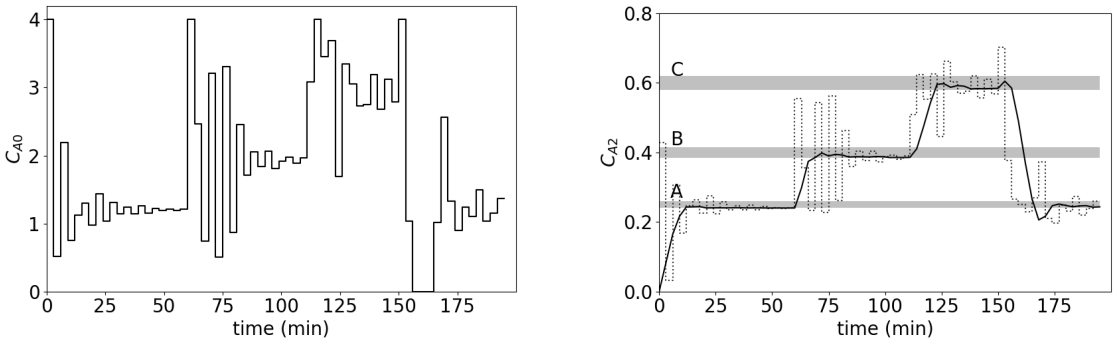

(a) (b)

Figure 3.5. (a) Input, (b) output (solid line) and reference trajectory (dashed line) for the robust DRTO implementation, and realization of the nominal value of the uncertainty in Case 1a.

Case 1a: $c^P = 0$ In this first subcase, we do not penalize the control performance on the DRTO objective function (Eq. (3.11)). The plant output, control and reference trajectory for the robust DRTO and realization of the nominal scenario are shown in Fig. 3.5.

Note that the reference trajectory and input values oscillate frequently, even during the production period. Moreover, the output is often at the boundary of the quality target band since this is economically optimal. This type of control performance may be undesirable in an industrial facility, and the output can be easily driven out of the target quality band by disturbances, since it is at its boundary.

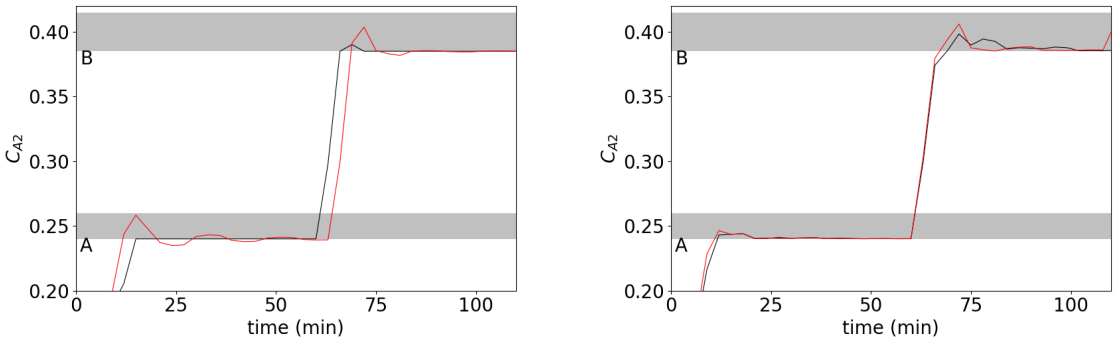

(a) (b)

Figure 3.6. Output trajectory for (a) nominal and (b) robust DRTO implementation, for realization of the nominal scenario (black line) and a randomly sampled scenario (red line) in Case 1a.

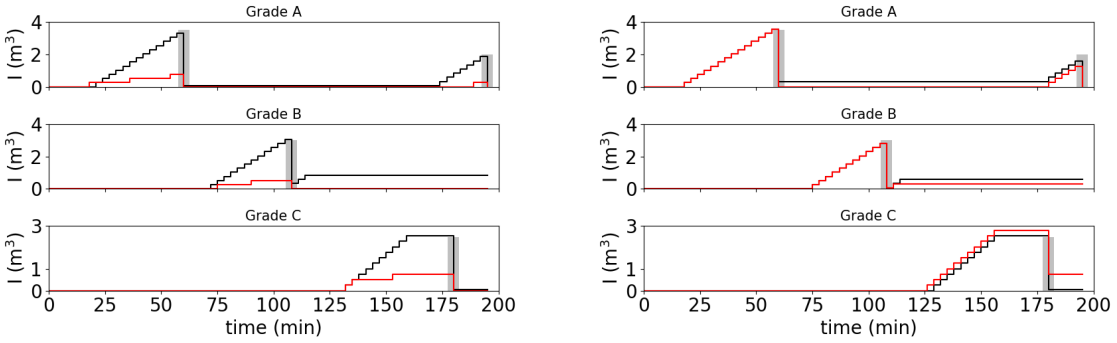

(a) (b)

Figure 3.7. Inventory trajectory for the (a) nominal and (b) robust DRTO implementation, for realization of the nominal scenario (black line) and a randomly sampled scenario (red line) in Case 1a.

The EPM values for the nominal and robust DRTO implementation, given in Table 3.3, indicate that it is advantageous to account for uncertainty in the DRTO formulation. This is largely due to the rather poor performance of the nominal DRTO that is unable to lead the plant to produce viable product in some of the scenarios. This is usually characterized by the output being just outside the quality target band. We can see this in Fig. 3.6a. On the other hand, the robust DRTO is able to drive the output to meet the quality specifications for different realizations of the model uncertainty k (Fig. 3.6b). These are also reflected on the inventory levels as shown in Fig. 3.7.

Table 3.3. Economic performance metric values ($) for nominal and robust DRTO implementations. In Cases 1a-1b, demand and model uncertainty are both accounted for in the robust DRTO formulation. In Case 1c, only model uncertainty is accounted for, and in Case 1d, only demand uncertainty.

Case	Nominal	Robust	VSS
Case 1a	-1,755.87	854.22	2,610.09
Case 1b	728.54	965.97	237.43
Case 1c	728.54	810.42	81.88
Case 1d	728.54	861.75	133.21

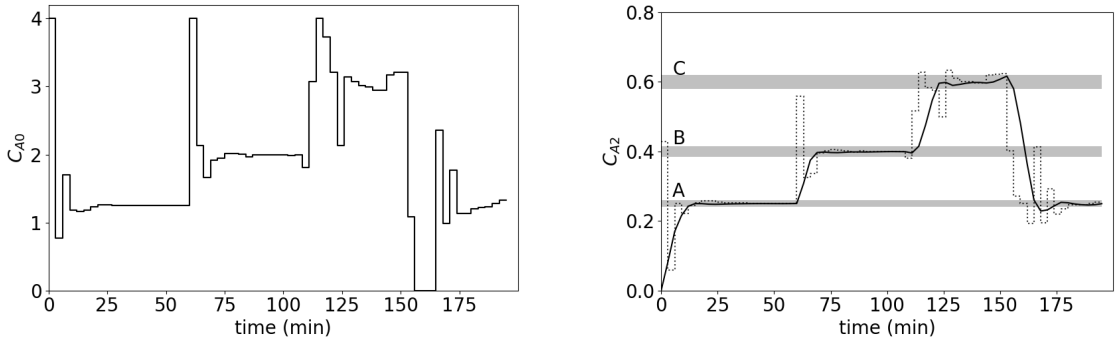

(a) (b)

Figure 3.8. (a) Input values and (b) output (solid line) and reference trajectory (dashed line) for robust DRTO implementation, assuming realization of the nominal scenario in Case 1b.

Case 1b: $c^P = 1$ In this case, we account for the control performance in the DRTO objective function (Eq. (3.11)). Input, output and reference trajectory values for the robust DRTO implementation assuming realization of the nominal scenario are given in Fig. 3.8. The input and reference trajectories oscillate considerably less than in Case 1a (see Fig. 3.5). The EPM value is given in Table 3.3.

There is a significant increase in the EPM value for the nominal DRTO implementation compared to the previous case. The reason is that the $c^P\Phi^P$ term in the objective function forces the output to the interior of the quality target band. Therefore, in case of disturbances affecting the system, there is room to react before the output is driven out of the quality target band. This is clear in Figs. 3.9-3.10, where the output trajectory and inventory levels for the same scenarios as given in Fig. 3.6 and 3.7 are displayed. For similar reasons, the EPM for the robust DRTO implementation is also better than in the previous subcase.

Despite significant improvement in the nominal DRTO, solving the stochastic problem at the

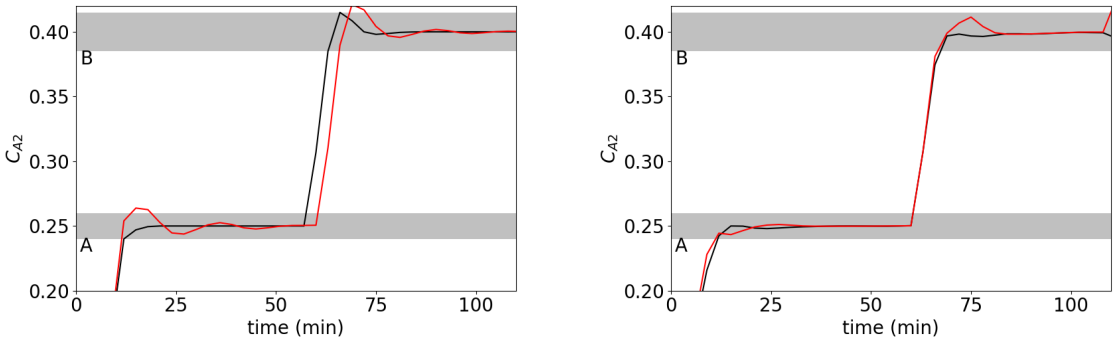

(a) (b)

Figure 3.9. Output trajectory for (a) nominal and (b) robust DRTO implementation, for realization of the nominal scenario (black line) and a randomly sampled scenario (red line) in Case 1b.

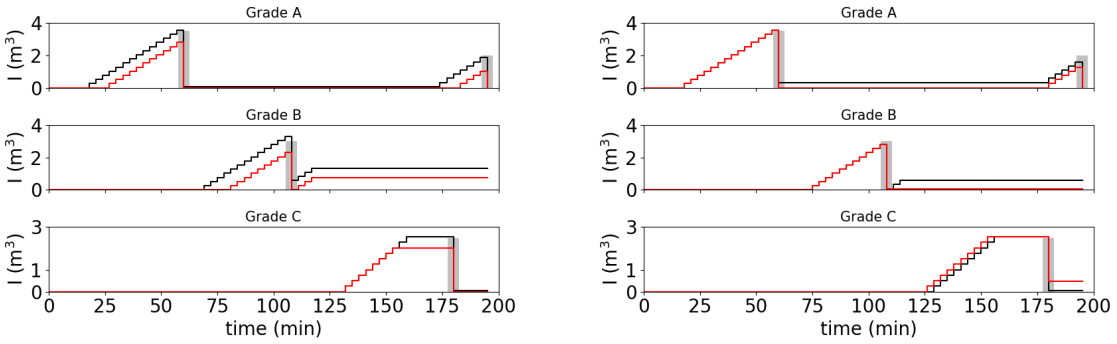

(a) (b)

Figure 3.10. Inventory trajectory for (a) nominal and (b) robust DRTO implementation, for realization of the nominal scenario (black line) and a randomly sampled scenario (red line) in Case 1b.

DRTO level is still advantageous since it leads to a 32% increase in the expected economic performance of the plant. One of the reasons why the robust DRTO outperforms the nominal is that it is able to damp the oscillatory behavior of the output in some of the scenarios, maximizing productivity (Fig. 3.9-3.10).

Cases 1c-1d: Effect of uncertainty In this case study, we explore the effect of accounting for different uncertainties in the DRTO formulation. As in the previous cases, model and demand uncertainty are neglected in the nominal DRTO formulation, and the uncertain parameters are assumed to equal their expected (nominal) values. We consider two distinct robust DRTO formulations. In the first one (Case 1c), we account only for model uncertainty, while in the second one (Case 1d), we account only for demand uncertainty. For all cases, there are always demand and model uncertainty at the plant level, and the scenario $\mathcal{S}^{plant}$ is the same used in the previous cases studies. The computed performance metric values are given in Table 3.3.

For this particular case study, the demand uncertainty has a more significant impact on the expected economic performance. Not accounting for demand uncertainty (Case 1c) leads to a 16% decrease in the EPM compared to Case 1b, while not accounting for model uncertainty (Case 1d) leads to a 11% decrease in the expected economic performance. This result is also influenced by the term $c^P\Phi^P$, which acts as a backoff constraint for both uncertainty types but has a greater impact on model uncertainty. In either case, accounting for at least one uncertainty type leads to better economic performance compared to the nominal case, and can be an alternative if the computational cost incurred when accounting for multiple uncertainty types is prohibitively high. The average solution times for the robust DRTO problem are 20.14, 9.02 and 4.45 seconds for Cases 1b, 1c and 1d, respectively.

Case 1e: The effect of $\Delta t^{DRTO}/\Delta t$ We study the effect of the frequency of execution of the DRTO layer for the case where model and demand uncertainty are accounted for in the DRTO formulation.

Overall, the EPM values, displayed in Table 3.4, decrease with decreasing frequency of

Table 3.4. Ecomomic performance metric values ($) for nominal and robust DRTO implementations for distinct Δt^{DRTO} in Case 1e.

Δt^{DRTO} (min)	N_{NAC}	Nominal	Robust	VSS
6	2	810.89	995.92	185.03
9	3	728.54	965.97	237.43
12	4	651.10	835.41	184.31
15	5	486.71	588.11	101.04
18	6	500.33	634.99	134.66

execution of the DRTO layer for both the nominal and robust DRTO implementations. That is partially due to the reduced feedback frequency regarding the plant states (i.e. inventory levels, output measurements), but the results are also influenced by how soon the DRTO sees new demand information. In particular, DRTOs executed at a higher frequency do not necessarily see new information earlier than DRTOs executed at lower frequencies. For example, for the present case, DRTOs executed at every 6, 9 and 18 min all see the demand of grade B for the first time at simulation time 18 min. DRTOs executed at every 12 and 15 min see the demand of grade B at simulation time 24 and 30 respectively, and have less time to react to the new information. Due to this, the DRTO executed every 15 min incurs higher costs for not meeting the demand of grade B, which helps to explain why the economic performance for $\Delta t^{\text{DRTO}} = 15$ min is lower than for $\Delta t^{\text{DRTO}} = 18$ min.

In Fig 3.11, we show the box plots for each case presented in Table 3.4. They show that the worst case scenario for the robust DRTO implementation is always better than for the nominal one, and that the objective range (difference between best and worst objective values) increases with decreasing feedback frequency.

For some of the lower frequencies, the robust DRTO problem could not be solved to the required optimality gap within the process sampling time Δt. The reason is that decreasing the DRTO frequency while having $N_{NAC} = \Delta t^{\text{DRTO}} / \Delta t$ leads to a problem more difficult to solve due to a higher number of non-anticipativity constraint (see Eq. (3.20)). In those cases, the best available feasible solution was then provided to the lower-level PI controller. Despite this, we see that the robust DRTO outperforms the nominal DRTO for all execution frequencies tested.

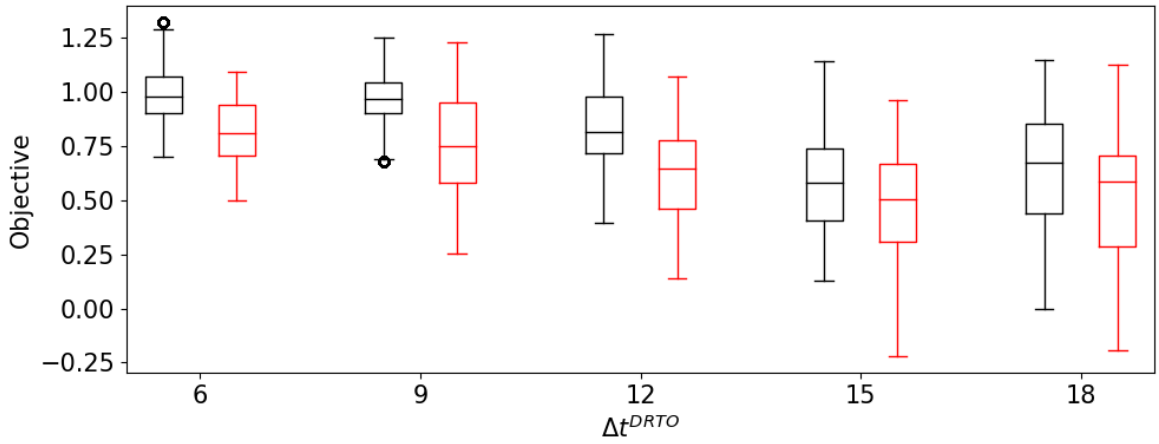

Figure 3.11. Box plots of objective (EPM) values for Case 1e for the robust (black) and nominal (red) DRTO implementations. Each box plot is built using 45 data-points, obtained from the simulation of each scenario in the set $\mathcal{S}^{plant}$. The objective values are in thousands of dollars.

3.3.2 Case 2: Nonlinear CSTR

In this second case study, we consider a nonlinear CSTR model, adapted from [10], where an exothermic reaction $A \rightarrow B$ takes place. The dynamic model is given by,

$$\frac{dT}{dt} = \frac{F}{V_R}(T_0 - T) - \frac{\Delta H k_0}{\rho c_p} e^{-E/RT} C_A + \frac{Q}{\rho c_p V_R} \tag{3.22a}$$

$$\frac{dC_A}{dt} = \frac{F}{V_R}(C_{A0} - C_A) - k_0 e^{-E/RT} C_A \tag{3.22b}$$

where T_0 and T are the temperature of the inlet and outlet stream, respectively, F is the inlet and outlet flow rate, V_R is the reactor volume, C_{A0} and C_A are the concentration of reactant A in the inlet and outlet stream, ΔH is the heat of reaction, k_0 is the rate constant, E is the activation energy, R is the ideal gas constant, ρ is the density of the contents of the reactor and c_p is the heat capacity. The parameter values can be found in Table 3.5.

The control inputs are $u = [Q, C_{A0}]^T$, and the outputs $y = [T, C_A]^T$. The lower and upper bounds on the outputs, reference trajectory, and control inputs are given by $y_{max} = [360, 6.0]^T$, $y_{min} = [310, 0.5]^T$, $y^{\text{ref}}_{max} = [360, 6.0]^T$, $y^{\text{ref}}_{min} = [300, 0.1]^T$, $u_{max} = [2 \times 10^5, 8]^T$, $u_{min} = [-2 \times 10^5, 0.5]^T$. Additionally, $f^m(\cdot) = F\Delta t$. We design PI controllers for this system with parameter values $K_c = [1, 2]^T$ and $\tau_I = [0.1, 0.2]^T$. This process produces

Table 3.5. Process model parameters values for Case 2.

F	5	m^3/h
V_R	1	m^3
T_0	300	K
R	8.314	kJ/kmolK
ΔH	-1.2×10^4	kJ/kmol
E	5×10^7	kJ/kmol
ρ	1000	kg/m^3
c_p	0.231	kJ/kg m^3

three different product grades. Additional information regarding the problem parameters is provided in Tables 3.6 and 3.7.

Table 3.6. DRTO parameter values for Case 2.

Parameter	Value
t^{sim}	12 h
Δt	0.1 h
N^z	1
N	30
H	3
L	5
c^{ECO}	0.1
c^P	10
c^I	0.1
c^y	$[5,5]^T$
c^u	$[1,1]^T$

Table 3.7. Quality targets y^{target} ($kmol/m^3$), quality target tolerance (ϵ), inventory cost C^I ($/m^3$), unmet demand cost C^B ($/m^3$), product value C^G ($/m^3$), inventory value C^S ($/m^3$), inventory level parameter I^{max} (m^3), mean demand level D^n (m^3) and demand time t^D (h) for Case 2.

Grade	y^{target}	ϵ	C^G	C^S	C^I	C^B	I^{max}	D^n [t^D]
A	$[340,1]^T$	$[2,0.05]^T$	50	50	0.16	350	2	6.0[3], 6.0[8], 6.0[12]
B	$[330,3]^T$	$[2,0.1]^T$	60	60	0.1	100	2	5.0[3], 5.0[7], 5.0[10.5]
C	$[320,5]^T$	$[2,0.1]^T$	40	40	0.32	400	2	6[5], 5[10], 4[14]

The model in Eq. (3.22) is nonlinear; however, we have considered a linear model in the DRTO formulation in Eq. (3.1). Thus, for each scenario $s \in \mathcal{S}$, we use the linearized version of the nonlinear model in the DRTO formulation. There is uncertainty in the rate constant k_0 and in the cost of input Q. There is no uncertainty in the demand level. At each DRTO

execution, the cost of input Q for the next one hour interval is known, but there is uncertainty thereafter. The corresponding scenario tree is shown in Fig. 3.12.

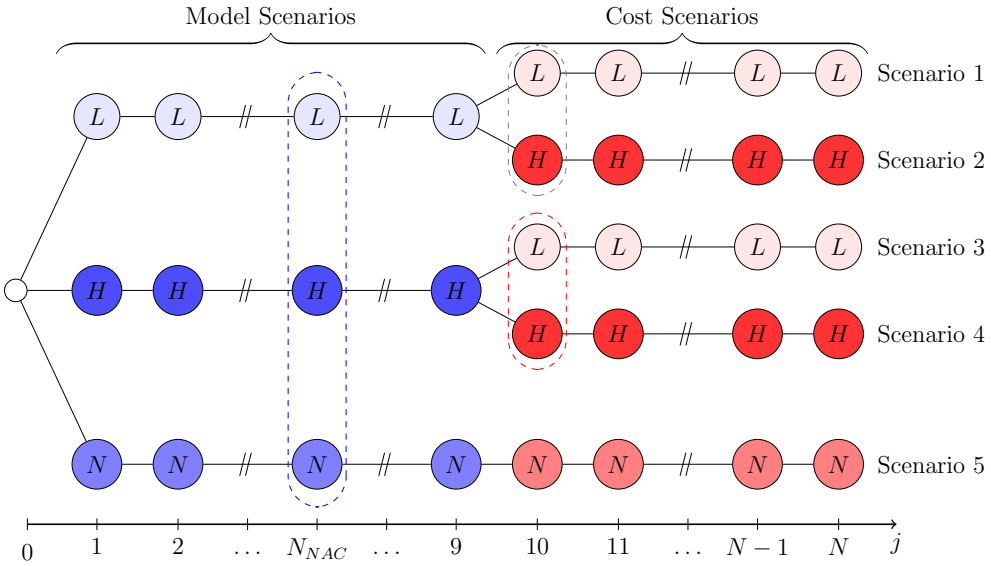

Figure 3.12. Schematic representation of scenario tree used in the robust DRTO in Case 2.

There is one set of nonanticipativity constraints due to model uncertainty

$$y^{\text{ref}}_{(L,L)_1,j} = y^{\text{ref}}_{s,j} \qquad \forall\, s \in \mathcal{S} - \{(L,L)_1\},\ j \in \mathcal{J}_1^{N_{NAC}} \tag{3.23a}$$

$$\gamma_{(L,L)_1,g,j} = \gamma_{s,g,j} \qquad \forall\, s \in \mathcal{S} - \{(L,L)_1\},\ j \in \mathcal{J}_1^{N_{NAC}},\ g \in \mathcal{G} \tag{3.23b}$$

and two sets due to cost uncertainty:

$$\text{Set 1} \begin{cases} y^{\text{ref}}_{(L,L)_1,j} = y^{\text{ref}}_{(L,H)_2,j} & j \in \mathcal{J}^{\tau_Q}_{N_{NAC}+1} \quad (3.24a) \\ \gamma_{(L,L)_1,g,j} = \gamma_{(L,H)_2,g,j} & j \in \mathcal{J}^{\tau_Q}_{N_{NAC}+1},\ g \in \mathcal{G} \quad (3.24b) \\ m_{(L,L)_1,g,j} = m_{(L,H)_2,g,j} & j \in \mathcal{J}^{\tau_Q}_{1},\ g \in \mathcal{G} \quad (3.24c) \end{cases}$$

$$\text{Set 2} \begin{cases} y^{\text{ref}}_{(H,L)_3,j} = y^{\text{ref}}_{(H,H)_4,j} & j \in \mathcal{J}^{\tau_Q}_{N_{NAC}+1} \quad (3.24d) \\ \gamma_{(H,L)_3,g,j} = \gamma_{(H,H)_4,g,j} & j \in \mathcal{J}^{\tau_Q}_{N_{NAC}+1},\ g \in \mathcal{G} \quad (3.24e) \\ m_{(H,L)_3,g,j} = m_{(H,H)_4,g,j} & j \in \mathcal{J}^{\tau_Q}_{1},\ g \in \mathcal{G} \quad (3.24f) \end{cases}$$

where τ_Q indicates the time step after which the cost of input Q is uncertain. Since for the

present case the cost of input Q is known for the next hour but becomes uncertain after that, we use $\tau_Q = 10$.

Similar to Case 1, the scenario set $\mathcal{S}$ used in the DRTO is given by

$$\mathcal{S} = \{(L,L)_1, (L,H)_2, (H,L)_3, (H,H)_4, (N,N)_5\}$$

where in the pair $(i,j)_s$, i and j indicate the value assumed by the uncertain parameters k_0 and $C^U_{s,1,j}$, respectively, in scenario s. The nominal value k_0^N of the uncertain parameter k_0 is taken as the mean of the respective uniform distribution and is given by $k_0^N = 3 \times 10^7$, the other discrete scenarios are taken as $k_0^L = 2.8 \times 10^7$ and $k_0^H = 3.2 \times 10^7$. The cost of input Q at the H and L scenarios is given by $(C^U_{1,j})^H = 1.2(C^U_{1,j})^N$ and $(C^U_{1,j})^L = 0.8(C^U_{1,j})^N$, where $(C^U_{1,j})^N \in \mathcal{R}$ is the nominal cost of input Q at a time step j. Similar to previous case studies, the scenario set $\mathcal{S}^{plant}$ is built via random sampling of the probability distributions of the uncertain parameters. The trajectory of $C^U_{s,1,j}$ for the discrete scenarios L, N and H and some $s \in \mathcal{S}^{plant}$ is shown in Fig 3.13d. $C^U_{s,2,j}$ is set to 1 \$/kmol.

As with the previous case study, 45 simulations are conducted, and the expected plant objective (EPM), without the control and process penalty term, is computed over the set $\mathcal{S}^{plant}$ for the nominal and robust DRTO implementations. The results are presented in Table 3.8. In Fig. 3.14 we present the box plots for Cases 2a-2f. Each box plot is constructed using the 45 simulation data points, one for the realization of each scenario s in the set $\mathcal{S}^{plant}$. Note that in the current case we have a situation of plant-model mismatch since the plant model is nonlinear, but a linear model is used at the DRTO level.

Table 3.8. Economic performance metric (\$) for nominal and robust DRTO implementations for distinct Δt^{DRTO} and N_{NAC} values for Case 2.

Case	Δt^{DRTO} (h)	N_{NAC}	Nominal	Robust	VSS
Case 2a	0.5	5	1,249.71	1,579.28	329.57
Case 2b	0.2	5	1,283.65	1,717.62	433.97
Case 2c	0.2	2	1,283.65	1,283.87	0.22
Case 2d	0.5	5	1,249.71	1,095.93	-153.78
Case 2e	0.5	5	1,249.71	1,522.77	273.06
Case 2f	0.5	5	429.28	1,125.07	695.79

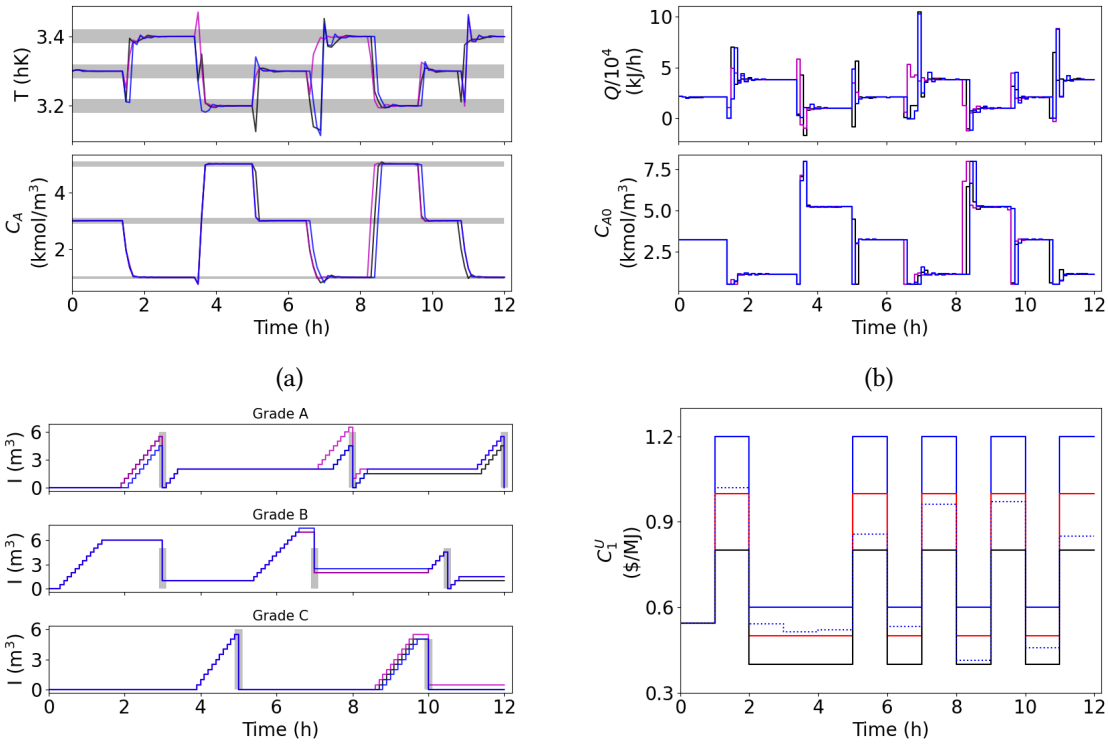

Figure 3.13. (a) Output, (b) input and (c) inventory trajectory for realization of a randomly sampled scenario in Case 2a (black line), 2b (magenta line) and 2c (blue line) and implementation of the robust DRTO. (d) $C^U_{s,1,j}$ trajectories for the discrete scenarios L (black solid line), N (red solid line) and H (blue solid line) and some $s \in \mathcal{S}^{plant}$ (blue dotted line)

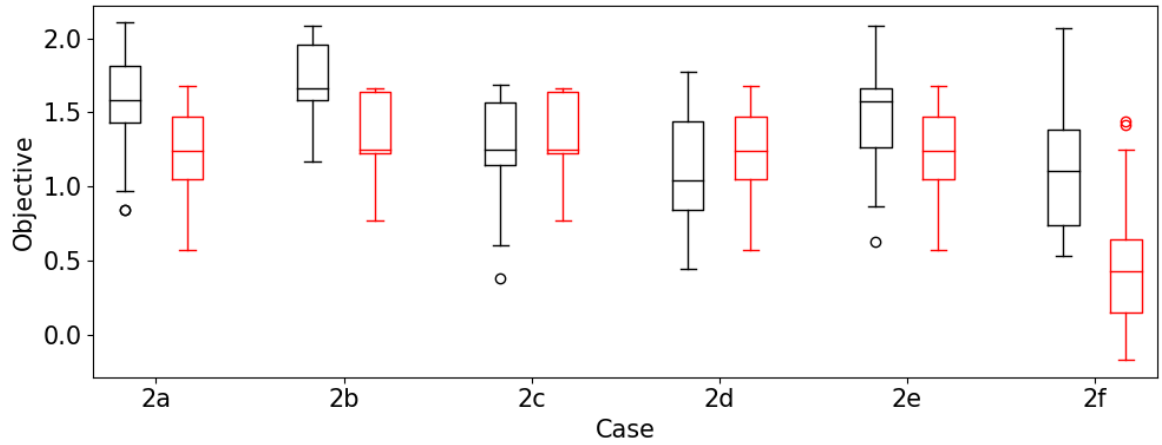

Figure 3.14. Box plots of plant objective (EPM) for the robust (black) and nominal (red) DRTO implementations. Each box plot is constructed from 45 simulation runs. The objective values are in thousands of dollars.

Cases 2a-2c: The effect of N_{NAC} and Δt^{DRTO} The N_{NAC} and Δt^{DRTO} values for each case are presented in Table 3.8. From Case 2a to 2b, we increase the DRTO execution frequency while keeping N_{NAC} constant. From Case 2b to 2c, we decrease N_{NAC} while keeping the execution frequency constant. For $N_{NAC} = 5$ (Cases 2a and 2b), we see that increasing the DRTO execution frequency leads to an improvement in economic performance (Table 3.8). This is similar to what was observed in Case 1e, where we saw that, generally, the economic performance increases with the execution frequency. The unexpected result is in Case 2c, where having $N_{NAC} = 2$ leads to a significant deterioration in the performance of the robust DRTO implementation compared to Cases 2a and 2b. This can also be observed in the box plots in Fig. 3.14, where we see that in Case 2c the robust formulation performs worse than the nominal one for some of the scenarios in $\mathcal{S}^{plant}$.

Output, input, inventory and cost trajectories for a scenario $s \in \mathcal{S}^{plant}$ are presented in Fig. 3.13 for the robust DRTO implementation in Cases 2a-2c. The profiles are not very different; however, only in Case 2b is the demand of grade A at 8h completely met. The evolution of the EPM for Cases 2a-2c is shown in Fig. 3.15a. The step-like increases can be attributed to the accrual of revenue at the discrete demand time points. On average, any revenue from the sales of grade A at 8h in Case 2a is offset by the cost incurred for not being able to completely meet the demand. This is the main cause of the worse performance of Case 2a compared to Case 2b. Additionally, note how the average economic performance achieved with the sales of grades A and B at 3h is lower in Case 2c. That is due to the large cost incurred for not being able to meet a significant amount of the demand of grade A, and the leading reason for the worse performance of the robust implementation in Case 2c. In Figs. 3.15b-3.15d, we show the expected inventory level of grade A, expected reactor temperature and expected reference trajectory across all scenarios in the set $\mathcal{S}^{plant}$. These plots show that, on average, the reference trajectory and reactor temperature in Case 2c take a little longer to settle within the quality target band for grade A between 1 and 3.5 hours. This causes production of grade A to start later, explaining the lower expected inventory level and consequent worse performance of the robust implementation in Case 2c compared to 2a and 2b. This result suggests that lower N_{NAC} values yield less conservative reference trajectories which, in the presence of unmodelled uncertainties, can lead to a deterioration

in performance.

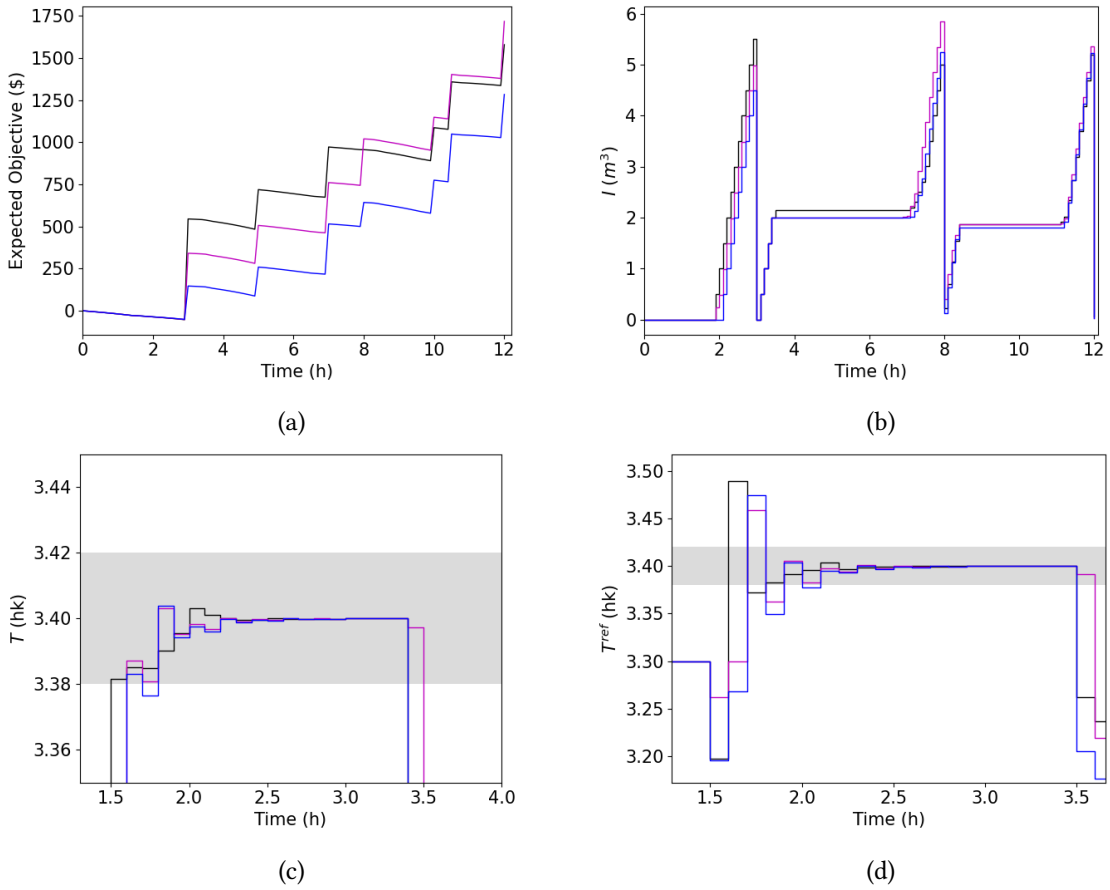

Figure 3.15. Evolution of the expected (a) objective (EPM), (b) inventory level of grade A, (c) reactor temperature, and (d) reference trajectory for the reactor temperature in Cases 2a (black line), 2b (magenta line) and 2c (blue line) for the robust DRTO implementation.

Cases 2d-2e In Case 2d, we only account for cost uncertainty, while in Case 2e, we only account for model uncertainty in the robust DRTO formulation. While in Case 2e we see an EPM value close to the one observed in Case 2a, in Case 2d the nominal DRTO performs better than the robust one. The reason is that it is able to drive the plant to meet a larger portion of the demand of grade A at 8h than the robust counterpart, which we can see in the plot of the economic performance trajectory in Fig. 3.16a. On average, 86% of the demand order of grade A at 8h is met for the robust implementation, against 90% for the nominal DRTO implementation. At 12h, 94% of the demand of grade A is met, on average, for the nominal implementation, against 90% for the robust. This is also reflected in Fig. 3.16b,

where we see that the expected inventory level of grade A at 8 and 12h is lower for the robust implementation.

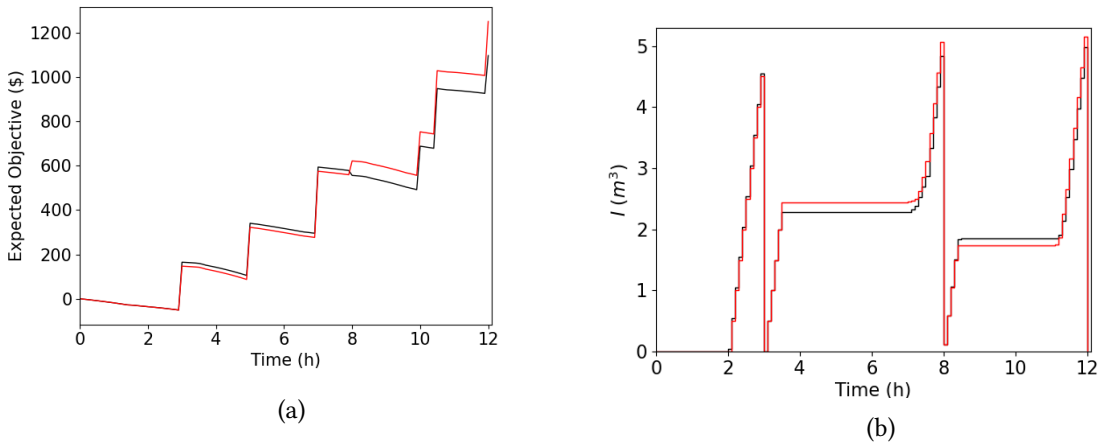

(a) (b)

Figure 3.16. Expected (a) objective (EPM), and (b) inventory level of grade A in Case 2d for the robust (black line) and nominal (red line) DRTO implementations.

The difference between the nominal and robust DRTO implementations in Case 2d is that the robust formulation has information about the cost uncertainty. However, this additional information is offset by the inaccurate process model, leading to worse performance of the robust DRTO. Note that different from Case 2e, in Case 2d the robust formulation does not have information about the model uncertainty.

The temperature required to produce grade A is the highest among all three grades, affecting the cost incurred with input Q. This could lead the DRTO to produce less of product A to minimize the input cost, an effect that is likely to become more pronounced in scenarios where the input cost is higher. Therefore, attempting to mitigate the effect of scenarios with higher input cost on the expected objective, the robust DRTO implementation may find it optimal to produce less of grade A. However, due to plant-model mismatch and missing information about the model uncertainty, the plant is not able to produce the optimal amounts computed by the DRTO.

Case 2f: detuned PI controller In this case, we detune the PI controllers by reducing the gain from $K_c = [1, 2]^T$ to $K_c = [0.5, 1]^T$. In Fig. 3.17, the simulated closed-loop response of the plant (without the DRTO) for the distinct controller gains is presented. The set-points

manually assigned to the PI controllers are given by the dashed line. Observe that the transition times for the temperature increase with decreasing controller gains.

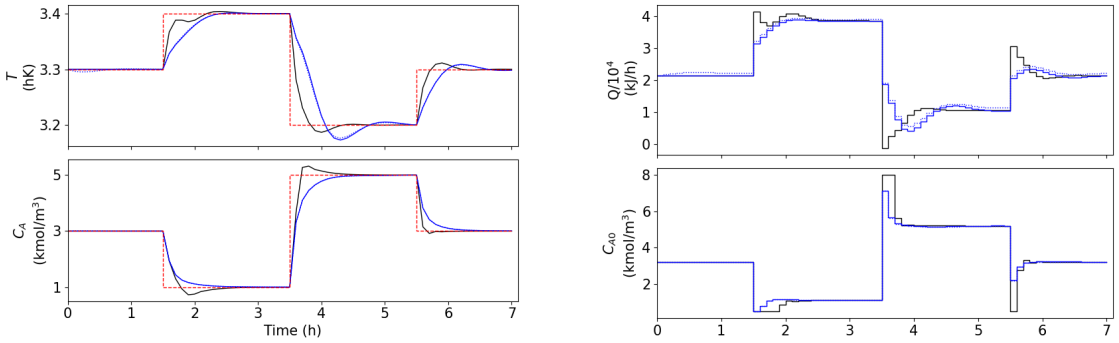

(a) (b)

Figure 3.17. Simulated closed-loop of the nonlinear plant for $k_0^N = 3 \times 10^7$ (solid lines) and $k_0^L = 2.8 \times 10^7$ (dotted line) for PI controllers gains $K_c = [1, 2]^T$ (black line) and $K_c = [0.5, 1]^T$ (blue line). The reference trajectory is given by the dashed red line.

The VSS for this case study is the highest, but there is deterioration in the EPM of the nominal and robust implementations compared to previous cases (Table 3.8). This deterioration is due to the loss of agility in the process transitions with the detuned PI controller, but it is more pronounced in the nominal case. The evolution of the expected plant economic performance and inventory level of grade A is shown in Fig. 3.18. The nominal implementation incurs significant losses at 3 and 8h for not being able to meet a large portion of the demand of grade A. On average, 73% of the demand of grade A at 3h and 74% at 8h is met for the nominal implementation, against 100% and 86% for the robust implementation.

In Fig. 3.19, we show the output, input and inventory trajectories for the nominal and robust DRTO implementations and some $s \in \mathcal{S}^{plant}$ where $k_0 = 2.83 \times 10^7$. The nominal DRTO fails to lead the plant to meet all three demands of grade A. Moreover, the production sequence is different between 0 and 4 hours for the two implementations. The nominal implementation performs worse because it underpredicts the transition time for producing A. This is made worse by the lower controller gain, which leads to a more sluggish system response to disturbances. Note that between 6 and 8h, the plant takes some time to start producing grade A after it finishes producing grade B. The reason is that the DRTO pushes production to start later to minimize inventory cost; however the plant is not able to meet

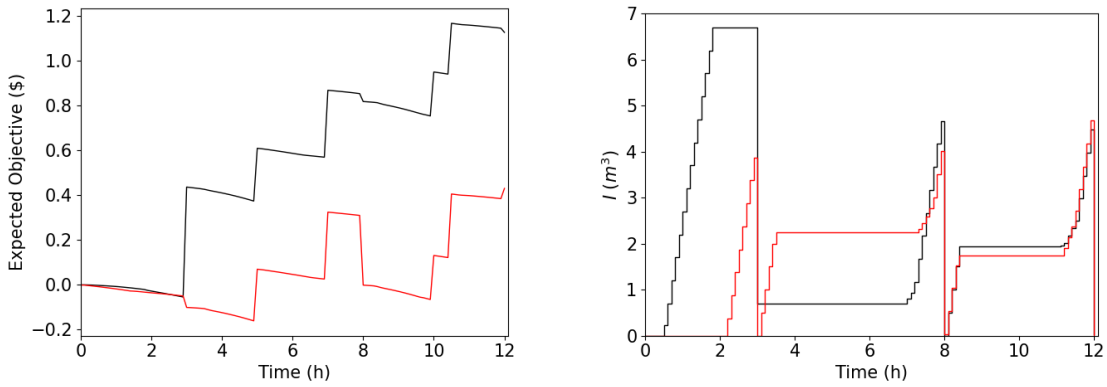

(a) (b)

Figure 3.18. Expected (a) objective (EPM), and (b) inventory level of grade A in Case 2f for the robust (black line) and nominal (red line) DRTO implementations. Expected objective is in thousands of dollars.

the DRTO production targets. The robust DRTO performs better because it has information about the different scenarios for k_0, and can act to mitigate the impact of scenarios that it predicts as having a more detrimental effect on the objective value.

3.4 Conclusion

Chemical manufacturers have traditionally followed a hierarchical decision-making architecture. However, increasingly dynamic market conditions have reduced the time scale gap between the decision-making layers, and require chemical processes to be operated in a more agile manner. Process response times can be improved by tighter integration of the decision-making layers, which can be accomplished, for example, by providing the scheduler with information about the process dynamics and control system.

In this study, we presented a scenario-based stochastic formulation for the integration of scheduling and control. The proposed formulation can accommodate multiple uncertainty types, including model, demand and cost uncertainty, and takes into account the action of the associated PI control system in order to predict the closed-loop system dynamics. Discrete scheduling decisions, and input saturation are appropriately modeled using binary variables. The resulting MILP problem is solved at the DRTO level, in a moving horizon fashion, to

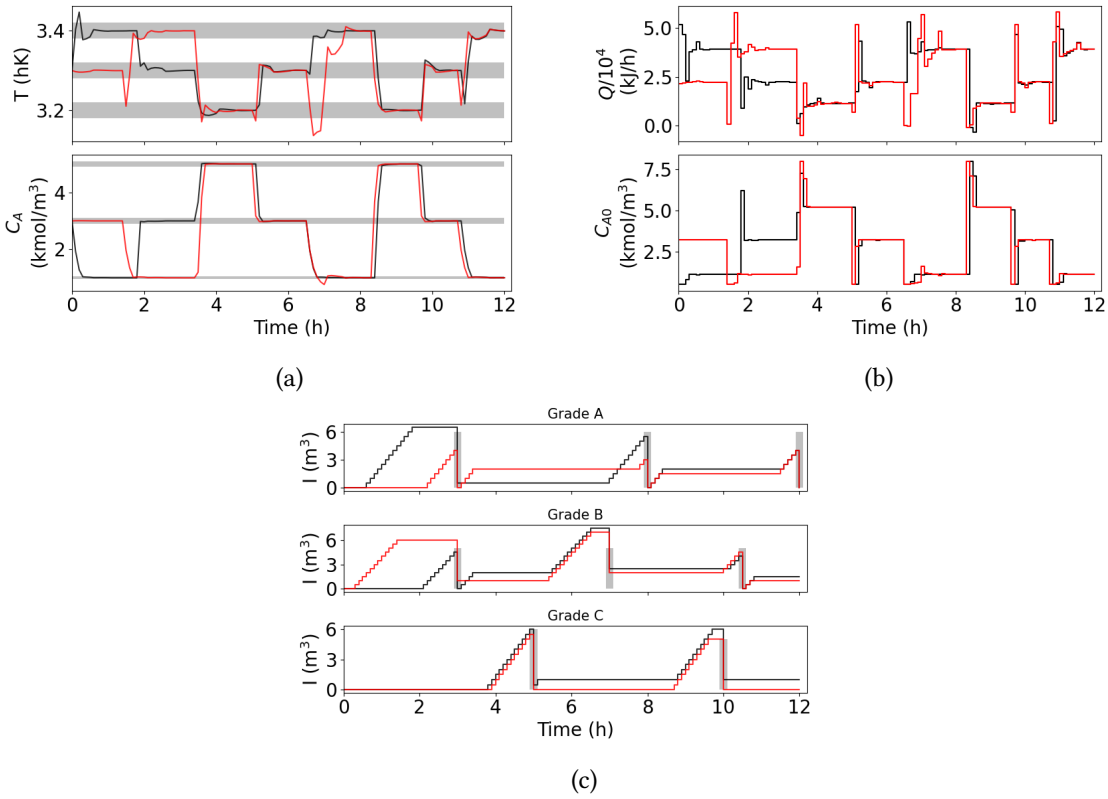

Figure 3.19. (a) Output, (b) input and (c) inventory trajectory for realization of a scenario $s \in \mathcal{S}^{plant}$ in Case 2f and implementation of the robust DRTO (black solid line) and nominal DRTO (red solid line).

compute optimal scheduling decisions and output set-points. Production sequencing is communicated to the plant via set-points to the PI control system. To assess the benefit of the proposed formulation, we ran closed-loop simulations for 45 random realizations of the uncertain parameters for nominal and robust implementations of the integrated scheduling and control problem, and used these simulation results to compute the value of the stochastic solution (VSS). Moreover, we explored the effect of the feedback frequency, and number of nonanticipativity constraints on the expected plant objective under perfect model knowledge and plant-model mismatch conditions.

The present study differs from previous works in literature on several fronts. We account for multiple uncertainty types in a closed-loop formulation for the integrated scheduling and control problem that also accommodates input saturation. The performance of the proposed framework is evaluated under real-time closed-loop implementation, and considers important practical aspects of an industrial application, such as execution frequency, plant-

model mismatch and unmodeled uncertainties. Via examples, we demonstrate conditions under which accounting for uncertainty leads to a better objective expectation, and others where accounting for uncertainty can have a detrimental effect on performance.

The value of the stochastic solution for all case studies suggests that accounting for uncertainty using the proposed formulation generally leads to significant improvement in process performance. Moreover, the objective value of the worst case scenario obtained with the robust DRTO implementation is often better than the worst case scenario in the nominal implementation where uncertainty is neglected. Our results also suggest that accounting for model uncertainty in a situation of plant-model mismatch can significantly improve process performance.

References

[1] R. Baker and C. L. E. Swartz. “Rigorous handling of input saturation in the design of dynamically operable plants”. In: *Industrial & engineering chemistry research* 43.18 (2004), pp. 5880–5887 (cit. on p. 65).

[2] J. Balasubramanian and I. Grossmann. “Approximation to multistage stochastic optimization in multiperiod batch plant scheduling under demand uncertainty”. In: *Industrial & engineering chemistry research* 43.14 (2004), pp. 3695–3713 (cit. on p. 74).

[3] J. R. Birge and F. Louveaux. *Introduction to stochastic programming*. Springer Science & Business Media, 2011 (cit. on p. 73).

[4] Y. Chu and F. You. “Integration of scheduling and dynamic optimization of batch processes under uncertainty: Two-stage stochastic programming approach and enhanced generalized Benders decomposition algorithm”. In: *Industrial & Engineering Chemistry Research* 52.47 (2013), pp. 16851–16869 (cit. on p. 61).

[5] D. Dering and C. L. E. Swartz. “A scenario-based framework for the integration of scheduling and control under multiple uncertainties”. In: *Journal of Process Control* 129 (2023), p. 103055 (cit. on p. 59).

[6] D. Dering and C. L. Swartz. “A stochastic optimization framework for integrated scheduling and control under demand uncertainty”. In: *Computers & Chemical Engineering* 165 (2022), p. 107931 (cit. on pp. 61, 62, 66).

[7] D. Dering and C. L. Swartz. “Dynamic Real-Time Scheduling and Control Under Uncertainty”. In: *2022 AIChE Annual Meeting*. AIChE. 2022 (cit. on p. 59).

[8] L. S. Dias and M. G. Ierapetritou. “Integration of scheduling and control under uncertainties: Review and challenges”. In: *Chemical Engineering Research and Design* 116 (2016), pp. 98–113 (cit. on p. 61).

[9] L. S. Dias, R. C. Pattison, C. Tsay, M. Baldea, and M. G. Ierapetritou. “A simulation-based optimization framework for integrating scheduling and model predictive control, and its application to air separation units”. In: *Computers & Chemical Engineering* 113 (2018), pp. 139–151 (cit. on p. 61).

[10] M. Ellis and P. D. Christofides. “Integrating dynamic economic optimization and model predictive control for optimal operation of nonlinear process systems”. In: *Control Engineering Practice* 22 (2014), pp. 242–251 (cit. on p. 85).

[11] D. Gupta and C. T. Maravelias. “On the design of online production scheduling algorithms”. In: *Computers & Chemical Engineering* 129 (2019), p. 106517 (cit. on p. 61).

[12] D. Gupta, C. T. Maravelias, and J. M. Wassick. “From rescheduling to online scheduling”. In: *Chemical Engineering Research and Design* 116 (2016), pp. 83–97 (cit. on pp. 61, 62).

[13] T. E. Marlin. “Process Control, 2nd edn.” In: McGraw-Hill, 2015. Chap. 7, pp. 64–65, 223–224, 366–367 (cit. on pp. 65, 76).

[14] P. Mathur, C. L. E. Swartz, D. Zyngier, and F. Welt. “Robust online scheduling for optimal short-term operation of cascaded hydropower systems under uncertainty”. In: *Journal of Process Control* 98 (2021), pp. 52–65 (cit. on p. 61).

[15] P. Mathur, C. L. E. Swartz, D. Zyngier, and F. Welt. “Uncertainty management via online scheduling for optimal short-term operation of cascaded hydropower systems”. In: *Computers & Chemical Engineering* 134 (2020), p. 106677 (cit. on p. 61).

[16] R. C. Pattison, C. R. Touretzky, T. Johansson, I. Harjunkoski, and M. Baldea. “Optimal process operations in fast-changing electricity markets: framework for scheduling with low-order dynamic models and an air separation application”. In: *Industrial & Engineering Chemistry Research* 55.16 (2016), pp. 4562–4584 (cit. on p. 61).

[17] J. M. Simkoff and M. Baldea. “Stochastic scheduling and control using data-driven nonlinear dynamic models: application to demand response operation of a chlor-alkali plant”. In: *Industrial & Engineering Chemistry Research* 59.21 (2020), pp. 10031–10042 (cit. on p. 61).

Chapter 4

Integration of scheduling and control for plants controlled by distributed MPC systems

An earlier version of this chapter has been published and presented in:

[1] D. Dering and C. Swartz. “An Integrated Scheduling and Control Framework for Plants Controlled by Distributed MPC Systems”. In: *IFAC-PapersOnLine*. Vol. 56. 2. Elsevier, 2023, pp. 1417–1422

[2] D. Dering and C. L. E. Swartz. “An Integrated Scheduling and Control Framework for

Plants Controlled by Distributed MPC Systems". In: *IFAC World Congress 2023*. IFAC. 2023

The contents of this chapter have be submitted to and presented in:

[3] D. Dering and C. L. E. Swartz. "Integration of scheduling and control for plants controlled by distributed MPC systems". In: *Industrial & Engineering Chemistry Research. Submitted* (2023)

[4] D. Dering and C. L. E. Swartz. "A closed-loop integrated scheduling and control formulation for processes controlled by distributed MPC systems". In: *2023 AICHE annual meeting in Orlando, FL, USA*. AICHE

4.1 Introduction

Almost all of the published work on the integration of scheduling and control for MPC controlled processes assume an underlying centralized MPC architecture[20, 10, 21, 9]. However, a collection of MPC regulators is commonly employed in refineries and chemical industries for reasons of reduced computational complexity, ease of maintenance, and safety[19, 17]. MPC control systems are commonly categorized as decentralized, distributed or hierarchical [19, 4, 17]. In decentralized MPC control, the process inputs and outputs are decoupled in disjoint SISO or MIMO subsystems. An MPC regulator is then independently designed for each of these subsystems. The MPC regulators do not communicate with each other, and are unaware of the interactions between the subsystems. This is known to hinder performance and stability in strongly coupled subprocesses. In distributed MPC control, each MPC regulator exchanges information with all (or a subset of) the other regulators, allowing it to predict the interaction between the subsystems. The information exchanged usually includes the computed input and state predictions. Design decisions include the frequency of information exchange, the subset of regulators with which to share information, and the type of metric optimized by each regulator (i.e. a global or local cost function). Algorithms that optimize a local performance metric are said to be noncooperative [19, 17]. On another hand,

cooperative regulators optimize a common global cost function. The MPC subsystems can also be coordinated by a supervisory upper-layer following a hierarchical control structure [19].

Few studies have considered the integration of scheduling and control for plants controlled by distributed MPC subsystems [3, 7]. Burnak et al. [3] include a case study involving two CSTRs operating in parallell where each CSTR is controlled by an independent MPC regulator. The MPC subsystems are coordinated by a supervisory controller-aware scheduler. Two optimization problems are solved in the supervisory layer to compute the set-point trajectories assigned to the lower-level MPCs. The first problem computes economically optimal scheduling decisions, while the second one translates these decisions into set-points to the lower-level controller. To reduce the online computational time, offline solution maps for each optimization problem are obtained via multiparametric programming. In Dering and Swartz [7], the MPC subsystems are coordinated by a control-aware scheduler at the dynamic real-time optimization (DRTO) level. While each MPC regulator has only local information about the plant dynamics, the DRTO has access to a full model of the plant, including its closed-loop dynamics. The DRTO computes set-point trajectories, tracked by the lower-level MPC subsystems, that optimize an economic performance metric. Therefore, coordination of the MPC subsystems is achieved via the set-point trajectories, and there is no direct exchange of information between the MPC regulators. They consider a linear case study where there is significant interaction between the process units to showcase the coordination capabilities of their integrated scheduling and control formulation.

While we acknowledge the benefits of the multiparametric programming formulation in Burnak et al. [3], it is known that as the number of parameters increase, it becomes increasingly challenging to obtain offline solution maps. Thus, in this study, we pursue a different paradigm to alleviate the computational burden of integrated scheduling and control formulations, centered on approximating the control input action. Particularly, we develop strategies to reduce the online solution time of the integrated scheduling and control formulation for plants controlled by distributed MPC systems introduced in Dering and Swartz [7]. Our approach is extremely versatile, in the sense that the level of conservativeness of the approximation can be easily adjusted. We demonstrate the economic and computational

performance of the strategies to reduce the solution time of the integrated scheduling and control problem via case studies. This includes industrially relevant scenarios, where there are, simultaneously, strong interactions between process units controlled by MPC subsystems, and plant-model mismatch. Our results demonstrate the efficacy of the approximation strategies to reduce the solution time, and the ability of the integrated scheduling and control layer to successfully coordinate the MPC subsystems, solely through the set-point trajectories. In summary, the key contributions of this study are: (i) an integrated scheduling and control framework capable of coordinating strongly interacting MPC control loops under conditions of plant-model mismatch, as demonstrated via case studies, (ii) strategies to reduce the solution time of the integrated scheduling and control problem, (iii) comprehensive case studies to assess the performance of the closed-loop approximations under different rescheduling frequencies, compared to a rigorous and open-loop integrated scheduling and control formulation. In all our case studies, the optimal solution of the integrated scheduling and control problem is implemented in closed-loop with the plant.

The proposed integrated scheduling and control formulation is presented in Section 4.2, the case studies in Section 4.3 and conclusion in Section 4.4.

4.2 Formulation

A schematic representation of the integrated scheduling and control framework proposed in this study is presented in Fig. 4.1. The inputs applied to the plant are computed by a distributed MPC system, where the s^{th} MPC subsystem computes the value of a subset of the inputs $u_j^{(\text{s})}$. Output measurements $y_j^{\text{m(s)}}$ and (estimated) inventory levels I_j are provided as feedback information from the plant to the upper layers. The output measurements are used to compute disturbance estimates for the DRTO and MPCs' linear process models. This strategy provides the MPC and DRTO formulations used in this study offset-free tracking properties. The output $y_j^{\text{SP(s)}}$ and input $u_j^{\text{SP(s)}}$ set-points assigned to the s^{th} MPC subsystem are computed in real-time via solution of the integrated scheduling and control problem at the DRTO level. The optimization problem in the DRTO layer is solved at an execution

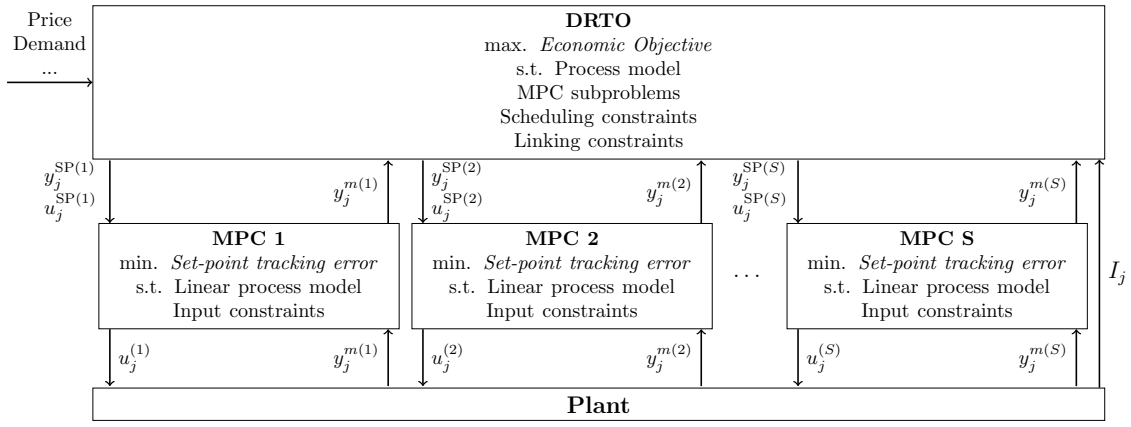

Figure 4.1. Schematic representation of the integrated scheduling and control framework considered in this study.

time interval of Δt^{DRTO}, while the lower-level MPC subsystems are executed at a higher frequency ($\Delta t \leq \Delta t^{\text{DRTO}}$) to rapidly reject disturbances.

Aiming to improve economic performance, we account for the distributed MPC system action in the formulation of the integrated scheduling and control problem. This leads to a closed-loop formulation at the DRTO layer. Conversely, if the feedback control action is neglected, the resulting DRTO problem formulation is said to be open-loop.

In the next section, we present the DRTO process model formulation. Different approaches to account for the MPC controller action are presented in Section 4.2.2. Our formulation also allows for the controller action to be neglected to yield an open-loop integrated scheduling and control problem. The constraints that link the DRTO process model and decision variables to the MPC subproblems are given in Section 4.2.3. The scheduling constraints and objective function are presented in Sections 4.2.4 and 4.2.5, respectively.

4.2.1 Process model

We consider a linear state-space representation of the plant model at the DRTO level:

$$\bar{x}_{j+1,i} = \sum_{k \in \mathcal{X}} \bar{A}_{i,k} \bar{x}_{j,k} + \sum_{k \in \mathcal{U}} \bar{B}_{i,k} \bar{u}_{j,k} \qquad \forall j \in \mathcal{J}_0^{N-1}, i \in \mathcal{X} \tag{4.1a}$$

$$\bar{y}_{j,i} = \sum_{k \in \mathcal{X}} \bar{C}_{i,k} \bar{x}_{j,k} + \bar{d}_i \qquad \forall j \in \mathcal{J}_1^N, i \in \mathcal{Y} \tag{4.1b}$$

where $\bar{A}_{i,k}$, $\bar{B}_{i,k}$ and $\bar{C}_{i,k}$ are state-space matrix coefficients. $\bar{x}_{j,i}$, $\bar{u}_{j,i}$, $\bar{y}_{j,i} \in \mathcal{R}$ denote the value of a state, input and output i at DRTO time-step j. $\mathcal{X}, \mathcal{U}$, and $\mathcal{Y}$ are the sets of state, input and output identifiers, respectively. $\mathcal{J}_a^b = \{i | a \leq i \leq b, i \in \mathcal{Z}\}$ is the set of time-steps between, and including, a and b. The disturbance estimate $\bar{d}_i$ is computed as follows,

$$\bar{d}_i = y_i^{\mathrm{m}} - \sum_{k \in \mathcal{X}} \bar{C}_{i,k} \bar{x}_{0,k}, \qquad \forall\, i \in \mathcal{Y} \tag{4.2}$$

where y_i^{m} is the measured value of output i, and $\bar{x}_{0,k}$ is the estimated value of state k at DRTO time step 0. Bounds are imposed on the states and outputs, where the subscripts min and max denote lower and upper bounds, respectively.

$$\bar{x}_{\min,i} \leq \bar{x}_{j,i} \leq \bar{x}_{\max,i}, \qquad \forall j \in \mathcal{J}_1^N,\ i \in \mathcal{X} \tag{4.3a}$$

$$\bar{y}_{\min,i} \leq \bar{y}_{j,i} \leq \bar{y}_{\max,i}, \qquad \forall j \in \mathcal{J}_1^N,\ i \in \mathcal{Y} \tag{4.3b}$$

Input bounds are imposed at the MPC level (Section 4.2.2).

The use of a linear model (Eq. (4.1)) is convenient because it limits the complexity of the DRTO problem to a mixed-integer linear programming (MILP) problem when all other constraints and objective function are linear or mixed-integer linear. Nonlinear process models can be either linearized, or approximated via piecewise linear segments. One of the advantages of MILP formulations is that they can be solved to global optimality by standard MILP solvers (e.g. Gurobi, CPLEX).

4.2.2 MPC subproblems

At the DRTO level, we consider two different MPC formulations: constrained, and unconstrained[14, 12]. The former corresponds to the MPC formulation used in the lower-level control layer, and it is based on the quadratic dynamic matrix control (QDMC) formulation of Garcia and Morshedi[11], but with the finite step response replaced with a state-space

model. The unconstrained formulation is obtained by dropping the input constraints from the QDMC-like formulation. We use $\mathcal{S}$ to denote the set of MPC subsystems. Each MPC subsystem is responsible for controlling a set of the outputs $\mathcal{Y}^{(s)}$ and inputs $\mathcal{U}^{(s)}$, such that $\mathcal{Y} = \cup_{s\in\mathcal{S}}\, \mathcal{Y}^{(s)}$, and $\mathcal{U} = \cup_{s\in\mathcal{S}}\, \mathcal{U}^{(s)}$.

In addition to the constrained and unconstrained MPC formulations, we also consider an open-loop formulation where the action of the lower-level controller is completely neglected. A hybrid formulation can also be employed: at every DRTO time-step j a different method (i.e. constrained, unconstrained, open-loop) can be used to compute the input action $\bar{u}_{j,k}$ in Eq. (4.1). We use $\mathcal{N}^{RCL} \subset \mathcal{J}_0^{N-1}$ to denote the set of DRTO time-steps for which the constrained MPC formulation is used to compute the input value $\bar{u}_{j,i}$, and $\mathcal{N}^{ACL} \subset (\mathcal{J}_0^{N-1} \backslash \mathcal{N}^{RCL})$ as the set of DRTO time-steps for which the unconstrained MPC formulation combined with an input-clipping method is used to compute $\bar{u}_{j,i}$. Thus, the subscripts RCL and ACL identify, respectively, the set of time-steps for which a rigorous or approximate closed-loop method is used to compute the input action. We define $\mathcal{N}^{OL} = \{j | j \in \mathcal{J}_0^{N-1}, j \notin \mathcal{N}^{RCL}, j \notin \mathcal{N}^{ACL}\}$ as the set of of time-steps for which the input values $\bar{u}_{j,i}$ are computed in an open-loop manner, that is, without taking into account the action of the underlying feedback control system. More detail on the different strategies to compute the input action is given in Section 4.2.2.

Constrained MPC formulation

The formulation of MPC subsystem s at DRTO time-step $j \in \mathcal{N}^{RCL}$ is presented in Eq. (4.4):

$$\min_{\substack{u_{j,k,i},\ \forall i\in\mathcal{U}^{(s)},\ k\in\mathcal{J}_0^{M^{(s)}-1},\\ x_{j,k,i},\ \forall i\in\mathcal{X}^{(s)},\ k\in\mathcal{J}_1^{P^{(s)}},\\ y_{j,k,i},\ \forall i\in\mathcal{Y}^{(s)},\ k\in\mathcal{J}_1^{P^{(s)}}}} \quad \sum_{k=1}^{P^{(s)}} \sum_{i\in\mathcal{Y}^{(s)}} Q_i \left(y_{j,k,i} - \bar{y}^{\mathrm{SP}}_{j,k,i}\right)^2 + \sum_{k=0}^{M^{(s)}-1} \sum_{i\in\mathcal{U}^{(s)}} \left[S_i \left(u_{j,k,i} - \bar{u}^{\mathrm{SP}}_{j,k,i}\right)^2 + R_i \left(\Delta u_{j,k,i}\right)^2\right] \quad (4.4a)$$

subject to:

$$x_{j,k+1,i} = \sum_{n\in\mathcal{X}^{(s)}} A_{i,n}x_{j,k,n} + \sum_{n\in\mathcal{U}^{(s)}} B_{i,n}u_{j,k,n} \qquad \forall k \in \mathcal{J}_0^{M^{(s)}-1},\ i \in \mathcal{X}^{(s)} \tag{4.4b}$$

$$x_{j,k+1,i} = \sum_{n\in\mathcal{X}^{(s)}} A_{i,n}x_{j,k,n} + \sum_{n\in\mathcal{U}^{(s)}} B_{i,n}u_{j,M^{(s)}-1,n} \qquad \forall k \in \mathcal{J}_{M^{(s)}}^{P^{(s)}-1},\ i \in \mathcal{X}^{(s)} \tag{4.4c}$$

$$y_{j,k,i} = \sum_{n\in\mathcal{Y}^{(s)}} C_{i,n}x_{j,k,n} + d_{j,i} \qquad \forall k \in \mathcal{J}_1^{P^{(s)}},\ i \in \mathcal{Y}^{(s)} \tag{4.4d}$$

$$\Delta u_{j,k,i} = u_{j,k,i} - u_{j,k-1,i} \qquad \forall k \in \mathcal{J}_0^{M^{(s)}-1},\ i \in \mathcal{U}^{(s)} \tag{4.4e}$$

$$u_{\min,i} \leq u_{j,k,i} \leq u_{\max,i} \qquad \forall k \in \mathcal{J}_0^{M^{(s)}-1},\ i \in \mathcal{U}^{(s)} \tag{4.4f}$$

where $x_{j,k,i}$, $u_{j,k,i}$, and $y_{j,k,i} \in \mathcal{R}$ are, respectively, the predicted value of a state, input and output i at MPC time-step k and DRTO time-step j. $\mathcal{X}^{(s)}$ is the set of state identifiers of MPC subsystem s. $\bar{y}^{\mathrm{SP}}_{j,k,i}$ and $\bar{u}^{\mathrm{SP}}_{j,k,i} \in \mathcal{R}$ are the output and input set-points, respectively. $u_{\max,i}$ and $u_{\min,i}$ are the upper and lower bounds, respectively, on input i. $A_{i,n}$, $B_{i,n}$ and $C_{i,n}$ are the MPC state-space model coefficients. $Q_i > 0$, $S_i \geq 0$ and $R_i \geq 0$ are, respectively, output set-point tracking, input set-point tracking and move repression weighting coefficients. $M^{(s)}$ and $P^{(s)}$ are the control and output horizon for MPC subsystem s. $d_{j,i} \in \mathcal{R}$ is a disturbance estimate. The expressions used to compute the values of $u_{j,-1,i}$, $x_{j,0,i}$, $d_{j,i}$, $\bar{y}^{\mathrm{SP}}_{j,k,i}$ and $\bar{u}^{\mathrm{SP}}_{j,k,i}$ for the MPC subproblems solved at DRTO time-step j are presented in Section 4.2.3.

The optimal input value $u_{j,0,i}$ obtained from the solution of Eq. (4.4) is linked to the input $\bar{u}_{j,k}$ in the DRTO process model (Eq. (4.1)) via:

$$\bar{u}_{j,i} = u_{j,0,i} \qquad \forall j \in \mathcal{N}^{RCL}, i \in \mathcal{U} \tag{4.5}$$

To avoid a multilevel optimization formulation, yielded by embedding $|\mathcal{S}| \times |\mathcal{N}^{RCL}|$ ($|i|$ denotes the number of elements in a set i) MPC problems within the DRTO economic optimization problem, Eq. (4.4) is replaced by its first-order Karush-Kuhn-Tucker (KKT) conditions[13]. Since the optimization problem in Eq. (4.4) is convex, its first-order KKT conditions are necessary and sufficient for optimality. The KKT-reformulation yields a system of linear equations with complementarity constraints that that can be solved for the optimum

of Eq. (4.4). Different approaches can be used to handle the complementarity constraints resulting from the KKT-reformulation, including the penalty approach[13, 20] and use of binary variables[18, 9]. For this study, we choose the latter to keep an overall MILP problem structure.

Unconstrained MPC formulation with input-clipping

The MPC formulation considered in this section is similar to the rigorous formulation presented in the previous section, except that the input constraints in Eq. (4.4f) are dropped from the MPC problem in Eq. (4.4). This leads to an unconstrained MPC problem whose KKT-reformulation yields a system of linear equations that can be explicitly solved for $u_{j,k,i}$[14]. The analytical solution of the unconstrained MPC subproblem at DRTO time-step $j \in \mathcal{N}^{ACL}$ can be stated as:

$$\begin{aligned} u_{j,k,i} = & \sum_{n \in \mathcal{X}^{(s)}} K^a_{k,i,n} x_{j,0,n} + \sum_{p \in \mathcal{J}_1^{P^{(s)}}} \sum_{n \in \mathcal{Y}^{(s)}} K^b_{k,i,n,p} (d_{j,n} - \bar{y}^{\mathrm{SP}}_{j,p,n}) \\ & + \sum_{p \in \mathcal{J}_0^{M^{(s)}-1}} \sum_{n \in \mathcal{U}^{(s)}} K^c_{k,i,n,p} \bar{u}^{\mathrm{SP}}_{j,p,n} + \sum_{n \in \mathcal{U}^{(s)}} K^d_{k,i,n} u_{j,-1,n} \\ & \forall\, s \in \mathcal{S}, k \in \mathcal{J}_0^{M^{(s)}-1},\ i \in \mathcal{U}^{(s)} \end{aligned} \tag{4.6}$$

where $K^a_{k,i,n}$, $K^b_{k,i,n,p}$, $K^c_{k,i,n,p}$ and $K^d_{k,i,n}$ are coefficients obtained from the KKT-reformulation. They are dependent on the MPC model coefficients $A_{i,n},\ B_{i,n},\ C_{i,n}$, on the objective function weighting coefficients $Q_i,\ S_i$ and R_i, and on the control $M^{(s)}$ and output $P^{(s)}$ horizon.

Because the above expression gives the solution of the unconstrained MPC problem, the values obtained for $u_{j,k,i}$ may violate the input bounds in Eq. (4.4f). To have only feasible input values applied to the process model in Eq. (4.1), we use a clipping mechanism[2]:

$$\bar{u}_{j,i} - u_{j,0,i} + \mu^1_{j,i} - \mu^2_{j,i} = 0 \qquad \forall j \in \mathcal{N}^{ACL}, i \in \mathcal{U} \tag{4.7a}$$

$$\bar{u}_{j,i} - u_{\min,i} \geq -(1 - \nu^2_{j,i})M \qquad \forall j \in \mathcal{N}^{ACL}, i \in \mathcal{U} \tag{4.7b}$$

$$\bar{u}_{j,i} - u_{\max,i} \geq -(1 - \nu^1_{j,i})M \qquad \forall j \in \mathcal{N}^{ACL}, i \in \mathcal{U} \tag{4.7c}$$

$$\bar{u}_{j,i} - u_{\min,i} \leq (1 - \nu^2_{j,i})M \qquad \forall j \in \mathcal{N}^{ACL}, i \in \mathcal{U} \tag{4.7d}$$

$$\bar{u}_{j,i} - u_{\max,i} \leq (1 - \nu^1_{j,i})M \qquad \forall j \in \mathcal{N}^{ACL}, i \in \mathcal{U} \tag{4.7e}$$

$$\mu^1_{j,i} \leq \nu^1_{j,i} M \qquad \forall j \in \mathcal{N}^{ACL}, i \in \mathcal{U} \tag{4.7f}$$

$$\mu^2_{j,i} \leq \nu^2_{j,i} M \qquad \forall j \in \mathcal{N}^{ACL}, i \in \mathcal{U} \tag{4.7g}$$

$$u_{\min,i} \leq \bar{u}_{j,i} \leq u_{\max,i} \qquad \forall j \in \mathcal{N}^{ACL}, i \in \mathcal{U} \tag{4.7h}$$

$$\mu^1_{j,i} \geq 0, \mu^2_{j,i} \geq 0 \qquad \forall j \in \mathcal{N}^{ACL}, i \in \mathcal{U} \tag{4.7i}$$

where $\mu^1_{j,i}$ and $\mu^2_{j,i} \in \mathcal{R}$ are slack variables, and $\nu^1_{j,i}$ and $\nu^2_{j,i} \in \{0,1\}$ are binaries. M is a sufficiently large positive constant. The construct in Eq. (4.7) captures the following logic:

$$\bar{u}_{j,i} = \begin{cases} u_{\min,i} & \text{if } u_{j,0,i} < u_{\min,i} \\ u_{j,0,i} & \text{if } u_{\min,i} \leq u_{j,0,i} \leq u_{\max,i} \\ u_{\max,i} & \text{if } u_{j,0,i} > u_{\max,i} \end{cases}, \quad \forall\, j \in \mathcal{N}^{ACL}, i \in \mathcal{U} \tag{4.8}$$

Open-loop formulation

We have defined $\mathcal{N}^{OL}$ as the set of of time-steps for which the input values $\bar{u}_{j,i}$ are computed in an open-loop manner, that is, without taking into account the action of the underlying feedback control system. To prevent $\bar{u}_{j,i}$ from violating the input bounds when $j \in \mathcal{N}^{OL}$, we have to impose the constraint:

$$u_{\min,i} \leq \bar{u}_{j,i} \leq u_{\max,i} \quad \forall j \in \mathcal{N}^{OL}, i \in \mathcal{U} \tag{4.9}$$

Closed-loop approximations

The complexity of the DRTO formulation, with respect to the modeling of the control action, can be adjusted using the sets $\mathcal{N}^{RCL}$, $\mathcal{N}^{ACL}$ and $\mathcal{N}^{OL}$. Basically three different DRTO formulations are possible:

- *Rigorous closed-loop formulation*: We have a rigorous closed-loop DRTO formulation when $\mathcal{N}^{RCL} = \{j | j \in \mathcal{J}_0^{N-1}\}$, $\mathcal{N}^{ACL} = \emptyset$, and $\mathcal{N}^{OL} = \emptyset$. That is, all input values $\bar{u}_{j,i}\ \forall j \in \mathcal{J}_0^{N-1}, i \in \mathcal{U}$ are computed using the rigorous MPC formulation (KKT-reformulation of Eq. (4.4), and Eq. (4.5)).

- *Input-clipping formulation*: An input-clipping formulation is obtained when $\mathcal{N}^{RCL} = \emptyset$, $\mathcal{N}^{ACL} = \{j | j \in \mathcal{J}_0^{N-1}\}$, and $\mathcal{N}^{OL} = \emptyset$. That is, all input values $\bar{u}_{j,i}\ \forall j \in \mathcal{J}_0^{N-1}, i \in \mathcal{U}$ are computed using the uncostrained MPC formulation (Eqs. (4.6) and (4.7))

- *Open-loop formulation*: An open-loop formulation is obtained when $\mathcal{N}^{RCL} = \emptyset$, $\mathcal{N}^{ACL} = \emptyset$, and $\mathcal{N}^{OL} = \{j | j \in \mathcal{J}_0^{N-1}\}$. The input values computed in this manner are said to be open-loop because the feedback control action is not taken into account (Eq. (4.9)).

- *Hybrid formulation*: A hybrid formulation results when at least two different methods are used to compute $\bar{u}_{j,i}$. That is, either $\mathcal{N}^{RCL} \neq \emptyset$ and $\mathcal{N}^{ACL} \neq \emptyset$, or $\mathcal{N}^{RCL} \neq \emptyset$ and $\mathcal{N}^{OL} \neq \emptyset$, or $\mathcal{N}^{ACL} \neq \emptyset$ and $\mathcal{N}^{OL} \neq \emptyset$.

We can compare the above DRTO formulations in terms of complexity and performance[12, 14]:

Complexity: The most complex and computationally intensive formulation is obtained with the rigorous approach because it requires the solution of $N \times |\mathcal{S}|$ constrained MPC problems at every DRTO execution. A comparatively less complex DRTO formulation is achieved with the input-clipping approach because it utilizes an analytical expression to compute the input values, leading to a lower number of variables and constraints compared to the rigorous approach[14]. The least computationally expensive formulation is obtained with the open-loop approach because it does not have additional constraints to account for the feedback control action.

Performance: The open-loop approach usually yields the worst plant performance[9]. Conversely, the best economic performance is usually achieved with the rigorous approach because it more accurately captures the closed-loop plant response. The input-clipping

formulation usually leads to a worse performance than the rigorous approach but significantly better than the open-loop solution. In cases where there is no input saturation, the input-clipping approach performs as well as the rigorous one[9].

4.2.3 Linking constraints

The disturbance estimate $d_{j,i}$, used in the rigorous and analytical MPC formulation (KKT-reformulation of Eq. (4.4), and Eq. (4.6)) is computed as:

$$d_{j,i} = y_i^{\mathrm{m}} - \sum_{n \in \mathcal{X}^{(s)}} C_{i,n} x_{j,k,0} \qquad \forall j \in (\mathcal{N}^{RCL} \cup \mathcal{N}^{ACL}),\ j = 0,\ s \in \mathcal{S},\ i \in \mathcal{Y}^{(s)} \quad (4.10a)$$

$$d_{j,i} = \bar{y}_{j,i} - \sum_{n \in \mathcal{X}^{(s)}} C_{i,n} x_{j-1,k,1} \quad \forall j \in (\mathcal{N}^{RCL} \cup \mathcal{N}^{ACL}),\ j \geq 1,\ s \in \mathcal{S},\ i \in \mathcal{Y}^{(s)} \quad (4.10b)$$

Note that for $j \geq 1$, the DRTO-predicted output $\bar{y}_{j,i}$ is used as a surrogate for the plant measurements y_i^{m}.

The output $\bar{y}_{j,k,i}^{SP}$ and input $\bar{u}_{j,k,i}^{SP}$ set-points are extracted from the reference trajectories $y_{j,i}^{\mathrm{ref}}$ and $u_{j,i}^{\mathrm{ref}} \in \mathcal{R}$ using:

$$\bar{y}_{j,k,i}^{\mathrm{SP}} = y_{j+1,i}^{\mathrm{ref}} \qquad \forall j \in \mathcal{J}_0^{N-1},\ s \in \mathcal{S}, i \in \mathcal{Y}^{(s)},\ k \in \mathcal{J}_1^{P^{(s)}} \quad (4.11a)$$

$$\bar{u}_{j,k,i}^{\mathrm{SP}} = u_{j,i}^{\mathrm{ref}} \qquad \forall j \in \mathcal{J}_0^{N-1}, s \in \mathcal{S}, i \in \mathcal{U}^{(s)}, k \in \mathcal{J}_0^{M^{(s)}-1} \quad (4.11b)$$

The reference trajectories $y_{j+1,i}^{\mathrm{ref}}$, $u_{j,i}^{\mathrm{ref}}\ \forall\ j \in \mathcal{J}_0^{N-1}$ are optimization degrees of freedom for the DRTO problem. There are various ways to obtain the MPC set-point trajectories from the reference trajectory [13, 9]. The one in Eq. (4.11) leads to a constant set-point trajectory for each MPC subproblem.

The reference trajectories are bounded in Eq. (4.12), where the subscripts min and max denote lower and upper bounds, respectively.

$$y_{\mathrm{min},i}^{\mathrm{ref}} \leq y_{j+1,i}^{\mathrm{ref}} \leq y_{\mathrm{max},i}^{\mathrm{ref}} \qquad \forall j \in (\mathcal{N}^{RCL} \cup \mathcal{N}^{ACL}), i \in \mathcal{Y} \quad (4.12a)$$

$$u_{\mathrm{min},i}^{\mathrm{ref}} \leq u_{j,i}^{\mathrm{ref}} \leq u_{\mathrm{max},i}^{\mathrm{ref}} \qquad \forall j \in (\mathcal{N}^{RCL} \cup \mathcal{N}^{ACL}), i \in \mathcal{U} \quad (4.12b)$$

For cases where $\mathcal{N}^{OL} \neq \emptyset$, we have that:

$$y^{\text{ref}}_{j+1,i} = \bar{y}_{j+1,i} \qquad \forall j \in \mathcal{N}^{OL}, i \in \mathcal{Y} \tag{4.13}$$

$$u^{\text{ref}}_{j,i} = \bar{u}_{j,i} \qquad \forall j \in \mathcal{N}^{OL}, i \in \mathcal{Y} \tag{4.14}$$

The initial state value for the MPC subproblems solved at DRTO time-steps $j \in \mathcal{J}_1^{N-1}$ is their predicted value in the previous time-step:

$$x_{j,0,i} = x_{j-1,1,i} \qquad \forall j \in (\mathcal{N}^{RCL} \cup \mathcal{N}^{ACL}),\ j \geq 1, s \in \mathcal{S},\ i \in \mathcal{Y}^{(s)} \tag{4.15}$$

Similar, $u_{j,-1,i}$ is set to equal the input values applied to the DRTO process model at the previous time-step:

$$u_{j,-1,i} = \bar{u}_{j-1,i} \qquad \forall j \in (\mathcal{N}^{RCL} \cup \mathcal{N}^{ACL}),\ j \geq 1,\ i \in \mathcal{U} \tag{4.16}$$

In a given DRTO execution, $x_{0,0,i}$ and $u_{0,-1,i}$ are set to match the value of the corresponding variable at the lower-level control layer.

4.2.4 Scheduling constraints

In this study, the scheduling constraints are used to define the production sequence, to check whether or not the outputs are within the quality band for the targeted grade (product is only stored if the quality targets are met), for limiting the number of target changes and for predicting production and inventory levels.

The grade targeted for production in a given time-step j is chosen via the binary variable $\gamma_{j,l,g}$ and Eq. (4.17).

$$\sum_{g \in \mathcal{G}} \gamma_{j,l,g} = 1 \qquad \forall j \in \mathcal{J}_1^N,\ l \in \mathcal{L} \tag{4.17a}$$

$$y^{\text{targ}}_{j,i} = \sum_{g \in \mathcal{G}} \gamma_{j,l,g} y^{\text{target}}_{g,i} \qquad \forall j \in \mathcal{J}_1^N,\ l \in \mathcal{L}, i \in \mathcal{I}^{(l)} \tag{4.17b}$$

Eq. (4.17a) ensures that only one grade is targeted for production at any time-step j in a given production line l. $\mathcal{L}$ is the set of parallel production lines. Eq. (4.17b) selects the quality target value $y_{g,i}^{\text{target}}$ associated with the targeted grade g and output i. $\mathcal{I}^{(l)} \subset \mathcal{Y}$ is the set of measured outputs in production line l.

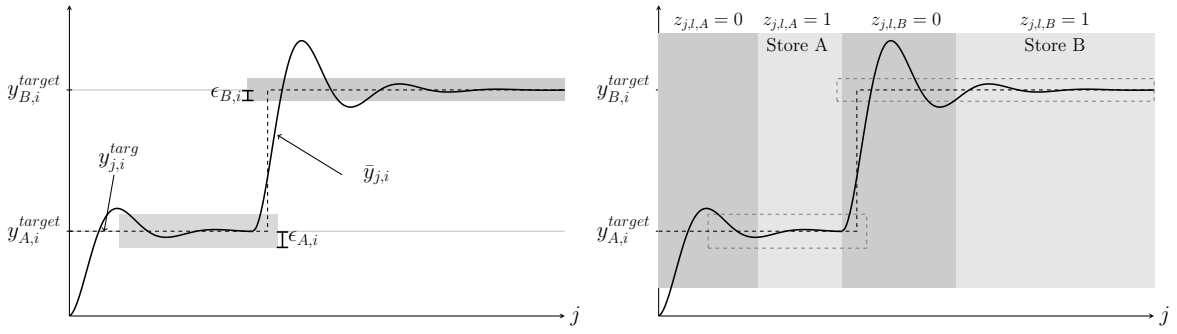

(a) (b)

Figure 4.2. Schematic representation of the quality target band, and the variable $z_{j,l,g}$.

The binary variable $z_{j,l,g}$ together with Eq. (4.18) is used to track whether or not all the outputs in the set $\mathcal{I}^{(l)}$ are within their respective quality target band for grade g. Output i is said to be within its quality target band for grade g at DRTO time-step j if $\bar{y}_{j,i} \in [y_{g,i}^{\text{target}} - \epsilon_{g,i}, y_{g,i}^{\text{target}} + \epsilon_{g,i}]$, where $\epsilon_{g,i}$ is the quality target tolerance as represented in Fig. 4.2a. Eq. (4.18) guarantees that $z_{j,l,g}$ equals one only if $\bar{y}_{j,i} \in [y_{g,i}^{\text{target}} - \epsilon_{g,i}, y_{g,i}^{\text{target}} + \epsilon_{g,i}]\ \forall i \in \mathcal{I}^{(l)}$ (Fig. 4.2b).

$$\bar{y}_{j,i} \geq \sum_{g \in \mathcal{G}} z_{j,l,g} \left(y_{g,i}^{\text{target}} - \epsilon_{g,i} \right) + (1 - \sum_{g \in \mathcal{G}} z_{j,l,g}) \bar{y}_{\min,i} \quad \forall j \in \mathcal{J}_1^N, l \in \mathcal{L}, i \in \mathcal{I}^{(l)} \tag{4.18a}$$

$$\bar{y}_{j,i} \leq \sum_{g \in \mathcal{G}} z_{j,l,g} \left(y_{g,i}^{\text{target}} + \epsilon_{g,i} \right) + (1 - \sum_{g \in \mathcal{G}} z_{j,l,g}) \bar{y}_{\max,i} \quad \forall j \in \mathcal{J}_1^N, l \in \mathcal{L}, i \in \mathcal{I}^{(l)} \tag{4.18b}$$

Eq. (4.19a) reflects the fact that only one grade can be produced at any time-step j in a production line l, while Eq. (4.19b) guarantees that $z_{j,l,g}$ can be one only if grade g has been targeted for production.

$$\sum_{g \in \mathcal{G}} z_{j,l,g} \leq 1, \qquad \forall j \in \mathcal{J}_1^N, l \in \mathcal{L} \tag{4.19a}$$

$$z_{j,g} \leq \gamma_{j,g}, \qquad \forall j \in \mathcal{J}_1^N, g \in \mathcal{G} \tag{4.19b}$$

Product g is stored if and only if $z_{j,l,g}$ is one (Fig. 4.2b). The amount of product $m_{j,l,g} \in \mathcal{R}$ produced at time-step j in production line l is computed as:

$$m_{j,l,g} - f_{j,l,g} \geq -(1 - z_{j,l,g}) f_{max,e} \qquad \forall j \in \mathcal{J}_1^N, l \in \mathcal{L}, g \in \mathcal{G} \tag{4.20a}$$

$$m_{j,l,g} - f_{j,l,g} \leq (1 - z_{j,l,g}) f_{min,e} \qquad \forall j \in \mathcal{J}_1^N, l \in \mathcal{L}, g \in \mathcal{G} \tag{4.20b}$$

$$m_{j,l,g} \geq 0 \qquad \forall j \in \mathcal{J}_1^N, l \in \mathcal{L}, g \in \mathcal{G} \tag{4.20c}$$

$$m_{j,l,g} \leq z_{j,l,g} f_{max,e} \qquad \forall j \in \mathcal{J}_1^N, l \in \mathcal{L}, g \in \mathcal{G} \tag{4.20d}$$

$f_{j,l,g} \in \mathcal{R}$ denotes the mass or volume of material produced in time-step j in production line l. $f_{\min}$ and $f_{\max}$ denote appropriate lower and upper bounds, respectively, on $f_{j,l,g}$. Note that $m_{j,l,g}$ equals $f_{j,l,g}$ if $z_{j,l,j}$ is one (Eqs. (4.20a) and (4.20b)), and it is zero otherwise (Eqs. (4.20c) and (4.20d)). The inventory level $I_{j,g}$ of grade g at time-step j is given by Eq. (4.21), where $D_{j,g}$ is the demand met, $B^d_{j,g}$ is the demand not met, and $D^{\mathrm{n}}_{j,g}$ is the actual size of the demand order.

$$I_{j,g} = I_{j-1,g} + \sum_{l \in \mathcal{L}} m_{j,l,g} - D_{j,g} \qquad \forall\, j \in \mathcal{J}_1^N, g \in \mathcal{G} \tag{4.21a}$$

$$D_{j,g} = D^{\mathrm{n}}_{j,g} - B^d_{j,g} \qquad \forall\, j \in \mathcal{J}_1^N, g \in \mathcal{G} \tag{4.21b}$$

$$I_{j,g}, D_{j,g}, B^d_{j,g} \geq 0 \qquad \forall\, j \in \mathcal{J}_1^N, g \in \mathcal{G} \tag{4.21c}$$

$$D_{j,g} \leq D^{\mathrm{n}}_{j,g}, \qquad \forall\, j \in \mathcal{J}_1^N, g \in \mathcal{G} \tag{4.21d}$$

The previously introduced equations do not constrain the number of times that $\gamma_{j,l,g}$ and $z_{j,l,g}$ can change from zero to one along the scheduling horizon N. To prevent excessive target changes, we introduce the variable $b_{j,l,g} \in [0, 1]$ and Eq. (4.22). $b_{j,l,g}$ is forced to equal one when storage of grade g stops, via Eq. (4.22a). That is, $z_{j,l,g}$ can only change values from 1 to 0 between consecutive time-steps if $b_{j,l,g}$ equals 1. Eq. (4.22b) limits the number of times that storage can stop to at most N_g^{target} per grade. Eq. (4.22c) prevents $b_{j,l,g}$ from being one if grade g is not being stored. We subtract $z_{N,l,g}$ from the right-hand side of Eq. (4.22b) to prevent a grade that has already been produced N_g^{target} times within the current DRTO execution from being produced once more time until time-step N.

$$z_{j,l,g} - z_{j-1,l,g} \geq -b_{j,l,g}, \qquad \forall\, l \in \mathcal{L}, g \in \mathcal{G}, j \in \mathcal{J}_1^N \tag{4.22a}$$

$$\sum_{j \in \mathcal{J}_1^N} b_{j,l,g} \leq N_g^{\text{target}} - z_{N,l,g}, \qquad \forall\, l \in \mathcal{L},\ g \in \mathcal{G} \tag{4.22b}$$

$$b_{j,l,g} \leq z_{j-1,l,g} \qquad \forall\, l \in \mathcal{L}, g \in \mathcal{G}, j \in \mathcal{J}_1^N \tag{4.22c}$$

$$\sum_{n \in \mathcal{J}_1^L} z_{j-n,l,g} \geq L b_{j,l,g}, \qquad \forall\, l \in \mathcal{L},\ g \in \mathcal{G}, j \in \mathcal{J}_1^N \tag{4.22d}$$

$$\gamma_{j,l,g} \leq 1 - b_{j,l,g}, \qquad \forall\, l \in \mathcal{L}, g \in \mathcal{G}, j \in \mathcal{J}_1^N \tag{4.22e}$$

$$\gamma_{j,l,g} - \gamma_{j-1,l,g} \geq -b_{j,l,g}, \qquad \forall\, l \in \mathcal{L}, g \in \mathcal{G}, j \in \mathcal{J}_1^N \tag{4.22f}$$

Eq. (4.22d) guarantees that once storage starts ($z_{j,l,g} = 1$), it will continue for at least L consecutive time-steps. Eq. (4.22e) forces a target change once storage of grade g stops. By Eq. (4.22f), a target change can only occur if $b_{j,l,g} = 1$.

Note that some of the variables accept a negative index j. This is to allow for previous information to be taken into account in the solution of the DRTO problem. In this study, this is accomplished using

$$z_{j,l,g} \leq z_{j,l,g}^{\text{plant}} \qquad \forall j \in \mathcal{J}_{-L+1}^0, l \in \mathcal{L}, g \in \mathcal{G} \tag{4.23}$$

where $z_{j,l,g}^{\text{plant}}$ is set to one if grade g was stored at the plant level at time-step j, and it is zero, otherwise. When the above inequality becomes active for consecutive values of j including $j = 0$ for some grade g, it allows storage of the given grade to cease at some time-step $j < L$ at the current DRTO execution.

We also impose the following tightening constraint in an attempt to reduce the time the MILP solver spends on infeasible solutions:

$$\sum_{g \in \mathcal{G}, j \in \mathcal{J}_1^N} \gamma_{j,l,g} = N \quad \forall l \in \mathcal{L} \tag{4.24}$$

4.2.5 Objective function

The objective function used in this study is

$$\Phi = \min \phi^E + \phi^C. \tag{4.25}$$

The term ϕ^E accounts for the economic performance of the plant, while ϕ^C is a control performance metric. More details on the computation of ϕ^E and ϕ^C are given bellow.

- *Economic Performance*: The economic objective is to minimize the input and inventory costs, and also the cost of not meeting the demand:

$$\phi^E = \sum_{j \in \mathcal{J}_0^{N-1}} \sum_{i \in \mathcal{U}} C_i^U \bar{u}_{j,i} + \sum_{j \in \mathcal{J}_1^N} \sum_{g \in \mathcal{G}} C_g^B B_{j,g}^d + \sum_{j \in \mathcal{J}_1^N} \sum_{g \in \mathcal{G}} C_g^I I_{j-1,g} \tag{4.26}$$

  where C_i^U, C_g^B and $C_g^I \geq 0$ are cost coefficients.

- *Control performance*: The term ϕ^C penalizes deviation of the output reference trajectory $y_{j,i}^{\text{ref}}$ and the output $\bar{y}_{j,i}$ from the quality target $y_{j,i}^{\text{targ}}$ during production mode ($z_{j,l,g} = 1$). It is computed using

$$\phi^C = \sum_{i \in \mathcal{Y}} \left(\sum_{j \in (\mathcal{N}^{RCL} \cup \mathcal{N}^{ACL})} \rho_i^{\text{ref}} \phi_{j,i}^{\text{ref}} + \sum_{j \in \mathcal{J}_1^N} \rho_i^{\bar{y}} \phi_{j,i}^{\bar{y}} \right) \tag{4.27a}$$

$$y_{j+1,i}^{\text{ref}} - y_{j+1,i}^{\text{targ}} + \eta_{j,i}^1 - \eta_{j,i}^2 = 0 \qquad \forall j \in (\mathcal{N}^{RCL} \cup \mathcal{N}^{ACL}), i \in \mathcal{Y} \tag{4.27b}$$

$$\phi_{j,i}^{\text{ref}} \geq \eta_{j,i}^1 + \eta_{j,i}^2 - (1 - \sum_{g \in \mathcal{G}} z_{j+1,l,g}) M_i^{\text{ref}} \qquad \forall j \in (\mathcal{N}^{RCL} \cup \mathcal{N}^{ACL}), l \in \mathcal{L}, i \in \mathcal{I}^{(l)} \tag{4.27c}$$

$$\eta_{j,i}^1,\ \eta_{j,i}^2,\ \phi_{j,i}^{\text{ref}} \geq 0 \qquad \forall j \in (\mathcal{N}^{RCL} \cup \mathcal{N}^{ACL}), i \in \mathcal{Y} \tag{4.27d}$$

$$\bar{y}_{j,i} - y_{j,i}^{\text{targ}} + \eta_{j,i}^3 - \eta_{j,i}^4 = 0 \qquad \forall j \in \mathcal{J}_1^N \tag{4.27e}$$

$$\phi^{\bar{y}}_{j,i} \geq \eta^3_{j,i} + \eta^4_{j,i} - (1 - \sum_{g \in \mathcal{G}} z_{j,l,g}) M^{\bar{y}}_i \qquad \forall j \in \mathcal{J}^N_1, l \in \mathcal{L}, i \in \mathcal{I}^{(l)} \tag{4.27f}$$

$$\eta^3_{j,i},\ \eta^4_{j,i},\ \phi^{\bar{y}}_{j,i} \geq 0 \qquad \forall j \in \mathcal{J}^N_1, i \in \mathcal{Y} \tag{4.27g}$$

where $\eta^1_{j,i}$, $\eta^2_{j,i}$, $\eta^3_{j,i}$, and $\eta^4_{j,i} \in \mathcal{R}$ are slack variables. $\phi^{\text{ref}}_{j,i}$ is forced to equal $\eta^1_{j,i} + \eta^2_{j,i}$ only when $\sum_{g \in \mathcal{G}} z_{j+1,l,g} = 1$. Otherwise, if $\sum_{g \in \mathcal{G}} z_{j+1,l,g} = 0$, $\phi^{\text{ref}}_{j,i}$ is allowed to take the value zero. A similar logic follows for $\phi^{\bar{y}}_{j,i}$. M^{ref}_i and $M^{\bar{y}}_i$ are sufficiently large positive constants (e.g. $M^{\text{ref}}_i = |y^{\text{ref}}_{\max,i} - y^{\text{ref}}_{\min,i}|$, $M^{\bar{y}}_i = |\bar{y}_{\max,i} - \bar{y}_{\min,i}|$). ρ^{ref}_i and $\rho^{\bar{y}}_i$ are weighting coefficients.

4.3 Case studies

To assess the performance of the integrated scheduling and control formulation proposed in this study, we consider a closed-loop implementation of the optimal set-point trajectories and scheduling decisions computed by the DRTO layer. That is, we simulate the plant response under the control scheme in Fig. 4.1, and use the simulated plant response to evaluate the economic performance of the proposed framework. The economic performance of the plant is measured using

$$EPM = -\sum_{j \in \mathcal{J}^{N^*-1}_0} \sum_{n \in \mathcal{U}} C^U_i \bar{u}_{*,j,i} - \sum_{j \in \mathcal{J}^{N^*}_1} \sum_{n \in \mathcal{G}} C^B_g B^d_{*,j,g} - \sum_{j \in \mathcal{J}^{N^*}_1} \sum_{n \in \mathcal{G}} C^I_g I_{*,j-1,g} \tag{4.28}$$

where N^* is the total number of simulation time-steps, $\bar{u}_{*,j,i}$ is the actual input value applied to the plant at simulation time-step j, $B^d_{*,j,g}$ corresponds to the actual value of the demand not met at the plant level, and $I_{*,j-1,g}$ is the actual inventory level of grade g at a simulation time-step j.

The integrated scheduling and control problem at the DRTO level is implemented in AMPL, via its Python programming interface, and solved using Gurobi. To solve the lower-level MPC problem and run the plant simulation, we use the python API of CasADi[1]. For all the

case studies, we use a Windows Server 2019 Standard, AMD EPYC 7H12 64-Core Processor 2.60 HGz (2 processors), 512 GB RAM.

For the first case study, we consider a linear plant with two reactors operating in parallel. Each reactor is controlled by an individual MPC subsystems, and there is no interaction between the feedback loops. However, the amounts produced in each reactor are determined by the DRTO, via the set-point trajectories assigned to the MPC subsystems. Therefore, the DRTO can coordinate the MPC subsystem to minimize the demand not met. We evaluate the plant performance for the hybrid, input-clipping and rigorous DRTO formulations for different values of the rescheduling period, Δt^{DRTO}.

For the second case study, we consider a a nonlinear reactor-separator that is controlled by two MPC subsystems. Different from the previous case study, there is significant interaction between the control loops. The nonlinear plant model is linearized to obtain the coefficients used in the linear DRTO process model (Eq. (4.1)), leading to a situation of plant-model mismatch.

4.3.1 Case Study I - Linear Dynamic Reactor System

For this case study, we consider a linear plant with two-parallel reactors $R1$ and $R2$. The transfer function of each reactor is given by[18]:

$$y_i(s) = \frac{1}{75s^2 + 15s + 1} u_i(s) \quad \forall i \in \{R1, R2\} \tag{4.29}$$

The manipulated inputs u_i are the inlet flow rates (L/min) to each reactor, and the measured outputs y_i are the outlet concentrations (mol/L). Each reactor is controlled by an MPC subsystem, such that $\mathcal{S} = \{S1, S2\}$. There are two production lines, $\mathcal{L} = \{L1, L2\}$. One output is monitored in each production line, $\mathcal{I}^{(L1)} = \{y_{R1}\}$, $\mathcal{I}^{(L2)} = \{y_{R2}\}$. Each MPC subsystem manipulates the inputs for the corresponding reactor, $\mathcal{U}^{(S1)} = \{u_{R1}\}$ and $\mathcal{U}^{(S2)} = \{u_{R2}\}$. Similarly, for the controlled outputs, $\mathcal{Y}^{(S1)} = \{y_{R1}\}$ and $\mathcal{Y}^{(S2)} = \{y_{R2}\}$. This plant produces three product grades, $\mathcal{G} = \{A, B, C\}$, for which the associated quality

target values, inventory costs and the cost of not meeting the demand are presented in Table 4.1. Additional parameter values, including input, output and reference trajectory bounds are presented in Table 4.2.

Table 4.1. Quality target band, molar mass, inventory cost, and cost of not meeting the demand for the linear case study.

g	$y_{g,i}^{\text{target}} \pm \epsilon_{g,i}\ \forall i \in \mathcal{Y}$ (mol/L)	m_g^w (kg/mol)	C_g^I (\$/kg)	C_g^B (\$/kg)
A	0.33 ± 0.01	3	0.05	1000
B	0.67 ± 0.02	1.5	0.03	1000
C	1 ± 0.03	1	0.02	1000

Table 4.2. MPC and DRTO parameters for linear case study.

MPC subsystems $S1$ and $S2$
$Q_{y_{R1}} = 1,\ Q_{y_{R2}} = 1\ R_{u_{R1}} = 1,\ R_{u_{R2}} = 1$
$P^{(S1)} = 15,\ P^{(S2)} = 15,\ M^{(S1)} = 3,\ M^{(S2)} = 3$
$u_{\min,u_{R1}} = 0.1,\ u_{\min,u_{R2}} = 0.1,\ u_{\max,u_{R1}} = 1.2,\ u_{\max,u_{R2}} = 1.2$
DRTO parameters
$N_A^{\text{target}} = 1,\ N_B^{\text{target}} = 1,\ N_C^{\text{target}} = 1,\ L = 3$
$N = 20,\ \Delta t = 2.5$ min
$C_{u_{R1}}^U = 1,\ C_{u_{R2}}^U = 1$
$\rho_{y_{R1}}^{\text{ref}} = 1 \times 10^4,\ \rho_{y_{R1}}^{\bar{y}} = 1 \times 10^4,\ \rho_{y_{R2}}^{\text{ref}} = 1 \times 10^4,\ \rho_{y_{R2}}^{\bar{y}} = 1 \times 10^4$
$\bar{y}_{\min,y_{R1}} = 0,\ \bar{y}_{\min,y_{R2}} = 0,\ \bar{y}_{\max,y_{R1}} = 1.2,\ \bar{y}_{\max,y_{R2}} = 1.2$
$y_{\min,y_{R1}}^{\text{ref}} = 0,\ y_{\min,y_{R2}}^{\text{ref}} = 0,\ y_{\max,y_{R1}}^{\text{ref}} = 1.5,\ y_{\max,y_{R2}}^{\text{ref}} = 1.5$

The mass of product $f_{j,l,g}$ (Eq. (4.21)) produced at each production line at a time-step j is given by[18]:

$$f_{j,L1,g} = \Delta t m_g^w y_{g,y_{R1}}^{\text{target}} \bar{u}_{j-1,u_{R1}} \qquad g \in \{A, B, C\} \tag{4.30}$$

$$f_{j,L2,g} = \Delta t m_g^w y_{g,y_{R2}}^{\text{target}} \bar{u}_{j-1,u_{R2}} \qquad g \in \{A, B, C\} \tag{4.31}$$

where m_g^w is the molar mass of grade g, presented in Table 4.1.

We perform a series of closed-loop plant simulations for different DRTO formulations, which are obtained by varying the sets $\mathcal{N}^{RCL}$, $\mathcal{N}^{ACL}$ and $\mathcal{N}^{OL}$ as shown in Table 4.3. We code name the formulations to facilitate referencing. For a given DRTO formulation, we also simulate the closed-loop plant response for several values of Δt^{DRTO}. While the set definition

has the potential to affect the solution time of the DRTO problem, and the quality of the solution, Δt^{DRTO} affects how soon the DRTO sees new information. For example, if we simulate the closed-loop plant response for 340 min using $\Delta t^{\text{DRTO}} = 5$, the DRTO layer is executed 68 times (once every 5 min). If $\Delta t^{\text{DRTO}} = 50$, the DRTO problem is solved 6 times (once every 50 min).

Table 4.3. Set definition for closed-loop simulation studies.

Code	$\mathcal{N}^{RCL}$	$\mathcal{N}^{ACL}$	$\mathcal{N}^{OL}$	DRTO formulation
R	$\{0,\ldots,19\}$	$\{\}$	$\{\}$	Rigorous
H10	$\{0,\ldots,9\}$	$\{10,\ldots,19\}$	$\{\}$	Hybrid
H8	$\{0,\ldots,7\}$	$\{8,\ldots,19\}$	$\{\}$	Hybrid
H4	$\{0,1,2,3\}$	$\{4,\ldots,19\}$	$\{\}$	Hybrid
H2	$\{0,1\}$	$\{2,\ldots,19\}$	$\{\}$	Hybrid
IC	$\{\}$	$\{0,\ldots,19\}$	$\{\}$	Input-clipping
OL	$\{\}$	$\{\}$	$\{0,\ldots,19\}$	Open-loop

Fig. 4.3 shows the time taken to solve the integrated scheduling and control problem every time that the DRTO layer is executed in a simulation case study. The x-axis indicates the DRTO formulation used in a particular simulation case study, as per Table 4.3. The red data points give the average time taken to solve the DRTO problem across one simulation. Any time that the DRTO problem is not solved to an optimality gap $\leq$0.01% in less than 30 min, the best feasible incumbent solution is ascribed to the lower-level control layer.

The data in Fig. 4.3 clearly indicates that the rigorous DRTO formulation (R) takes more time to solve compared to the hybrid and input-clipping formulations for all Δt^{DRTO} values considered. As the number of time-steps for which the rigorous closed-loop approach is used decreases, the average solution time also decreases. Among the closed-loop DRTO formulations considered, the input-clipping approach (IC) leads to the lowest solution times. However, as expected, its computational cost is still higher than for the open-loop formulation (OL). In fact, the computational cost of accounting for the control action within the DRTO formulation can be inferred by comparing the solution times of the hybrid, rigorous and input-clipping formulations with the open-loop (OL) one. The average solution time for the open-loop (OL) and input-clipping (IC) DRTO formulation for the case $\Delta t^{\text{DRTO}} = 5$ is 0.02 min and 0.13 min, respectively. Therefore, there is an added computational cost of 0.11

min to account for the control action using the input-clipping formulation (IC). This cost increases to 1.09 min when using the rigorous formulation (R).

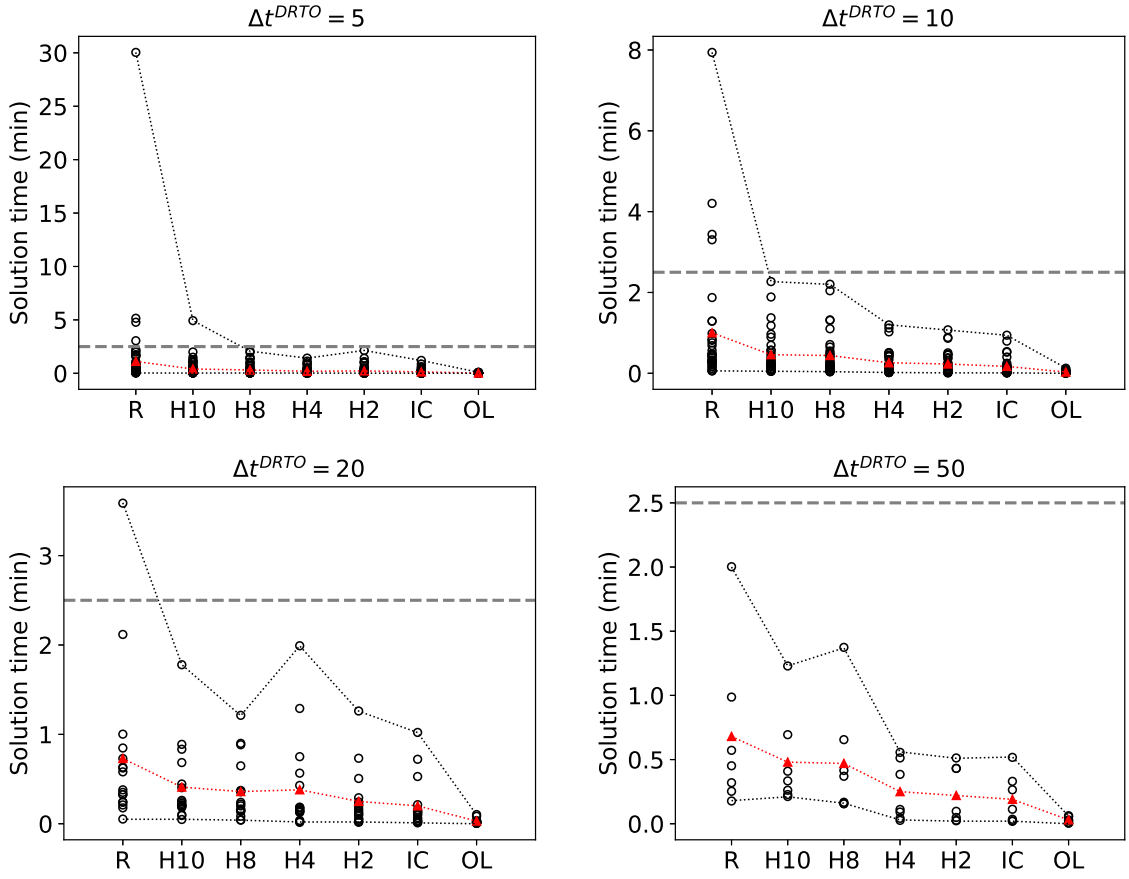

Figure 4.3. DRTO run-times (black circle) and average DRTO solution time (red circle) for different simulation case studies. The dashed gray line indicates the MPC sampling time. The black dotted lines are to help visualize the maximum and minimum DRTO run-times within a case study.

The plant economic performance metric (EPM) (Eq. (4.28)) for each case study is shown in Fig. 4.4. Lower EPM values indicate a poorer plant performance. The results indicate that a better performance can generally be achieved with the hybrid and rigorous formulations than with the input-clipping and open-loop approximations. The reason is that they better approximate the action of the lower-level controller. In fact, the rigorous formulation provides an exact representation of the lower-level controller in the absence of unmeasured disturbances and plant-model mismatch. The OL formulation neglects the control action leading to a significantly poorer closed-loop performance (EPM values displayed in red).

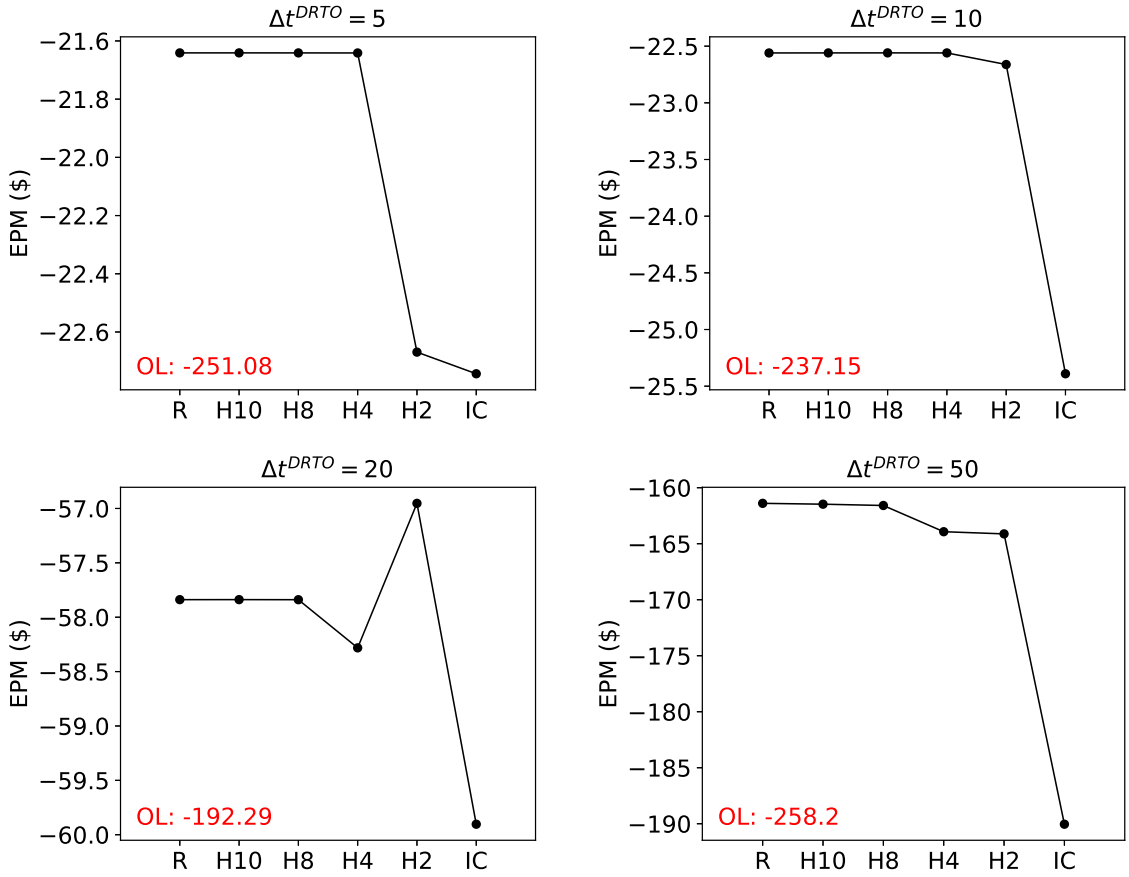

Figure 4.4. EPM values, in thousands of dollars, for the DRTO formulations in Table 4.3 and different Δt^{DRTO}.

There is a sharp decrease in performance as Δt^{DRTO} increases. This is expected because the higher the Δt^{DRTO}, the less frequently the DRTO problem is solved, impacting the frequency with which new information is taken into account. The later the DRTO becomes aware of a new demand order, the less time there is for the new demand order to fulfilled. In Fig. 4.5, we show the closed-loop plant response when using DRTO formulation H2 (Table 4.3) for Δt^{DRTO} = 5 min and Δt^{DRTO} = 20 min. Since $N = 20$ (DRTO horizon) and $\Delta t = 2.5$ min, every time the DRTO is executed, it receives information about the demand orders due 50 min ($N \times \Delta t$) ahead of the current simulation time. Consider the demand order of grade C at time 135 min, shown by the shaded area in Figs. 4.5e and f. If Δt^{DRTO} = 5 min, the DRTO becomes aware of the order at simulation time 85 min ($85 + N * \Delta t = 85 + 20 * 2.5 = 135$). Otherwise if $\Delta t^{\text{DRTO}} = 20$, the DRTO becomes aware of the same order only at simulation

time 100 min since the DRTO executed at 80 min only sees the demand orders until 130 min. This is reflected on the plots of y_{R1} in Figs. 4.5a and b. In Fig. 4.5b we have that the transition to produce grade C starts only at time 100 min while in Fig. 4.5a the transition starts earlier. This impacts the inventory level and the amount of the demand order met at 135 min (Figs. 4.5e and 4.5f). The plant response for the case where $\Delta t^{\text{DRTO}} = 50$ min and a rigorous DRTO formulation is used is displayed in Fig. 4.6. The main reason for the poor EPM is the delay in accounting for new information due to the large Δt^{DRTO}.

The H2 DRTO formulation, used to simulate the plant response shown on the right in Fig. 4.5, leads to a better EPM than the other formulations, including the rigorous, for $\Delta t^{\text{DRTO}} =$ 20 min (Fig. 4.4). This is due to the finite DRTO horizon. While the inventory of grade C remaining after time 170 min (Fig. 4.6e) would ordinarily lead to higher inventory costs, it actually helps to meet the next order of grade C at 215 min. Note that the DRTO is not aware of the demand of grade C at 215 min when it decides to produce more of grade C than that required to meet the demand at time 170 min. Due to the discrete nature of the DRTO model, the DRTO executed at time 160 min has the option to either not completely meet the demand of grade C at time 170 min, or to produce C for one more time-step. Since the cost of not meeting even a small value of the demand order is very high, it prefers to produce a little more of grade C leading to the nonzero inventory value after time 170 min.

The open-loop DRTO formulation (OL) leads to the worst performance among all formulations considered (EPM values in red in Fig.4.4). In Fig. 4.6, we show the simulated plant response for the OL DRTO formulation and Δt^{DRTO}= 20 min. The reference trajectories computed by the OL formulation leads to a more sluggish plant response compared to the other closed-loop formulations. As a result, it also incurs in higher costs for not meeting the demand.

Ideally, the time taken to solve the DRTO problem should not be higher than Δt. The results presented in Figs. 4.3 and 4.4 suggest that a good compromise between the integrated scheduling and control problem complexity and plant performance can be achieved using a hybrid formulation. The execution frequency of the DRTO layer plays a significant role on the performance, and should more or less match the frequency of new information updates,

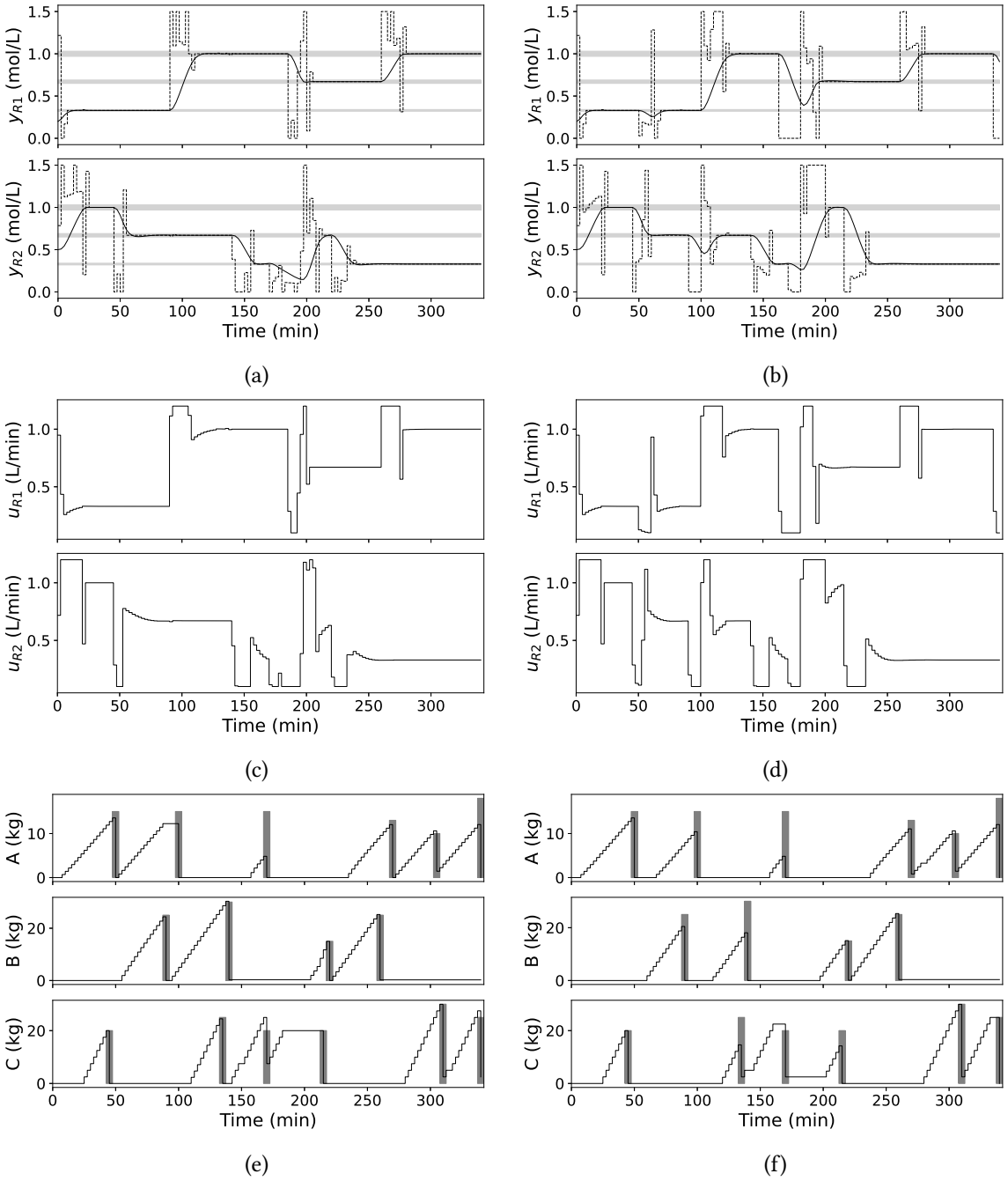

Figure 4.5. (a) Output, (c) input, and (e) inventory trajectories for $\Delta t^{\mathrm{DRTO}} = 5$ min. (b) Output, (d) input, and (f) inventory trajectories for $\Delta t^{\mathrm{DRTO}} = 20$ min. These results are for the DRTO formulation code H2. The reference trajectory is given by the dashed lines in (a) and (b). The shaded area indicates the quality target band in (a) and (b), and the size of the demand orders in (e) and (f).

such that the response time is improved.

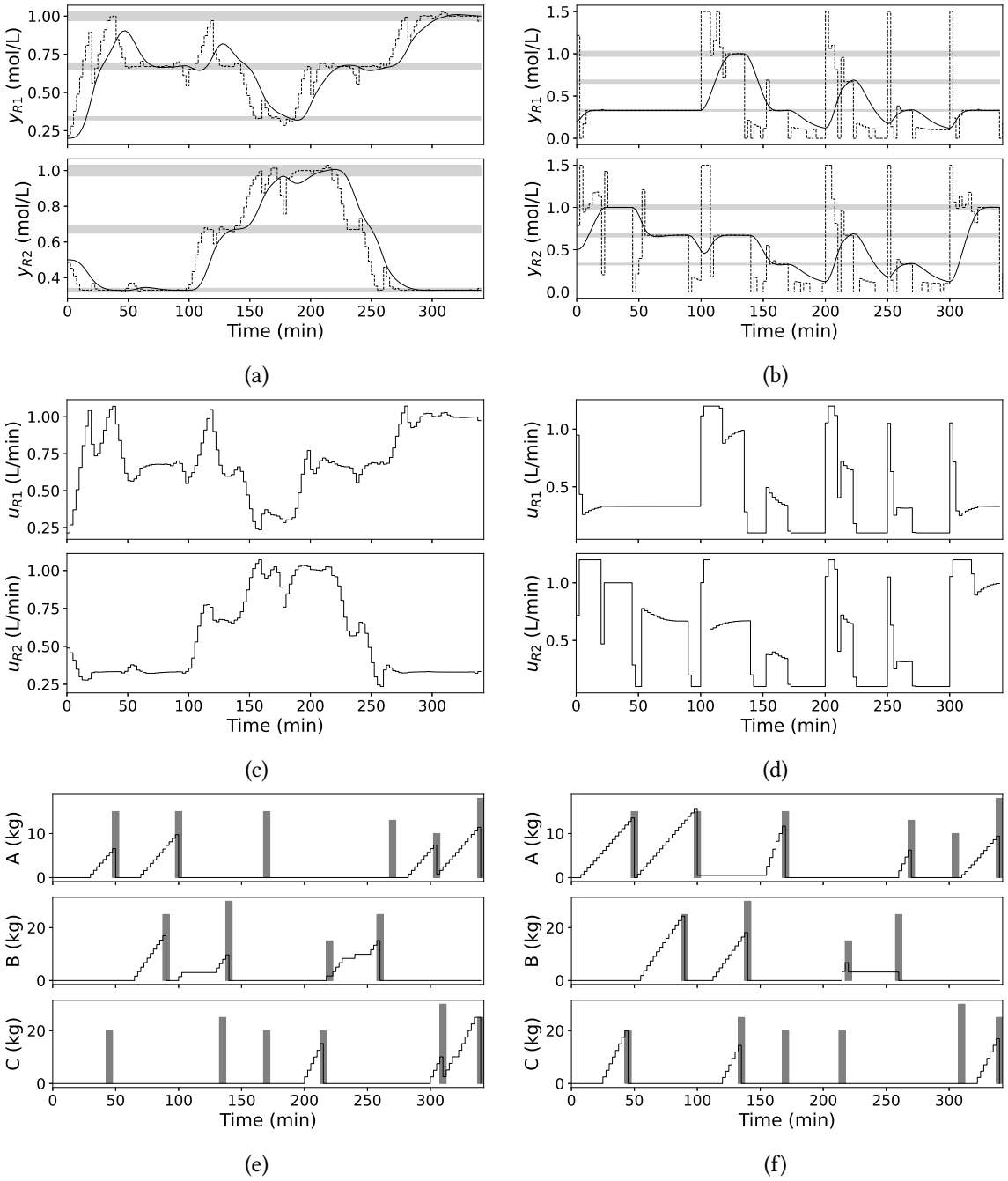

Figure 4.6. (a) Output, (c) input, and (e) inventory trajectories for $\Delta t^{\mathrm{DRTO}} = 20$ min and the open-loop (OL) DRTO formulation. (b) Output, (d) input, and (f) inventory trajectories for $\Delta t^{\mathrm{DRTO}} = 50$ min and the rigorous (R) DRTO formulation. The reference trajectory is given by the dashed lines in (a) and (b). The shaded area indicates the quality target band in (a) and (b), and the size of the demand orders in (e) and (f).

As seen in the in Fig. 4.5, the DRTO layer successfully coordinates the MPC subsystems to produce each grade according to the demand. Considering Fig. 4.5a, the DRTO-computed set-point trajectories lead to production of grade A in line 1 and production of grade C in line 2, between 0-50min. Between time 200-250 min, the bulk amount of grade B is produced in line 1, while line 2 is used just to complement the production to meet the demand of B at 220 min. We highlight that the transition trajectory and production sequencing are communicated to the plant exclusively through the set-point trajectories assigned to the lower-level MPC subsystem. This is possible because the DRTO is aware of the control dynamics, that is, of the control law (or an approximation thereof) that defines the relationship between the set-points and the input action. From a maintenance perspective, any changes to the lower-level control tuning parameters can be easily implemented at the DRTO level, and the derivation of new solution maps for the control action, as when using multiparametric programming, is not necessary.

4.3.2 Case Study II - Nonlinear Reactor-Separator System

For this case study, we consider a nonlinear reactor-separator system adapted from Liu et al.[16] and Li and Swartz[15], and presented in Fig. 4.7. This system produces a product C via the reaction $A \rightarrow B \rightarrow C$ that takes place in CSTR-1 and CSTR-2. No reaction takes place in the flash tank. F_{10} and F_{20} are inlet flow rates, F_r is the recycle stream flow rate and F_p is the purge stream flow rate. The bottom stream from the flash tank is the product stream. The flow rate of product from the flash tank is equal to $F_{20} + F_{10} - F_r - F_p$. V_i and T_i, $\forall i \in \{1,2,3\}$ are, respectively, the volume and temperature of the contents in vessel i. x_{Ai} and x_{Bi} are, respectively, the mass fraction of A, and mass fraction of B in vessel i. Q_i $\forall i \in \{1,2,3\}$ is the heat input to vessel i. We consider the production of three grades, instead of a single operating steady-state point in Liu et al. [16] and Li and Swartz [15].

The dynamic mathematical model of this process is as follows [16].

$$\frac{dx_{A1}}{dt} = \frac{F_{10}}{V_1}(x_{A10} - x_{A1}) + \frac{F_r}{V_1}(x_{Ar} - x_{A1}) - k_1 e^{\frac{-E_1}{RT_1}} x_{A1} \tag{4.32a}$$

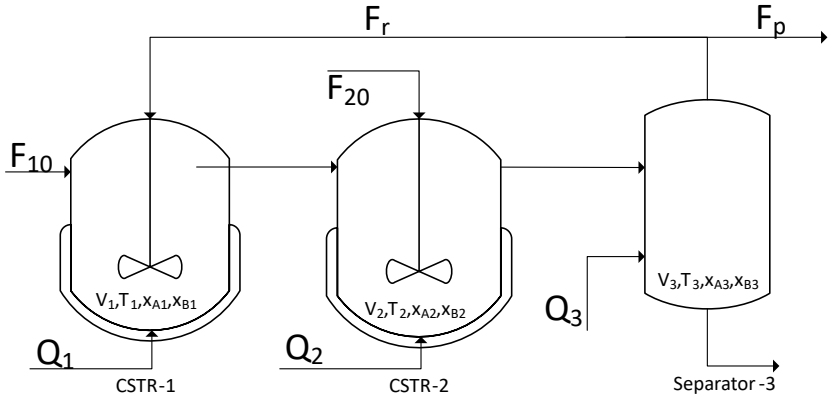

Figure 4.7. Schematic representation of the nonlinear reactor-separator process[16].

$$\frac{dx_{B1}}{dt} = \frac{F_{10}}{V_1}(x_{B10} - x_{B1}) + \frac{F_r}{V_1}(x_{Br} - x_{B1}) + k_1 e^{\frac{-E_1}{RT_1}} x_{A1} - k_2 e^{\frac{-E_2}{RT_1}} x_{B1} \tag{4.32b}$$

$$\frac{dT_1}{dt} = \frac{F_{10}}{V_1}(T_{10} - T_1) + \frac{F_r}{V_1}(T_3 - T_1) + \frac{-\Delta H_1}{C_p} k_1 e^{\frac{-E_1}{RT_1}} x_{A1} + \frac{-\Delta H_2}{C_p} k_2 e^{\frac{-E_2}{RT_1}} x_{B1} + \frac{Q_1}{\rho C_p V_1} \tag{4.32c}$$

$$\frac{dx_{A2}}{dt} = \frac{F_1}{V_2}(x_{A1} - x_{A2}) + \frac{F_{20}}{V_2}(x_{A20} - x_{A2}) - k_1 e^{\frac{-E_1}{RT_2}} x_{A2} \tag{4.32d}$$

$$\frac{dx_{B2}}{dt} = \frac{F_1}{V_2}(x_{B1} - x_{B2}) + \frac{F_{20}}{V_2}(x_{B20} - x_{B2}) + k_1 e^{\frac{-E_1}{RT_2}} x_{A2} - k_2 e^{\frac{-E_2}{RT_2}} x_{B2} \tag{4.32e}$$

$$\frac{dT_2}{dt} = \frac{F_1}{V_2}(T_1 - T_2) + \frac{F_{20}}{V_2}(T_{20} - T_2) + \frac{-\Delta H_1}{C_p} k_1 e^{\frac{-E_1}{RT_2}} x_{A2} + \frac{-\Delta H_2}{C_p} k_2 e^{\frac{-E_2}{RT_2}} x_{B2} + \frac{Q_2}{\rho C_p V_2} \tag{4.32f}$$

$$\frac{dx_{A3}}{dt} = \frac{F_2}{V_3}(x_{A2} - x_{A3}) - \frac{F_r + F_p}{V_3}(x_{Ar} - x_{A3}) \tag{4.32g}$$

$$\frac{dx_{B3}}{dt} = \frac{F_2}{V_3}(x_{B2} - x_{b3}) - \frac{F_r + F_p}{V_3}(x_{Br} - x_{B3}) \tag{4.32h}$$

$$\frac{dT_3}{dt} = \frac{F_2}{V_3}(T_2 - T_3) + \frac{Q_3}{\rho C_p V_3} \tag{4.32i}$$

$$x_{Ar} = \frac{\alpha_A x_{A3}}{\alpha_A x_{A3} + \alpha_B x_{B3} + \alpha_C x_{C3}} \tag{4.32j}$$

$$x_{Br} = \frac{\alpha_B x_{B3}}{\alpha_A x_{A3} + \alpha_B x_{B3} + \alpha_C x_{C3}} \tag{4.32k}$$

$$x_{Cr} = \frac{\alpha_C x_{C3}}{\alpha_A x_{A3} + \alpha_B x_{B3} + \alpha_C x_{C3}} \tag{4.32l}$$

x_{A10} and x_{B10} are the mass fractions of A and B in the inlet stream F_{10}, and x_{A20} and x_{B20} are the mass fractions of A and B in the inlet stream F_{20}. E_1, ΔH_1 and k_1 are the activation energy, heat of reaction and rate constant for the reaction $A \rightarrow B$, and E_2, ΔH_2 and k_2 are the activation energy, heat of reaction and rate constant for reaction $B \rightarrow C$. R is the ideal gas constant. α_A, α_B and α_C are the relative volatility of species A, B and C, respectively.

x_{C3} is the mass fraction of C in the product stream. We use $F_p = 0.01F_r$ for the purge stream. The parameter values are given in Table 4.4.

Table 4.4. Parameter values for reactor-separator system model[15].

Name	Value	Unit	Name	Value	Unit
V_1	89.4	m^3	ρ	0.15	kg/m^3
V_2	90	m^3	ΔH_1	-40	kJ/kg
V_3	13.27	m^3	ΔH_2	-50	kJ/kg
k_1	0.336	min^{-1}	x_{A10}	1	-
k_2	0.089	min^{-1}	x_{A20}	1	-
E_1	831.4	J/mol	x_{B10}	0	-
E_2	1247.1	J/mol	x_{B20}	0	-
T_{10}	313	K	α_A	3.5	-
T_{20}	313	K	α_B	0.5	-
C_p	2.5	kJ/(kg K)	α_C	1.1	-

This process is controlled by a distributed MPC system $\mathcal{S} = \{S1, S2\}$, configured as follows

$$\mathcal{U}^{(S1)} = \{F_{10}, Q_1\} \qquad \mathcal{U}^{(S2)} = \{F_{20}, Q_2, F_r, Q_3\}$$
$$\mathcal{Y}^{(S1)} = \{T_1\} \qquad \mathcal{Y}^{(S2)} = \{T_2, T_3, x_{B3}\}$$
$$\mathcal{X}^{(S1)} = \{x_{A1}, x_{B1}, T_1\} \qquad \mathcal{X}^{(S2)} = \{x_{A2}, x_{B2}, T_2, x_{A3}, x_{B3}, T_3\}$$

To obtain the model coefficients for subsystem s (Eqs. (4.4b) - (4.4d)), we take the relevant equations for that subsystem from Eq. (4.32) and set any input or state i that is not part of subsystem s ($i \notin \mathcal{U}^{(s)}$ and $i \notin \mathcal{X}^{(s)}$) to its corresponding steady-state value. Then, we linearize the resulting system with respect to the inputs and states that belong to subsystem s. The last step is to obtain a discrete-time representation. For example, to obtain the linear model for MPC subsystem $S1$, we take Eqs. (4.32a)-(4.32c), set x_{A2}, x_{B2}, T_2, x_{A3}, x_{B3}, T_3, F_{20}, Q_2, F_r, and Q_3 to their respective steady-state values, and linearize the resulting system around the steady-state value of the variables x_{A1}, x_{B1}, T_1, F_{10}, and Q_1. We also linearize and obtain a discrete-time representation of the full model (Eq. (4.32)) that is used as the DRTO process model (Eq. (4.1)). The steady-state point used for linearization is $F_{10}^{ss} = 5.64992$, $Q_1^{ss} = 10.1$, $F_{20}^{ss} = 3.28279$, $Q_2^{ss} = 44.6758$, $F_r^{ss} = 5, Q_3^{ss} = 13.5321$, $x_{A1}^{ss} = 0.212011$, $x_{B1}^{ss} = 0.376558$, $T_1^{ss} = 347.019988$, $x_{A2}^{ss} =$

0.150814, $x_{B2}^{ss} = 0.388438$, $T_2^{ss} = 354.429994$, $x_{A3}^{ss} = 0.079414$, $x_{B3}^{ss} = 0.475$, $T_3^{ss} = 357.019986$. The plant response is simulated using the nonlinear model in Eq. (4.32). This leads to a situation of plant model mismatch since a linear model is used in the DRTO and MPC subsystems.

The quality target set-points for the different product grades, $\mathcal{G} = \{C1, C2, C3\}$, are presented in Table 4.5. The MPC and DRTO parameter values are given in Table 4.6. There is only one production line $\mathcal{L} = \{L1\}$, and $\mathcal{I}^{(L1)} = \{T_1, T_2, T_3, x_{B3}\}$.

Table 4.5. Quality target band $y_{g,i}^{\text{target}} \pm \epsilon_{g,i}$ for nonlinear case study.

$g \backslash i$	T_1	T_2	x_{B3}	T_3
C1	349.9 ± 1.5	352.2 ± 1.5	0.4 ± 0.01	355.0 ± 1
C2	341.6 ± 1.5	347.6 ± 1.5	0.5 ± 0.01	350.0 ± 1
C3	333.6 ± 1.5	336.9 ± 1.5	0.6 ± 0.02	338.1 ± 1

Table 4.6. MPC and DRTO parameters for nonlinear case studies.

MPC subsystem $S1$
$P^{(S1)} = 5$, $M^{(S1)} = 2$, $Q_{T_1} = 1 \times 10^{-6}$, $R_{F_{10}} = 6.7 \times 10^{-4}$, $R_{Q_1} = 1 \times 10^{-4}$, $S_{Q_1} = 2 \times 10^{-5}$
$u_{\min,F_{10}} = 0$, $u_{\min,Q_1} = 0$, $u_{\max,F_{10}} = 15$, $u_{\max,Q_1} = 50$
MPC subsystem $S2$
$P^{(S2)} = 5$, $M^{(S2)} = 2$, $Q_{T_2} = 1 \times 10^{-6}$, $Q_{T_3} = 1 \times 10^{-6}$, $Q_{x_{B3}} = 1$
$R_{F_{20}} = 5 \times 10^{-4}$, $R_{Q_2} = 1 \times 10^{-4}$, $R_{F_r} = 1 \times 10^{-2}$, $R_{Q_3} = 1 \times 10^{-4}$, $S_{Q_3} = 5 \times 10^{-5}$
$u_{\min,F_{20}} = 0$, $u_{\min,Q_2} = 0$, $u_{\min,F_r} = 0$, $u_{\min,Q_3} = 0$
$u_{\max,F_{20}} = 20$, $u_{\max,Q_2} = 100$, $u_{\max,F_r} = 15$, $u_{\max,Q_3} = 20$
DRTO Parameters
$\Delta t = 5$ min, $\Delta t^{\text{DRTO}} = 10$ min, $N = 30$, $L = 3$
$\mathcal{N}^{RCL} = \{0,1,2,3\}$, $\mathcal{N}^{ACL} = \{4,\ldots,29\}$, $\mathcal{N}^{OL} = \{\}$
$N_{C1}^{\text{target}} = 1$, $N_{C2}^{\text{target}} = 1$, $N_{C3}^{\text{target}} = 1$
$C_{F10}^{U} = 1 \times 10^{-4}$, $C_{F20}^{U} = 4 \times 10^{-4}$, $C_{F_r}^{U} = 7 \times 10^{-4}$
$C_{C1}^{B} = 10$, $C_{C2}^{B} = 10$, $C_{C3}^{B} = 10$
$\rho_{T_1}^{\text{ref}} = 10$, $\rho_{T_2}^{\text{ref}} = 10$, $\rho_{T_3}^{\text{ref}} = 10$, $\rho_{x_{B3}}^{\text{ref}} = 1 \times 10^4$
$\rho_{T_1}^{\bar{y}} = 10$, $\rho_{T_2}^{\bar{y}} = 10$, $\rho_{T_3}^{\bar{y}} = 10$, $\rho_{x_{B3}}^{\bar{y}} = 1 \times 10^4$
$\bar{y}_{\min,T_1} = 326$, $\bar{y}_{\min,T_2} = 324$, $\bar{y}_{\min,x_{B3}} = 0.2$, $\bar{y}_{\min,T_3} = 326$
$\bar{y}_{\max,T_1} = 357$, $\bar{y}_{\max,T_2} = 364$, $\bar{y}_{\max,x_{B3}} = 0.65$, $\bar{y}_{\max,T_3} = 366$
$y_{\min,T_1}^{\text{ref}} = 300$, $y_{\min,T_2}^{\text{ref}} = 300$, $\bar{y}_{\min,x_{B3}} = 0$, $y_{\min,T_3}^{\text{ref}} = 300$
$y_{\max,T_1}^{\text{ref}} = 380$, $y_{\max,T_2}^{\text{ref}} = 380$, $y_{\max,x_{B3}}^{\text{ref}} = 0.8$, $y_{\max,T_3}^{\text{ref}} = 380$
$u_{\min,Q_1}^{\text{ref}} = 0$, $u_{\min,Q_3}^{\text{ref}} = 0, u_{\max,Q_1}^{\text{ref}} = 50$, $u_{\max,Q_3}^{\text{ref}} = 20$

Fig. 4.8 shows the simulated plant response for different values of the heat input coefficients,

which are presented in Table 4.7. At every DRTO execution, the integrated scheduling and control problem was always solved to an optimality gap $\leq$3% in less than the MPC sampling time Δt. Despite the plant-model mismatch, the DRTO is able to drive the plant to produce all three different products grades in all cases. This is largely due to the disturbance estimate $\bar{d}_i$ in Eq. (4.1), which acts as a correction term for the linear DRTO process model. Note that steady-state operation is not reached, and the different grades are produced while in transient operation. The capability of producing valuable product while in transition is highly attractive for processes with large time-constants.

We highlight that the DRTO attempts to drive the plant to the optimal operating point computed using the linear process model, which may not coincide with the actual economically optimal operating point of the nonlinear plant, leading to suboptimal performance. While undesirable, this is typically the case in situations involving plant-model mismatch, and it is not within the scope of this paper to address this particular issue.

A breakdown of the input costs and usage is presented in Table 4.7. In case B, less is consumed of resource Q_2 compared to case A due to its higher cost. This is more evident during production of grade $C2$ ($\approx$ 175 - 275 min in Fig. 4.8a). Note also the increase in consumption of input Q_3 during the same period in order to satisfy the temperature quality constraints for grade $C2$ in the separator (T_3 in Fig. 4.8c). In case C, the cost of input Q_1 is 10 times higher than in case A leading the DRTO to compute set-point trajectories that reduce the usage of this resource (Fig. 4.8a). The flow-rate F_{10} to the first reactor is also reduced (Fig. 4.8b), allowing the quality constraints on $T1$ (Fig. 4.8c) for each one of the grades to be met. Observe that there is also a slight increase in the recycling rate to CSTR-1 (F_r Fig. 4.8b). The production level is not severely compromised due to a higher inlet flow-rate F_{20} to the second reactor (Fig. 4.8b), and associated increase in Q_2 (Fig. 4.8a) to meet the temperature constraints.

Note that F_{10} and Q_1 belong to MPC subsystem $S1$, while F_{20} and Q_2 are computed by MPC subsystem $S2$. If Q_1 is higher, less of Q_2 is required to maintain the temperature of the second reactor within the desired bounds. Consider the production of $C2$ between 150 and 300 min in Cases A and C. In Case A, Q_1 is higher compared to Case C, and conversely, $Q2$ is lower in

Case A than in Case C. The DRTO is cognizant of the interactions between the feedback loops, and ensures that the target constraints are met while reducing costs. Remarkably, as we mentioned before, a truly steady-state operation is never reached. Therefore, the DRTO can effectively coordinate the MPC subsystems via the set-point trajectories, under conditions of plant-model mismatch and transient operations, both of which occur simultaneously in this case study.

Table 4.7. Heat input cost coefficient, total input usage ($\sum_{j\in\mathcal{J}_0^{N^*-1}} \Delta t \bar{u}_{*,j,i}$) and associated input cost ($\sum_{j\in\mathcal{J}_0^{N^*-1}} C_i^U \bar{u}_{*,j,i}$).

	i	Case A	Case B	Case C
Cost coefficient C_i^U	Q_1	0.08	0.08	0.8
	Q_2	0.008	0.024	0.008
	Q_3	0.006	0.006	0.006
Usage/Cost	F_{10}	787/0.12	784/0.12	723/0.11
	Q_1	2366/189.26	2339/187.13	1858/1,486.15
	F_{20}	203/0.08	203/0.08	237/0.09
	Q_2	1012/8.10	996/23.91	1184/9.48
	F_r	425/0.30	423/0.30	466/0.33
	Q_3	1150/6.90	1179/7.08	1214/7.28
Total Input cost		204.76	218.62	1503.44

4.4 Conclusion

In recent years, there have been several publications on the integration of scheduling and control. Most studies that propose a closed-loop formulations for the integrated scheduling and control problem consider a centralized MPC as the underlying controller. However, for various reasons[19, 17], distributed MPC architectures are also used in the chemical industry. In this paper, we presented a closed-loop integrated scheduling and control formulation for plants controlled by distributed MPC systems.

A formulation is deemed closed-loop when it accounts for the action of the underlying control system in some manner. While it has been shown that closed-loop formulations have the potential to significantly improve process performance[13, 20, 9], compared to the open-loop counterpart that neglects the controller action, this often comes at a significant

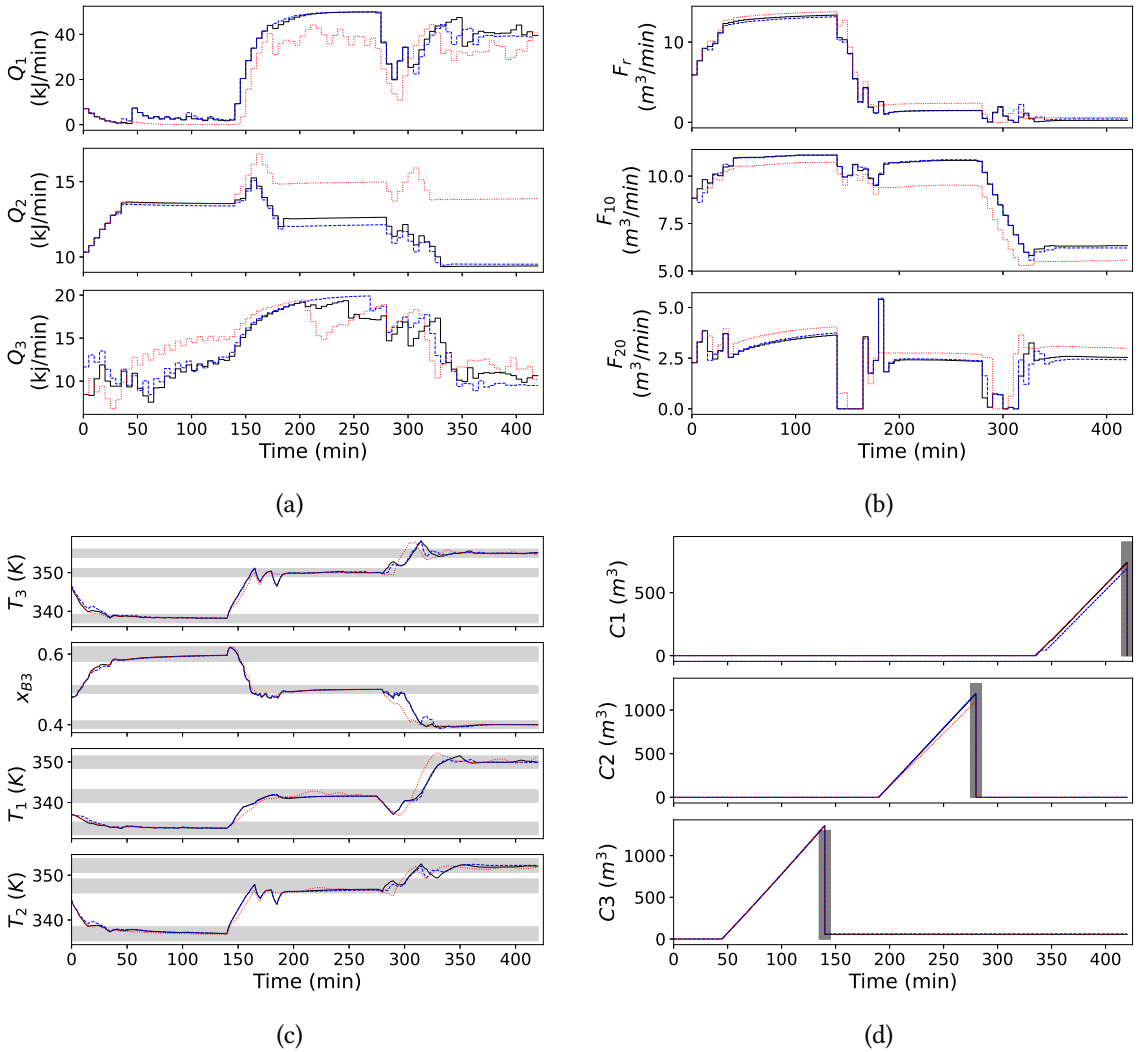

Figure 4.8. Simulated output, input and inventory trajectories for Case Study II, cases A (black solid line), B (blue dashed line) and C (red dotted line).

computational cost. With that mind, we first considered the rigorous closed-loop problem to establish a base case scenario. Then, we proposed closed-loop approximation strategies to reduce the computational burden. These strategies were compared from the perspective of the solution time and plant performance.

A rigorous closed-loop formulation for the integrated scheduling and control problem, where the underlying controller if of the MPC type, leads to a multilevel dynamic optimization problem. In this study, we recover a single-level formulation by replacing the embedded constrained MPC problems by their equivalent first order Karush-Kuhn-Tucker conditions.

The KKT-complementarity conditions are reformulated as mixed-integer linear constraints using binary variables. Moreover, we assume that a linear model with a disturbance estimate correction term is able to capture the process dynamics sufficiently well. As all the other constraints and objective function are linear the resulting integrated scheduling and control formulation is mixed-integer linear programming (MILP) problem, that can be solved by standard MILP solvers to global optimality. In this study, the integrated problem is solved at the DRTO level to compute set-points to the lower-level MPC subsystems.

In the case studies we showed that performance comparable to the rigorous formulation can be achieved using the proposed closed-loop approximations at a significantly lower computational cost. Our results also demonstrate the importance of frequent rescheduling to account for new information. Furthermore, we demonstrated the ability of the proposed framework to coordinate the MPC subsystems under perfect model knowledge and plant-model mismatch conditions. In the latter, the plant itself is nonlinear but a linear approximation is used at the DRTO level. Despite that, the proposed integrated scheduling and control formulation was able to drive the nonlinear plant to meet the quality constraints for different product grades while in transient operation. Its capability of coordinating the MPC subsystems to change the operating conditions in response to changes in the cost coefficients of utilities was also demonstrated. The ability to produce valuable product during transient operation has the potential to significantly enhance the profit of processes with large time constants.

References

[1] J. A. E. Andersson, J. Gillis, G. Horn, J. B. Rawlings, and M. Diehl. "CasADi – A software framework for nonlinear optimization and optimal control". In: *Mathematical Programming Computation* 11.1 (2019), pp. 1–36 (cit. on p. 116).

[2] R. Baker and C. L. E. Swartz. "Rigorous handling of input saturation in the design of dynamically operable plants". In: *Industrial & engineering chemistry research* 43.18 (2004), pp. 5880–5887 (cit. on p. 107).

[3] B. Burnak, J. Katz, N. A. Diangelakis, and E. N. Pistikopoulos. "Simultaneous process scheduling and control: a multiparametric programming-based approach". In: *Industrial & Engineering Chemistry Research* 57.11 (2018), pp. 3963–3976 (cit. on p. 101).

[4] P. D. Christofides, R. Scattolini, D. M. de la Pena, and J. Liu. "Distributed model predictive control: A tutorial review and future research directions". In: *Computers & Chemical Engineering* 51 (2013), pp. 21–41 (cit. on p. 100).

[5] D. Dering and C. Swartz. "An Integrated Scheduling and Control Framework for Plants Controlled by Distributed MPC Systems". In: *IFAC-PapersOnLine*. Vol. 56. 2. Elsevier, 2023, pp. 1417–1422 (cit. on p. 99).

[6] D. Dering and C. L. E. Swartz. "A closed-loop integrated scheduling and control formulation for processes controlled by distributed MPC systems". In: *2023 AICHE annual meeting in Orlando, FL, USA*. AICHE (cit. on p. 100).

[7] D. Dering and C. L. E. Swartz. "An Integrated Scheduling and Control Framework for Plants Controlled by Distributed MPC Systems". In: *IFAC World Congress 2023*. IFAC. 2023 (cit. on pp. 99, 101).

[8] D. Dering and C. L. E. Swartz. "Integration of scheduling and control for plants controlled by distributed MPC systems". In: *Industrial & Engineering Chemistry Research. Submitted* (2023) (cit. on p. 100).

[9] D. Dering and C. L. Swartz. "A stochastic optimization framework for integrated scheduling and control under demand uncertainty". In: *Computers & Chemical Engineering* 165 (2022), p. 107931 (cit. on pp. 100, 107, 109, 110, 130).

[10] L. S. Dias, R. C. Pattison, C. Tsay, M. Baldea, and M. G. Ierapetritou. "A simulation-based optimization framework for integrating scheduling and model predictive control, and its application to air separation units". In: *Computers & Chemical Engineering* 113 (2018), pp. 139–151 (cit. on p. 100).

[11] C. E. Garcia and A. Morshedi. "Quadratic programming solution of dynamic matrix control (QDMC)". In: *Chemical Engineering Communications* 46.1-3 (1986), pp. 73–87 (cit. on p. 104).

[12] M. Z. Jamaludin and C. L. E. Swartz. "Approximation of closed-loop prediction for dynamic real-time optimization calculations". In: *Computers & Chemical Engineering* 103 (2017), pp. 23–38 (cit. on pp. 104, 109).

[13] M. Z. Jamaludin and C. L. E. Swartz. "Dynamic real-time optimization with closed-loop prediction". In: *AIChE Journal* 63.9 (2017), pp. 3896–3911 (cit. on pp. 106, 107, 110, 130).

[14] H. Li and C. L. E. Swartz. "Approximation techniques for dynamic real-time optimization (DRTO) of distributed MPC systems". In: *Computers & Chemical Engineering* 118 (2018), pp. 195–209 (cit. on pp. 104, 107, 109).

[15] H. Li and C. L. Swartz. "Dynamic real-time optimization of distributed MPC systems using rigorous closed-loop prediction". In: *Computers & Chemical Engineering* 122 (2019), pp. 356–371 (cit. on pp. 125, 127).

[16] J. Liu, D. Muñoz de la Peña, and P. D. Christofides. "Distributed model predictive control of nonlinear process systems". In: *AIChE journal* 55.5 (2009), pp. 1171–1184 (cit. on pp. 125, 126).

[17] G. Pannocchia. "Distributed Model Predictive Control, In: Encyclopedia of Systems and Control". In: Springer London, 2015, pp. 301–308 (cit. on pp. 100, 130).

[18] J. E. Remigio and C. L. E. Swartz. "Production scheduling in dynamic real-time optimization with closed-loop prediction". In: *Journal of Process Control* 89 (2020), pp. 95–107 (cit. on pp. 107, 117, 118).

[19] R. Scattolini. "Architectures for distributed and hierarchical model predictive control–a review". In: *Journal of process control* 19.5 (2009), pp. 723–731 (cit. on pp. 100, 101, 130).

[20] J. M. Simkoff and M. Baldea. “Production scheduling and linear MPC: Complete integration via complementarity conditions”. In: *Computers & Chemical Engineering* 125 (2019), pp. 287–305 (cit. on pp. 100, 107, 130).

[21] J. Zhuge and M. G. Ierapetritou. “Integration of scheduling and control for batch processes using multi-parametric model predictive control”. In: *AIChE Journal* 60.9 (2014), pp. 3169–3183 (cit. on p. 100).

Chapter 5

Integration of scheduling and control for NMPC-controlled plants

An earlier version of this chapter has been published and presented in:

[1] D. Dering and C. L. E. Swartz. “Dynamic Real–Time Optimization with Closed-Loop Prediction for Nonlinear MPC–Controlled Plants”. In: *Computer Aided Chemical Engineering*. Vol. 51. Elsevier, 2022, pp. 1099–1104

[2] D. Dering and C. L. E. Swartz. “Dynamic Real-Time Optimization with Closed-Loop Prediction for Nonlinear MPC-Controlled Plants”. In: *ESCAPE 32 Conference*. 2022

The contents of this chapter will be submitted to:

[3] D. Dering and C. L. E. Swartz. "Integration of scheduling and control for NMPC-controlled plants". In: *Manuscript in preparation* (2023)

5.1 Introduction

While widely popular [27], LMPC is sometimes considered unsuitable for the operation of highly nonlinear processes owing to the limited accuracy of a linear model representation [25, 3]. In this situation, practitioners may resort to a nonlinear control system that utilizes a more accurate nonlinear model representation of the process dynamics. Examples of nonlinear processes that pose challenges to linear control systems are processes characterized by gain sign changes, input multiplicities [3], and multiple operating regimes [16]. Several nonlinear control strategies can be found in the literature [3]; however, in this study we focus on nonlinear model predictive control (NMPC) [25]. Practical NMPC applications include refineries and polymerization processes [16, 33], while simulation and experimental studies with NMPC encompass air-separation units [6, 32, 19], polymerization reactors [21], and pH neutralization [26].

To the author's knowledge, a control-aware scheduling formulation that directly accounts for NMPC has not yet been developed. In Andrés-Martínez and Ricardez-Sandoval [1], an NMPC controller is used to track the optimal trajectories computed by a plant dynamics-aware scheduler. Brengel and Seider [5], Palma-Flores and Ricardez-Sandoval [23], and Palma-Flores and Ricardez-Sandoval [24] account for the NMPC feedback action in a integrated design and control framework. Li and Swartz [20] and Dering and Swartz [9] propose a DRTO formulation (without scheduling) that utilizes the NMPC-KKT conditions to model the closed-loop dynamics of processes operated by distributed and centralized NMPC controllers, respectively. In our previous studies [13, 8], we considered PI and LMPC controlled processes. We used binary variables to model discrete scheduling decisions, and linearized the nonlinear process model to obtain an MILP formulation for the ISC problem that was solved using Gurobi.

In this study, we develop a closed-loop integrated scheduling and control formulation for

multiproduct plants controlled by NMPC. The integrated problem is solved at the DRTO level to compute set-point trajectories to the lower-level NMPC. Our formulation shares some similarities with previous studies regarding the scheduling formulation [34, 29, 13, 8], and the method used to account for the NMPC action [23] within the integrated framework. We use the first-order NMPC-KKT conditions to compute the input action within the integrated scheduling and control formulation [23]. However, due to the nonconvexity of the NMPC problem, the first-order KKT conditions are necessary but not sufficient for optimality. This means that the first-order KKT conditions are not guaranteed to yield a local optimum of the NMPC optimization problem. Moreover, we use complementarity conditions to capture discrete scheduling decisions, which leads to a mathematical program with complementarity constraints (MPCC) for the integrated scheduling problem. This MPCC problem is solved using a regularization method, to compute set-point trajectories tracked by the NMPC controller.

For the case studies, we consider a single input, multi-output (SIMO) process and a MIMO polymerization reactor system. We show that the complementarity formulation captures the discrete scheduling decisions sufficiently well. Moreover, knowledge of the control system enables the framework to adapt the set-point trajectories to different controller settings, including detuned conditions. In all cases, (i) the proposed formulation leads to good economic and process performance, (ii) the NMPC-KKT conditions at the DRTO level yield a local minimum of the NMPC problem, and (iii) the DRTO computed set-point trajectories guide the plant to meet the demand for all product grades.

5.2 Formulation

A schematic representation of the integrated scheduling and control framework proposed in this study is presented in Figure 5.1. The control-aware scheduler problem is solved at the DRTO level at simulation time-step j^* to compute the output y^{SP}_{j*} and input u^{SP}_{j*} set-point trajectories for the lower-level NMPC layer. Inventory levels I_{j*} and output measurements y^{m}_{j*} may be provided as feedback information from the plant to the NMPC and DRTO layers.

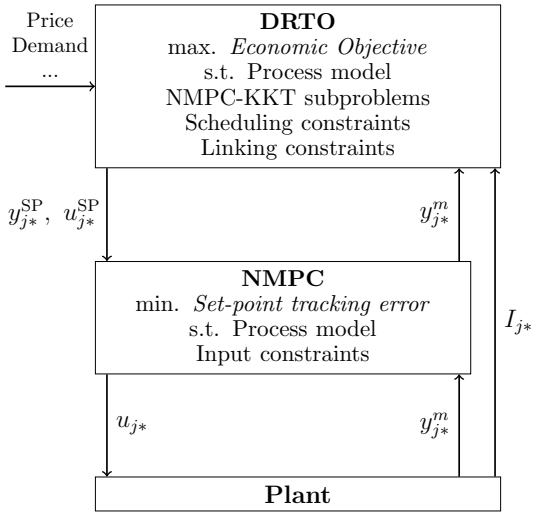

Figure 5.1. Integrated scheduling and control framework.

Market information regarding raw material costs, product prices and demand levels are also provided to the DRTO layer. The NMPC problem is solved at control intervals Δt, while the DRTO problem is solved at an execution interval Δt^{DRTO}.

In the next sections, we present the formulation of the dynamic optimization problem solved at the DRTO layer.

5.2.1 Process model

A discrete-time model is utilized to represent the plant at the DRTO level:

$$f(x_{j+1}, x_j, u_j, y_{j+1}) = 0 \qquad j \in \mathcal{J}_0^{N-1} \tag{5.1a}$$

$$g(x_j, y_j) = 0 \qquad j \in \mathcal{J}_1^{N} \tag{5.1b}$$

where $x_j \in \mathcal{R}^{n_x}$, $u_j \in \mathcal{R}^{n_u}$ and $y_j \in \mathcal{R}^{n_y}$ are vectors of the predicted states, inputs and outputs at DRTO time-step j. N is the DRTO horizon. $f : \mathcal{R}^{2n_x+n_u+n_y} \rightarrow \mathcal{R}^{n_x}$ and $g : \mathcal{R}^{n_x+n_u+n_y} \rightarrow \mathcal{R}^{n_y}$ are the discrete-time process model equations for the differential states and algebraic states (i.e. outputs), respectively. We use the notation $\mathcal{J}_a^b = \{i | a \leq i \leq b, i \in \mathcal{Z}\}$ to represent the set of discrete time-steps. Moreover, we define $\mathcal{Y} = \{1, \ldots, n_y\}$,

and $\mathcal{U} = \{1, \ldots, n_u\}$ as the set of the indices of the elements of the column vectors y_j and u_j.

Bounds are imposed on the state and output predictions as:

$$x_{\min} \leq x_j \leq x_{\max} \qquad j \in \mathcal{J}_1^N \tag{5.2a}$$

$$y_{\min} \leq y_j \leq y_{\max} \qquad j \in \mathcal{J}_1^N \tag{5.2b}$$

where the subscripts "min" and "max" denote the vectors of lower and upper bounds, respectively. Input bounds are enforced on the NMPC-KKT subproblems discussed in Section 5.2.3.

5.2.2 Scheduling constraints

The scheduling formulation presented in this section includes constraints to indicate the production sequencing, whether or not the outputs are meeting quality constraints, and whether or not product that meets the quality specifications is sent to storage.

Departing from standard scheduling formulations where discrete decisions are typically modeled using binary or integer variables, in this study, we capture discrete decisions using complementarity constraints. This choice is motivated by the presence of nonlinearities, which when combined with discrete scheduling decisions yield a mixed-integer nonlinear programming (MINLP) problem. MINLP problems are known to be very challenging and time consuming to solve. In our previous studies [13, 8], we linearized the plant model to yield a mixed-integer linear programming (MILP) problem, which is usually more tractable than a MINLP. By capturing the discrete scheduling decisions through complementarity conditions in the current study, the resulting problem can be cast as a nonlinear programming (NLP) problem, and solved using standard nonlinear optimization solvers. A similar strategy has been used in Simkoff and Baldea [34].

Figure 5.2 shows a schematic representation of a grade transition. The quality target band for quality i of product grades A and B is represented by the shaded area.

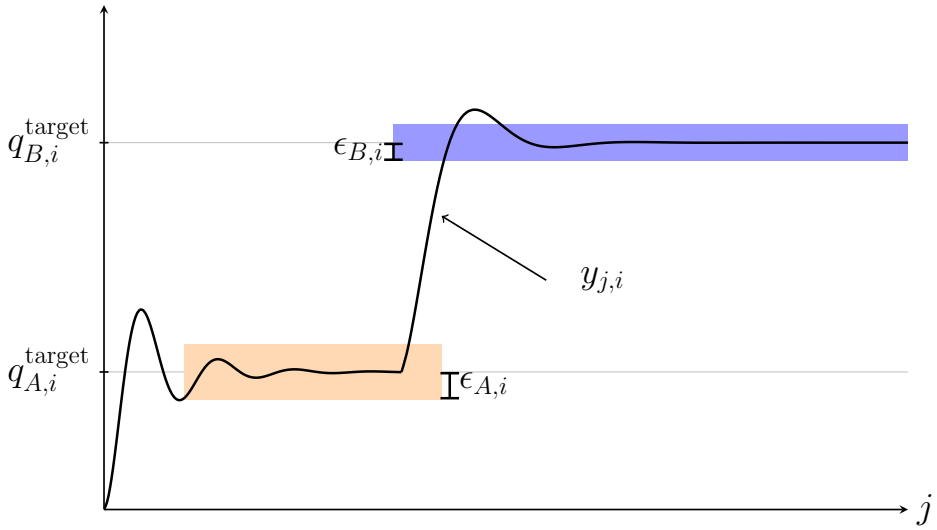

Figure 5.2. Schematic representation of the quality target band.

Eq. (5.3) is utilized to define whether or not output $y_{j,i}$, where $y_{j,i}$ is the i^{th} element of the vector y_j, is within the quality target band for grade g. $\mathcal{G}$ is the set of product grades, and $\mathcal{Q} \subset \mathcal{Y}$ is a subset of indices of the elements of y_j. $q_{g,i}^{\text{target}}$ denotes the target value for output i and grade g. $\epsilon_{g,i}$ is the quality target tolerance, as indicated in Figure 5.2. $s_{j,g,i}^{\text{a}}$, $s_{j,g,i}^{\text{b}}$, $s_{j,g,i}^{\text{c}}$, $s_{j,g,i}^{\text{d}} \in \mathcal{R}$ are positive slack variables. $\mu_{j,g,i}^{\text{lb}}$, $\mu_{j,g,i}^{\text{ub}} \in \mathcal{R}$ are complementarity constraint multipliers and serve that indicate whether the output is within the quality target band.

$$y_{j,i} - (q_{g,i}^{\text{target}} - \epsilon_{g,i}) - s_{j,g,i}^{\text{a}} + s_{j,g,i}^{\text{b}} = 0 \qquad j \in \mathcal{J}_1^N,\ g \in \mathcal{G},\ i \in \mathcal{Q} \tag{5.3a}$$

$$\left(1 - \mu_{j,g,i}^{\text{lb}}\right) s_{j,g,i}^{\text{a}} = 0 \qquad j \in \mathcal{J}_1^N,\ g \in \mathcal{G},\ i \in \mathcal{Q} \tag{5.3b}$$

$$\mu_{j,g,i}^{\text{lb}} s_{j,g,i}^{\text{b}} = 0 \qquad j \in \mathcal{J}_1^N,\ g \in \mathcal{G},\ i \in \mathcal{Q} \tag{5.3c}$$

$$(q_{g,i}^{\text{target}} + \epsilon_{g,i}) - y_{j,i} - s_{j,g,i}^{\text{c}} + s_{j,g,i}^{\text{d}} = 0 \qquad j \in \mathcal{J}_1^N,\ g \in \mathcal{G},\ i \in \mathcal{Q} \tag{5.3d}$$

$$\left(1 - \mu_{j,g,i}^{\text{ub}}\right) s_{j,g,i}^{\text{c}} = 0 \qquad j \in \mathcal{J}_1^N,\ g \in \mathcal{G},\ i \in \mathcal{Q} \tag{5.3e}$$

$$\mu_{j,g,i}^{\text{ub}} s_{j,g,i}^{\text{d}} = 0 \qquad j \in \mathcal{J}_1^N,\ g \in \mathcal{G},\ i \in \mathcal{Q} \tag{5.3f}$$

$$s_{j,g,i}^{\text{a}}, s_{j,g,i}^{\text{b}}, s_{j,g,i}^{\text{c}}, s_{j,g,i}^{\text{d}} \geq 0 \qquad j \in \mathcal{J}_1^N,\ g \in \mathcal{G},\ i \in \mathcal{Q} \tag{5.3g}$$

$$0 \leq \mu_{j,g,i}^{\text{lb}} \leq 1 \qquad j \in \mathcal{J}_1^N,\ g \in \mathcal{G},\ i \in \mathcal{Q} \tag{5.3h}$$

$$0 \leq \mu_{j,g,i}^{\text{ub}} \leq 1 \qquad j \in \mathcal{J}_1^N,\ g \in \mathcal{G},\ i \in \mathcal{Q} \tag{5.3i}$$

The complementarity conditions in Eq. (5.3c) ensure that either $\mu^{\text{lb}}_{j,g,i}$ or $s^{\text{b}}_{j,g,i}$ are zero at a given time-step j. If $\mu^{\text{lb}}_{j,g,i} = 0$, then $s^{\text{b}}_{j,g,i} \geq 0$, and $s^{\text{a}}_{j,g,i} = 0$ by Equation (5.3b). This implies, from Eq. (5.3a), that

$$y_{j,i} - (q^{\text{target}}_{g,i} - \epsilon_{g,i}) = -s^{\text{b}}_{j,g,i} \leq 0 \quad \rightarrow \quad y_{j,i} \leq q^{\text{target}}_{g,i} - \epsilon_{g,i}$$

Otherwise, if $\mu^{\text{lb}}_{j,g,i} > 0$, then $s^{\text{b}}_{j,g,i} = 0$, and from Eq. (5.3a) we have

$$y_{j,i} - (q^{\text{target}}_{g,i} - \epsilon_{g,i}) = s^{\text{a}}_{j,g,i} \geq 0 \quad \rightarrow \quad y_{j,i} \geq q^{\text{target}}_{g,i} - \epsilon_{g,i}$$

If a strict equality holds in the second expression, then $s^{\text{a}}_{j,g,i} = 0$, and any value of $\mu^{\text{lb}}_{j,g,i} \in (0, 1]$ satisfies Eq. (5.3b). However, if

$$y_{j,i} > q^{\text{target}}_{g,i} - \epsilon_{g,i}$$

then $s^{\text{a}}_{j,g,i} > 0$, and $\mu^{\text{lb}}_{j,g,i}$ is forced to equal 1 via Eq. (5.3b). A similar analysis can be done for Eqs. (5.3d)-(5.3f) to show that

$$(q^{\text{target}}_{g,i} + \epsilon_{g,i}) - y_{j,i} = s^{\text{c}}_{j,g,i} \geq 0 \quad \rightarrow \quad y_{j,i} \leq q^{\text{target}}_{g,i} + \epsilon_{g,i}$$

if $s^{\text{d}}_{j,g,i} = 0$. If in addition $s^{\text{c}}_{j,g,i} > 0$, then $\mu^{\text{ub}}_{j,g,i}$ is forced to equal one and

$$y_{j,i} < q^{\text{target}}_{g,i} + \epsilon_{g,i}.$$

Therefore, by the construct in Eq. (5.3), $\mu^{\text{lb}}_{j,g,i}$ and $\mu^{\text{ub}}_{j,g,i}$ are both simultaneously equal one only if $y_{j,i} \in [q^{\text{target}}_{g,i} - \epsilon_{g,i}, q^{\text{target}}_{g,i} + \epsilon_{g,i}]$. This is a *only if* instead of a *if and only if* condition because strict complementarity does not hold at the boundaries of the quality target band. $\mu^{\text{lb}}_{j,g,i}$ and $s^{\text{b}}_{j,g,i}$ can both be zero when $y_{j,i}$ is at the lower boundary of the quality target band, and $\mu^{\text{ub}}_{j,g,i}, s^{\text{d}}_{j,g,i}$ can both be zero when $y_{j,i}$ is at the upper boundary of the quality target band. Note however, that $\mu^{\text{lb}}_{j,g,i}$ and $\mu^{\text{ub}}_{j,g,i}$ will never be simultaneously one if $y_{j,i} \notin [q^{\text{target}}_{g,i} - \epsilon_{g,i}, q^{\text{target}}_{g,i} + \epsilon_{g,i}]$. That is, $\mu^{\text{lb}}_{j,g,i}\mu^{\text{ub}}_{j,g,i} = 0$ if $y_{j,i} \notin [q^{\text{target}}_{g,i} - \epsilon_{g,i}, q^{\text{target}}_{g,i} + \epsilon_{g,i}]$.

Moreover, based on the above analysis, the following tightening constraint holds

$$1 \leq \mu^{\text{lb}}_{j,g,i} + \mu^{\text{ub}}_{j,g,i} \leq 2 \tag{5.4}$$

since $\mu^{\text{lb}}_{j,g,i}$ and $\mu^{\text{ub}}_{j,g,i}$ can not both be simultaneously zero. That is, the output $y_{j,i}$ is either above the lower boundary (i.e. $y_{j,i} > q^{\text{target}}_{g,i} - \epsilon_{g,i}$) and/or below the upper boundary (i.e. $y_{j,i} < q^{\text{target}}_{g,i} + \epsilon_{g,i}$) of the quality target band .

We introduce $z^{\text{sto}}_{j,g} \in \mathcal{R}$ and Eq. (5.5) to define whether or not product that meets the quality specifications is sent to storage.

$$z^{\text{sto}}_{j,g} \leq \mu^{\text{lb}}_{j,g,i}\mu^{\text{ub}}_{j,g,i} \qquad j \in \mathcal{J}^N_1,\ g \in \mathcal{G}, i \in \mathcal{Q} \tag{5.5a}$$

$$0 \leq z^{\text{sto}}_{j,g} \leq 1 \qquad j \in \mathcal{J}^N_1,\ g \in \mathcal{G} \tag{5.5b}$$

Note that by Eq. (5.5a), $z^{\text{sto}}_{j,g}$ can be greater than zero only if all outputs simultaneously meet the quality requirements for grade g at time-step j. However, $z^{\text{sto}}_{j,g}$ is not guaranteed to have a binary value.

As we will see later in this section, $z^{\text{sto}}_{j,g}$ affects the inventory level predictions via Eq. (5.8b). In particular, if $z^{\text{sto}}_{j,g} < 1$ when all the predicted outputs are within the quality target band, the DRTO-predicted inventory level will be an underestimate of the actual inventory level (under perfect model conditions). The following complementarity constraint could be imposed to guarantee $z^{\text{sto}}_{j,g} \in \{0,1\}$:

$$z^{\text{sto}}_{j,g}(1 - z^{\text{sto}}_{j,g}) = 0 \qquad j \in \mathcal{J}^N_1,\ g \in \mathcal{G} \tag{5.6}$$

However, this type of constraint is usually avoided since it leads to a disjoint feasible region [4]. A binary solution for $z^{\text{sto}}_{j,g}$ can alternatively be achieved via careful formulation of the objective function, without necessitating Eq. (5.6). An example is the case where the objective function is to maximize the inventory level, since this would incentivize $z^{\text{sto}}_{j,g}$ to be one via Eq. (5.8b).

We also restrict the number of times that grade g can be produced in the DRTO horizon N

to one using the variable $z^{\text{aux}}_{j,g} \in \mathcal{R}$ and Eq. (5.7).

$$z^{\text{sto}}_{j+1,g} - z^{\text{sto}}_{j,g} \geq -z^{\text{aux}}_{j,g} \qquad j \in \mathcal{J}_1^{N-1},\ g \in \mathcal{G} \tag{5.7a}$$

$$\sum_{j=1}^{N-1} z^{\text{aux}}_{j,g} \leq 1 - \prod_{i \in \mathcal{Q}} \mu^{\text{lb}}_{N,g,i} \mu^{\text{ub}}_{N,g,i} \qquad g \in \mathcal{G} \tag{5.7b}$$

$$0 \leq z^{\text{aux}}_{j,g} \leq 1 \qquad j \in \mathcal{J}_1^{N-1},\ g \in \mathcal{G} \tag{5.7c}$$

Provided that $z^{\text{sto}}_{j,g}$ is integral, $z^{\text{aux}}_{j,g}$ is forced to equal one any time grade g stops being stored via Eq. (5.7a). Eq. (5.7b) guarantees that $z^{\text{aux}}_{j,g}$ is one only once in the DRTO horizon. We subtract $\prod_{i \in \mathcal{Q}} \mu^{\text{lb}}_{N,g,i} \mu^{\text{ub}}_{N,g,i}$ to prevent a grade that has already been produced one time, from being produced once more until the end of the prediction horizon. A similar construct is used in our previous studies [13, 8].

The amount of grade g in inventory at time-step j is then given by:

$$I_{j,g} = I_{j-1,g} + m_{j,g} - D^{\text{nom}}_{j,g} \qquad j \in \mathcal{J}_1^{N},\ g \in \mathcal{G} \tag{5.8a}$$

$$m_{j,g} = z^{\text{sto}}_{j,g} f^{\text{m}}(x_j, u_{j-1}, y_j) \qquad j \in \mathcal{J}_1^{N},\ g \in \mathcal{G} \tag{5.8b}$$

$$I_{j,g}, m_{j,g} \geq 0 \qquad j \in \mathcal{J}_1^{N},\ g \in \mathcal{G} \tag{5.8c}$$

where $I_{g,j} \in \mathcal{R}$ is the inventory level of grade g at time-step j, $m_{j,g} \in \mathcal{R}$ is the amount of grade g sent to storage at time-step j, $D^{\text{nom}}_{j,g}$ is the nominal demand of grade g at time-step j, and $f^{\text{m}} : \mathcal{R}^{n_x+n_u+n_y} \to \mathcal{R}$ is a scalar valued function to compute the product throughput. Note that in this formulation the demand must always be met.

Remarks A non-integral value for the variables $\mu^{\text{lb}}_{j,g,i}$, $\mu^{\text{ub}}_{j,g,i}$, and $z^{\text{sto}}_{j,g}$ will affect the inventory predictions via Eq. (5.8b). More specifically, if $z^{\text{sto}}_{j,g} < 1$ when all outputs are within the quality target band, the DRTO prediction will be an underestimate of the actual inventory level (under perfect model conditions). However, as we will show in the case studies, the complementarity formulation captures sufficiently well the discrete scheduling decisions.

5.2.3 NMPC-KKT subproblems

At a given time-step j, the following nonlinear set-point tracking problem is solved at the lower NMPC level to compute the inputs $\bar{u}_{j,0}$ applied to the plant:

$$\min_{\bar{u}_j,\bar{x}_j,\bar{y}_j} \quad \Phi^{MPC}(\bar{x}_j,\bar{u}_j,\bar{y}_j) = \sum_{k=1}^{P}\left(\bar{y}_{j,k}-y_{j,k}^{\mathrm{SP}}\right)^T Q\left(\bar{y}_{j,k}-y_{j,k}^{\mathrm{SP}}\right) + \sum_{k=0}^{M-1}\left(\bar{u}_{j,k}-u_{j,k}^{\mathrm{SP}}\right)^T S\left(\bar{u}_{j,k}-u_{j,k}^{\mathrm{SP}}\right) + \tag{5.9a}$$

$$\sum_{k=0}^{M-1}\left(\bar{u}_{j,k}-\bar{u}_{j,k-1}\right)^T R\left(\bar{u}_{j,k}-\bar{u}_{j,k-1}\right) \tag{5.9b}$$

subject to:

$$\bar{f}(\bar{x}_{j,k+1},\bar{x}_{j,k},\bar{u}_{j,k},\bar{y}_{j,k+1}) = 0 \qquad k \in \mathcal{J}_0^{P-1} \tag{5.9c}$$

$$\bar{g}(\bar{x}_{j,k},\bar{u}_{j,k-1},\bar{y}_{j,k}) = 0 \qquad k \in \mathcal{J}_1^{P} \tag{5.9d}$$

$$\bar{u}_{j,k}-\bar{u}_{j,M-1} = 0 \qquad k \in \mathcal{J}_M^{P-1} \tag{5.9e}$$

$$\bar{x}_{\min} \le \bar{x}_{j,k} \le \bar{x}_{\max} \qquad k \in \mathcal{J}_1^{P} \tag{5.9f}$$

$$\bar{y}_{\min} \le \bar{y}_{j,k} \le \bar{y}_{\max} \qquad k \in \mathcal{J}_1^{P} \tag{5.9g}$$

$$\bar{u}_{\min} \le \bar{u}_{j,k} \le \bar{u}_{\max} \qquad k \in \mathcal{J}_0^{P-1} \tag{5.9h}$$

$\bar{x}_{j,k} \in \mathcal{R}^{n_x}$, $\bar{u}_{j,k} \in \mathcal{R}^{n_u}$ and $\bar{y}_{j,k} \in \mathcal{R}^{n_y}$ are the predicted state, input and output vectors at NMPC time-step k. $\bar{u}_j$, $\bar{x}_j$ and $\bar{y}_j$ are composite vectors:

$$\bar{u}_j = [\left(\bar{u}_{j,0}\right)^T,\ldots,\left(\bar{u}_{j,P-1}\right)^T]^T \tag{5.10a}$$

$$\bar{x}_j = [\left(\bar{x}_{j,1}\right)^T,\ldots,\left(\bar{x}_{j,P}\right)^T]^T \tag{5.10b}$$

$$\bar{y}_j = [\left(\bar{y}_{j,1}\right)^T,\ldots,\left(\bar{y}_{j,P}\right)^T]^T \tag{5.10c}$$

$y_{j,k}^{\mathrm{SP}} \in \mathcal{R}^{n_y}$ and $u_{j,k}^{\mathrm{SP}} \in \mathcal{R}^{n_x}$ are output and input set-points. $Q \in \mathcal{R}^{n_y \times n_y}$, $R \in \mathcal{R}^{n_u \times n_u}$ and $S \in \mathcal{R}^{n_u \times n_u}$ are weighting matrices. $\bar{f} : \mathcal{R}^{2n_x+n_u+n_y} \to \mathcal{R}^{n_x}$ and $\bar{g} : \mathcal{R}^{n_x+n_u+n_y} \to \mathcal{R}^{n_y}$ denote the discrete-time model representation of the plant utilized at the NMPC level. $\bar{x}_{\min}$

and $\bar{x}_{\max}$ are vectors of lower and upper bounds on the NMPC state predictions, $\bar{u}_{\min}$ and $\bar{u}_{\max}$ are vectors of lower and upper bounds on the computed input values, $\bar{y}_{\min}$ and $\bar{y}_{\max}$ are vectors of lower and upper bounds on the NMPC output predictions. Note that $y^{\mathrm{SP}}_{j,k}$, $u^{\mathrm{SP}}_{j,k}$, $\bar{x}_{j,0}$, and $\bar{u}_{j,-1}$ are parameters for the j^{th} NMPC problem.

At the DRTO level, we use the first-order KKT conditions of Eq. (5.9) to compute $\bar{u}_j$ at every DRTO time-step j. Defining the Lagrangian of Eq. (5.9) as:

$$\begin{aligned}\mathcal{L}(\bar{x}_j, \bar{u}_j, \bar{y}_j, \mu_j^{\min}, \mu_j^{\max}, \lambda_j) = \Phi^{MPC}(\bar{x}_j, \bar{u}_j, \bar{y}_j) - \lambda_j^T F(\bar{x}_j, \bar{u}_j, \bar{y}_j) \\ - \left(\mu_j^{\min}\right)^T X_{\min}(\bar{x}_j, \bar{u}_j, \bar{y}_j) - \left(\mu_j^{\max}\right)^T X_{\max}(\bar{x}_j, \bar{u}_j, \bar{y}_j)\end{aligned} \tag{5.11}$$

where $\mu_j^{\min} \in \mathcal{R}^{(n_x+n_y+n_u)P}$, $\mu_j^{\max} \in \mathcal{R}^{(n_x+n_y+n_u)P}$ is a vector of positive Lagrange multipliers for the inequality constraints, and $\lambda_j \in \mathcal{R}^{(n_x+n_y)P+n_u(P-M)}$ is a vector of Lagrange multipliers for the equality constraints. $F(\cdot)$ is a vector-valued function of all the equality constraints in Eqs. (5.9c)-(5.9e):

$$F = \begin{bmatrix} \bar{f}(\bar{x}_{j,1}, \bar{x}_{j,0}, \bar{u}_{j,0}, \bar{y}_{j,1}) \\ \bar{g}(\bar{x}_{j,1}, \bar{u}_{j,0}, \bar{y}_{j,1}) \\ \vdots \\ \bar{f}(\bar{x}_{j,P}, \bar{x}_{j,P-1}, \bar{u}_{j,P-1}, \bar{y}_{j,P}) \\ \bar{g}(\bar{x}_{j,P}, \bar{u}_{j,P-1}, \bar{y}_{j,P}) \\ \bar{u}_{j,M} - \bar{u}_{j,M-1} \\ \vdots \\ \bar{u}_{j,P-1} - \bar{u}_{j,M-1} \end{bmatrix} \tag{5.12}$$

$X_{\min}(\cdot)$ and $X_{\max}(\cdot)$ are vector-valued functions of the inequality constraints:

$$X_{\min}(\bar{x}_j, \bar{u}_j, \bar{y}_j) = \begin{bmatrix} \bar{u}_{j,0} - \bar{u}_{\min} \\ \vdots \\ \bar{u}_{j,P-1} - \bar{u}_{\min} \\ \bar{x}_{j,1} - \bar{x}_{\min} \\ \vdots \\ \bar{x}_{j,P} - \bar{x}_{\min} \\ \bar{y}_{j,1} - \bar{y}_{\min} \\ \vdots \\ \bar{y}_{j,P} - \bar{y}_{\min} \end{bmatrix} \qquad X_{\max}(\bar{x}_j, \bar{u}_j, \bar{y}_j) = \begin{bmatrix} \bar{u}_{\max} - \bar{u}_{j,0} \\ \vdots \\ \bar{u}_{\max} - \bar{u}_{j,P-1} \\ \bar{x}_{\max} - \bar{x}_{j,1} \\ \vdots \\ \bar{x}_{\max} - \bar{x}_{j,P} \\ \bar{y}_{\max} - \bar{y}_{j,1} \\ \vdots \\ \bar{y}_{\max} - \bar{y}_{j,P} \end{bmatrix} \tag{5.13}$$

Assuming that a suitable constraint qualification holds (e.g. linear independence constraint qualification (LICQ)), and that $\bar{f}(\cdot)$, $\bar{g}(\cdot)$ and $\Phi^{\text{MPC}}(\cdot)$ are differentiable, the first-order KKT conditions of problem (5.9) can be written as:

$$\frac{\delta \mathcal{L}}{\delta \bar{u}_j}(\bar{x}_j, \bar{u}_j, \bar{y}_j, \mu_j^{\min}, \mu_j^{\max}, \lambda_j) = 0 \tag{5.14a}$$

$$\frac{\delta \mathcal{L}}{\delta \bar{x}_j}(\bar{x}_j, \bar{u}_j, \bar{y}_j, \mu_j^{\min}, \mu_j^{\max}, \lambda_j) = 0 \tag{5.14b}$$

$$\frac{\delta \mathcal{L}}{\delta \bar{y}_j}(\bar{x}_j, \bar{u}_j, \bar{y}_j, \mu_j^{\min}, \mu_j^{\max}, \lambda_j) = 0 \tag{5.14c}$$

$$F(\bar{x}_j, \bar{u}_j, \bar{y}_j) = 0 \tag{5.14d}$$

$$X_{\min}(\bar{x}_j, \bar{u}_j, \bar{y}_j) \geq 0 \tag{5.14e}$$

$$X_{\max}(\bar{x}_j, \bar{u}_j, \bar{y}_j) \geq 0 \tag{5.14f}$$

$$\mu_j^{\min} \odot X_{\min}(\bar{x}_j, \bar{u}_j, \bar{y}_j) = 0 \tag{5.14g}$$

$$\mu_j^{\max} \odot X_{\max}(\bar{x}_j, \bar{u}_j, \bar{y}_j) = 0 \tag{5.14h}$$

$$\mu_j^{\min} \geq 0, \mu_j^{\max} \geq 0 \tag{5.14i}$$

The left-hand sides of Eqs. (5.14a)-(5.14c) are the gradient of the Lagrangian function with respect to the optimization variables. Eqs. (5.14d)-(5.14f) define the primal feasibility

conditions, Eqs. (5.14g)-(5.14h) are the complementarity conditions. Equations (5.14a)-(5.14c) together with (5.14i) give the dual feasibility conditions. Any point $\bar{u}_j, \bar{x}_j, \bar{y}_j$ that solves Eq. (5.14) is said to be a KKT-point. For nonlinear-nonconvex $\bar{f}(\cdot)$, $\bar{g}(\cdot)$, further analysis is necessary to check whether or not a KKT-point is a local mimimum of problem (5.9). For convex $\bar{f}(\cdot)$, $\bar{g}(\cdot)$, any solution to (5.14) is a global minimizer of (5.9).

We use Eq. (5.14) to compute $\bar{u}_{j-1}, \bar{x}_j$ and $\bar{y}_j$ at every prediction time-step $j \in \mathcal{J}_1^N$ at the DRTO level. However, at the lower NMPC level, problem (5.9) is solved using a suitable nonlinear optimization solver. After solving the DRTO problem, it is possible to verify if the DRTO computed values for $\bar{u}_j$ for all $j \in \mathcal{J}_0^{N-1}$ is a local minimum of (5.9), by solving the actual NMPC problem (formulated as in (5.9)) for every DRTO time-step j using an optimization solver.

5.2.4 Linking constraints

The value for u_j used in Eqs. (5.1) and (5.8) is obtained via the solution of the NMPC-KKT subproblems (Eq. (5.14)) as:

$$u_j = \bar{u}_{j,0} \qquad j \in \mathcal{J}_0^{N-1} \tag{5.15}$$

Mirroring the lower-level NMPC, the predicted value for $\bar{x}_{j,1}$, by the j^{th} NMPC-KKT subproblem, is the initial state value $\bar{x}_{j+1,0}$ for the NMPC-KKT subproblem solved at the subsequent DRTO time-step:

$$\bar{x}_{j,0} = \bar{x}_{j-1,1} \qquad j \in \mathcal{J}_1^N \tag{5.16}$$

Similarly, the computed values for $\bar{u}_{j,0}$ are required by the subsequent NMPC-KKT subproblems:

$$\bar{u}_{j,-1} = \bar{u}_{j-1,0} \qquad j \in \mathcal{J}_1^{N-1} \tag{5.17}$$

The NMPC set-point trajectories are related to the output $y_j^{\text{ref}} \in \mathcal{R}^{n_y}$ and input $u_j^{\text{ref}} \in \mathcal{R}^{n_u}$ reference trajectories via Eq. (5.18):

$$y_{j-1,k}^{\text{SP}} = y_j^{\text{ref}} \qquad j \in \mathcal{J}_1^N,\ k \in \mathcal{J}_1^P \tag{5.18a}$$

$$u_{j,k}^{\text{SP}} = u_j^{\text{ref}} \qquad j \in \mathcal{J}_0^{N-1},\ k \in \mathcal{J}_0^{M-1} \tag{5.18b}$$

The reference trajectories are degrees of freedom for the ISC problem, and there are other schemes, different from the one in Eq. (5.18), by which the set-point trajectory can be extracted from the reference trajectory [13]. We constrain the move of the output and input reference trajectory between time-steps using Eq. (5.19), where $\xi \in [0,1]$ is a user-defined parameter, and the subscripts min and max indicates lower and upper bound vectors.

$$y_j^{\text{ref}} - y_{j-1}^{\text{ref}} \leq \xi \left(y_{\text{max}}^{\text{ref}} - y_{\text{min}}^{\text{ref}} \right) \qquad j \in \mathcal{J}_1^N \tag{5.19a}$$

$$y_j^{\text{ref}} - y_{j-1}^{\text{ref}} \geq -\xi \left(y_{\text{max}}^{\text{ref}} - y_{\text{min}}^{\text{ref}} \right) \qquad j \in \mathcal{J}_1^N \tag{5.19b}$$

$$u_j^{\text{ref}} - u_{j-1}^{\text{ref}} \leq \xi \left(u_{\text{max}}^{\text{ref}} - u_{\text{min}}^{\text{ref}} \right) \qquad j \in \mathcal{J}_0^{N-1} \tag{5.19c}$$

$$u_j^{\text{ref}} - u_{j-1}^{\text{ref}} \geq -\xi \left(u_{\text{max}}^{\text{ref}} - u_{\text{min}}^{\text{ref}} \right) \qquad j \in \mathcal{J}_0^{N-1} \tag{5.19d}$$

$$y_{\text{min}}^{\text{ref}} \leq y_j^{\text{ref}} \leq y_{\text{max}}^{\text{ref}} \qquad j \in \mathcal{J}_1^N \tag{5.19e}$$

$$u_{\text{min}}^{\text{ref}} \leq u_j^{\text{ref}} \leq u_{\text{max}}^{\text{ref}} \qquad j \in \mathcal{J}_0^{N-1} \tag{5.19f}$$

5.2.5 Objective function

The economic objective function utilized at the DRTO level is defined as:

$$\min \quad \Phi^{DRTO} = \Phi^{eco} + \Phi^{control} + \Phi^{inv} \tag{5.20}$$

where:

$$\Phi^{eco} = \sum_{j \in \mathcal{J}_0^{N-1}} \left(\sum_{i \in \mathcal{U}} C_{j,i}^{U} u_{j,i} + \sum_{g \in \mathcal{G}} C_g^I I_{j,g} \right) \tag{5.21a}$$

$$\Phi^{control} = \sum_{j \in \mathcal{J}_1^N} \sum_{g \in \mathcal{G}} z_{j,g}^{\text{sto}} \left(\sum_{i \in \mathcal{Q}} P_i^Y (y_{j,i} - q_{g,i}^{\text{target}})^2 + \sum_{i \in \mathcal{U}} P_i^U (u_{j-1,i} - u_{j-2,i})^2 \right) \tag{5.21b}$$

Φ^{eco} computes the input and inventory cost, $\Phi^{control}$ penalizes deviation of the output from the quality target, and movement of the inputs during the storage mode (i.e. when $z_{j,g}^{\text{sto}} > 0$). $C_{j,i}^U$ is the cost of input i at time-step j, and C_g^I is the inventory cost of grade g. P_i^Y and P_i^U are user-defined coefficients, for which appropriate values can be chosen based on closed-loop simulations. The construct in (5.21b) prevents the outputs from sitting at the boundary of the target band, and also works as a buffer against modeling errors. Alternatively (or in addition) the quality target band parameter $\epsilon_{g,i}$, at the DRTO level, can be set to a smaller value than that used in the plant. In cases where $0 < z_{j,g}^{\text{sto}} < 1$, the importance of the term $\Phi^{control}$ is reduced. Φ^{inv} can be set-up as a soft constraint on the inventory level, such as:

$$\phi_g^{inv} \geq V_g^I (0.2 D_{j,g}^{\text{nom}} - I_{j,g}) \qquad \forall j \in \mathcal{J}_1^N,\ g \in \mathcal{G} \tag{5.22a}$$

$$\Phi^{inv} = \sum_{g \in \mathcal{G}} \phi_g^{inv} \tag{5.22b}$$

$$\phi_g^{inv} \geq 0 \qquad \forall g \in \mathcal{G} \tag{5.22c}$$

where V_g^I is a user-defined coefficient. In (5.22a), the right-hand side is the difference between a targeted inventory value, defined in terms of the nominal demand (the targeted inventory value corresponds to 20% of the nominal demand at the associated time-step), and the inventory level at the corresponding time-step. If $I_{j,g} \geq 0.2 D_{j,g}^{\text{nom}}$, ϕ_g^{inv} assumes a value of zero due to the constraint in Eq. (5.22c) and the fact that this is a minimization problem. If $I_{j,g} \leq 0.2 D_{j,g}^{\text{nom}}$, ϕ_g^{inv} is forced to assume a value greater than zero to satisfy Eq. (5.22a). That is, there is a penalization for not meeting the inventory targets.

5.2.6 NLP reformulation of the MPCC problem

It is widely accepted that mathematical programs with complementarity constraints (MPCC) are challenging to solve. The reason is that constraints of the type

$$x \odot y = 0$$
$$x, y \geq 0$$

where $\odot$ denotes element-wise multiplication of vectors, violate the linear independence constraint qualification (LICQ), and also the weaker Magasarian-Fromovitz constraint qualification (MFCQ) at every feasible point [4, 28]. Assuming that the KKT-Lagrange multipliers of an optimization problem exist, satisfaction of the LICQ guarantees that the multipliers are unique. On another hand, the MFCQ is necessary and sufficient for boundedness of the multipliers [4]. The violation of the constraint qualifications can lead to numerical instability of standard NLP solvers [18, 22, 31]. For example, algorithms that rely on a linearization of the active constraint set may fail or face numerical difficulties because the gradient of the active constraint set of a MPCC problem is singular. To overcome these challenges, MPCC problems are usually reformulated using a regularization or penalty approach [4, 28, 18, 30, 2]. A general MPCC problem of the form

$$\min_{x,y,z} \quad f(x,y,z) \tag{5.23a}$$
$$\text{subject to:} \quad h(x,y,z) = 0 \tag{5.23b}$$
$$g(x,y,z) \leq 0 \tag{5.23c}$$
$$x \odot y = 0 \tag{5.23d}$$
$$x, y \geq 0 \tag{5.23e}$$

can be reformulated using a regularization scheme as:

$$\min_{x,y,z} \quad f(x,y,z) \tag{5.24a}$$

$$\text{subject to:} \quad h(x,y,z) = 0 \tag{5.24b}$$
$$g(x,y,z) \leq 0 \tag{5.24c}$$
$$x \odot y \leq t_{\text{reg}} \tag{5.24d}$$
$$x, y \geq 0 \tag{5.24e}$$

where $t_{\text{reg}} > 0$ is the value of the regularization parameter. Usually, problem (5.24) is solved for a sequence of decreasing values of t_{reg}. Assume that problem (5.24) is first solved for a value of $t_{\text{reg}} = t^0_{\text{reg}}$, t_{reg} is then reduced by $\alpha < 1$ at every iteration until $||x \odot y||_\infty \leq t^f_{\text{reg}} \approx 0$. For a given choice of t^0_{reg} and α, the value of the regularization parameter in iteration n is given by:

$$t_{\text{reg}} = \max(\alpha^{n-1} t^0_{\text{reg}}, t^f_{\text{reg}}) \tag{5.25}$$

At every iteration, the optimal solution of the previous problem is used as initial guess for the current problem. A penalty reformulation scheme for (5.23) is given as:

$$\min_{x,y,z} \quad f(x,y,z) + \rho x^T y \tag{5.26a}$$
$$\text{subject to:} \quad h(x,y,z) = 0 \tag{5.26b}$$
$$g(x,y,z) \leq 0 \tag{5.26c}$$
$$x, y \geq 0 \tag{5.26d}$$

where $\rho > 0$ is the penalty parameter. An alternative formulation is:

$$\min_{x,y,z} \quad f(x,y,z) + \rho t \tag{5.27a}$$
$$\text{subject to:} \quad h(x,y,z) = 0 \tag{5.27b}$$
$$g(x,y,z) \leq 0 \tag{5.27c}$$
$$x \odot y \leq t \tag{5.27d}$$
$$x, y \geq 0 \tag{5.27e}$$

While problems (5.26) and (5.27) may be sequentially solved for increasing values of ρ, they are usually solved only once for a sufficiently large value of ρ [2]. Whether or not the optimal solution is feasible for (5.23), that is $x \odot y \approx 0$, has to be checked afterwards. It has been shown that the penalty method can get stuck in local solutions where the complementarities are not satisfied [18, 4].

5.3 Case studies

In this section, we present two case studies. The first one is for a SIMO system. We consider an offline solution of the integrated scheduling and control formulation, with the optimal set-point trajectories tracked online (in closed-loop) by the lower-level NMPC. For the second case study, we implement the proposed control-aware scheduler online and in closed-loop for a MIMO polymerization reactor system.

For all case studies, the control-aware scheduler (DRTO), lower-level NMPC and plant are implemented using CasADi (Python interface), in a Windows 10 64-bit, 16GB RAM, 3.6 GHz Intel Core i7-7700 processor machine. The plant model is integrated using IDAS [15]. We utilize the regularization method (Eq. (5.24)) with $t_{\text{reg}}^0 = 1$, $\alpha = 0.2$ and $t_{\text{reg}}^f = 9 \times 10^{-6}$, and IPOPT[35] with the linear solver MA97[17] to solve the DRTO-MPCC problem. IPOPT with the linear solver MA57[17] is used to solve the lower-level NMPC problem.

5.3.1 Case 1: SIMO system

For this case study, we consider the nonlinear model of a CSTR (Eq. (5.28)), adapted from Bequette [3], where the reaction

$$A \rightarrow B \rightarrow C$$

takes place.

$$\dot{C_A} = \frac{F}{V}(C_{Ai} - C_A) - k_1 C_A^2 \tag{5.28a}$$

$$\dot{C_B} = -\frac{F}{V}C_B + k_1 C_A^2 - k_2 C_B \tag{5.28b}$$

$$\dot{T} = \frac{F}{V}(Ti - T) + \frac{(-\Delta H_1)}{\rho C_p})k_1 C_A^2 + \frac{(-\Delta H_2)}{\rho C_p})k_2 C_B + \frac{Q}{\rho C_p V} \tag{5.28c}$$

$$k_1 = A_{10} e^{-E_{a1}/RT} \tag{5.28d}$$

$$k_2 = A_{20} e^{-E_{a2}/RT} \tag{5.28e}$$

C_{Ai} is the inlet concentration of reactant A, C_A and C_B are the outlet concentration of species A and B. T_i is the temperature of the inlet stream, and T is the temperature of the contents of the reactor. V is the volume, C_p is the heat capacity and ρ is the density of the contents of the reactor. R is the ideal gas constant, and Q is the heat input to the reactor. k_i, E_{ai} and ΔH_i are the pre-exponential rate constant, activation energy and heat of reaction, respectively, for reaction i. The parameter values are given in Table 5.1.

Table 5.1. Parameter values for Case 1.

Parameter	Value	Units
C_{Ai}	1.0	kmol/m^3
A_{10}	11.0	m^3/(kmol·s)
A_{20}	172.2	1/s
E_{a1}	4,180	kJ/(kmol·K)
E_{a2}	34,833	kJ/(kmol·K)
ρ	1,000	kg/m^3
C_p	1.0	kJ/(kg·°C)
ΔH_1	418,000	kJ/kmol
ΔH_2	418,000	kJ/kmol
R	8.314	kJ/(kmol·K)
V	100	m^3
T_i	25	°C
F	10	m^3/s

We assume that this plant produces three product grades, $\mathcal{G} = \{A, B, C\}$, for which the quality target values and inventory costs are given in Table 5.2. The DRTO and NMPC parameter values are presented in Table 5.3. We take $x = [C_A, C_B, T]^T$ as states, $y = [C_B, T]^T$ as outputs, and $u = Q$ as input. We use the Backward Euler scheme to discretize Eq. (5.28), and obtain a discrete system of equations of the form in (5.1) and (5.9c)-(5.9d). We use a smaller Euler step-size for Eq. (5.1) (0.5s) than for Eqs. (5.9c)-(5.9d) (2.5s).

Table 5.2. Quality target values (q_g^{target}), and inventory cost (C_g^I) for Case 1.

Parameter	A	B	C
C_B (kmol/m^3)	0.6	0.7	0.8
T (°C)	231	192	123
C_g^I (\$/m^3)	5×10^{-5}	7×10^{-5}	2×10^{-5}

Table 5.3. DRTO and NMPC parameters.

Parameter	Value
Δt	2.5
N	80
P	10
M	3
Q	diag(10, 0)
R	5×10^{-13}
S	0
$C_{j,1}^U$	1×10^{-8}
P_1^U	1×10^{-14}
P_1^Y	200
P_2^Y	1×10^{-4}
$\tilde{\zeta}$	0.1

Bounds on the input, output and state trajectories $\forall j \in \mathcal{J}_1^N, k \in \mathcal{J}_1^P$ are given by:

$$1 \times 10^6 \leq \bar{u}_{j-1,k-1} \leq 7 \times 10^6, \qquad \begin{bmatrix} 0 \\ 0 \\ 110 \end{bmatrix} \leq x_j, \bar{x}_{j-1,k} \leq \begin{bmatrix} 1 \\ 1 \\ 250 \end{bmatrix}$$

$$\begin{bmatrix} 0 \\ 110 \end{bmatrix} \leq y_j, \bar{y}_{j-1,k}, \leq \begin{bmatrix} 1 \\ 250 \end{bmatrix}$$

The bounds on the reference trajectory for C_B are,

$$0.1 \leq y_{j,1}^{\text{ref}} \leq 1 \qquad \forall j \in \mathcal{J}_1^N$$

The optimization problem at the DRTO level is given by Eqs. (5.1) - (5.5), (5.7), (5.8), (5.14)-

(5.21), with Φ^{inv} in Eq. (5.20) defined as:

$$\Phi^{inv} \geq -0.10 I_{N,g} \qquad \forall g \in \mathcal{G} \tag{5.29}$$

The expression above aims to maximize the inventory level of all grades at the end of the scheduling horizon.

Case 1a For this first case, the demand of each of the grades is due at 200h (end of scheduling horizon): $D^{\text{nom}}_{N,g} = 300 \; \forall g \in \mathcal{G}$. The simulated plant response is given by the solid lines in Figure 5.3, while the dashed lines correspond to the trajectory used as initial guess for the C_A, C_B, T and Q variables in the DRTO problem. We highlight that the DRTO problem is solved only once to compute the reference trajectory, given by the blue dotted line in the upper right plot in Figure 5.3. This reference trajectory is tracked by the lower-level NMPC controller in closed-loop. The lower-level NMPC problem is solved every 2.5s using IPOPT. The solid line in the lower right plot in Figure 5.3 corresponds to the input values computed by the lower-level NMPC and applied to the plant. The input trajectory computed by the lower-level NMPC matches the input trajectory computed using the NMPC-KKT conditions at the DRTO level at every sampling-time. Therefore, the NMPC-KKT conditions at the DRTO yield a local optimum of the NMPC problem.

The evolution of the inventory at the plant level is shown in Figure 5.4a, where we see that the DRTO computed reference trajectory leads to the demand of all the grades being satisfied. The Φ^{inv} term in the DRTO objective function incentivizes production beyond what is required to meet the demand, because of that there is some remaining inventory after the demand is met at time 200h.

Case 1b For this case study, the demand order of grade B is due at 75h instead of 200h. We solve the DRTO problem, using the same initial guess as in Case 1a, to compute the reference trajectory to be tracked by the lower-level NMPC.

The closed-loop plant response is given by the black solid lines in Figure 5.5, while the red dotted lines are the predicted DRTO response, and the blue dotted line is the reference

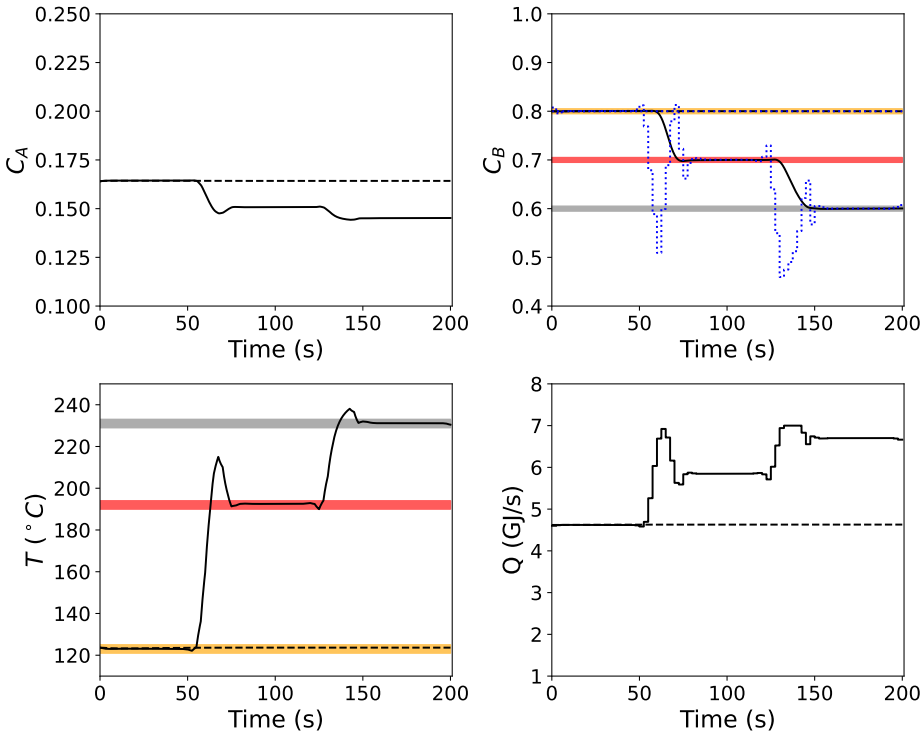

Figure 5.3. Simulated plant response (solid lines), and reference trajectory (blue dotted line) for Case 1a. Initial guess for the corresponding variable in the DRTO problem in Cases 1a and 1b (dashed lines). The shaded area indicates the quality target band.

trajectory computed by the DRTO. For example, the red dotted line in the lower right plot correspond to the predicted u_j trajectory $(u_0, \ldots, u_{N-1})$ at the DRTO level. As we can see, the input trajectory computed by the lower-level NMPC matches the u_j value computed via the NMPC-KKT solution at the DRTO level for all $j \in \mathcal{J}_0^{N-1}$, that is, at every sampling time. The reference trajectory computed by the DRTO leads grade B to be produced first in order to meet the demand at 75h, as shown in Figure 5.4b.

The optimal objective value and solution time for the DRTO problem in Cases 1a and 1b are shown in Table 5.4.

Table 5.4. Optimal objective value and solution time for the DRTO problem in Cases 1a and 1b. The solution time is the total time taken to solve the respective MPCC using the regularization approach.

Case	Objective (Φ^{DRTO})	Solution Time (min)
1a	-16.74	7.7
1b	-5.7	15.53

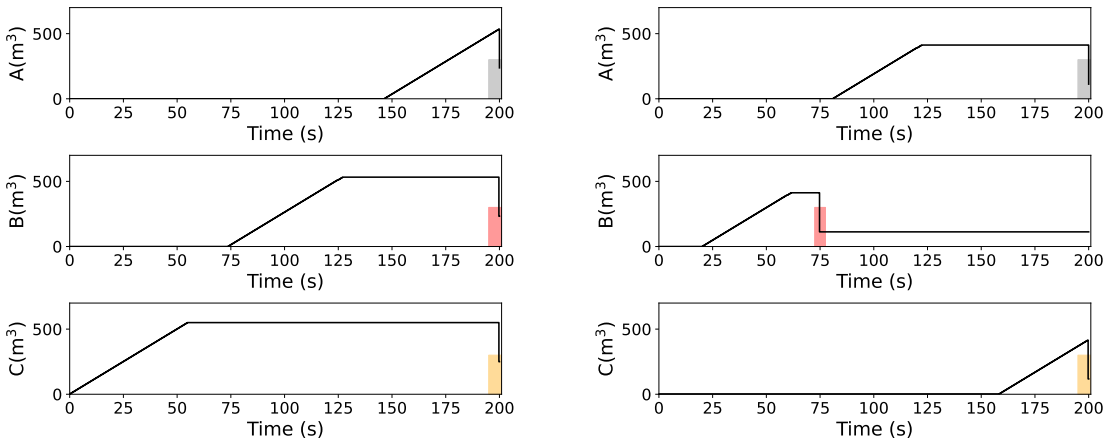

(a) (b)

Figure 5.4. Inventory trajectory for (a) Case 1a and (b) Case 1b. The bars indicate the demand level.

The difference in objective value is due mainly to the Φ^{inv} term in the DRTO objective function. As we can see in Figure 5.4, there is less inventory build-up in Case 1b than in Case 1a. The inventory of each grade after the demand is met is 240 m^3 in Case 1a and 120 m^3 in Case 1b. Therefore, the difference in the Φ^{inv} term (Eq. Eq. (5.29)) between the two cases is $-0.1 \times (240 - 120) = -12$, which is roughly the difference between the objective values in Table 5.4 $(-16.74 - (-5.7) = -11.07)$. Note that the total cost incurred with the inputs and inventory is also different between the cases, making up for the remaining difference between the objective values.

In the DRTO formulation, we use a complementarity formulation to model the discrete scheduling decisions. To check the adequacy of the proposed formulation, we compute the integrality error as

$$\text{integrality error} = |b - 0.5| - 0.5$$

where b stands for the variables $\mu^{\text{lb}}_{j,g,i}$, $\mu^{\text{ub}}_{j,g,i}$, $z^{\text{sto}}_{j,g}$ and $z^{\text{aux}}_{j,g}$ for all $j \in \mathcal{J}_1^N, i \in \mathcal{Q}, g \in \mathcal{G}$. These variables are expected to assume a binary value. The integrality error for Cases 1a and 1b are presented in Figure 5.6. Since most of the data points are very close to zero, the integrality error is small and the proposed DRTO formulation captures the discrete scheduling decisions well.

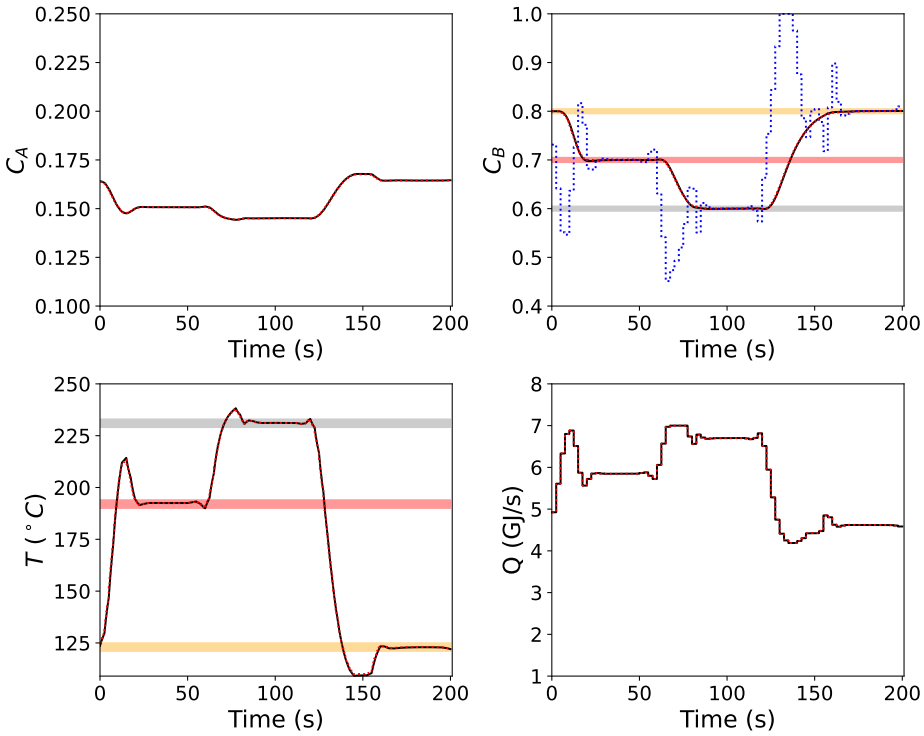

Figure 5.5. Simulated plant response (solid lines), reference trajectory (blue dotted line), and DRTO-predicted trajectories (red dotted line) for Case 1b. The shaded area indicates the quality target band.

5.3.2 Case 2: MIMO system

In this case study, we consider a polymerization reactor system. Instead of solving the integrated scheduling and control problem only once offline, as in the previous case, we solve it periodically at pre-established time intervals. The polymerization reactor model is adapted from Daoutidis et al. [7]. The mathematical model is given as follows.

$$\frac{dC_\mathrm{m}}{dt} = -\left(Z_\mathrm{P} e^{-\frac{E_\mathrm{P}}{RT}} + Z_\mathrm{fm} e^{-\frac{E_\mathrm{fm}}{RT}}\right) C_\mathrm{m} P_0 + \frac{F(C_\mathrm{m}^{in} - C_\mathrm{m})}{V} \tag{5.30a}$$

$$\frac{dC_\mathrm{I}}{dt} = -Z_\mathrm{I} e^{-\frac{E_\mathrm{I}}{RT}} C_\mathrm{I} + \frac{F_\mathrm{I} C_\mathrm{I}^{in} - F C_\mathrm{I}}{V} \tag{5.30b}$$

$$\frac{dT}{dt} = Z_\mathrm{P} e^{-\frac{E_\mathrm{P}}{RT}} C_\mathrm{m} \left(\frac{-\Delta H_\mathrm{P}}{\rho C_\mathrm{p}}\right) P_0 - \frac{UA}{\rho C_\mathrm{p} V}(T - T_\mathrm{j}) + \frac{F(T_\mathrm{in} - T)}{V} \tag{5.30c}$$

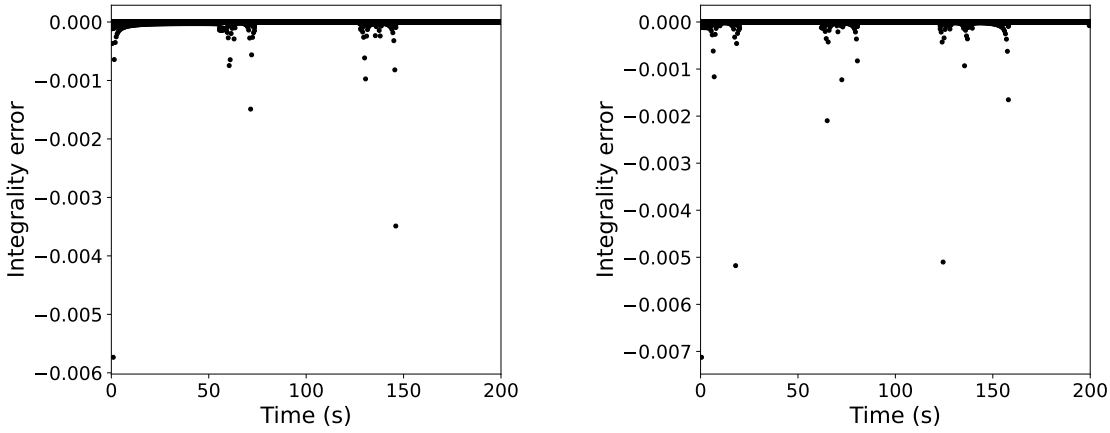

(a) (b)

Figure 5.6. Integrality error in $\mu^{\text{lb}}_{j,g,i}$, $\mu^{\text{ub}}_{j,g,i}$, $z^{\text{sto}}_{j,g,i}$ and $z^{\text{aux}}_{j,g}$ for all $j \in \mathcal{J}_1^N, i \in \mathcal{Q}, g \in \mathcal{G}$ in (a) Case 1a and (b) Case 1b.

$$\frac{dD_0}{dt} = \left(0.5 Z_{\text{Tc}} e^{-\frac{E_{\text{Tc}}}{RT}} + Z_{\text{Td}} e^{-\frac{E_{\text{Td}}}{RT}}\right) P_0^2 + Z_{\text{fm}} e^{-\frac{E_{\text{fm}}}{RT}} C_{\text{m}} P_0 - \frac{F D_0}{V} \tag{5.30d}$$

$$\frac{dD_1}{dt} = M_{\text{m}} \left(Z_{\text{P}} e^{-\frac{E_{\text{P}}}{RT}} + Z_{\text{fm}} e^{-\frac{E_{\text{fm}}}{RT}}\right) C_{\text{m}} P_0 - \frac{F D_1}{V} \tag{5.30e}$$

$$\frac{dT_{\text{j}}}{dt} = \frac{F_{\text{cw}}}{V_{\text{o}}}(T_{\text{wo}} - T_{\text{j}}) + \frac{UA}{\rho_{\text{w}} C_{\text{w}} V_{\text{o}}}(T - T_{\text{j}}) \tag{5.30f}$$

$$P_0 = \left(\frac{2 f C_{\text{I}} Z_{\text{I}} e^{-\frac{E_{\text{I}}}{RT}}}{Z_{\text{Td}} e^{-\frac{E_{\text{Td}}}{RT}} + Z_{\text{Tc}} e^{-\frac{E_{\text{Tc}}}{RT}}}\right)^{0.5} \tag{5.30g}$$

C_{m} and C_{I} are, respectively, the concentration of monomer and initiator in the reactor. D_1/D_0 is the average molecular weight (AMW), T is the reactor temperature, T_j is the jacket temperature. F, F_{I} and F_{cw} are the volumetric flow rate of product, initiator, and cooling water, respectively. C_{m}^{in} is the concentration of monomer in the inlet stream. The model parameter values are given in Table 5.5.

The state vector is $x = [C_{\text{m}}, C_{\text{I}}, T, D_1, D_0, T_{\text{j}}]^T$. We take $y = [D_1/D_0, T]^T$ as outputs, and $u = [F_{\text{I}}, F_{\text{cw}}]^T$ as inputs. The DRTO and NMPC parameter values are provided in Table 5.6.

Table 5.5. Model parameter values for case 2 [14].

Parameter	Value	Units	Parameter	Value	Units
Z_{Tc}	3.8223×10^{10}	kmol/m^3.h	Z_{Td}	3.1457×10^{11}	kmol/m^3.h
Z_{I}	3.7920×10^{18}	h^{-1}	Z_{P}	1.7700×10^{9}	kmol/m^3.h
Z_{fm}	1.0067×10^{15}	kmol/m^3.h	f	0.58	-
E_{Tc}	2.9442×10^{3}	kJ/kmol	E_{Td}	2.9442×10^{3}	kJ/kmol
E_{I}	1.2877×10^{5}	kJ/kmol	E_P	1.8283×10^{4}	kJ/kmol
E_{fm}	7.4478×10^{4}	kJ/kmol	F	1	m^3/h
V	0.1	m^3	ρ	866	kg/m^3
C_{I}^{in}	8	kmol/m^3	Cp	2.0	kJ/kg.K
A	2	m^2	ρ_{w}	$1,000$	kg/m^3
Vo	0.02	m^3	R	8.314	kJ/kmol.K
M_{m}	100.12	kg/kmol	C_{m}^{in}	6.0	Kmol/m^3
$-\Delta H_{\text{P}}$	$57,800$	kJ/kmol	U	720	kJ/h.K.m^2
c_{w}	4.2	kJ/kg.K	T_{in}	350	K
T_{wo}	293.2	K			

The bounds are set $\forall j \in \mathcal{J}_1^N, k \in \mathcal{J}_1^P$ as:

$$\begin{bmatrix} 0.001 \\ 1 \end{bmatrix} \leq \bar{u}_{j-1,k-1} \leq \begin{bmatrix} 0.04 \\ 4 \end{bmatrix}, \qquad \begin{bmatrix} 0 \\ 0 \\ 325 \\ 1 \times 10^{-5} \\ 5 \\ 270 \end{bmatrix} \leq x_j, \bar{x}_{j-1,k} \leq \begin{bmatrix} 10 \\ 0.3 \\ 335 \\ 1 \times 10^{-3} \\ 45 \\ 335 \end{bmatrix}$$

$$\begin{bmatrix} 30,000 \\ 325 \end{bmatrix} \leq y_j, \bar{y}_{j-1,k} \leq \begin{bmatrix} 100,000 \\ 335 \end{bmatrix}, \qquad \begin{bmatrix} 30,000 \\ 300 \end{bmatrix} \leq y_j^{\text{ref}} \leq \begin{bmatrix} 100,000 \\ 335 \end{bmatrix}$$

The quality targets, inventory costs and nominal demand values are given in Table 5.7.

The model equations (Eq. (5.30)) are discretized using the Backward Euler method with a time-step of $\Delta t = 1$h. At every 10 hours, we use the regularization approach to solve the DRTO optimization problem (Eqs. (5.1) - (5.5), (5.7), (5.8), (5.14)-(5.22)) and compute the reference trajectories to be tracked by the lower-level NMPC. The lower-level NMPC then computes the input values applied to the plant. The DRTO layer receives feedback

Table 5.6. DRTO and NMPC parameter values for case 2.

Parameter	Value
Δt	1
Δt^{DRTO}	10
N	40
P	10
M	3
$C^U_{j,1}$	10
$C^U_{j,1}$	0.01
P^U_1	1×10^5
P^U_2	0.01
P^Y_1	2×10^{-7}
P^Y_2	0
ξ	0.2

Table 5.7. Quality target values (q_g^{target}), inventory cost (C_g^I), inventory target penalty (V_g^I), demand ($D_{j,g}^{\text{nom}}$) and time (t) that the demand should be met for case 2.

Parameter	A	B	C	D
AMW	44,000	55,000	77,000	96,000
C_g^I (\$/m^3)	8×10^{-3}	9×10^{-3}	1×10^{-2}	2×10^{-2}
V_g^I (\$/m^3)	0.7	1	1.1	1.2
$D_{j,g}^{\text{nom}}[t]$ (m^3[h])	14[20], 12[80], 13[180]	12[40], 12[160]	13[60],13[120]	16[100], 14[140]

information from the plant regarding the inventory levels. This implementation scheme follows the schematic diagram in Figure 5.1.

After each DRTO execution, we check the input trajectories given by the NMPC-KKT conditions at DRTO time-step j against the solution of the equivalent NMPC optimization problem solved using IPOPT. Since we do this for all $j \in \mathcal{J}_0^{N-1}$, a total of 40 NMPC optimization problems are solved after each DRTO execution. For the present case study, the NMPC-KKT solution always matched the IPOPT solution. During our studies, NMPC-KKT conditions did not match the solution of the stand-alone NMPC problem only when the DRTO problem itself was infeasible. For example, the DRTO problem is infeasible when the demand can not be met.

Case 2a We consider the case of a detuned NMPC controller with weighting matrices (Eq. (5.9a))

$$Q = \begin{bmatrix} 1 \times 10^{-8} & 0 \\ 0 & 5 \times 10^{-3} \end{bmatrix}$$

$$R = \begin{bmatrix} 1 \times 10^{6} & 0 \\ 0 & 5 \end{bmatrix}$$

and

$$S = \begin{bmatrix} 0 & 0 \\ 0 & 0 \end{bmatrix}$$

In Figure 5.7, we present the plant output and input trajectories for a total simulation time of 160 hours. The inventory trajectories are presented in Figure 5.8a.

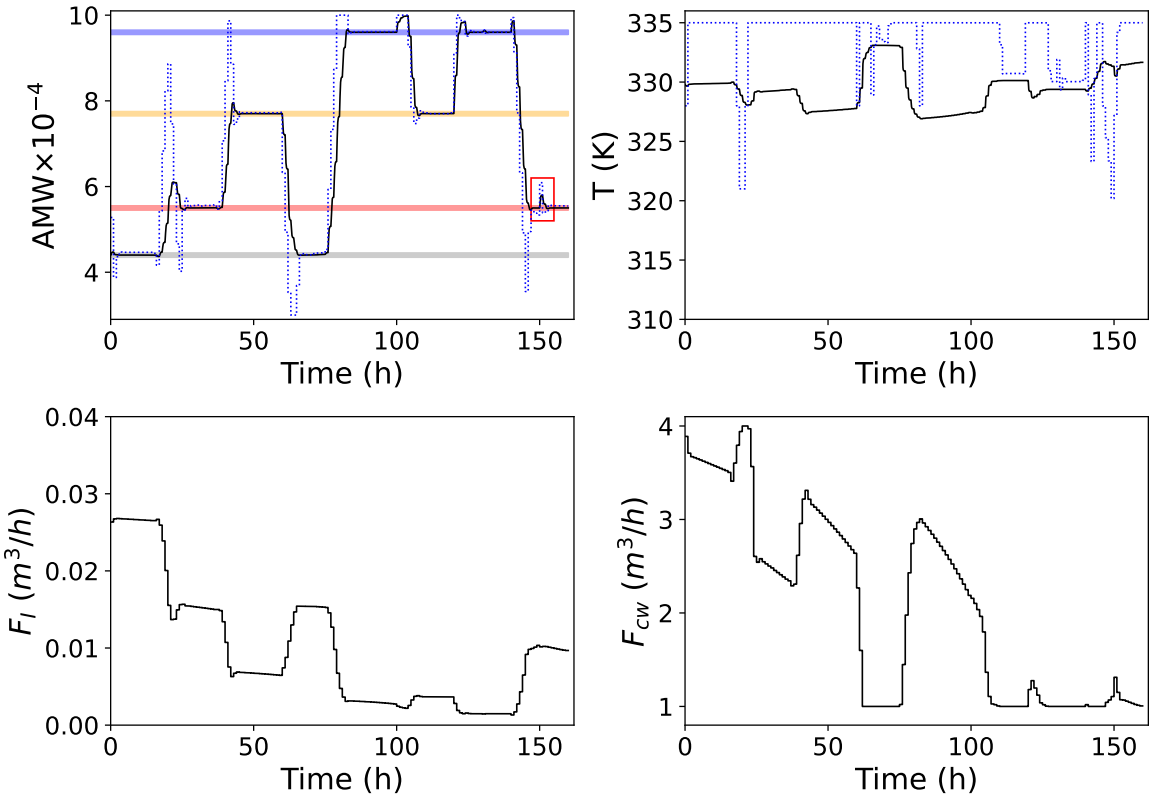

Figure 5.7. Reference (dotted line), output and input trajectories for Case 2a.

The reference trajectories computed by the DRTO (blue dotted line in the two upper plots in

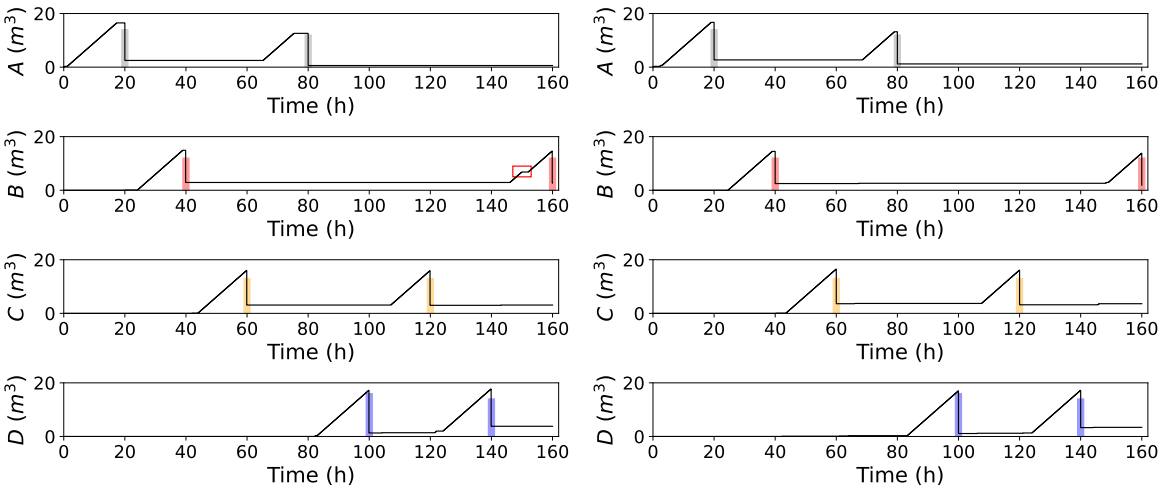

(a) (b)

Figure 5.8. Inventory trajectories for (a) Case 2a, (b) Case 2b. The bars indicate the demand level.

Figure 5.7) drive the plant to produce the demand amount of each grade (Figure 5.8a). Due to the Φ^{inv} term in the DRTO objective function more may be produced of each grade than what is required to meet the demand.

After 150 hours, we see we see a small disturbance on the AMW trajectory during the production of grade B. This disturbance is indicated by a red rectangle in the upper left plot in Figure 5.7. Note that a DRTO problem is solved at simulation time 140 hours and another one at 150 hours. The DRTO problem solved at 140 hours predicts uninterrupted build-up of the inventory of grade B until 158 hours. It also predicts 6.4 m^3 of grade B in inventory at 150 hours. However, the actual amount in inventory at 150 hours is 6.8 m^3. Therefore, there is 0.4 m^3 more of grade B in inventory at 150 hours than it was predicted by the DRTO executed at 140 hours. To compensate for this mismatch, the DRTO executed at 150 hours adjusts the reference trajectory, temporarily halting production of grade B. This is the cause of the indicated disturbance in the AMW trajectory. The predicted amount of grade B in inventory at 160 hours is the same for the DRTOs executed at 140 and 150 hours. The reason for the 0.4 m^3 inventory mismatch is that $z^{\text{sto}}_{j,B}$ assumes a non-binary value in one of the time steps for the DRTO executed at 140 hours, which affects the inventory prediction via Eq. (5.8b). Considering all the 16 DRTO executions for Case 2a, $z^{\text{sto}}_{j,g} \in [0.05, 0.95]$ 0.8% of the time (22 occurrences in total out of 2560).

In Figure 5.7, we see that the lower-level NMPC tracks the reference trajectory for the AMW better than for the reactor temperature. One of the reasons is the high input suppression move weight on the cooling water flow-rate, and the lower set-point tracking weight for the temperature.

Case 2b For this case study, we consider a different NMPC controller tuning (Eq. (5.9a)):

$$Q = \begin{bmatrix} 1 \times 10^{-8} & 0 \\ 0 & 0.1 \end{bmatrix}$$

$$R = \begin{bmatrix} 1 \times 10^{5} & 0 \\ 0 & 0.1 \end{bmatrix}$$

$$S = \begin{bmatrix} 0 & 0 \\ 0 & 0 \end{bmatrix}$$

The closed-loop plant response is presented in Figure 5.9, and the inventory in Figure 5.8b. Comparing the two upper plots in Figures 5.7 and 5.9, we observe that the reactor temperature follows the reference trajectory (blue dotted line) more closely in Case 2b than in Case 2a. This is due to the lower input suppression move weights (R in Eq. (5.9a)), and the higher set-point tracking weight (Q in Eq. (5.9a)) for the reactor temperature in Case 2b. However, it is also important to make a distinction between the DRTO and NMPC objectives. The DRTO provides set-point trajectories ($y^{\mathrm{SP}}_{j,k}$ in Eq. (5.9a)) to the NMPC that lead the NMPC to compute input values that optimize the DRTO objective function, while the NMPC computes input values that minimize its own objective function. There are no constraints regarding how well the NMPC should be able to track the set-point trajectories provided by the DRTO. The NMPC in Case 2b is more sensitive to the temperature set-point trajectory because of the lower input suppression move weight and higher set-point tracking weight for the temperature, which lead the DRTO to compute more conservative set-point trajectories.

On another hand, the lower input suppression move leads to larger variations in the initiator flow-rate F_{I} and overshoots in the AMW trajectory in Case 2b (left plots in Figure 5.9)

compared to Case 2a (left plots in Figure 5.7). The overshoots at 20 and 40 hours are particularly noticeable (upper left plot in Figure 5.9), and the upper bound of 100,000 on the AMW is momentarily violated at approximately 10 and 80 hours. While the DRTO would predict these large overshoots, the accuracy of the Backward Euler method is not high enough to capture the bound violations. Therefore, from the DRTO perspective, these overshoots neither violate constraints nor negatively impact the objective function. While we could improve the accuracy of the Backward Euler method by reducing the integration step size, this would significantly increase the computational burden. Alternative options are to reduce the upper bound on the reference trajectory, or restrict the change in the reference trajectory between time-steps (reduce the value ξ).

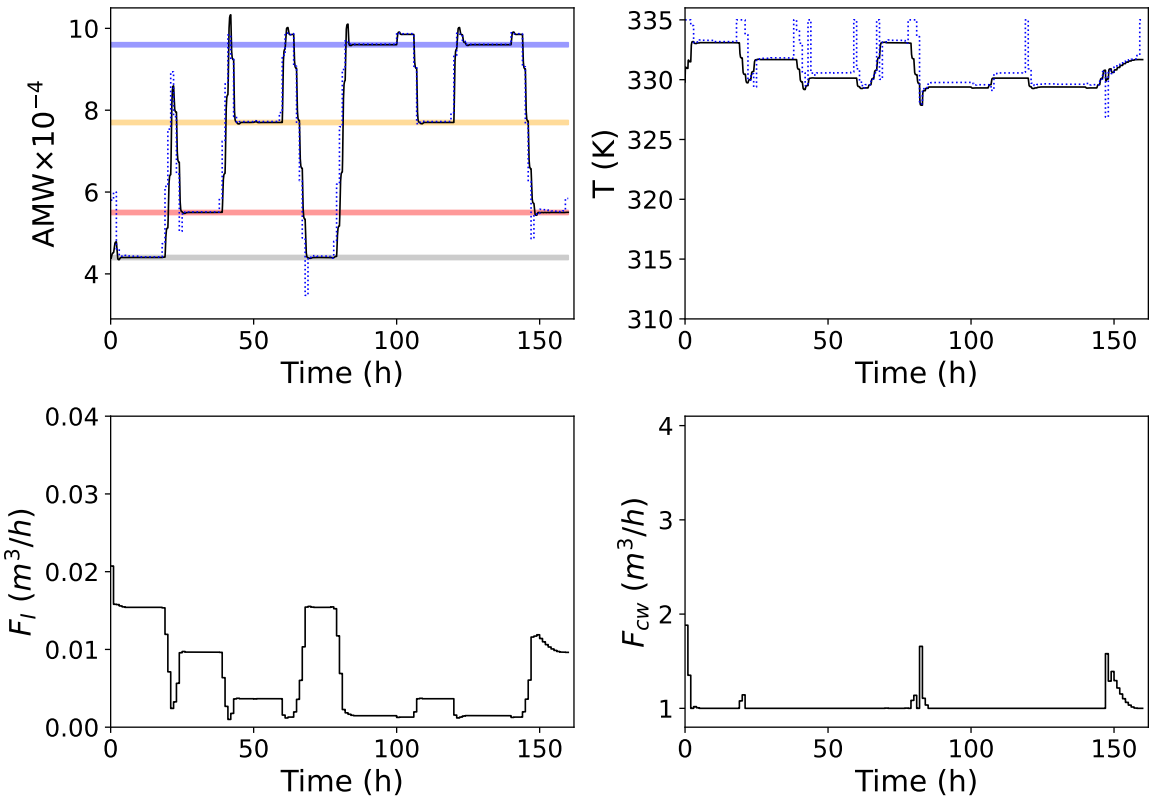

Figure 5.9. Reference (dotted line), output and input trajectories for Case 2b.

For each case, the DRTO problem was solved 16 times. In Table 5.8, we present the total input and inventory costs (Φ^{eco}) incurred by the plant, as well as the average, minimum and maximum solution times for DRTO problem. The cost is lower in Case 2b compared to Case

2a, because the change in controller tuning allows the DRTO to compute trajectories that reduce the usage of cooling water and initiator. Overall, this case shows that the proposed integrated scheduling and control formulation is able to adapt the reference trajectories in response to changes in controller tuning, successfully guiding the plant to meet the demand order of each grade on time while minimizing cost.

Table 5.8. Total input and inventory cost Φ^{eco} at the plant level. Average, maximum and minimum DRTO solution times.

	Case 2a	Case 2b
Φ^{eco} ($)	41.15	33.89
Average sol. time (min)	3.3	4.8
Maximum sol. time (min)	4.7	6.7
Minimum sol. time (min)	1.6	2.7

5.4 Conclusion

Volatile market conditions have fueled interest in the integration of scheduling and control in recent years. As a result, several integrated scheduling and control (ISC) frameworks for processes controlled by linear control systems have been developed. In this study, we propose a control-aware scheduling formulation for processes controlled by nonlinear model predictive control (NMPC). NMPC is usually employed in processes that are highly nonlinear and/or operate over wide regimes where a linear model approximation is not considered sufficiently accurate.

We use the NMPC first-order Karush-Kuhn-Tucker (KKT) conditions to compute the input action applied to the dynamic nonlinear model in the ISC problem, which leads to a control-aware ISC formulation. Discrete scheduling decisions are captured using complementarity conditions. These, together with the NMPC-KKT complementarity constraints render the ISC problem a mathematical program with complementarity constraints (MPCC). This MPCC problem is solved at the DRTO level, using a regularization method and IPOPT as the NLP solver, to compute optimal reference trajectories tracked by the lower-level NMPC. The production sequencing and production amounts are communicated to the plant exclusively

through these reference trajectories. We demonstrate the performance of the framework for a multiproduct SIMO and MIMO systems, where the MIMO system is a polymerization reactor.

Our results demonstrate that the proposed framework is able to successfully guide the plant to meet the demand of all the grades on time. Moreover, knowledge of the control systems enables it to adapt the set-points trajectories to different controller settings. For the cases considered, the NMPC-KKT conditions always led to a local minimum, despite the nonconvexity of the NMPC problem.

References

[1] O. Andrés-Martínez and L. A. Ricardez-Sandoval. "A nested online scheduling and nonlinear model predictive control framework for multi-product continuous systems". In: *AIChE Journal* 68.5 (2022), e17665 (cit. on p. 137).

[2] B. Baumrucker, J. G. Renfro, and L. T. Biegler. "MPEC problem formulations and solution strategies with chemical engineering applications". In: *Computers & Chemical Engineering* 32.12 (2008), pp. 2903–2913 (cit. on pp. 151, 153).

[3] B. W. Bequette. "Nonlinear predictive control using multi-rate sampling". In: *The Canadian Journal of Chemical Engineering* 69.1 (1991), pp. 136–143 (cit. on pp. 137, 153).

[4] L. T. Biegler. "Process Optimization with Complementarity Constraints". In: *Nonlinear Programming*. Society for Industrial and Applied Mathematics, 2010, pp. 325–362. DOI: 10.1137/1.9780898719383.ch11 (cit. on pp. 143, 151, 153).

[5] D. Brengel and W. Seider. "Coordinated design and control optimization of nonlinear processes". In: *Computers & Chemical Engineering* 16.9 (1992), pp. 861–886 (cit. on p. 137).

[6] Z. Chen, M. A. Henson, P. Belanger, and L. Megan. "Nonlinear model predictive control of high purity distillation columns for cryogenic air separation". In: *IEEE transactions on control systems technology* 18.4 (2009), pp. 811–821 (cit. on p. 137).

[7] P. Daoutidis, M. Soroush, and C. Kravaris. "Feedforward/feedback control of multivariable nonlinear processes". In: *AIChE Journal* 36.10 (1990), pp. 1471–1484 (cit. on p. 159).

[8] D. Dering and C. L. E. Swartz. "A scenario-based framework for the integration of scheduling and control under multiple uncertainties". In: *Journal of Process Control* 129 (2023), p. 103055 (cit. on pp. 137, 138, 140, 144).

[9] D. Dering and C. L. E. Swartz. "An Integrated Scheduling and Control Framework for Plants Controlled by Distributed MPC Systems". In: *IFAC World Congress 2023*. IFAC. 2023 (cit. on p. 137).

[10] D. Dering and C. L. E. Swartz. “Dynamic Real–Time Optimization with Closed-Loop Prediction for Nonlinear MPC–Controlled Plants”. In: *Computer Aided Chemical Engineering*. Vol. 51. Elsevier, 2022, pp. 1099–1104 (cit. on p. 136).

[11] D. Dering and C. L. E. Swartz. “Dynamic Real-Time Optimization with Closed-Loop Prediction for Nonlinear MPC-Controlled Plants”. In: *ESCAPE 32 Conference*. 2022 (cit. on p. 136).

[12] D. Dering and C. L. E. Swartz. “Integration of scheduling and control for NMPC-controlled plants”. In: *Manuscript in preparation* (2023) (cit. on p. 137).

[13] D. Dering and C. L. Swartz. “A stochastic optimization framework for integrated scheduling and control under demand uncertainty”. In: *Computers & Chemical Engineering* 165 (2022), p. 107931 (cit. on pp. 137, 138, 140, 144, 149).

[14] F. J. Doyle III, B. A. Ogunnaike, and R. K. Pearson. “Nonlinear model-based control using second-order Volterra models”. In: *Automatica* 31.5 (1995), pp. 697–714 (cit. on p. 161).

[15] D. J. Gardner, D. R. Reynolds, C. S. Woodward, and C. J. Balos. “Enabling new flexibility in the SUNDIALS suite of nonlinear and differential/algebraic equation solvers”. In: *ACM Transactions on Mathematical Software (TOMS)* (2022). DOI: 10.1145/3539801 (cit. on p. 153).

[16] M. A. Henson. “Nonlinear model predictive control: current status and future directions”. In: *Computers & Chemical Engineering* 23.2 (1998), pp. 187–202 (cit. on p. 137).

[17] *HSL, a Collection of Fortran Codes for Large-Scale Scientific Computation*. URL: http://www.hsl.rl.ac.uk/ (cit. on p. 153).

[18] X. M. Hu and D. Ralph. “Convergence of a penalty method for mathematical programming with complementarity constraints”. In: *Journal of Optimization Theory and Applications* 123 (2004), pp. 365–390 (cit. on pp. 151, 153).

[19] R. Huang, V. M. Zavala, and L. T. Biegler. “Advanced step nonlinear model predictive control for air separation units”. In: *Journal of Process Control* 19.4 (2009), pp. 678–685 (cit. on p. 137).

[20] H. Li and C. L. E. Swartz. "Economic Coordination of Distributed Nonlinear MPC Systems using Closed-loop Prediction of a Nonlinear Dynamic Plant". In: *IFAC-PapersOnLine* 51.20 (2018), pp. 35–40 (cit. on p. 137).

[21] S. Lucia, T. Finkler, and S. Engell. "Multi-stage nonlinear model predictive control applied to a semi-batch polymerization reactor under uncertainty". In: *Journal of process control* 23.9 (2013), pp. 1306–1319 (cit. on p. 137).

[22] J. Nocedal and S. J. Wright. "Quadratic Programming". In: *Numerical Optimization*. Springer New York, 0206, p. 467. DOI: https://doi.org/10.1007/978-0-387-40065-5 (cit. on p. 151).

[23] O. Palma-Flores and L. A. Ricardez-Sandoval. "Integration of design and NMPC-based control for chemical processes under uncertainty: An MPCC-based framework". In: *Computers & Chemical Engineering* 162 (2022), p. 107815 (cit. on pp. 137, 138).

[24] O. Palma-Flores and L. A. Ricardez-Sandoval. "Simultaneous design and nonlinear model predictive control under uncertainty: A back-off approach". In: *Journal of Process Control* 110 (2022), pp. 45–58 (cit. on p. 137).

[25] A. A. Patwardhan, J. B. Rawlings, and T. F. Edgar. "Nonlinear model predictive control". In: *Chemical Engineering Communications* 87.1 (1990), pp. 123–141 (cit. on p. 137).

[26] M. Pottmann and D. E. Seborg. "A nonlinear predictive control strategy based on radial basis function models". In: *Computers & chemical engineering* 21.9 (1997), pp. 965–980 (cit. on p. 137).

[27] S. J. Qin and T. A. Badgwell. "A survey of industrial model predictive control technology". In: *Control Engineering Practice* 11.7 (2003), pp. 733–764 (cit. on p. 137).

[28] D. Ralph* and S. J. Wright. "Some properties of regularization and penalization schemes for MPECs". In: *Optimization Methods and Software* 19.5 (2004), pp. 527–556 (cit. on p. 151).

[29] J. E. Remigio and C. L. E. Swartz. "Production scheduling in dynamic real-time optimization with closed-loop prediction". In: *Journal of Process Control* 89 (2020), pp. 95–107 (cit. on p. 138).

[30] S. Scholtes. “Convergence properties of a regularization scheme for mathematical programs with complementarity constraints”. In: *SIAM Journal on Optimization* 11.4 (2001), pp. 918–936 (cit. on p. 151).

[31] S. Scholtes and M. Stöhr. “Exact penalization of mathematical programs with equilibrium constraints”. In: *SIAM Journal on Control and Optimization* 37.2 (1999), pp. 617–652 (cit. on p. 151).

[32] J. C. Schulze, A. Caspari, C. Offermanns, A. Mhamdi, and A. Mitsos. “Nonlinear model predictive control of ultra-high-purity air separation units using transient wave propagation model”. In: *Computers & chemical engineering* 145 (2021), p. 107163 (cit. on p. 137).

[33] H. Seki, M. Ogawa, S. Ooyama, K. Akamatsu, M. Ohshima, and W. Yang. “Industrial application of a nonlinear model predictive control to polymerization reactors”. In: *Control Engineering Practice* 9.8 (2001), pp. 819–828 (cit. on p. 137).

[34] J. M. Simkoff and M. Baldea. “Production scheduling and linear MPC: Complete integration via complementarity conditions”. In: *Computers & Chemical Engineering* 125 (2019), pp. 287–305 (cit. on pp. 138, 140).

[35] A. Wächter and L. T. Biegler. “On the implementation of an interior-point filter line-search algorithm for large-scale nonlinear programming”. In: *Mathematical Programming* 106.1 (2006), pp. 25–57 (cit. on p. 153).

Chapter 6

Conclusion

In this chapter, we summarize the key contributions of this thesis and make recommendations for future research avenues.

6.1 Conclusion

Typically, scheduling decisions are based on steady-state process models. However, increasing volatile market conditions shaped by the deregulation of the energy market, and growing participation of intermittent energy sources in the power grid, are forcing industries to conform to a more dynamic and flexible operating setting. Under this new operating environment, set-point transitions are likely to be performed more frequently, leading to increased relevance of the transition dynamics to the scheduling decisions, ultimately rendering the

traditional steady-state approach to the scheduling problem suboptimal. In this context, the integration of scheduling and control can lead to improved process economics by providing the scheduling problem with needed dynamic information about the process.

Paradigms for the integration of scheduling and control [1, 3] include economic model predictive approach and the two-layer approach. The economic model predictive control approach dispenses the use of a dedicated control system layer. It physically combines the scheduling and control problem into a single decision making layer. In the two-layer approach, the existing control system is kept intact, but the set-points to be tracked are computed by a supervisory integrated scheduling and control layer that has access to a suitable dynamic process model. This dynamic model represents either the open or closed-loop process response. Closed-loop integrated scheduling and control formulations have been shown to be superior to open-loop formulations [7].

This thesis is dedicated to the development of closed-loop integrated scheduling and control frameworks for process controlled by various control systems. In Chapters 2 and 3, we developed a robust integrated scheduling and control formulation for processes controlled by linear model predictive control and PI control, respectively. We accounted for uncertainty using a scenario-based approach, where each scenario corresponds to a different realization of the uncertainty. The scenarios are linked via the so called nonanticipativity constraints to ensure that decisions based on the same information are equal. Following the standard approach in stochastic programming, we used the value of the stochastic solution (VSS), to access the benefits of the robust formulation against a nominal one where uncertainty is neglected. The robust formulation largely outperforms the nominal one, even under conditions of plant-model mismatch, because it is able to compute set-point trajectories that are robust to demand, and model uncertainty. The difference in performance is even more accentuated when the controller is detuned.

In Chapter 4, we developed an integrated scheduling and control formulation for processes controlled by distributed linear model predictive control, and propose strategies for reducing the computational time. Our formulation also accounts for multiple production lines. Knowledge of the control system, and interactions between the control loops, enables the

framework to coordinate the MPC subsystem via the set-point trajectories. In particular, the integrated framework computes set-point trajectories that take advantage of, or mitigate, the control loop interactions to achieve optimal economic performance. We compare the economic and computational performance of various strategies to enhance the solution time, and explore the effect of the DRTO sampling time on the plant performance. The framework leads to acceptable performance under conditions of plant-model mismatch.

In Chapter 5, an integrated scheduling and control framework for plants controlled by nonlinear model predictive control was developed. We departed from the formulation in the previous studies, by utilizing a nonlinear model of the plant instead of a linear one, and complementarities to model the discrete scheduling decisions instead of binary variables. Consequently, the final problem took the form of a mathematical program with complementarity constraints (MPCC), as opposed to the mixed-integer linear programming formulation of the previous chapters. This problem was solved using a regularization approach. Through simulation case studies, we confirmed that complementarity conditions can effectively capture discrete scheduling decisions. Challenges associated with the MPCC formulation were demonstrated, and potential strategies for addressing them proposed. We carefully explored and explained seemingly paradoxical results.

6.2 Future Research Directions

The integration of scheduling and control is a rapidly evolving field of research with various opportunities for future research.

Model uncertainty In this study, we assumed a fixed probability distribution for the model uncertainty. However, a more careful treatment of the model uncertainty may be beneficial. For example, the model uncertainty, as measured by the standard deviation in a model parameter, should decrease as more information about the process, in the form of measurements, becomes available. A more accurate description of the model uncertainty has the potential to improve the economic performance of the stochastic DRTO formulation.

Additionally, it could reduce the number of discrete scenarios required to appropriately model the uncertainty probability distribution, effectively decreasing the complexity and solution time of the DRTO problem. In this context, methods for obtaining a more accurate description of the model uncertainty is warranted.

State-estimation For the current work, we used the state prediction at the previous DRTO iteration together with a disturbance estimate to correct for plant-model mismatch. This approach is similar to the one utilized in the MPC formulation of Garcia and Morshedi [4] to achieve offset-free tracking. However, a more advanced method for state-estimation such as Kalman filter or moving horizon estimation could improve the accuracy of the DRTO predictions and, consequently, the economic performance of the framework, especially for cases where a nonlinear model representation of the plant is utilized at the DRTO level. The state-estimation method could be extended to some of the scheduling variables, such as the inventory level, since measurements may not be available at every sampling time.

Surrogate modelling for large scale application Throughout this study, we used first-principles model, or a linearization thereof (for cases where the first-principles model was nonlinear in Chapters 2-4), to represent the plant at the DRTO level. However, for large scale dynamic processes, other strategies may be more efficient. For example, machine learning methods such as artificial neural network could be used to develop surrogate models with a good level of compromise between accuracy and computational complexity. Additionally, an efficient strategy for updating the model should be developed in order to ensure good accuracy over wide operating regimes.

Decomposition and parallelization For more efficient solution of the stochastic DRTO formulation presented in Chapters 2 and 3, decomposition methods should be explored. Decomposition methods tailored to linear problems with first and second-stage mixed continuous and binary variables include Carøe and Tind [2], Ntaimo and Tanner [5] and Sherali and Zhu [6]. The implementation of existing methods is likely to be challenging, and the development of more accessible and transparent methods would be beneficial. Decomposition

methods that allow for efficient parallelization are particularly attractive because they offer the opportunity for significant decrease in the computational time. Moreover, decomposition methods for nonlinear problems with mixed-integer first and second stage variables should also be explored for efficient solution of the stochastic DRTO problems where a nonlinear representation of the plant model is used.

References

[1] M. Baldea and I. Harjunkoski. “Integrated production scheduling and process control: A systematic review”. In: *Computers & Chemical Engineering* 71 (2014), pp. 377–390 (cit. on p. 174).

[2] C. C. Carøe and J. Tind. “L-shaped decomposition of two-stage stochastic programs with integer recourse”. In: *Mathematical Programming* 83 (1998), pp. 451–464 (cit. on p. 176).

[3] A. Caspari, C. Tsay, A. Mhamdi, M. Baldea, and A. Mitsos. “The integration of scheduling and control: Top-down vs. bottom-up”. In: *Journal of Process Control* 91 (2020), pp. 50–62 (cit. on p. 174).

[4] C. E. Garcia and A. Morshedi. “Quadratic programming solution of dynamic matrix control (QDMC)”. In: *Chemical Engineering Communications* 46.1-3 (1986), pp. 73–87 (cit. on p. 176).

[5] L. Ntaimo and M. W. Tanner. “Computations with disjunctive cuts for two-stage stochastic mixed 0-1 integer programs”. In: *Journal of Global Optimization* 41 (2008), pp. 365–384 (cit. on p. 176).

[6] H. D. Sherali and X. Zhu. “On solving discrete two-stage stochastic programs having mixed-integer first-and second-stage variables”. In: *Mathematical programming* 108 (2006), pp. 597–616 (cit. on p. 176).

[7] J. M. Simkoff and M. Baldea. “Production scheduling and linear MPC: Complete integration via complementarity conditions”. In: *Computers & Chemical Engineering* 125 (2019), pp. 287–305 (cit. on p. 174).